Metal-organic Frameworks (MOFs) for building applications

Menghao Qin
Technical University of Denmark (DTU)

Preface

The regulation of the balance of the sensible and latent loads remains a critical problem for built environment control. Unlike the traditional vapor compression system that features high-energy consumption and environmental-unfriendly processes, desiccants represent an alternative air-conditioning method that takes advantage of the low-grade energy, decreases energy consumption, and even employs the use of water vapor. Though the desiccant-based systems can achieve spatial moisture transfer through the periodic adsorption/desorption process, however, the water-stable desiccants with high water uptake and mildly reversible adsorption are required, and the traditional desiccants (e.g. silica gel, zeolite, etc.) cannot meet these requirements.

Metal-organic Frameworks (MOFs) are an emerging class of porous materials. Most MOFs can exhibit very high surface areas and large adsorption capacity for gas. Due to their structural and functional tunability, MOFs have become one of the most fascinating classes of materials for both scientists and engineers. In the area of built environment, MOFs can be used for moisture regulation, pollutant removal, air purification, thermal storage, and atmosphere water harvesting, etc. This report contains 8 recent selected papers of DTU Building Physics concerning preparation, characterization, and applications of metal-organic frameworks for built environment control.

For more information of relevant research at DTU Building Physics group, please visit: https://www.staff.dtu.dk/menqin

Contact information:
Prof. Menghao Qin
Department of Civil Engineering
Technical University of Denmark
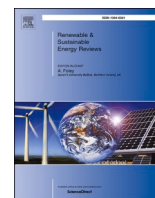Tel. +45 45 25 40 15
Email: menqin@byg.dtu.dk

Content

Progress and potential of metal-organic frameworks (MOFs) as novel desiccants for built environment control: A review

Kan Zu, Menghao Qin [*], Shuqing Cui

Department of Civil Engineering, Technical University of Denmark, Lyngby, Denmark

A B S T R A C T

The regulation of the balance of the sensible and latent loads remains a critical problem for built environment control. Unlike the traditional vapor compression system that features high-energy consumption and environmental-unfriendly processes, desiccants represent an alternative air-conditioning method that takes advantage of the low-grade energy, decreases the energy consumption and even employs use of water vapor. Though the desiccant-based systems can achieve spatial moisture transfer through the periodic adsorption/desorption process, however, the water-stable desiccants with high water uptake and mildly reversible adsorption are required, and the traditional desiccants cannot meet these requirements. In this respect, metal-organic frameworks (MOFs), possessing a variety of structures and precise functional ability to optimize their properties, are promising porous materials exhibiting high potential for rational design and sorption-based applications. In this review, intrinsic properties and prevalent water adsorption mechanisms of the potential micro/mesoporous MOF desiccants have been elucidated. Subsequently, the selection criteria of the promising MOF desiccants for water loading removal from air in the built environment is proposed and some currently available water-stable MOFs based on different working humidity ranges have been analyzed for the potential humidity control from the aspects of microstructure, isotherms and regeneration conditions. Finally, approaches for screening the well-suited MOFs from material and system levels is presented. Overall, the cases of actual applications in the active or passive way have confirmed that MOF-based systems can effectively regulate the humidity load within the desirable range, thus, underlining the high potential of large-scale applications in the near future.

1. Introduction

Benefitting from the scientific inventions of the contemporary era, people's lifestyle has evolved from early open-air living spaces into more comfortable and enclosed air-conditioned ones. The energy consumption by the air conditioning systems represents more than 40% of the total building energy consumption. In the traditional cooling dehumidification, the cooling air below the dew point, used to remove both sensible and latent loads, gives rise to a large extent of energy waste owing to the low trigger temperature for the latent load removal [1,2]. Therefore, the critical problem in the indoor air-conditioned zones is to achieve an independent control of temperature and humidity [3,4]. It is to be noted that either moisture accumulation or deficiency will cause discomfort to human beings and damage to building materials, and 45% ~65% relative humidity (RH) in residential buildings has been recommended by the American Society of Heating, Refrigerating and Air-Conditioning Engineers (ASHRAE) [5]. In this regard, the introduction of desiccant materials is an alternative method to achieve effective humidity control within a desirable range, and extensive studies have been devoted to the synthesis and application of new desiccants possessing high water capacity and gentle regeneration conditions [6,7].

Desiccants can generally be classified into liquid and solid phase. As the liquid desiccant dehumidifiers suffer from large and complicated systems, metal corrosion, etc., the solid desiccant systems (SDSs) progressively exhibit potential as promising methods for indoor humidity control [8,9]. Some commercially used materials, like zeolites and silica gels, have been incorporated into the air-conditioning systems, but these are incapable of achieving high-performance dehumidification due to the harsh regeneration condition or low work loading [10,11]. Therefore, research efforts are going for the development of novel solid desiccants with an ability to improve the whole system performance with respect to the built environment control. Recently, micro- and mesoporous materials such as metal-organic frameworks (MOFs) have

emerged as an effective alternative to the currently used desiccants [9]. The MOFs are constructed by the formation of strong chemical bonds to bridge inorganic metal-related units with organic ligands, thus, creating open frameworks with ordered structure [12,13]. A high level of structural flexibility and ultra-high porosity make these materials promising desiccants in the sorption-based applications [14]. In addition, most of the MOFs have S-shaped isotherms with a steep rise in a narrow relative humidity (RH) range. The observed steep rise is directly correlated with the special adsorption mechanism of MOFs, however, it does not rely on the formation of strong bonding sites in the crystalline frameworks, thus, partly indicating their gentle regeneration condition [15].

To date, more than 80000 different MOFs have been reported, but only a small number of literature studies have investigated their distinct advantages over traditional materials in the air-conditioning system [16, 17]. One critical challenge appears to be the effective screening of the available MOF desiccants. First, the long-term water stability is the precondition that ensures the conservation of their frameworks [10]. Hydrothermal stability tests over several thousands of adsorption/ desorption cycles have been proven only for a few structures [18–21], while most reports have presented only a few dozen cycles on laboratory scale. Second, the working performance (adsorption and desorption) of MOF desiccants is of importance for the working efficiency. At present, a small number of studies have been reported on the MOF-based open SDSs (directly contacting the ambient air) for humidity regulation in buildings. However, water-harvesting applications [22–24] and explorations of the sorption-based close SDSs (without contacting the ambient air) such as heat pumps [25–31] and adsorption-based refrigeration [20, 32–34] provide more information about the basic hydrothermal properties of MOFs. Third, the intrinsic properties of the MOF chemicals decide the application area. In general, it is also preferred to use green and safe materials with low cost in the practical applications [35]. Besides, the other challenge is to classify the MOF desiccants. In general, MOFs such as MOF-801 [36], MOF-841 [37], MIL-160 [25], CAU-10 [38], $Co_2Cl_2(BTDD)$ [39], etc., have been investigated for good working capacity in the 0–30% RH range, while MIL-100 (Cr, Fe, Al) [27,40], MIL-101(Cr) [41],Cr-**soc**-MOF-1 [42], Y-**shp**-MOF-5 [21], UiO-66 [37], etc., exhibit high working capacity in the 30%~65% RH range. Especially, Y-**shp**-MOF-5 [21] and Cr-**soc**-MOF-1 [42] demonstrate autonomous humidity control within a desirable range (45%~65% RH) for the building environment. Thus, the ongoing work on the classification of MOFs should be intensively developed.

To the best of our knowledge, most previous review papers on the topic of water adsorption applications of MOFs are mainly focused on heat transformation in mechanical systems (e.g. heat pump, adsorption chiller, etc. [16,17,43]) and atmospheric water harvesting (AWH) [44]. Very few reviews have a special emphasis on the MOF application for built environment. In this review, we will discuss in detail the potential applications of MOF materials for built environment control from both the material and system levels. A brief review of the compositions and intrinsic properties of the MOF materials has been presented. Some basic selection criteria of MOFs for humidity load control have been subsequently proposed, and three groups of MOFs have been classified and discussed based on their different trigger point (a turning point P/P_0 before a steep rise in isotherms). At the end of this review, the strategy and design of systems using MOF materials have been provided for either passive or active methods. Though it is hard to review the vast number of literature studies on MOFs and make a well-considered evaluation on this subject, it is still hoped that the review provides some insights into the selection of the most suitable MOFs depending on the different conditions with reference to their application in the built environment control.

2. Compositions and intrinsic properties of MOFs

2.1. Compositions

A specific MOF requires the provision of metal ions derived from the inorganic metal salts, organic ligands, and possibly solvents. MOFs with desirable structures can be prepared through the component exchanges in the metal ions, ligands or solvents.

Metal ions: metal-containing units are used for bonding with organic groups. To date, many metal ions have been reported for developing MOFs with high hydrolytic stability, most of which traditionally are divalent metal ions such as Cu^{2+}, Zn^{2+}, Zr^{2+}, Ni^{2+}, Co^{2+}, Mg^{2+} and Cd^{2+} [30,39,45–47], trivalent metal ions such as Fe^{3+}, Cr^{3+} and Al^{3+} [27], and even tetravalent ions such as Ti^{+4} and Hf^{+4} [48,49]. In past decades, many studies have also been conducted on lanthanide series (i.e., Ce, Pr and Eu), p-block elements (i.e., Ga and In) and even mix-metals [10,50, 51].

Ligands (linkers): the ligands are used to connect the metal clusters, which shape the crystal framework. The structure of ligands can provide insights about the hydrophilicity/ hydrophobicity of the pore surface. Theoretically, longer ligands bear larger surface area, thus, providing more adsorption sites and storage space, and correspondingly affecting the adsorption capacity. Common ligands used in the synthesis of water-stable MOFs include BTC (1, 3, 5-benzene tricarboxylic acid), TPA (terephthalic acid), TDC (thiophene-2, 5-dicarboxylic acid), fumaric acid, etc. [40,41,49].

Solvents: the solvents are not a necessity during the synthesis of MOFs, especially for mechanochemical synthesis. However, the solvents can provide a benign environment for the chemical reactions, resulting in the diversity of the formed structures. Besides, the solvents can also determine the thermodynamics and activation energy for a specific reaction. The commonly used solvents are water and organic solvents such as ethanol, acetone and ethyl acetate. A few non-green solvents (e.g. dimethyl sulfoxide, tetrahydrofuran, toluene, formic acid etc.) can also be used in the large-scale production by strictly following the standard procedures [52,53].

2.2. Intrinsic properties

The remarkable performance of MOFs has advanced their synthesis, accompanied by the development of geometric topology design, post-synthetic modification and multivariate MOFs. It is to be noted that the interaction between the acceptor and target pairs (i.e. MOF- water vapor) makes the MOFs competent desiccants. Namely, the intrinsic properties of MOFs drive the performance for water uptake and corresponding applications (Table 1 and Table 2).

2.2.1. Metal sites

There are many coordinatively unsaturated metal sites inside the MOF structure, where the guest molecules such as water or other organic solvents can be coordinated after synthesis [54]. Prior to the practical usage, activation is needed to help remove these guest molecules from the metal nodes by heating in a vacuum environment. As the exposed sites exhibit strong polarity, MOFs demonstrate relatively high affinity towards vapor molecules even at low vapor pressure. Correspondingly, the amount of the recovered unsaturated metal sites can enhance the adsorption capacity of MOFs for vapor molecules [55,56].

2.2.2. Functionality and expansion of structures

Apart from metal sites, the combination of functional groups with ligands is also an alternative to improve the hydrophobicity/ hydrophilicity of MOF chemicals, tune the shape of isotherms or move their trigger points (P/P_0). Commonly used hydrophilic functional groups, such as $-NO_2$ (nitro), $-NH_2$ (amino), $-OH$ (hydroxyl), etc., have been reported for the synthesis of MOFs [57–62]. In comparison with the original MOFs without functionalities, the functionalized MOFs

Table 1
Reported real applications of MOFs in water adsorption.

Materials	Surface area (m^2 g^{-1})	Pore Volume (cm^3 g^{-1})	Pore diameter (nm)	Uptake (g g^{-1})	P/P_0 of the steep adsorption	Possible regeneration condition	Refs.
CAU-10(Al)	635	0.43	0.7	0.36	0.15–0.25	70°C	[32, 38]
MIL-53-FA (Al)	1080	0.49	0.6	0.53	0.2–0.35	90°C	[52, 71]
MIL-100 (Fe)	1917	1.0	2.5/2.9	0.77	0.25–0.45	<70°C	[27, 72]
MOF-801(Zr)	990	0.45	0.48/0.56/0.77	0.36	0.05–0.15	80–85°C	[37, 73]
MOF-303(Al)	–	0.54	0.6	0.48	0.1–0.25	85°C	[22, 74]

Table 2
Promising MOFs in water adsorption applications.

Materials	Surface area (m^2 g^{-1})	Pore Volume (cm^3 g^{-1})	Pore diameter (nm)	Uptake (g g^{-1})	P/P_0 of the steep adsorption	Possible regeneration condition	Refs.
BIT-66(V)	1417	0.87	0.65/2.58	0.71	0.6	–	[75]
BUT-46A(Zr)	1550	0.69	1.6–3.5	0.52	0.44–0.49	–	[76]
BUT-46B(Zr)	1430	0.65	1.6–3.5	0.49	0.51–0.55	–	[76]
BUT-46F(Zr)	1563	0.71	1.6–3.5	0.59	0.39–0.43	–	[76]
BUT-46W(Zr)	1565	0.71	1.6–3.5	0.63	0.27–0.37	–	[76]
CAU-1(Al)	1300	0.55	0.5/1.0	0.55	0.38	–	[77]
CAU-23(Al)	1250	0.48	–	0.37	0.3	60°C	[20]
CUK-1(Co)	510	0.26	–	0.28	0.12	–	[30]
CUK-1(Mg)	580	0.28	–	0.36	0.23–0.28	–	[30]
CUK-1(Ni)	520	0.26	–	0.3	0.12	–	[30]
Cr-soc-MOF-1	4549	2.1	–	1.95	0.58–0.72	25°C, RH<45%	[42]
DUT-67(Hf)	810	0.33	–	0.29	0.25–0.45	–	[49]
DUT-67(Zr)	1064	0.44	–	0.41	0.25–0.45	–	[49]
DUT-68(Hf)	749	0.34	–	0.29	0.38–0.42	–	[49]
DUT-68(Zr)	891	0.41	0.8/1.3/1.4/2.8	0.34	0.38–0.42	–	[49]
DUT-69(Hf)	450	0.22	–	0.2	–	–	[49]
DUT-69(Zr)	560	0.31	–	0.26	–	–	[49]
MIL-100(Al)	1814	1.14	2.5/2.9	0.5	0.25–0.45	–	[27]
MIL-100 (Cr)	1517	–	2.5/2.9	0.8	0.25–0.42	–	[40]
MIL-101(Cr)	5900	2.0	2.9/3.4	–	–	–	[41]
	4150	–	–	>1.5	0.4–0.5	70°C	[78]
+NO$_2$(Cr)	2146	1.19	<2.9/3.4	1.08	0.41–0.52	–	[57]
+NH$_2$(Cr)	2509	1.27	<2.9/3.4	0.9	0.37–0.44	–	[57]
+SO$_3$H(Cr)	1920	0.94	<2.9/3.4	0.62	0.28–0.36	–	[57]
MAF-7(Zn)	1870	0.67	–	0.43	0.26–0.3	–	[79]
MIL-160(Al)	1070	0.398	–	0.37	0.05–0.16	90°C	[25]
MIL-125-NH$_2$(Ti)	1509	0.66	–	0.68	0.2	–	[48, 80]
MIP-200(Zr)	1000	0.4	–	0.46	0.17	65–70°C	[46]
MOF-74(Mg)	1250	0.53	1.11	0.75	0–0.05	–	[37]
MOF-808	2360	0.84	1.84	0.6	0.28–0.32	–	[37]
MOF-841(Zr)	1390	0.53	0.92	0.5	0.26	80°C	[37, 81]
Co$_2$Cl$_2$(BTDD)	1912	–	2.2	0.97	0.28	55°C	[39]
Ni$_2$Cl$_2$(BTDD)	1752	–	2.2	0.77	0.3–0.32	–	[39]
Ni-BPP	2039	0.88	1.7	0.72	0.08–0.32	–	[33]
Ni-TPP	1975	1.14	2.3	0.84	0.26–0.64	–	[33]
Ni-IRMOF74-III	–	–	–	0.35	0–0.05	<65°C,	[82]
NU-1500(Cr)	3580	1.28	1.4	1.09	0.45–0.49	25°C, RH<20%	[83]
PIZOF-2(Zr)	1250	0.68	2.0	0.68	0.7–0.74	–	[37, 84]
SIM-1(Zn)	570	0.3	0.65	0.14	–	–	[51]
UiO-66(Zr)	1290	0.49	0.74/ 0.84	0.44	0.3–0.35	–	[37]
+NH$_2$(Zr)	1328	0.7	0.75/ 1.2	0.38	0–0.3	–	[80]
Y-shp-MOF-5	1550	0.63	1.2	0.45	0.55–0.72	25°C, RH<45%	[21]
ZJNU-30(Zr)	3116	1.24	0.7/1.4/2.1	1.2	0.21	<60°C	[81]

demonstrate strong tunability in isotherms, however, at the expense of surface area or pore volume. On the other hand, the exploitation of MOF-based composite materials has also gained interest. In order to facilitate the heat and mass transfer of desiccants, MOFs have also been combined with inorganic salts or carbon substrates to improve the adsorption performance. For instance, CaCl$_2$@UiO-66 and MIL-101(Cr) @graphene oxide have been reported to possess high water capacity

[63–67].

In addition, a few research studies have expanded the MOF structures based on the same topology, which indicates that it is possible to develop identically topological and uniquely functional MOFs. An example of such cases is HKUST-1 [Cu$_3$(BTC)$_2$], which results from the bridging of copper metal ions (Cu^{2+}) with tritopic ligand (BTC^{3-}). Identically topological structures were constructed through ligand

expansion from BTC to TATB, and further to BBC. The BBC analog has been reported to possess 17.4 times volume as compared to the original HKUST-1 [68]. Accordingly, the developed extension exhibits the potential to provide more adsorption sites for achieving diverse functionalities.

2.2.3. Porosity, surface area and pore apertures

From the perspective of topology, MOFs consist of the units of nodes (metal ions) and rods (ligands), and the rods generally encompass a number of void spaces therefore making MOFs porous materials. To date, the flexibility of the selection of both metal ion sources and organic ligands has resulted in various internal structures, leading to a wide range of surface area (from hundreds to thousands m^2/g) and porosity up to 90% [69], with pore size in micropore range (~nm) or even smaller [70]. Furthermore, according to the synthesis methods reported in literature, the reaction conditions have a direct correlation with the intrinsic structure through the control on the residence time, feed mass, reaction temperature, etc., thus, allowing flexibility during synthesis.

3. Mechanisms and selection criteria of MOFs for applications in the built environment

Considering the operational performance of traditional desiccants, solid desiccant technology suffers from the bulky systems and low efficiency, thus, leading to limited applications [11]. Some efforts have also been made to mix the inorganic salt with desiccants (i.e. silica gel) to improve the working capacity. However, the regeneration condition is closely related to the nature of the desiccants, not to ignore the corrosion hazard of the inorganic salts on the metal framework. It is expected that the novel desiccants could well overcome these drawbacks. In the following section, the detailed information about the promising MOF-based desiccants has been presented. The adsorption mechanisms are also noted to disclose the moisture transfer within the MOF desiccants (Section 3.1). Based on their properties, the selection criteria of available MOFs have been discussed to further elucidate the advantages of MOF desiccants in practice (Section 3.2).

3.1. Water adsorption mechanisms in MOFs

Owing to the remarkable features of MOFs, the water adsorption mechanism has drawn significant research attention, which can be divided into three subgroups: I) chemisorption in metallic clusters, II) reversible physisorption in layers or cluster adsorption, and III) irreversible capillary condensation.

Chemisorption in metallic clusters: Due to the accumulation of charges, the unsaturated metal sites in MOFs evolve into strong adsorption nodes [85]. These strong adsorption nodes can form initial adsorption sites, followed closely by the weaker nodes. However, to regenerate MOFs to their full adsorption capacity, extensive extent of thermal energy is needed, which is undesirable for sorption-based applications. Besides, some studies have reported that the repeated adsorption/desorption of vapor molecules on these sites may lead to gradual degradation [56,86].

Physisorption in layers or cluster adsorption: Surface water molecules initially gather at the hydrophilic surface sites (i.e. hydroxyl), followed by the adsorbed water molecules acting as nucleation sites to grow into large water clusters (nucleation growth process). As these clusters connect with each other through the surface or pores (pore filling process), the continuous moisture transfer is observed to occur [87]. This mechanism is similar to other conventional materials like activated carbon, and observed in some MOFs as well.

Capillary condensation: As some porous materials have a hysteretic capillary condensation phenomenon, the definition of critical diameter indicates that the capillary condensation in desiccants with certain pore size is generally accompanied by a hysteresis loop in the isotherms [51]. In contrast to pore filling, it should be noted that the

capillary condensation is an irreversible process. As for MOFs with pore size <2 nm, the presence of hysteresis is generally assigned to the deformation of inner frameworks [88].

3.2. Selection criteria for MOF desiccants

MOFs with special intrinsic properties and adsorption mechanisms have been identified in the previous sections. Here, the selection criteria were discussed in detail to further elucidate the assessment of MOFs. To do so, some criteria related to material properties have been presented, namely stability, performance and safety. Other factor such as scalability belongs to the manufacturing technologies depend on the improvement of industrial level.

3.2.1. Stability

In many cases, the employment of MOF materials is held back due to the weak long-term stability. In built environment, the MOF material may quickly break down after moisture exposure, thus, it is preferable to identify the promising candidates based on the stability studies reported in literature. Previously, the stability of MOFs upon exposure to water in vapor and liquid phase has been reviewed in Refs. [14], based on which the relationship between the structure and stability has also been discussed with respect to metal-ligand bonds and degradation mechanisms (including ligand displacement and hydrolysis) [29,89–96]. Moreover, a comprehensive review of heat pumps using MOF desiccants is also available [16]. Burtch et al. have expediently identified MOF water stability in the thermodynamic and kinetic regimes, as shown in Fig. 1 [17]. However, the balance between thermodynamic and kinetic control over MOF water stability remains under debate [97].

Thermodynamic stability relates the free energy in a hydrolysis reaction to the structural properties of MOFs. In other words, the inert degree of the metal cluster directs the coordination with water, followed by the destruction of the crystal structure. It is believed that a thermodynamically stable MOF can maintain the framework avoiding breakdown after a long-time exposure to moisture, and it is concluded to contribute to the strength of metal-ligand bond [89,95,98] and the lability with water [92,99]. Under a built environment, the thermal stability of MOF materials during moisture transfer still requires further exploitation.

Kinetic stability is dependent on the activation energy barrier related to the specific reaction. Even if a structure may not be thermodynamically stable, high activation energy can still restrict the hydrolysis reaction and keep the structure stable in the presence of water. Here, the kinetic stability represents the material resistance to water in the vapor phase [100]. In addition, some MOFs have been reported to effectively perform in humid air without any degradation, though breakdown is observed after exposure to liquid water [101]. These MOFs still exhibit strong potential of use in humid air [38,78,102].

3.2.2. Performance

With respect to the assessment of a practical system, it is inevitable to mention the water capacity, regeneration condition and sorption dynamics of the desiccant employed. Some research studies have indicated that a regeneration temperature less than 80°C can lead to significant improvement in the system performance [20]. High water capacity and dynamic sorption instead can reduce the time spent in the periodic cycles or system volume. Consequently, it is desirable to select MOFs with high water capacity and dynamic sorption, along with gentle regeneration condition.

Isotherm is a vital tool for characterizing the water capacity and affinity to water vapor for the desiccant materials [51]. It is known that the water capacity and affinity to water vapor can affect the adsorption and desorption process. High affinity between the water vapor and desiccants indicates the difficulty for the adsorbed water molecules to break away from the formed chemical bonds, thus, signifying a strict regeneration condition. In Fig. 2, IUPAC (International Union of Pure
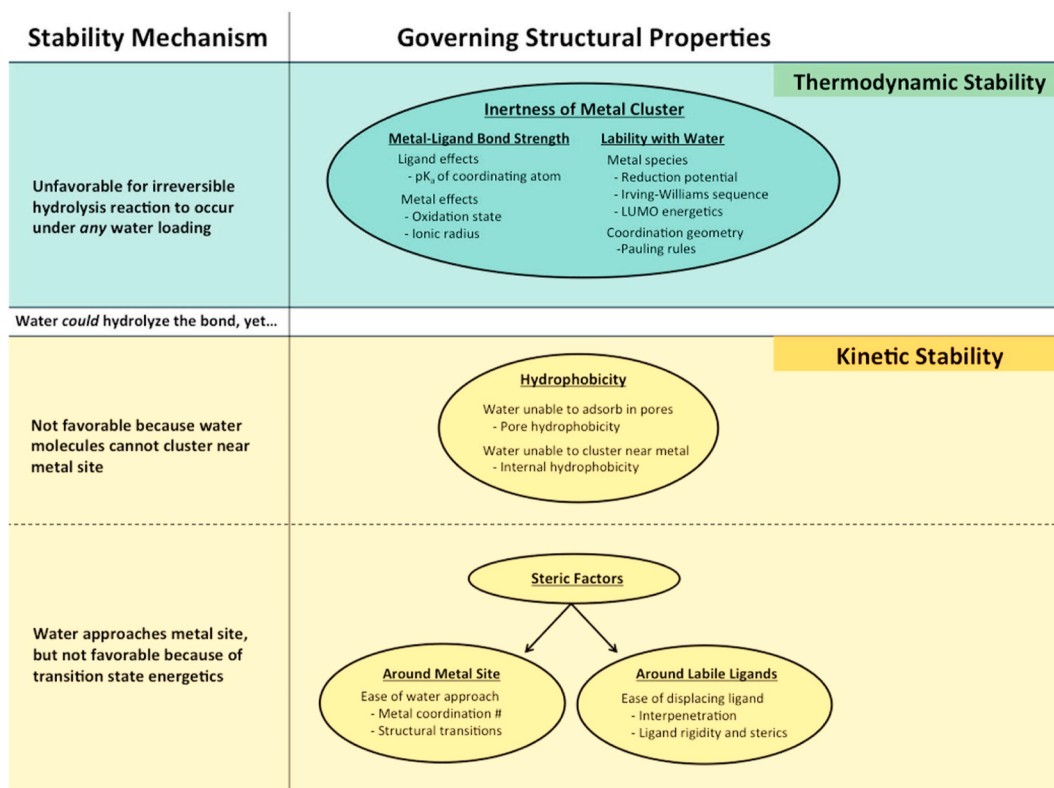
Stability Mechanism | Governing Structural Properties

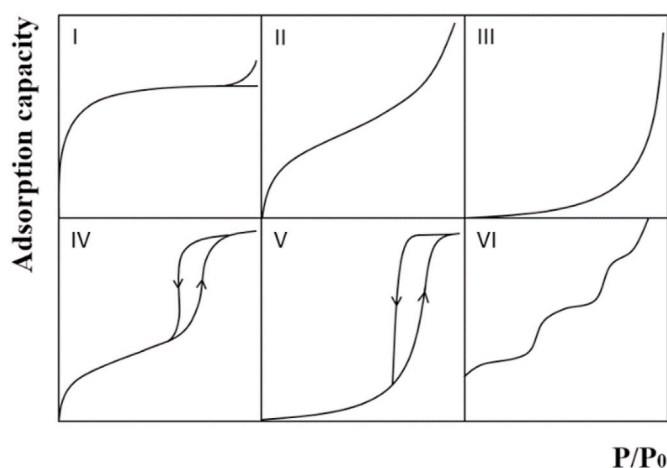**Fig. 1.** Structural factors affecting MOF water stability [17].

Fig. 2. Classification of isotherms based on IUPAC (International Union of Pure and Applied Chemistry) [103].

and Applied Chemistry) has classified isotherms for thermodynamic analysis [103]. However, only desiccants (e.g. MOFs) with type V isotherm (sigmoidal or S-shaped curve, which enables a sharp change within a narrow P/P_0) are the optimal candidates for sorption-based systems [11]. A sharp increase in adsorption capacity at low RH is the characteristic of highly hydrophilic desiccants, as presented in Type I, II, IV and step-like Type VI isotherms. These desiccants (e.g. zeolite (I) and silica gel (II)) generally require more energy to drive the regeneration process. Type III isotherm belongs to the hydrophobic group, which is not suitable for the system operation due to the higher trigger point (P/P_0). Thus, the selection criteria should at least meet $>0.2g_{H2O}$ g-1 water capacity and $<90°C$ regeneration condition.

With respect to dynamic sorption that indicates the adsorption and

desorption equilibrium in cycles, Thomas et al. initially investigated the adsorption performance of traditional desiccants [104]. Afterwards, many research studies have reported experimental analysis on activated carbon and silica gel [105,106]. Recently, the dynamic nature of the MOF materials has been evaluated by means of in-situ EDXRD [58], thermogravimetric analysis [107], etc. Solovyeva et al. have reported the high potential of MOF-801 in adsorption cooling through water adsorption dynamics [73]. In this regard, the dynamic nature of MOFs correlated to material properties of heat and mass transfer can help to anticipate the future applications [64,72,108,109].

3.2.3. Scalability

The translation of novel materials into practical technologies faces the challenge to produce MOFs at the required scale and quality. For the built environment, an open SDS generally requires MOFs at the kilogram or ton scale to regulate the latent load, which is quite different from the gram-scale production of MOFs in laboratory. Recently, factors affecting the scale-up methods have been comprehensively reviewed, and two aspects can be concluded [110]: synthesis process and raw materials. Normally, a complete synthesis process includes synthesis and post-synthesis. The development in the chemical synthesis methods of MOFs have been discussed for the past 20 years (See Fig. S1, Supporting Information). It is desirable that the emerging methods are capable to significantly reduce the time spent in the chemical reactions [111]. After synthesis, careful processing is required in order to qualify the materials,
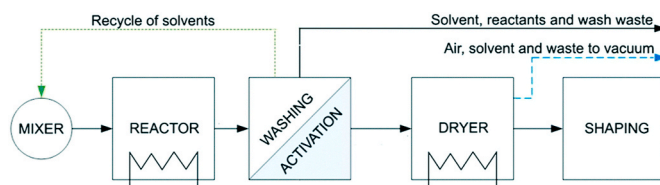

Fig. 3. Basic processes for MOF production [110].

as shown in Fig. 3. Here, processes such as washing and activation lead to the extension of the cycle time. Thus, meaningful studies on shorting the post-synthesis processes are needed. On the other hand, raw materials correspond to the possibility of large-scale preparation of MOFs. It is encouraged to use cost-effective and environmentally friendly raw materials to obtain the functional MOF materials. To date, large-scale production of some MOF materials has been reported [6,16,44,112, 113].

3.2.4. Safety

Toxicity of MOFs is one of the most important concerns, as these materials may be harmful to human health on direct contact. The selection of green materials should be of high priority for specific applications. Thus, among the raw materials for MOF synthesis, the use of environmentally unfriendly ingredients should be reduced or avoided. Green transition metals such as Al, Fe, Zr and Cu have been widely recognized as alternatives to Cr-based MOFs due to the low toxicity and cost [35,114–116]. Green solvents are also employed during MOF synthesis. Some of the accepted green solvents such as water, ethanol, ethyl acetate, etc., are highly recommended, and less green solvents including formic acid, dimethyl sulfoxide, dimethyl formamide, etc., should be used in moderation [32,35]. In short, natural or biomass-based products are good candidates to generate ideal MOFs using low-toxicity metal clusters. Besides, it is noteworthy that other safety hazards such as inflammability and bacteriostatic activity all have certain effects on the quality of the built environment.

4. Material-level water vapor capture of MOFs

As many MOFs have desired water uptake and regeneration condition, care is necessary to screen the MOFs suitable for the specific use under specified conditions. Many literature studies have reported the MOF materials for water harvesting in water scarcity regions and heat transformation in heat pumps [23,27,32,81,117]. As an open SDS employed for humidity regulation of the built environment, it is noteworthy that different MOFs may correspond to different trigger points, corresponding to different climate conditions. Based on the classification of the trigger point, MOFs with the following features are focused in this section (*material level*): 1) high water uptake (more than $0.2 \, g \, g^{-1}$) and stability, 2) gentle regeneration condition, and 3) steep rise in water uptake.

4.1. Low range (<30% RH)

Desiccants with high water uptake at the low relative pressure have strong affinity towards water molecules, generally requiring strict regeneration conditions. In comparison with the traditional desiccants such as silica gel, zeolites, etc., many MOF materials with low trigger point can still have a low regeneration temperature and high water uptake. With these properties, active SDS can significantly improve the system performance, while passive SDS can maintain the low RH level, which is a requirement in some special installations. The humidity control can effectively avoid, for example, ageing of the batteries in battery factories and deterioration of artefacts in museums [118]. Thus, the search for MOFs with low trigger point P/P_0 in isotherms deserves more intensive efforts.

CAU-10 (CAU: Christian Albrechts University) is a kind of porous aluminum isophthalate, which combines aluminum clusters with BDC (1,3-benzene dicarboxylic acid) ligand. As a commercially available MOF, the synthesis method has been greatly improved by substituting toxic DMF-water solvent (dimethylformamide) with green options [32]. In the framework of CAU-10, corner-sharing AlO_6 polyhedra are connected with each other, forming a helical arrangement and square channels with up to 0.7 nm pore diameter [19,38]. Fröhlich et al. [119] were the first to investigate the hydrothermal stability through 700 adsorption-desorption cycles with no observed irreversible degradation,

as shown in Fig. 4 (a). A $0.34 \, g \, g^{-1}$ of water uptake at thermodynamic equilibrium has been observed, accompanied by 0.18 P/P_0 trigger point in the isotherm. CAU-10 coated adsorption chillers [32] have been subsequently prepared, which indicates that a regeneration temperature of 70°C can generate a specific cooling power over 1200W kg_{ads}^{-1}. Additionally, several functional groups in the ligands have also been investigated, such as CAU-10(-OH, -OCH$_3$, -NO$_2$). Reference [38] presents different shapes of isotherms with even less water uptake at adsorption equilibrium, as shown in Fig. 4 (b), probably resulting from the change in pore volume and heterogeneous character.

CAU-23 is a new class of Al-based MOF with TDC (thiophene-2, 5-dicarboxylic acid) as its ligand. A recent study has indicated that CAU-23 can be synthesized using a green and scalable method by using water as the only solvent, and it is stable in air up to 400°C, thus, exhibiting high thermal stability [20]. In the three-dimensional structure of CAU-23, the metal cluster unit comprises of the combination of helix and straight AlO_6 polyhedra, joined with TDC to form square channels. CAU-23 has been tested for 5000 cycles with nearly no loss in water uptake as shown in Fig. 5 (a). Water isotherm indicates that a maximum water uptake of $0.43 \, g \, g^{-1}$ can be obtained without hysteresis loop at room temperature. Correspondingly, the trigger point is noted to be around 0.24 $P/P0$. Besides, the findings from the desorption analysis have pointed out an ultralow regeneration temperature of <60°C for the adsorption-driven chillers, along with a cycling water capacity of $0.37 \, g \, g^{-1}$ [20]. As the temperature increases, the trigger point of the isotherms in Fig. 5 (b) is observed to move right to a larger P/P_0 with lower water capacity. Other analogs of CAU-23 such as CAU-22 [120], CAU-28 [121] and CAU-39 [122] are more or less limited by the low hydrothermal stability or low uptake capacity.

MIL-53 (Al, Fe, Cr) [MIL: Material Institut Lavoisier] is one of the most frequently investigated MOF series. Among the various analogs, MIL-53 (Al) is currently produced at industrial levels and features corner-sharing AlO_6 chains connected by terephthalate ligands in the crystal structure. To date, MIL-53(Al) has been prepared at large scale by sole use of water as solvent, however, the recorded water capacity is far less than $0.2 \, g \, g^{-1}$ [123]. Subsequently, Alvarez et al. have investigated a new MOF [114], MIL-53-FA (or aluminum fumarate), which has an isoreticular structure to MIL-53(Al). Although these have similar cornering-sharing aluminum-based octahedra, MIL-53-FA uses fumarate as its ligands. As a commercially available product with green synthesis, MIL-53-FA has been widely applied for gas storage and water vapor capture [71]. Henninger et al. [18,52] also reported the highly stable nature of the hydrophilic MIL-53-FA. As shown in Fig. 6, the cycling adsorption capacity is observed to be constant at around $0.37 \, g \, g^{-1}$ after 4500 cycles. The isotherm shows a steep rise in water uptake between 0.2 and 0.35 P/P_0. Regeneration at 90°C achieved the release of more than half of the adsorbed water molecules within several minutes, which is superior to the zeolites (>100°C).

Serre et al. reported hydrophilic MOF (MIL-160), a promising material for heat reallocation, which consisted of aluminum ions and FDCA (2, 5-furandicarboxylic acid, derived from renewable biomass feedstock) ligand [25]. As an isostructure to CAU-10, hydrothermally stable MIL-160 has helically cis-connected chains with four surrounding carboxylates forming square-shaped channels as shown in Fig. 7. The subsequent studies indicated that MIL-160 with 0.5 nm pore size outperforms CAU-10 in surface area and pore volume [25]. Though the water uptake of MIL-160 is almost identical to CAU-10, its 0.05 P/P_0 trigger point exhibits better hydrophilicity than 0.16 P/P_0 for CAU-10 due to the presence of many hydroxyl groups at the pore surface. The measured water uptake is around $0.37 \, g \, g^{-1}$, and most of the water adsorption is below 0.18 P/P_0. The high water affinity enables a heat source around 363K (90°C) to achieve the release of 75% of the water molecules (regeneration). Lately, the authors have also investigated the energy-storage capacity and cycling loading lift of MIL-160, which are noted to be 6 times as compared to zeolite 13X [124]. Based on these features, MIL-160 is a promising desiccant for adsorption heat
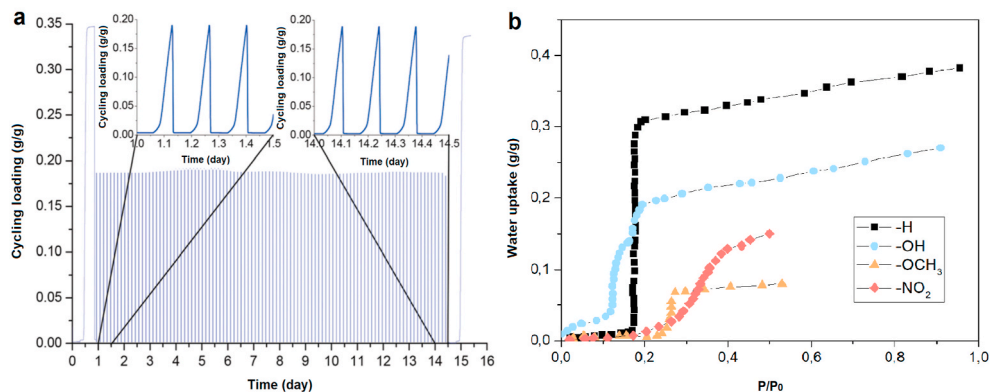
Fig. 4. (a) Cycling performance of CAU-10 [119] and (b) water adsorption isotherms with different functional groups (25°C) [38].
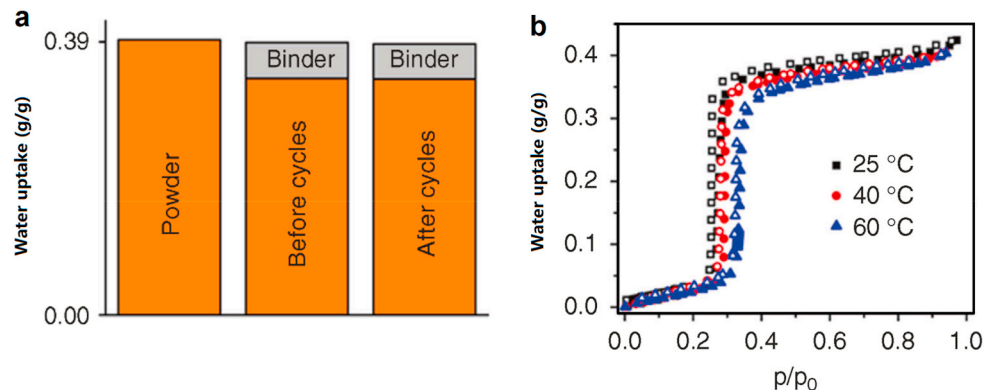

Fig. 5. (a) Water uptake of CAU-23 coatings before and after 5000 cycles and (b) water adsorption/desorption isotherms of CAU-23 at different temperatures [20].
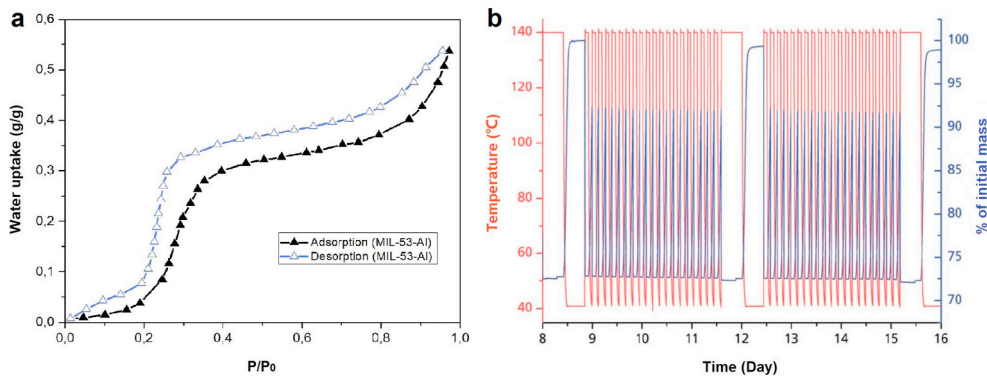

Fig. 6. Water adsorption/desorption isotherms of MIL-53-FA at 25 °C [48] and cycling tests [52].

transformation (i.e. heat pump) [125] and even in places requiring an ultralow relative humidity with gentle regeneration condition.

MIL-125-NH$_2$ is a Ti-based MOF comprised of titanium clusters and BDC-NH$_2$ (2-amino benzene dicarboxylic acid) with two types of cages (0.51 nm and 1.25 nm). Since Dan-Hardi et al. [126] reported the synthesis of highly porous MIL-125, the ligand functionalization has been applied to generate MIL-125-NH$_2$ [127,128]. MIL-125-NH$_2$ has a three-dimensional bipyramidal structure with Ti$_8$O$_8$(OH)$_4$ as metal node connected with eight BDC-NH$_2$ ligands. It is reasonable to expect a reduction in pore size and surface area owing to the introduction of the amino group, but isotherms exhibit an obvious increase in the water uptake for MIL-125-NH$_2$ compared to unusual adsorption and desorption behavior of MIL-125. This indicates that MIL-125-NH$_2$ is more

hydrothermally stable in presence of water [129]. A recorded 0.67 g g^{-1} water uptake with 0.2 P/P$_0$ trigger point in Fig. 8 confirm the competence of MIL-125-NH$_2$ for hygrothermal control at low RH range. Kim et al. have investigated its potential use in the adsorption heat transformation, and regeneration at 80°C with a constant cycling water capacity of 0.45 g g^{-1} at working conditions confirm its superiority as compared to most of the currently used desiccants [48].

In recent years, MOF-801 has attracted research attraction for use in applications requiring low RH range, such as water harvesting in deserts. Behrens et al. [36] first reported the preparation of MOF-801 by combining a zirconium cluster (Zr^{4+}) with fumaric acid. The structure of MOF-801 is composed of cubic spaces with three independent cavities, two tetrahedral cavities of size 0.56 nm and 0.48 nm, and one octahedral
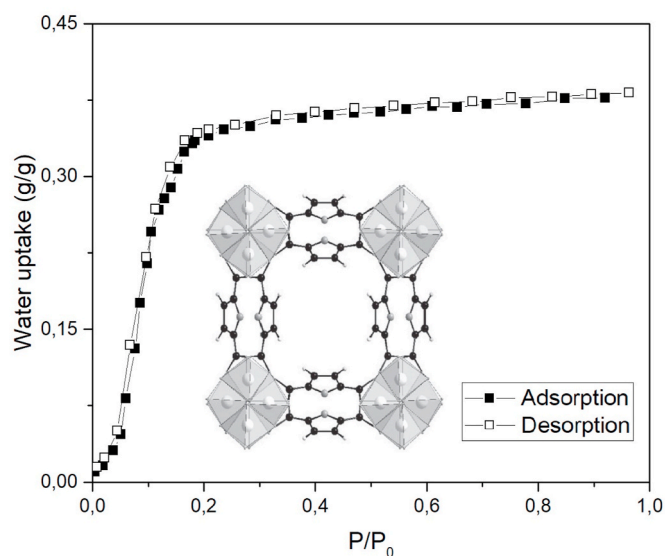
Fig. 7. Water adsorption/desorption isotherms for MIL-160 [25].

cavity with a diameter of 0.74 nm. MOF-801 has been demonstrated to be stable in hygrothermal conditions, and its cycling water uptake remains stable after five adsorption-desorption cycles [37]. The adsorption isotherm in Fig. 10 displays a steep rise around trigger point (P/P_0) of 0.05 and reaches a saturated state around 0.5, from which a water uptake capacity of 0.36 g g^{-1} at room temperature can be observed, greatly outperforming the traditional desiccants (i.e. silica gel). Subsequently, Yaghi et al. have prepared MOF-841 and other analogs such as MOF-802, MOF-805, MOF-806 and MOF-808, however, the latter ones demonstrate unstable water adsorption during initial cycles owing to the loss of porosity [37]. MOF-841 is prepared by employing MTB (4,4',4'', 4''-methanetetrayltetrabenzoic acid) as connecting ligand. In the three-dimensional framework of MOF-841, the metal cluster bound with eight ligands constructs the basic structural unit. Cycling performance indicated that MOF-841 exhibits relatively constant adsorption after several cycles. Its steep rise in Fig. 9 occurs around 0.26 P/P_0, and it reaches saturation around 0.3 P/P_0, at which the water uptake accounts for nearly 90% of total water uptake (0.5 g g^{-1}). Recently, Yaghi et al. [23,117] applied MOF-801 for water harvesting from air. The experiments were conducted with a regeneration temperature of 65°C, and the set-up was predicted to produce a 2.8L_{water} kg_{MOF}^{-1} each day at 0.2 P/P_0. Based on this study, the authors also developed a next-generation desiccant MOF-303, synthesized by using aluminum-based metal cluster and HPDC [1H-pyrazole-3,5-dicarboxylate] [22]. The green hydrophilic MOF featured pore volume and pore size of 0.54 cm^3 g^{-1} and 0.6

nm, with up to 0.48 g g^{-1} of water capacity. The trigger point is noted to be around 0.15P/P_0, which is comparable to its predecessor MOF-801. In addition, 150 cycling experiments verified the hydrolytic stability of the material owing to no measurable mass loss. Fig. 10 shows the evolution and cycling performance of the crystal structure from MOF-801 to MOF-303. MOF-303 with higher cycling water lift is theoretically superior to MOF-801 for humidity regulation.

MIP-200 is a newly developed MOF material constructed using the zirconium cluster and H_4mdip ligand (3, 3', 5, 5'-tetracarboxydiphenylmethane). In the three-dimensional structure, Zr-based metal cluster is connected with eight carboxylate groups and four formate groups, thus, forming a triangular tunnel of 0.68 nm and a hexagonal channel of 1.3 nm. A surface area of 1000 m^2 g^{-1} as well as a pore volume of 0.4 cm^3 g^{-1} were measured as well. Serre et al. [46] explored the application of MIP-200 in adsorption-based chillers. From isotherm in Fig. 11, MIP-200 is noted to exhibit high water capacity of around 0.46 g g^{-1}, however, a two steep rise occurred at 0.01P/P_0 and 0.17 P/P_0, respectively. It is also found that the material is stable against different chemicals and temperatures over 300°C. One intriguing property is the facile regeneration temperature below 70°C, which outperforms most of currently reported desiccants, such as MIL-160 (90°C), SAPO-34(~90°C), aluminum fumarate (90°C), etc. [20]. Other family members such as MIP-202, MIP-203 and MIP-204 have also been synthesized. However, the ultra-small porosity limits their application [130].

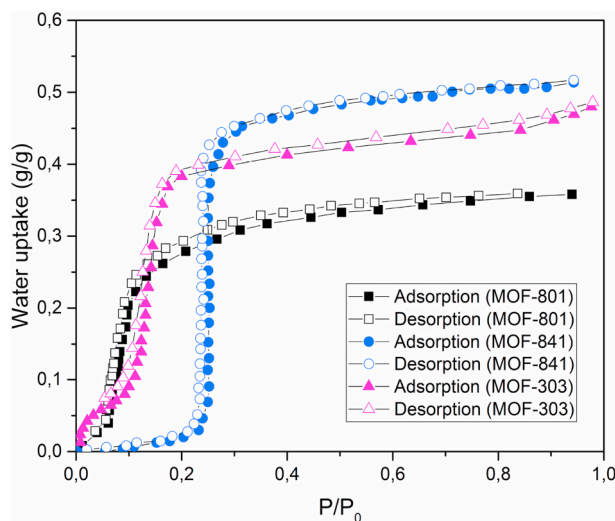The MOFs described so far represent both widely used desiccants as

Fig. 9. Water adsorption/desorption isotherms of different MOFs used for water harvesting [22,37].
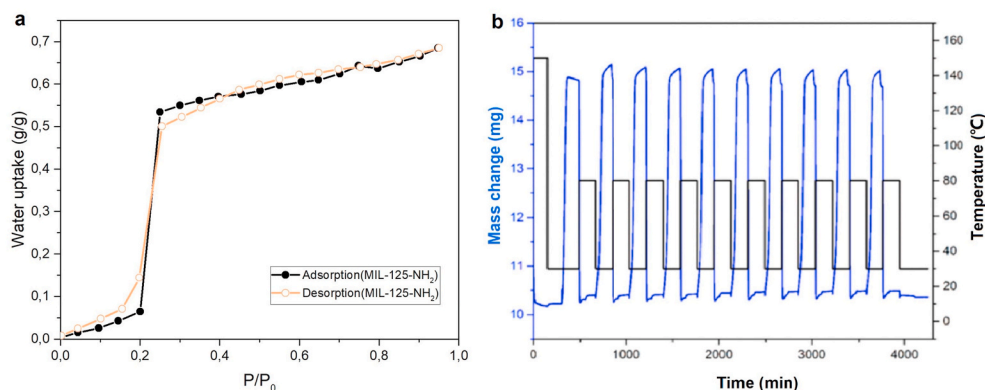

Fig. 8. (a) Water adsorption/desorption isotherms for MIL-125-NH$_2$ and (b) dynamic water uptake with adsorption at 30 °C and desorption at 80 °C [48].
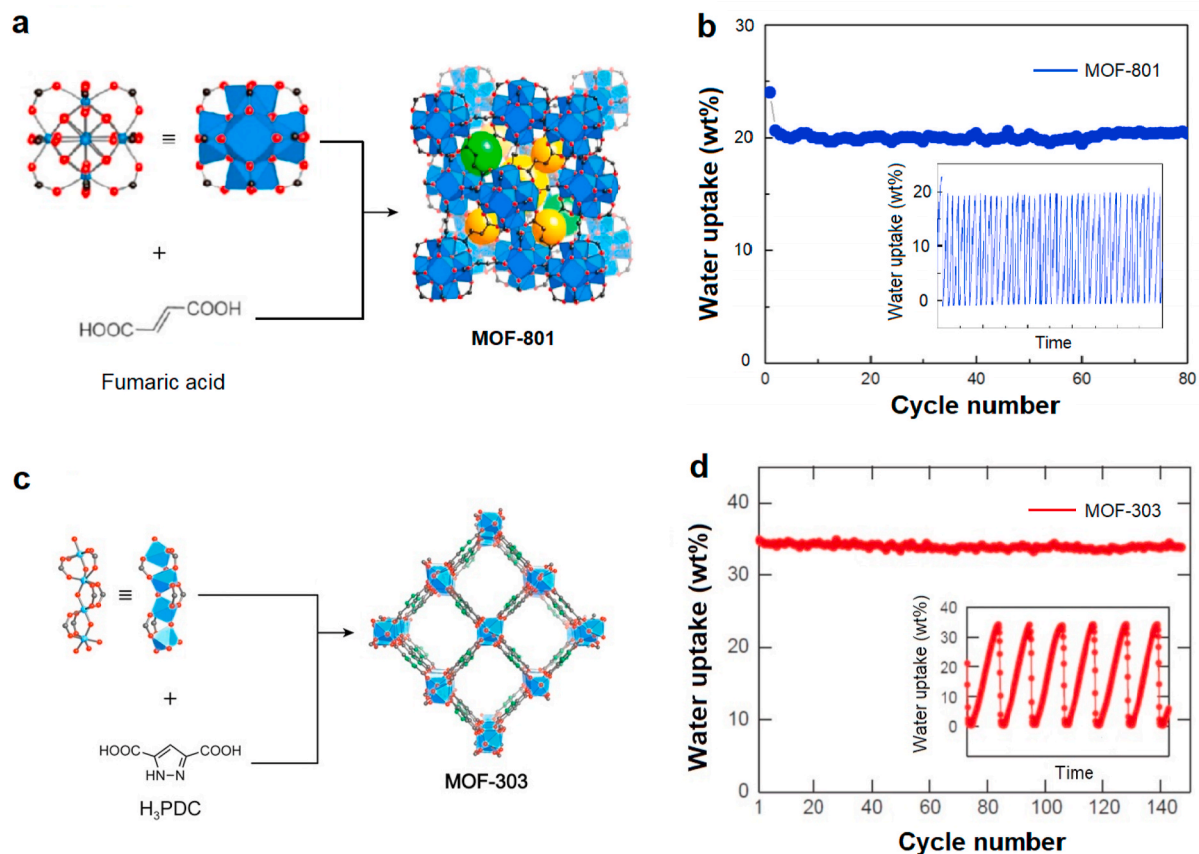
Fig. 10. Crystal structure (a and c) and cycling performance (b and d) of MOF-801 and MOF-303 [22,37].
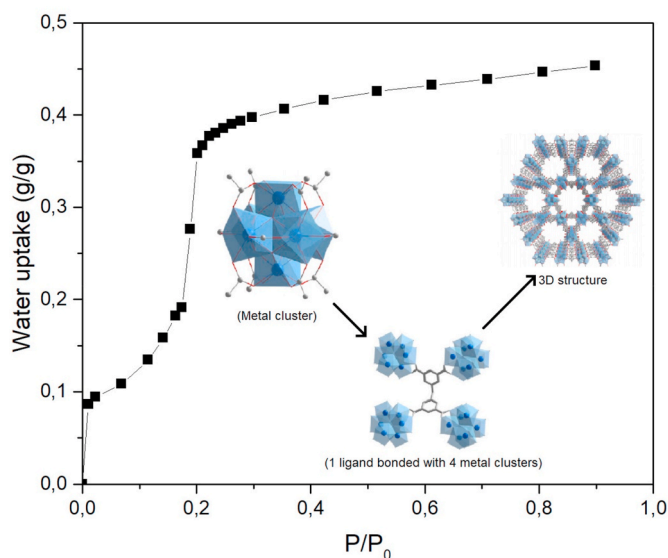

Fig. 11. Water sorption isotherms of MIP-200 at 25 °C [20,46].

well as newly developed desiccants. These desiccants feature low trigger point (0-30%), exhibiting great potential of application for the control in built environment. In addition, other promising desiccants such as $M_2Cl_2(BTDD)$ (M = Co, Ni) [26,39], mixed-metal MOF [10], ZJNU-30 [81], CUK-1 [30], etc., demonstrate strong capability for humidity control. The exploitation of these MOFs is still an ongoing research.

4.2. Medium range (30–65% RH)

In the past few years, a few MOFs have been reported with a medium trigger point. Though these MOFs may have weak affinity towards water molecules, the water capacity and regeneration condition are still significant. Hydrophilic MOFs might be preferred for the active systems due to high working efficiency. However, a few studies carried out by using these neutral MOFs have also indicated that these desiccants are well capable of sorption-based heat transformation [27]. One the other hand, as ASHRAE has recommended the comfort zone of relative humidity, >65%RH and <30%RH to a degree make human beings to feel uncomfortable. Materials that can adsorb water vapor at higher humidity levels and desorb it at lower humidity levels can well meet the demand for humidity control in a passive way. Traditional materials have limited performance in both active and passive SDS. Many research studies have focused on exploring neutral desiccants and most of these deserve further study.

CAU-1 was first synthesized by the combination of H_2N–H_2bdc (aminoterephthalic acid) and $Al_8(OH)_4(OCH_3)_8$ (aluminum-based octameric cluster) by Stock et al. [131]. The AlO_6-based octameric clusters are connected to other units to form two types of cages, an octahedral cage of 1 nm and a tetrahedral cage of 0.5 nm. The remarkable water uptake at 25°C is recorded around 0.55 g g^{-1} [77,132], and the TGA data exhibit that the material can keep stable under hygrothermal conditions and preserve its framework up to 310°C [131]. Subsequently, a new Al-based MOF named CAU-3 has been synthesized, which exhibits water uptake of up to 0.51 g g^{-1}. However, the thermal stability tests indicate that the decomposition of framework may occur in air under 200°C [133]. Reinsch et al. have reported the green synthesis of CAU-15-Cit [134]. CAU-15-Cit exhibited a 23.8% water uptake at the trigger point of $0.5P/P_0$, and the powder X-ray diffraction (PXRD) disclosed the reversible de- and rehydration behaviors, which greatly

outperform the unstable form CAU-15 [135].

As a member of DUT series (DUT, Dresden University of Technology), DUT-68 has been synthesized by using TDC (2, 5-thiophenedicarboxylate) as ligand with different metal clusters (Z-based and hf-based). Senkovska et al. [136] reported the structure of DUT-68 to contain a complicated pore system with four types of pore size (0.8 nm, 1.25 nm, 1.39 nm and 2.77 nm). From water adsorption studies, it is observed that a steep rise in water uptake takes place at $0.38P/P_0$ exhibiting a value of 0.29 g g^{-1}, along with structural stability verified by using repeated water adsorption tests. Besides, it is noted to adsorb nearly 40% of total water uptake at <30% RH, which may result from the complex hierarchical pore system. Recently, an insight into water adsorption by DUT-67 has been proposed for exploring its potential in adsorption-based heat transformation. Bon et al. [49] conducted more than 20 adsorption-desorption cycles to prove its stability and investigated the pore filling process through neutron powder diffraction. In comparison with the other Zr-based DUT-68, Fig. 12 indicates that DUT-67 has a water capacity of 0.44 g g^{-1} at 0.6 of P/P_0 with a steep rise in relative pressure range 0.3–0.4. In this respect, DUT-67 is confirmed to be potential desiccant for water adsorption [31]. Other DUT series such as DUT-52, DUT-53 and DUT-69 have been prepared. Though a few of these may have S-shaped adsorption isotherms, the shape of desorption branch is significantly different from Type-V isotherms, thus, these are not suitable for humidity control [49,136].

MIL-100 is one of the most studied MOF benchmarks for water adsorption applications. To date, three metal elements such as Fe, Al and Cr have been mostly used with BTC (1,3,5-benzene tricarboxylic acid) as ligand to prepare MIL-100 series. Since Férey et al. [137] reported the three-dimensional (3D) structure of MIL-100(Cr), a corner-sharing tetrahedral MOF(Cr) with 2.5–3 nm and 0.65 nm sized mesopores and micropores respectively, many research studies have reported the stability for water adsorption, along with its application in sensible and latent load control [40,138]. Kitagawa et al. [40] conducted more than 2000 adsorption-desorption cycles with no observed structural decomposition, and the water uptake was maintained at 0.8 g g^{-1}. However, the undesirable isotherms have also driven the efforts to graft some hydrophilic groups on the coordinately unsaturated metal sites to tune the isotherm shape of MIL-100(Cr). The introduction of hydrophilic groups tunes the hydrophilicity of MIL-100(Cr), however, decreases the surface area and pore volume, thus, resulting in different trigger point (P/P_0) as well as water uptake capacity [139].

In addition, considering the potentially harmful chromium

compounds, Horcajada et al. have successfully synthesized Fe-based MOF, MIL-100(Fe) with non-toxic nature [140]. Subsequently, Henninger et al. [27] have used MIL-100(Al, Fe) for heat transformation applications. From the comparison of isotherms in Fig. 13, the water uptake of 0.77 g g^{-1} for MIL-100(Fe) is noted to be superior than 0.5 g g^{-1} for MIL-100(Al) with, and all of the studied MOFs bear hydrothermal cycling stability under 40 cycling experiments (6.4% loss for MIL-100(Fe) and 6.6% loss for MIL-100(Al)), as shown in Fig. 14. From the adsorption behavior, it is interesting to find two step steep rise at 0.24 and $0.35P/P_0$ for MIL-100(Fe, Al), respectively, which is similar to 0.24 and $0.38P/P_0$ observed for MIL-100(Cr). The observed behavior is explained as follows: the open metal sites start adsorbing a fraction of water molecules below $0.2P/P_0$, and subsequently the two steep rise steps contribute to the sudden adsorption in the cage of different size [45]. The resulting features therefore render MIL-100 series very interesting alternatives for sorption-based heat and humidity control.

MIL-101 was first prepared and reported by Férey et al. [41] with 5900 $\text{m}^2 \text{ g}^{-1}$ surface area and 2.9–3.4 nm pore size. The three-dimensional structure is constructed by joining Cr-based inorganic trimers (octahedra) with ligand 1, 4-BDC (1, 4-benzenedicarboxylate) to form a super tetrahedron, which is closely related to the structure of MIL-100, as seen in Fig. 15. With an aim to surpass its predecessor's merit of reversible water adsorption, Henninger et al. [29] evaluated MIL-101(Cr) and pointed out its more desirable isotherm, with a steep rise at $0.4P/P_0$. The results indicated nearly 1g g^{-1} of cycling water loading under a typical condition with only 3.2% of loading loss after 40 cycles on applying MIL-101(Cr) in a heat-transformation cycling system. Thus, MIL-101(Cr) is confirmed to demonstrate high water loading along with strong hydrothermal stability. Fig. 16 shows several isotherms extracted from the literature studies indicating ultrahigh adsorption capacity of MIL-101(Cr) with a maximum value reaching up to 1.6 g g^{-1} [28,57,78]. Owing to the larger pore size (>2 nm), hysteresis loops occurred in isotherms, therefore reducing the usable loading lift in active SDSs. Kitagawa et al. [57] also examined the adsorption/desorption behavior of functionalized MIL-101 derivatives. These compounds with different substituents (-NO_2, -NH_2, -SO_3H) are noted to reach a water capacity in the range 0.8–1.2 g g^{-1} with great stability and regeneration under 80°C [28,57]. Different from MIL-100 series, little research has been carried out on MIL-101 analogs with different metal clusters (i.e. Fe^{3+}, Al^{3+}) due to the hydrolysis.

Many MOFs based on NU series (NU, Northwestern University) have emerged recently, however, their use for water adsorption has been
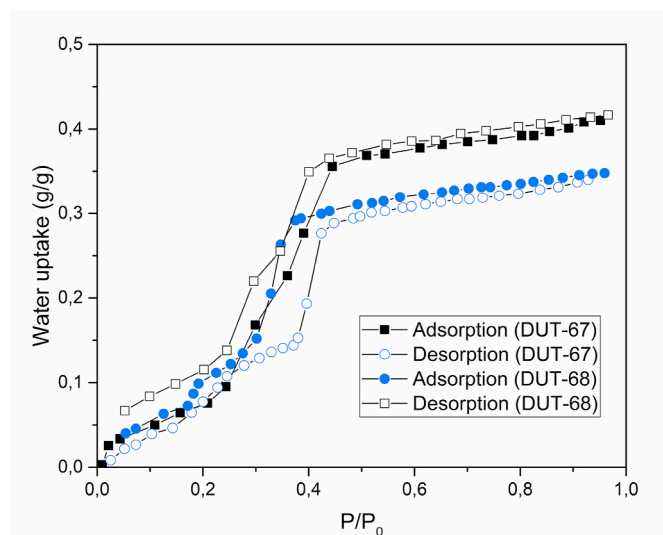

Fig. 12. Water adsorption/desorption isotherms of water-stable DUT series [49].
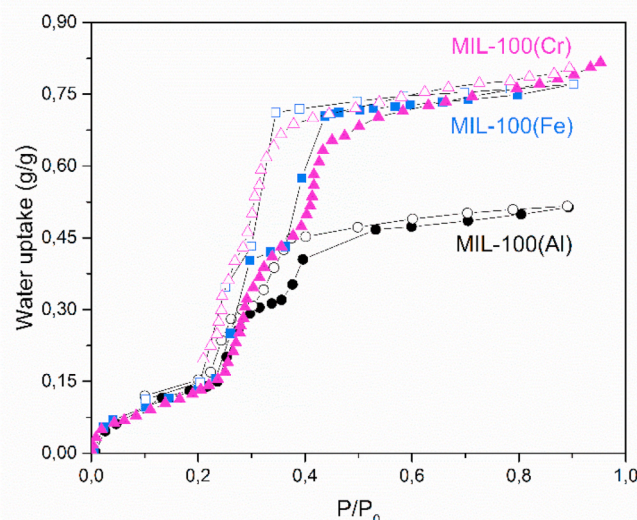

Fig. 13. Water adsorption/desorption isotherms of MIL-100 (Al, Cr, Fe) [27, 40,138].
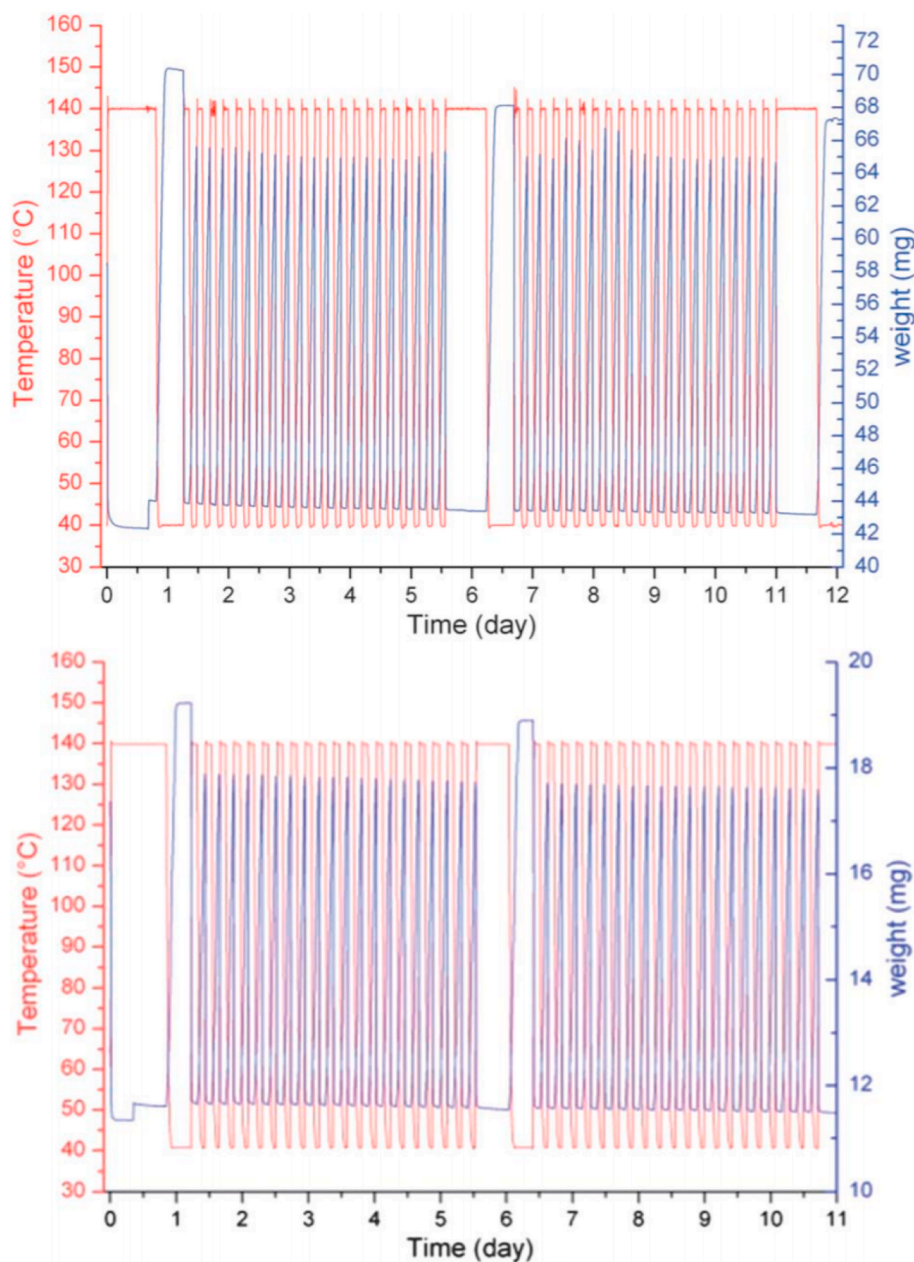
Fig. 14. Temperature profiles and mass loading of MIL-100 (Al, Fe) in cyclic tests [27].

limited except NU-1500 [142,143]. Farha et al. [83] reported that NU-1500 consisted of trivalent trinuclear metal cluster (Fe^{3+}, Sc^{3+} and Cr^{3+}) and trigonal prismatic ligand, while the Cr-based NU-1500 was also noted to exhibit water stability after 20 cycling experiments. In Fig. 17(a), water adsorption capacity of NU-1500 is observed to approach 1.09 g g^{-1} without hysteresis loop between the adsorption and desorption branches. This may have resulted due to only one kind of small hexagonal channels with a 1.4 nm of pore size. The trigger point in Fig. 17(b) is around 0.45P/P_0 followed by a narrow steep rise. Consequently, compared with more hydrophilic MOFs (low trigger point), it is reasonable to predict that NU-1500 can be desorbed using a gentler regeneration condition in heat-transformation application.

Recently, two excellent MOFs aimed towards autonomous indoor humidity control have been proposed, namely, Y-shp-MOF-5 and Cr-soc-MOF-1. Y-shp-MOF-5 is the rare earth metal-based MOF composed of the yttrium-based metal cluster and tetratopic ligand [BTEB, 1,2,4,5-tetrakis (4-carboxyphenyl) benzene]. Eddaoudi et al. [21] have evaluated the water adsorption/desorption isotherms and cyclic behavior of hexagonal prism-shaped Y-shp-MOF-5. The trigger points of adsorption and desorption branches are 0.56 and 0.47P/P_0 respectively, as shown in Fig. 18(a), after which two steep rise steps occur within 30%–47% RH and 56%-70%RH. The water uptake is noted to reach up to 0.45 g g^{-1}, which indicates superior performance as compared to most traditional desiccants. In addition, 200 adsorption-desorption cycles display its stable water uptake variation for relative humidity between 25% and 85% (Fig. 18(b)), exhibiting the capacity to regulate the humidity within a desirable range.

Cr-soc-MOF-1 is the other MOF with potential for autonomous humidity regulation. Eddaoudi et al. [42] reported this hydrolytically stable material together with its remarkable water capacity (~1.95 g g^{-1}), much better than the MOFs reported so far. Cr-soc-MOF-1 consists of the trinuclear chromium cluster and deprotonated organic ligand (TCPT; 3, 3'', 5, 5''-tetrakis(4-carboxyphenyl)-p-terphenyl), developed through post-synthetic modification of Fe-soc-MOF-1. The isotherm in
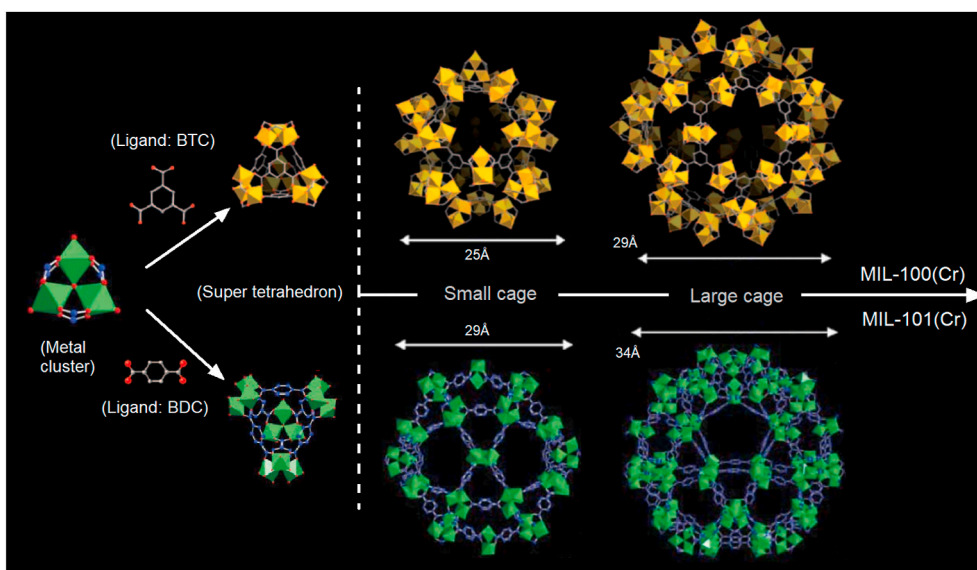
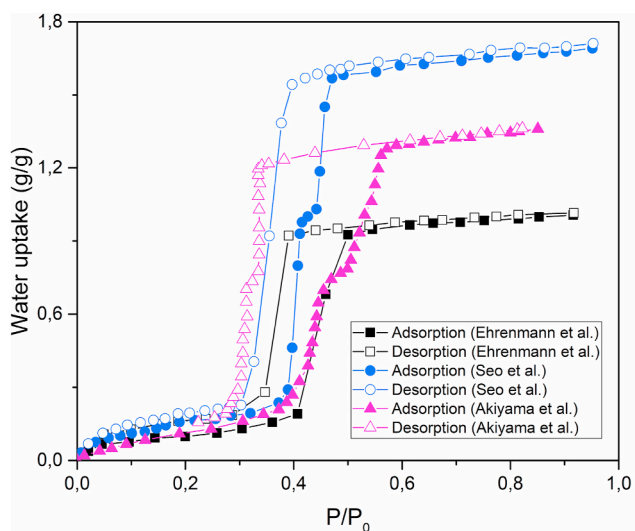**Fig. 15.** Structure of MIL-100(Cr) and MIL-101(Cr) [6,141].

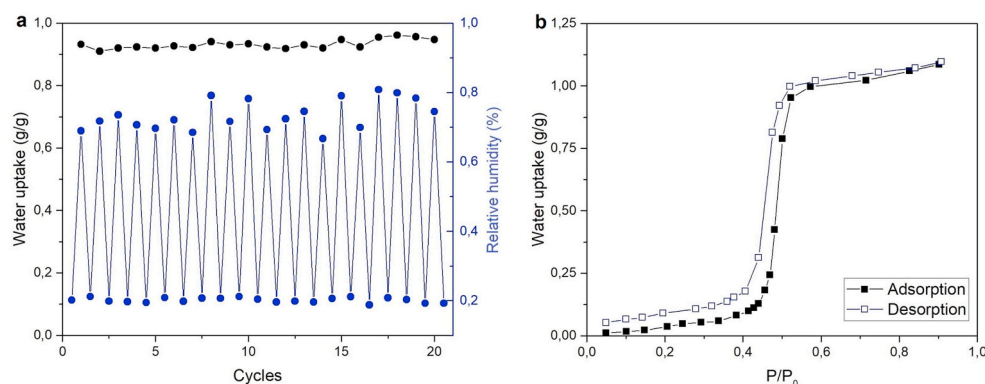**Fig. 16.** Water adsorption/desorption isotherms of different MIL-101(Cr) samples [29,57,78].

Fig. 19(a) indicates its intriguing ability for the passive control of indoor humidity load in view of the strong hydrolytically stable nature, with 3 times higher working capacity (1.95 g g^{-1} at 0.7P/P$_0$) than the predecessor, Y-shp-MOF-5, at room temperature (298K). The rectangular hysteresis loop with two trigger points in adsorption (0.6P/P$_0$) and desorption (0.42P/P$_0$) branches comply with the recommended comfort zone by ASHRAE. Besides, the adsorption-desorption cycles were conducted to confirm the durability of the material within 25%–85% humidity level at room temperature. After 100 cycling experiments as shown in Fig. 19(b), the water capacity remained unchanged, which indicated that the adsorbed water molecules can be desorbed at 298K by lowering the humidity level. However, the hydrothermal stability at different temperatures is required for active control in SDSs.

On the basis of the previous discussion, the relatively hydrophobic MOFs have less affinity towards water molecules, thus these theoretically allow swift release of the adsorbed water molecules. In fact, little research has been carried out to investigate the active heat transformation owing to the low water uptake at the low relative pressure range. Moreover, most of these MOFs have an unwanted hysteresis loop, which reduces the actual loading lift. Luckily, the design and synthesis of these MOFs with hysteresis loop is potentially qualified for the autonomous humidity regulation in a built environment. The benchmark material Y-shp-MOF-5 [21] and its successor Cr-soc-MOF-1 [42] have been the most mentioned for the passive control of indoor humidity load in open SDSs due to their desirable isotherms, high hydrolytical stability
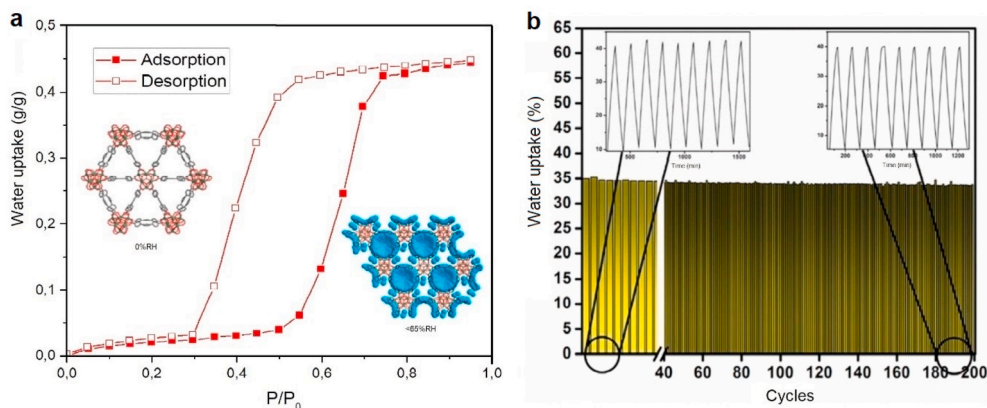

Fig. 17. Water adsorption/desorption isotherms and cycling tests between 20% and 80%RH [83].

Fig. 18. (a) Water adsorption/desorption isotherms of Y-shp-MOF-5 and (b) 200 cycles in the relative humidity range between 25% and 85% [21].
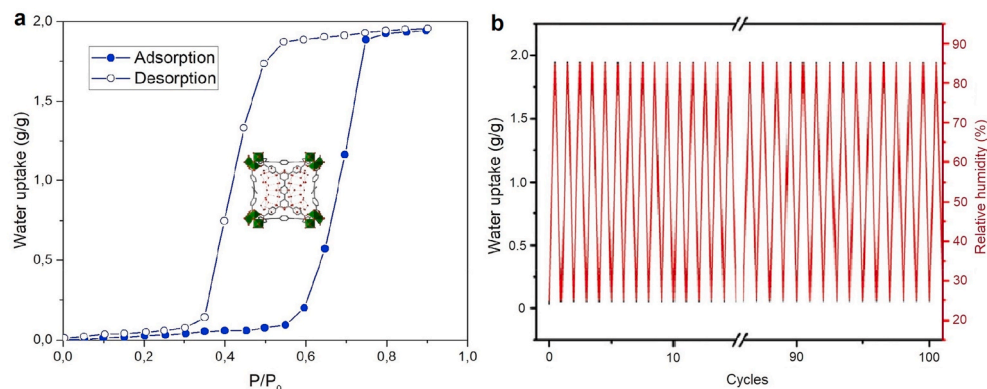

Fig. 19. (a) Water adsorption/desorption isotherms of Cr-soc-MOF-1 and (b) 100 cycles in relative humidity range between 25% and 85% [42].

and water uptake. However, these materials have undesirable metal clusters (i.e. Y, Cr), which may limit their application range. Moreover, further cycling experiments under different temperature pairs (adsorption-desorption) are needed to be conducted to evaluate their hydrothermal stability for active SDS systems. Besides, other water stable materials such as MAF [79], DMOF [89], Ni-BPP [33], BUT [76] and functionalized MOFs [62,144] have been developed, all of which need further intensive studies for passive and active humidity control.

4.3. High range (>65%RH)

Some MOF materials with the adsorption process starting after 0.65 P/P_0 trigger point have also been synthesized. Compared to the earlier-mentioned MOFs, these ultra-hydrophobic MOFs are less competitive towards the sorption-based humidity regulation due to their low efficiency for passive (adsorption at >65%RH) and active control (<30% RH) in SDSs. To date, it is reported that PIZOF-2 [23,37] initiates water vapor adsorption after $0.7P/P_0$ and reaches 68 wt% of water capacity at $0.9P/P_0$. Kitagawa et al. [123] investigated MIL-53 (Al) with different functional groups, and isotherms show a steep rise of water uptake after $0.7P/P_0$ in MIL-53(Al)–OH. Though these MOFs exhibit more or less good stability and S-shaped isotherms with high water uptake, the hydrophobicity makes them ineffective to take up the water vapor molecules at the desirable humidity range. It is expected that modification/functionalization of these MOFs can tune their inner structure, enabling them to exhibit improved performance based on water adsorption.

5. System-level screening and applications for the built environment

5.1. Working principles of the open solid desiccant system (SDS)

In general, an open SDS is designed to deal with the hygrothermal load in air, in which the desiccants directly contact with the indoor air to regulate the sensible and latent load. Open SDSs based on different working principles can be classified into active and passive types. The passive-type SDS can remove the moisture fluctuation by virtue of the nature of the desiccant materials that autonomously adsorb or release the water vapor under high or low indoor humidity levels. As the intrinsic properties of the desiccant decide the operational performance, limited progress has been made in passive-type SDS systems [145–148]. As for active-type SDS, the adsorption loop forces the process air to flow through the desiccant and dehumidifies the air to the desired room temperature. The regeneration loop can reject the trapped water vapor out of the desiccant so that the desiccant can be recovered and utilized in the next operation loop. In this regard, the regeneration can be achieved by heating the desiccant to the regeneration temperature, which relies on the intrinsic properties of the desiccants (i.e. zeolite, ~100°C; MOF, 50–90°C) [11,20,72].

To date, passive-type SDS systems (Fig. 20) primarily act as moisture buffer for building environment control, which contains classical hygroscopic materials such as wood, plasterboard, etc. Qin et al. have recently developed a new type of MOF-based precise humidity control material (MOF-PHCM) to autonomously control the indoor moisture [149]. In contrast, active-type SDS systems (Fig. 21) generally have three complex components, namely, dehumidification unit, regeneration unit and cooling unit [150]. The configuration of these units may
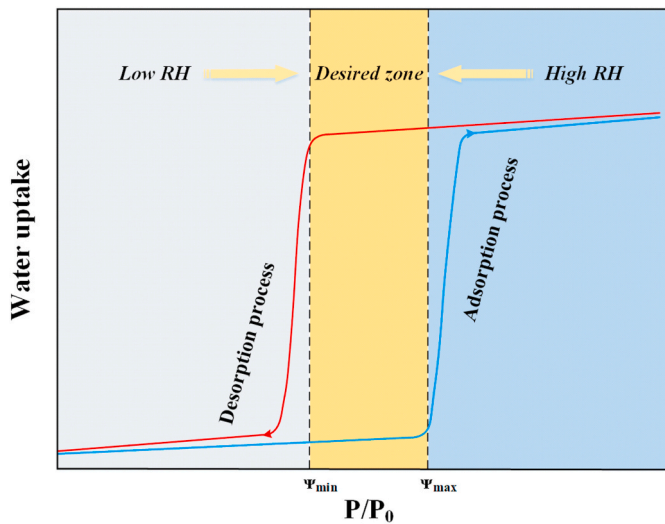
Fig. 20. The variation of water uptake in desiccant materials at high and low RH.
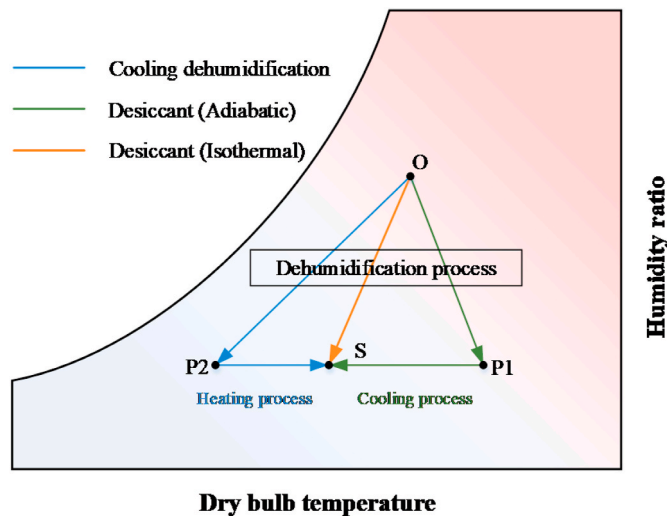

Fig. 21. The psychrometric processes of active-type desiccant dehumidifiers in comparison with cooling dehumidification. O: outside air; S: supply air; P1 and P2: medium process.

1) Dehumidifier

vary largely based on the desiccant and the employed operation modes, as shown in the following section.

In the case where SDS has been employed, the dehumidifier can generally work in two different manners: adiabatic [151,152] and isothermal [9]. The process air stream directly flows through the solid desiccant in the adiabatic dehumidifiers, while in the case of isothermal dehumidifiers, the solid desiccant is not only in contact with the air stream, but is also cooled down by the cooling medium to improve the performance of desiccants. The psychrometric processes are shown in Fig. 21. It is clear that the isothermal desiccant system is more desirable than the adiabatic process.

The commonly used dehumidifier types are fixed bed, rotary wheel and desiccant-coated heat exchangers (DCHEs). Since the desiccant can directly affect the performance of SDS, the selection of the desiccant for the above-mentioned systems become a focal point. Traditional desiccants such as silica gel and zeolite have been widely embedded into fixed bed [153,154], rotary wheel [152,155,156] and desiccant-coated heat exchangers (DCHEs) [9,157,158]. However, metal-organic frameworks

with superior adsorption capacity and gentler regeneration condition have found little evaluation for use in dehumidifiers, thus, presenting a high potential of their application [23,52,159].

2) Cooling and regeneration

The cooling medium handles the sensible load in the cooling unit in SDS. In case an adiabatic type dehumidifier is implemented, the adsorption heat released during adsorption process gradually heats up the process air. The cooling unit can cool the air down to the desired supply air temperature. In case an isothermal type dehumidifier is employed, the cooling unit can immediately remove the adsorption heat to keep a high adsorption capacity of the desiccants. To the best of our knowledge, the common cooling unit can be a cold coil, an evaporative cooler or even an evaporator in the air conditioner.

In addition, the regeneration unit in SDS is of vital significance as it supplies the thermal energy to drain the adsorbed water vapor out of the desiccants. The regenerated desiccant can therefore continue the subsequent adsorption process. As the regeneration condition is primarily decided by the intrinsic properties of the desiccants, SDS makes it possible to use a variety of energy sources, including waste heat, solar energy, electricity, etc.

5.2. Matching the sorption operation with the given condition

Based on the review on the MOF materials, it is confirmed that MOFs exhibit highly tunable structures, thus, laying promising foundation for the sorption-based humidity control. For this application, the optimal MOF materials should possess hydrothermal stability and recyclability. In real life situations, air-conditioning systems usually experience multiple climate conditions during days or years. In MOF-used desiccant systems, hydrothermally stable MOFs with a steep rise in a narrow humidity range (S-shaped isotherm) are expected to maintain the humidity level during the long-term cycling operations [14]. Thus, for SDSs, the ideal MOFs for built environment control should be qualified as follows:

(1) In an active-type system, it is favorable to pick up desiccants with high water lift loading, milder regeneration condition and no or minimal hysteresis loop at the working humidity range.
(2) In a passive-type system, it is desirable that the hysteresis loop of the MOF desiccant formed by the adsorption-desorption branches appears during the working humidity range, and the MOF can be easily regenerated around room temperature. Moreover, these MOFs should not be temperature-sensitive, which implies that these materials are able to maintain almost the same isotherms within a certain temperature range.

In fact, many commercial and laboratory developed MOFs cannot strictly meet these requirements, especially related to hydrothermal stability. Most of heat-transformation studies on MOFs are carried out focusing on the heat pumps, adsorption-driven chillers or water harvesting etc. [23,28,32], however, a little knowledge is available on the open SDSs for building humidity control or the introduction of MOF-based system concept [160]. Chang et al. [78] investigated the potential of MIL-100 and MIL-101 for the energy-efficient dehumidification. Obviously, the used MOFs are promising desiccants, however, the study primarily focused on the properties of materials, rather than practical application. Lately, Henninger et al. [52] studied the MOF-coated heat exchanger at full scale considering pretreatment and coating processes. The coefficient of performance (COP) of the cooling system was estimated under different evaporator and heat rejection temperatures, and the results revealed a maximum COP up to 0.72 without heat recovery. As mentioned in the study [52], the preparation and coating processes are arduous for large-scale applications, and the recyclability of the system may need more field experiments. This work thus offers a benchmark for MOF-based open SDSs. Besides, Eddaoudi

et al. [21,42] prepared two novel desiccants with the most favorable isotherms, designed for autonomous humidity control (section 3.2.2) at room temperature. As a whole, the climate conditions, material properties and system requirements determine the design and assembly of an open SDS.

5.3. Alternative applications

The sorption-based air-conditioning system is a critical technology for achieving energy saving in building environment control. From material to system design, the selected MOFs considering the above-mentioned criteria will be integrated into a real SDS. In this context, most of currently available water-stable MOFs have been classified into three groups, and each of these groups remains a focal point of research. It is noted that significant research efforts have been focused on the some common material properties such as water stability, water uptake capacity and regeneration of MOFs. Some other factors such as processing techniques (i.e. coating process) have been scarcely reported [52,125,161], which partly affect the size and performance of SDSs along with initial investment. Thus, it is needed to conduct more field measurements to assess all factors affecting MOF-based SDSs. In the following sections, we propose the case of two MOF-based systems with potential of high energy saving for the built environment control. Here, the promising candidate, MIL-100(Fe), has been applied to the systems working in active or passive mode and detailed parameters have been documented in previous studies [72,162].

5.3.1. Active system

Through the literature reviews on the development of sorption-based air-conditioning systems, it is clear that the traditional adiabatic dehumidification approaches (i.e. rotary wheel [152,163]) experience the severe effect of adsorption heat, which adversely reduces the total dehumidification efficiency. Therefore, a new system with desiccant-coated heat exchangers may be preferable as shown in Fig. 22. The evaporator will remove the sensible load and adsorption heat to keep an isothermal adsorption, which helps to enlarge the usable water loading lift and avoid the low evaporation temperature. Although there is no heat recovery or mixing of new and exhaust air, the ultralow condensation temperature (less than 60°C) has been noted to result in COP of 7.9, which is comparable to the traditional desiccants based cooling systems [164]. As MOF is saturated in the evaporator as well as dried in the condenser, switching of the flow direction can achieve a continuous operation. Besides, the sorption kinetics confirms MIL-100 (Fe) to outperform many desiccants in both adsorption rate and cycling water loading. Apparently, this system can achieve a fast regulation of sensible and latent load.

On the other hand, mathematical models of SDS have also been developed for several decades. To date, many research studies have been dedicated to the mathematical prediction of supply air conditioning [158,165–167]. MOF-based model [159] has also been used recently, which helps to disclose the potential application of MOFs in the low and medium humidity environment.

5.3.2. Passive system

In 2005, Rode et al. [149] introduced a concept of moisture buffer value (MBV), which indicates that the hygroscopic materials can autonomously relieve indoor humidity fluctuation. Since then, many intensive research studies have been carried out for the model development [145,147,168,169] and the assessment of buffer performance of the hygroscopic materials [170–172]. However, MBV test of the traditional hygroscopic materials such as wood, cellular concrete, etc., have been conducted on the laboratory scale, and their low moisture buffer capacity indicates their inability of effective humidity control (see Table S1 in the Supporting information). Eddaoudi et al. [21,42] proposed two promising MOF materials with desirable isotherms, however, these materials need more field experimental verifications at different temperature conditions. Lately, we have applied MIL-100(Fe) as a moisture buffer panel to investigate the changes in indoor humidity load at different climate conditions. The MBV ($\sim$10 g m^{-2} RH%$^{-1}$) of MIL-100(Fe) has been measured to be one order of magnitude larger than the traditional hygroscopic material ($\sim$1g m^{-2} RH%$^{-1}$) [162]. The configuration of the room model is shown in Fig. 23.

Considering the inner moisture gain and ventilation, the results indicate that MIL-100(Fe) can remove a majority of the latent load by night ventilation under dry and moderate climate conditions, and more than 70% of the latent load under humid climate is removed with the help of a regenerator driven by the low-grade energy such as waste heat. As the passive control of MOF-based SDSs can remove most of the latent load, it is expected that the COP of air-conditioning system will be raised without cooling dehumidification. Thus, MOFs become promising candidates as hygroscopic materials.
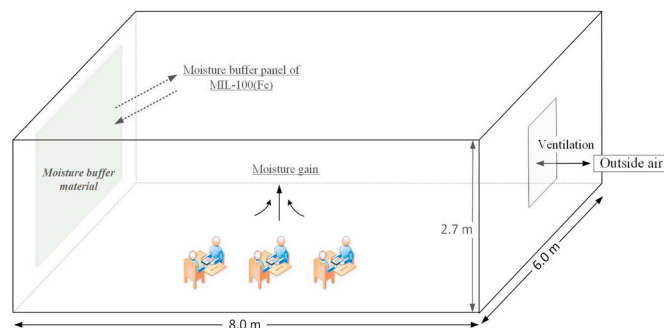

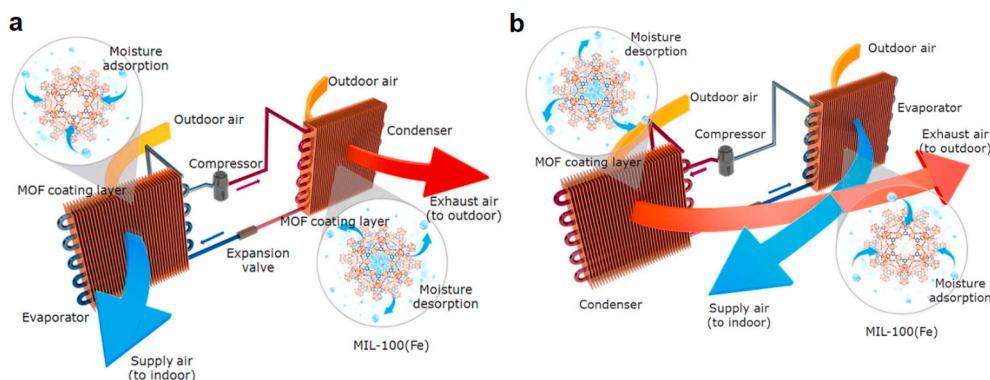**Fig. 23.** The room office using a MIL-100(Fe) panel [162].

Fig. 22. Configuration of MOF-based cooling system [72]. (a–b) The working operation of the cooling system.

6. Summary and potential

Solid desiccant system is considered as a promising approach to provide a comfortable and hygienic environment, by taking advantage of the low-grade energy. The desiccant is primarily used to remove the latent load in a target room. Therefore, the desiccants with higher water capacity and stable structure become potential candidates. Metal-organic frameworks (MOFs) derived from the combination of metal clusters and organic ligands are one of the potential categories, which possess remarkable microstructure and adsorption mechanisms, together with structural tunability. All of the mentioned MOFs in the review fulfill the basic requirements for SDSs, and some of them have been reported with mild regeneration conditions, usually between 60 and 90°C (or even <60°C). Moreover, these MOFs with S-shaped isotherms are also noted to outperform many traditional desiccants, as a sudden tunable change in water uptake can take place in the working humidity range. A comprehensive comparison of the water capacity of MOF desiccants in different pressure ranges is presented in Fig. 24.

In the past years, the synthesis and application of MOFs have made significant progress. The balance among the water stability, adsorption capacity and regeneration condition can be achieved through the subtle structure tailoring of the porous MOFs such as functionality or modification. The advances in the development of topology design and synthesis of MOFs [173] raise the chances of large-scale practical applications in both active and passive SDSs, and the research studies devoted to these systems are still increasing (Section 5). Despite the remarkable progresses in MOFs, no single MOF can currently meet all of the requirements owing to the drawbacks more or less related to material or system level. From the reviewed literature studies, some suggestions can be summarized as follows:

1) Chemical synthesis of MOF materials affects their intrinsic structure and material performance. The selection of green and nontoxicity raw materials (metal ions, organic ligand and solvent) is preferable to produce environment-friendly MOFs [35].
2) Conventional synthetic methods for MOF desiccants are considered convenient, however, these may be less productive and time-consuming. Assisted synthesis [174] or flow chemistry [175] can be expected as an alternative way to produce MOFs at large scale.
3) The flexibility of structural tunability makes MOF remarkable intrinsic properties, which helps explain the unique water adsorption mechanisms [14].
4) The screening of the available MOFs based on hydrothermal stability, water adsorption and regeneration, dynamic sorption equilibrium, large-scale production and non-toxicity helps to identify the high priority of MOFs among different MOF series.
5) In a specific environment, open SDSs can sustain the corresponding climate change with superior recyclability. The operation in active or passive way leads to different requirements for these MOF desiccants, generally focused on the shape of isotherm (i.e. hysteresis loop) and regeneration condition.
6) It is expected that more research studies will be available in future on the heat and mass properties of MOF desiccants, such as thermal conductivity, thermal and moisture effusivity, etc. [125]. Moreover, the applications in the desiccant-coated heat exchangers have been reported, but a little knowledge is available about the rotary wheel or fixed bed systems. In short, these properties and applications of open SDSs can prompt the use of MOF materials in built environment control.

The remarkable advances in the chemistry of MOF materials during the past years have revealed many alluring properties in comparison with the traditional solid desiccants. A systematic exploitation on the novel desiccants for SDSs is the need of the hour. In order to apply an optimal MOF to a specific SDS for the built environment control, it is essential to conduct an intensive research on the material and system
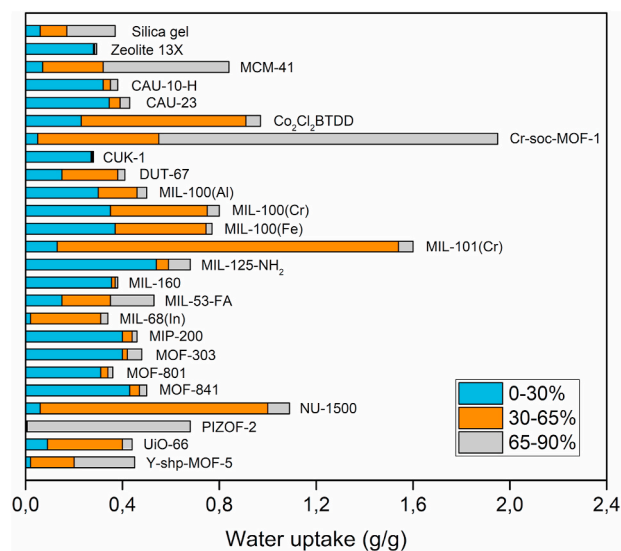

Fig. 24. Water uptake of some representative MOFs in different relative pressure ranges.

levels, from structural design to material preparation, from gram scale in laboratory to ton scale in production facility, from properties assessment to system application. As some studies have confirmed that SDS using MOFs exhibits superior performance over the traditional systems, it is important to conduct further field experiments and identify the appropriate MOFs for safe, cost-effective, and energy efficient processes.

Declaration of competing interests

The authors declare that they have no known competing financial interests or personal relationships that could have appeared to influence the work reported in this paper.

Declaration of competing interest

The authors declare that they have no known competing financial interests or personal relationships that could have appeared to influence the work reported in this paper.

Acknowledgements

Appendix A. Supplementary data

Supplementary data to this article can be found online at https://doi.org/10.1016/j.rser.2020.110246.

### References

[1] Lin B, Liu H. China's building energy efficiency and urbanization. Energy Build 2015;86:356–65.
[2] Chua K, Chou S, Yang W, Yan J. Achieving better energy-efficient air conditioning- A review of technologies and strategies. Appl Energy 2013;104: 87–104.
[3] Zhang T, Liu X, Jiang Y. Development of temperature and humidity independent control (THIC) air-conditioning systems in China- A review. Renew Sustain Energy Rev 2014;29:793–803.
[4] Xu X, Zhong Z, Deng S, Zhang X. A review on temperature and humidity control methods focusing on air-conditioning equipment and control algorithms applied in small-to-medium-sized buildings. Energy Build 2018;162:163–76.
[5] ASHRAE, Ventilation for Acceptable Indoor Air Quality. American Society of Heating, Refrigerating, and Air Conditioning Engineering. 2010. Atlanta, GA(US).

[6] Chaemchuen S, Xiao X, Klomkliang N, Yusubov M. Tunable metal-organic frameworks for heat transformation applications. Nanomaterials 2018;8(9).

[7] Wang W, Wu L, Li Z, Fang Y, Ding J, et al. An overview of adsorbents in the rotary desiccant dehumidifier for air dehumidification. Dry Technol 2013;31(12): 1334–45.

[8] Jain S, Bansal PK. Performance analysis of liquid desiccant dehumidification systems. Int J Refrig 2007;30(5):861–72.

[9] Vivekh P, Kumja M, Bui D, Chua K. Recent developments in solid desiccant coated heat exchangers - a review. Appl Energy 2018;229:778–803.

[10] Tsobnang PK, Hastürk E, Fröhlich D, Wenger E, Durand P, et al. Water vapor single-gas selectivity via flexibility of three potential materials for autonomous indoor humidity control. Cryst Growth Des 2019;19(5):2869–80.

[11] Zheng X, Ge TS, Wang RZ. Recent progress on desiccant materials for solid desiccant cooling systems. Energy 2014;74:280–94.

[12] Furukawa H, Cordova K, Keeffe M, Yaghi O. The chemistry and applications of metal-organic frameworks. Science 2013;341(6149):1230444.

[13] Yaghi OM, Keeffe M, Ockwig N, Chae H, Eddaoudi M, et al. Reticular synthesis and the design of new materials. Nature 2003;423(6941):705–14.

[14] Canivet J, Fateeva A, Guo Y, Coasne B, Farrusseng D. Water adsorption in MOFs: fundamentals and applications. Chem Soc Rev 2014;43(16):5594–617.

[15] Hastürk E, Ernst SJ, Janiak C. Recent advances in adsorption heat transformation focusing on the development of adsorbent materials. Curr Opin Chem Eng 2019; 24:26–36.

[16] Lange MF, Verouden K, Vlugt T, Gascon J, Kapteijn F. Adsorption-driven heat pumps: the potential of metal-organic frameworks. Chem Rev 2015;115(22): 12205–50.

[17] Burtch NC, Jasuja H, Walton KS. Water stability and adsorption in metal-organic frameworks. Chem Rev 2014;114(20):10575–612.

[18] Jeremias F, Fröhlich D, Janiak C, Henninger S. Advancement of sorption-based heat transformation by a metal coating of highly-stable, hydrophilic aluminium fumarate MOF. RSC Adv 2014;4(46):24073–82.

[19] Fröhlich D, Pantatosaki E, Kolokathis P, Markey K, Reinsch H, et al. Water adsorption behaviour of CAU-10-H: a thorough investigation of its structure–property relationships. J Mater Chem 2016;4(30):11859–69.

[20] Lenzen D, Zhao J, Ernst S, Wahiduzzaman M, Inge A, et al. A metal-organic framework for efficient water-based ultra-low-temperature-driven cooling. Nat Commun 2019;10(1):3025.

[21] AbdulHalim RG, Bhatt PM, Belmabkhout Y, Shkurenko A, Adil K, et al. A fine-tuned metal-organic framework for autonomous indoor moisture control. J Am Chem Soc 2017;139(31):10715–22.

[22] Fathieh F, Kalmutzki MJ, Kapustin EA, Waller PJ, Yang JJ, et al. Practical water production from desert air. Sci Adv 2018;4(6):eaat3198.

[23] Kim H, Yang S, Rao SR, Narayanan S, Kapustin EA, et al. Water harvesting from air with metal-organic frameworks powered by natural sunlight. Science 2017; 356(6336):430.

[24] Tu Y, Wang R, Zhang Y, Wang J. Progress and expectation of atmospheric water harvesting. Joule 2018;2(8):1452–75.

[25] Cadiau A, Lee JS, Borges DD, Fabry P, Devic T, et al. Design of hydrophilic metal organic framework water adsorbents for heat reallocation. Adv Mater 2015;27 (32):4775–80.

[26] Rieth AJ, Wright AM, Rao S, Kim H, LaPotin AD, et al. Tunable metal-organic frameworks enable high-efficiency cascaded adsorption heat pumps. J Am Chem Soc 2018;140(50):17591–6.

[27] Jeremias F, Khutia A, Henninger SK, Janiak C. MIL-100(Al, Fe) as water adsorbents for heat transformation purposes—a promising application. J Mater Chem 2012;22(20):10148–51.

[28] Khutia A, Rammelberg U, Schmidt T, Henninger S, Janiak C. Water sorption cycle measurements on functionalized MIL-101Cr for heat transformation application. Chem Mater 2013;25(5):790–8.

[29] Ehrenmann J, Henninger SK, Janiak C. Water adsorption characteristics of MIL-101 for heat-transformation applications of MOFs. Eur J Inorg Chem 2011;2011 (4):471–4.

[30] Lee JS, Yoon JW, Mileo PGM, Cho KH, Park J, et al. Porous metal-organic framework CUK-1 for adsorption heat allocation toward green applications of natural refrigerant water. ACS Appl Mater Interfaces 2019;11(29):25778–89.

[31] Bon V, Senkovska I, Evans JD, Wöllner M, Hölzel M, et al. Insights into the water adsorption mechanism in the chemically stable zirconium-based MOF DUT-67- a prospective material for adsorption-driven heat transformations. J Mater Chem 2019;7(20):12681–90.

[32] Lenzen D, Bendix P, Reinsch H, Fröhlich D, Kummer H, et al. Scalable green synthesis and full-scale test of the metal-organic framework CAU-10-H for Use in Adsorption-Driven Chillers. Adv Mater 2018;30(6):1705869.

[33] Zheng J, Vemuri RS, Estevez L, Koech PK, Varga T, et al. Pore-engineered metal-organic frameworks with excellent adsorption of water and fluorocarbon refrigerant for cooling applications. J Am Chem Soc 2017;139(31):10601–4.

[34] Rezk A, Al-Dadah R, Mahmoud S, Elsayed A, et al. Characterisation of metal organic frameworks for adsorption cooling. Int J Heat Mass Tran 2012;55(25): 7366–74.

[35] Wang S, Serre C. Toward green production of water-stable metal-organic frameworks based on high-valence metals with low toxicities. ACS Sustainable Chem Eng 2019;7(14):11911–27.

[36] Wißmann G, Schaate A, Lilienthal S, Bremer I, Schneider AM, et al. Modulated synthesis of Zr-fumarate MOF. Microporous Mesoporous Mater 2012;152:64–70.

[37] Furukawa H, Gandara F, Zhang YB, Jiang JC, Queen WL, et al. Water adsorption in porous metal-organic frameworks and related materials. J Am Chem Soc 2014; 136(11):4369–81.

[38] Reinsch H, Veen MAVD, Gil B, Marszalek B, Verbiest T, et al. Structures, sorption characteristics, and nonlinear optical properties of a new series of highly stable aluminum MOFs. Chem Mater 2013;25(1):17–26.

[39] Rieth AJ, Yang S, Wang EN, Dincă M. Record atmospheric fresh water capture and heat transfer with a material operating at the water uptake reversibility limit. ACS Cent Sci 2017;3(6):668–72.

[40] Akiyama G, Matsuda R, Kitagawa S. Highly porous and stable coordination polymers as water sorption materials. Chem Lett 2010;39(4):360–1.

[41] Férey G, Mellot-Draznieks C, Serre C, Millange F, Dutour J, et al. A chromium terephthalate-based solid with unusually large pore volumes and surface area. Science 2005;309(5743):2040.

[42] Abtab SMT, Alezi D, Bhatt PM, Shkurenko A, Belmabkhout Y, et al. Reticular chemistry in action: a hydrolytically stable MOF capturing twice its weight in adsorbed water. Inside Chem 2018;4(1):94–105.

[43] Karmakar A, Prabakaran V, Zhao D, Chua KJ. A review of metal-organic frameworks (MOFs) as energy-efficient desiccants for adsorption driven heat-transformation applications. Appl Energy 2020;269:115070.

[44] Kalmutzki MJ, Diercks CS, Yaghi OM. Metal-organic frameworks for water harvesting from air. Adv Mater 2018;30(37):1704304.

[45] Küsgens P, Rose M, Senkovska I, Fröde H, Henschel A, et al. Characterization of metal-organic frameworks by water adsorption. Microporous Mesoporous Mater 2009;120(3):325–30.

[46] Wang S, Lee JS, Wahiduzzaman M, Park J, Muschi M, et al. A robust large-pore zirconium carboxylate metal–organic framework for energy-efficient water-sorption-driven refrigeration. Nat Energy 2018;3(11):985–93.

[47] Kundu T, Sahoo SC, Banerjee R. Variable water adsorption in amino acid derivative based homochiral metal organic frameworks. Cryst Growth Des 2012; 12(9):4633–40.

[48] Sohail M, Yun YN, Lee E, Kim SK, Cho K, et al. Synthesis of highly crystalline NH2-MIL-125(Ti) with S-shaped water isotherms for adsorption heat transformation. Cryst Growth Des 2017;17(3):1208–13.

[49] Bon V, Senkovska I, Baburin IA, Kaskel S. Zr- and Hf-based metal-organic frameworks: tracking down the polymorphism. Cryst Growth Des 2013;13(3): 1231–7.

[50] Guo X, Zhu G, Fang Q, Xue M, Tian G, et al. Synthesis, structure and luminescent properties of rare earth coordination polymers constructed from paddle-wheel building blocks. Inorg Chem 2005;44(11):3850–5.

[51] Canivet J, Bonnefoy J, Daniel C, Legrand A, Coasne B, et al. Structure-property relationships of water adsorption in metal–organic frameworks. New J Chem 2014;38(7):3102–11.

[52] Kummer H, Jeremias F, Warlo A, Füldner G, Fröhlich D, et al. A functional full-scale heat exchanger coated with aluminum fumarate metal-organic framework for adsorption heat transformation. Ind Eng Chem Res 2017;56(29):8393–8.

[53] Prat D, Wells A, Hayler J, Sneddon H, McElroy CR, et al. CHEM21 selection guide of classical- and less classical-solvents. Green Chem 2016;18(1):288–96.

[54] Yoon JW, Seo YK, Hwang YK, Chang JS, Leclerc H, et al. Controlled reducibility of a metal-organic framework with coordinatively unsaturated sites for preferential gas sorption. Angew Chem Int Ed 2010;49(34):5949–52.

[55] Liu Y, Kabbour H, Brown CM, Neumann DA, Ahn CC. Increasing the density of adsorbed hydrogen with coordinatively unsaturated metal centers in metal-organic frameworks. Langmuir 2008;24(9):4772–7.

[56] Dietzel PDC, Johnsen RE, Blom R, Fjellvåg H, et al. Structural changes and coordinatively unsaturated metal atoms on dehydration of honeycomb analogous microporous metal-organic frameworks. Chem Eur J 2008;14(8):2389–97.

[57] Akiyama G, Matsuda R, Sato H, Hori A, Takata M, et al. Effect of functional groups in MIL-101 on water sorption behavior. Microporous Mesoporous Mater 2012;157:89–93.

[58] Ragon F, Campo B, Yang Q, Martineau C, Wiersum AD, et al. Acid-functionalized UiO-66(Zr) MOFs and their evolution after intra-framework cross-linking: structural features and sorption properties. J Mater Chem 2015;3(7):3294–309.

[59] Devic T, Horcajada P, Serre C, Salles F, Maurin G, et al. Functionalization in flexible porous solids: effects on the pore opening and the host-guest interactions. J Am Chem Soc 2010;132(3):1127–36.

[60] Juan-Alcañiz J, Gielisse R, Lago AB, Ramos-Fernandez EV, Serra-Crespo P, et al. Towards acid MOFs-catalytic performance of sulfonic acid functionalized architectures. Catal Sci Technol 2013;3(9):2311–8.

[61] Eddaoudi M, Kim J, Rosi N, Vodak D, Wachter J, et al. Systematic design of pore size and functionality in isoreticular MOFs and their application in methane storage. Science 2002;295(5554):469.

[62] Jasuja H, Zang J, Shollet DS, Walton KS. Rational tuning of water vapor and CO_2 adsorption in highly stable Zr-based MOFs. J Phys Chem C 2012;116(44): 23526–32.

[63] Shi W, Zhu Y, Shen C, Shi J, Xu G, et al. Water sorption properties of functionalized MIL-101(Cr)-X ($X=-NH_2$, $-SO_3H$, -H, $-CH_3$, -F) based composites as thermochemical heat storage materials. Microporous Mesoporous Mater 2019; 285:129–36.

[64] Yan J, Yu Y, Ma C, Xiao J, Xia Q, et al. Adsorption isotherms and kinetics of water vapor on novel adsorbents MIL-101(Cr)@GO with super-high capacity. Appl Therm Eng 2015;84:118–25.

[65] Yuan Y, Zhang H, Yang F, Zhang N, Cao X. Inorganic composite sorbents for water vapor sorption: a research progress. Renew Sustain Energy Rev 2016;54:761–76.

[66] Elsayed E, Raya ALD, Mahmoud S, Anderson P, Elsayed A. Adsorption cooling system employing novel MIL-101(Cr)/$CaCl_2$ composites: numerical study. Int J Refrig 2019;107:246–61.

[67] Jabbari V, Veleta JM, Zarei-Chaleshtori M, Gardea-Torresdey J, Villagrán D. Green synthesis of magnetic MOF@GO and MOF@CNT hybrid nanocomposites

with high adsorption capacity towards organic pollutants. Chem Eng J 2016;304: 774–83.

[68] Furukawa H, Go YB, Ko N, Park YK, Uribe-Romo FJ, et al. Isoreticular expansion of metal-organic frameworks with triangular and square building units and the lowest calculated density for porous crystals. Inorg Chem 2011;50(18):9147–52.

[69] Furukawa H, Ko N, Go YB, Aratani N, Choi SB, et al. Ultrahigh porosity in metal-organic frameworks. Science 2010;329(5990):424.

[70] Deng H, Grunder S, Cordova KE, Valente C, Furukawa H, et al. Large-pore apertures in a series of metal-organic frameworks. Science 2012;336(6084):1018.

[71] Alvarez E, Guillou N, Martineau C, Bueken B, Voorde BVD, et al. The structure of the aluminum fumarate metal-organic framework A520. Angew Chem Int Ed 2015;127(12):3735–9.

[72] Cui S, Qin M, Marandi A, Steggles V, Wang S, et al. Metal-organic frameworks as advanced moisture sorbents for energy-efficient high temperature cooling. Sci Rep 2018;8(1):15284.

[73] Solovyeva MV, Gordeeva LG, Krieger TA, Aristov YI. MOF-801 as a promising material for adsorption cooling: equilibrium and dynamics of water adsorption. Energy Convers Manag 2018;174:356–63.

[74] Hanikel N, Prévot MS, Fathieh F, Kapustin EA, Lyu H, et al. Rapid cycling and exceptional yield in a metal-organic framework water harvester. ACS Cent Sci 2019;5:1699–706.

[75] Ma D, Li P, Duan X, Li J, Shao P, et al. A hydrolytically stable vanadium(IV) metal-organic frameworkwith photocatalytic bacteriostatic activity for autonomous indoor humidity control. Angew Chem Int Ed 2020;59:3905–9.

[76] Zhang YZ, He T, Kong XJ, Lv XL, Wu XQ, et al. Tuning water sorption in highly stable Zr(IV)-metal-organic frameworks through local functionalization of metal clusters. ACS Appl Mater Interfaces 2018;10(33):27868–74.

[77] Ahnfeldt T, Gunzelmann D, Wack J, Senker J, Stock N. Controlled modification of the inorganic and organic bricks in an Al-based MOF by direct and post-synthetic synthesis routes. CrystEngComm 2012;14(12):4126–36.

[78] Seo YK, Yoon JW, Lee JS, Hwang YK, Jun CH, et al. Energy-efficient dehumidification over hierachically porous metal-organic frameworks as advanced water adsorbents. Adv Mater 2012;24(6):806–10.

[79] Zhang JP, Zhu AX, Lin RB, Qi XL, Chen XM. Pore surface tailored SOD-type metal-organic zeolites. Adv Mater 2011;23(10):1268–71.

[80] Jeremias F, Lozan V, Henninger SK, Janiak C. Programming MOFs for water sorption: amino-functionalized MIL-125 and UiO-66 for heat transformation and heat storage applications. Dalton Trans 2013;42(45):15967–73.

[81] Luna-Triguero A, Sławek A, Huinink HP, Vlugt TJH, Poursaeidesfahani A, et al. Enhancing the water capacity in Zr-based metal-organic framework for heat pump and atmospheric water generator applications. ACS Appl Nano Mater 2019; 2(5):3050–9.

[82] Suh BL, Chong S, Kim JH. Photochemically induced water harvesting in metal-organic framework. ACS Sustainable Chem Eng 2019;7:15854–9.

[83] Chen Z, Li P, Zhang X, Li P, Wasson MC, et al. Reticular access to highly porous acs-MOFs with rigid trigonal prismatic linkers for water sorption. J Am Chem Soc 2019;141(7):2900–5.

[84] Schaate A, Roy P, Preuße T, Lohmeier SJ, Godt A, et al. Porous interpenetrated zirconium-organic frameworks (PIZOFs): a chemically versatile family of metal-organic frameworks. Chem Eur J 2011;17(34):9320–5.

[85] Vimont A, Goupil JM, Lavalley JC, Daturi M, Surblé S, et al. Investigation of acid sites in a zeotypic giant pores chromium(III) carboxylate. J Am Chem Soc 2006; 128(10):3218–27.

[86] Valenzano L, Civalleri B, Chavan S, Bordiga S, Nilsen MH, et al. Disclosing the complex structure of UiO-66 metal organic framework: a synergic combination of experiment and theory. Chem Mater 2011;23(7):1700–18.

[87] Coasne B, Galarneau A, Pellenq RJM, Renzo FD. Adsorption, intrusion and freezing in porous silica: the view from the nanoscale. Chem Soc Rev 2013;42(9): 4141–71.

[88] Coudert FX, Boutin A, Fuchs AH, Neimark AV. Adsorption deformation and structural transitions in metal-organic frameworks: from the unit cell to the crystal. J Phys Chem Lett 2013;4(19):3198–205.

[89] Jasuja H, Huang YG, Walton KS. Adjusting the stability of metal-organic frameworks under humid conditions by ligand functionalization. Langmuir 2012; 28(49):16874–80.

[90] Taylor JM, Vaidhyanathan R, Iremonger SS, Shimizu GKH. Enhancing water stability of metal-organic frameworks via phosphonate monoester linkers. J Am Chem Soc 2012;134(35):14338–40.

[91] Lv XL, Yuan S, Xie LH, Darke HF, Chen Y, et al. Ligand rigidification for enhancing the stability of metal-organic frameworks. J Am Chem Soc 2019;141 (26):10283–93.

[92] Kang IJ, Khan NA, Haque E, Jhung SH. Chemical and thermal stability of isotypic metal-organic frameworks: effect of metal ions. Chem Eur J 2011;17(23): 6437–42.

[93] Bosch M, Zhang M, Zhou HC. Increasing the stability of metal-organic frameworks. Adv Chem 2014;2014:182327.

[94] Schoenecker PM, Carson CG, Jasuja H, Cjj Flemming, Walton KS. Effect of water adsorption on retention of structure and surface area of metal-organic frameworks. Ind Eng Chem Res 2012;51(18):6513–9.

[95] Low JJ, Benin AI, Jakubczak P, Abrahamian JF, Faheem SA, et al. Virtual high throughput screening confirmed experimentally: porous coordination polymer hydration. J Am Chem Soc 2009;131(43):15834–42.

[96] DeCoste JB, Peterson GW, Jasuja H, Glover TG, Huang Y, et al. Stability and degradation mechanisms of metal-organic frameworks containing the $Zr_6O_4(OH)_4$ secondary building unit. J Mater Chem 2013;1(18):5642–50.

[97] Cheetham AK, Kieslich G, Yeung HHM. Thermodynamic and kinetic effects in the crystallization of metal-organic frameworks. Acc Chem Res 2018;51(3):659–67.

[98] Guillerm V, Ragon F, Dan-Hardi M, Devic T, Vishnuvarthan M, et al. A series of isoreticular, highly stable, porous zirconium oxide based metal-organic frameworks. Angew Chem Int Ed 2012;51(37). 9188-9188.

[99] Liu J, Benin AI, Furtado AMB, Jakubczak P, Willis RR, et al. Stability effects on CO2 adsorption for the DOBDC series of metal-organic frameworks. Langmuir 2011;27(18):11451–6.

[100] Ming Y, Purewal J, Yang J, Xu C, Soltis R, et al. Kinetic stability of MOF-5 in humid environments: impact of powder densification, humidity level, and exposure time. Langmuir 2015;31(17):4988–95.

[101] Jasuja H, et al. Kinetic water stability of an isostructural family of zinc-based pillared metal-organic frameworks. Langmuir 2013;29(2):633–42.

[102] Bon V, et al. Zr(iv) and Hf(iv) based metal-organic frameworks with reo-topology. Chem Commun 2012;48(67):8407–9.

[103] Kitagawa S, Kitaura R, Noro SI. Functional porous coordination polymers. Angew Chem Int Ed 2004;43(18):2334–75.

[104] Foley NJ, Thomas KM, Forshaw PL, Stanton D, Norman PR. Kinetics of water vapor adsorption on activated carbon. Langmuir 1997;13(7):2083–9.

[105] Harding AW, Foley NJ, Norman PR, Francis DC, Thomas TK. Diffusion barriers in the kinetics of water vapor adsorption/ desorption on activated carbons. Langmuir 1998;14(14):3858–64.

[106] Aristov YI, Tokarev MM, Freni A, Glaznev IS, Restuccia G. Kinetics of water adsorption on silica Fuji Davison RD. Microporous Mesoporous Mater 2006;96(1): 65–71.

[107] Hou C, Liu Q, Okamura T, Wang P, Sun WY. Dynamic porous metal-organic frameworks: synthesis, structure and sorption property. CrystEngComm 2012;14 (24):8569–76.

[108] Munusamy K, Sethia G, Patil DV, Rallapalli PBS, Somani RS, et al. Sorption of carbon dioxide, methane, nitrogen and carbon monoxide on MIL-101(Cr): volumetric measurements and dynamic adsorption studies. Chem Eng J 2012; 195–196:359–68.

[109] Fletcher AJ, Cussen EJ, Prior TJ, Rosseinsky MJ, Kepert CJ, et al. Adsorption dynamics of gases and vapors on the nanoporous metal organic framework material $Ni_2(4,4'$-Bipyridine$)_3(NO_3)_4$: Guest modification of host sorption behavior. J Am Chem Soc 2001;123(41):10001–11.

[110] Rubio-Martinez M, Avci-Camur C, Thornton AW, Imaz I, Maspoch D, et al. New synthetic routes towards MOF production at scale. Chem Soc Rev 2017;46(11): 3453–80.

[111] Dey C, Kundu T, Biswal BP, Mallick A, Banerjee R. Crystalline metal-organic frameworks (MOFs): synthesis, structure and function. Acta Crystallogr B 2014;70 (1):3–10.

[112] Gaab M, Trukhan N, Maurer S, Gummaraju R, Müller U. The progression of Al-based metal-organic frameworks-From academic research to industrial production and applications. Microporous Mesoporous Mater 2012;157:131–6.

[113] Bazer-Bachi D, Assié L, Lecocq V, Harbuzaru B, Falk V. Towards industrial use of metal-organic framework: impact of shaping on the MOF properties. Powder Technol 2014;255:52–9.

[114] Alvarez E, Guillou N, Martineau C, Bueken B, deVoorde BV, et al. The structure of the aluminum fumarate metal-organic framework A520. Angew Chem Int Ed 2015;54(12):3664–8.

[115] Simon-Yarza T, Mielcarek A, Couvreur P, Serre C. Nanoparticles of metal-organic frameworks: on the road to in vivo efficacy in biomedicine. Adv Mater 2018;30 (37):1707365.

[116] Reinsch H, Fröhlich D, Waitschat S, Chavan S, Lillerud KP, et al. Optimisation of synthesis conditions for UiO-66-CO2H towards scale-up and its vapour sorption properties. React Chem Eng 2018;3(3):365–70.

[117] Kim H, Rao SR, Kapustin EA, Zhao L, Yang S. Adsorption-based atmospheric water harvesting device for arid climates. Nat Commun 2018;9(1):1191.

[118] Strlič M, Thickett D, Taylor J, Cassar M. Damage functions in heritage science. Stud Conserv 2013;58(2):80–7.

[119] Fröhlich D, Henninger SK, Janiak C. Multicycle water vapour stability of microporous breathing MOF aluminium isophthalate CAU-10-H. Dalton Trans 2014;43(41):15300–4.

[120] Waitschat S, Reinsch H, Stock N. Water-based synthesis and characterisation of a new Zr-MOF with a unique inorganic building unit. Chem Commun 2016;52(86): 12698–701.

[121] Dreischarf AC, Lammert M, Stock N, Reinsch H. Green synthesis of Zr-CAU-28: structure and properties of the first Zr-MOF based on 2,5-furandicarboxylic acid. Inorg Chem 2017;56(4):2270–7.

[122] Waitschat S, Reinsch H, Arpacioglu M, Stock N. Direct water-based synthesis and characterization of new Zr/Hf-MOFs with dodecanuclear clusters as IBUs. CrystEngComm 2018;20(35):5108–11.

[123] Shigematsu A, Yamada T, Kitagawa H. Wide control of proton conductivity in porous coordination polymers. J Am Chem Soc 2011;133(7):2034–6.

[124] Permyakova A, Skrylnyk O, Courbon E, Affram M, Wang SJ, et al. Synthesis optimization, shaping, and heat reallocation evaluation of the hydrophilic metal-organic framework MIL-160(Al). ChemSusChem 2017;10(7):1419–26.

[125] Cui SQ, Marandi A, Lebourleux G, Thimon M, Bourdon M, et al. Heat properties of a hydrophilic carboxylate-based MOF for water adsorption applications. Appl Therm Eng 2019;161:114135.

[126] Dan-Hardi M, Serre C, Frot T, Rozes L, Maurin G, et al. A new photoactive crystalline highly porous titanium(IV) dicarboxylate. J Am Chem Soc 2009;131 (31):10857–9.

[127] Hendon CH, Tiana D, Fontecave M, Sanchez C, D'arras L, et al. Engineering the optical response of the titanium-MIL-125 metal-organic framework through ligand functionalization. J Am Chem Soc 2013;135(30):10942–5.

[128] Logan MW, Adamson JD, Le D, Uribe-Romo FJ. Structural stability of N-Alkyl-functionalized titanium metal-organic frameworks in aqueous and humid environments. ACS Appl Mater Interfaces 2017;9(51):44529–33.

[129] Kim SN, Kim J, Kim HY, Cho HY, Ahn WS. Adsorption/catalytic properties of MIL-125 and NH2-MIL-125. Catal Today 2013;204:85–93.

[130] Wahiduzzaman M, Wang SJ, Sikora BJ, Serre C, Maurin G. Computational structure determination of novel metal-organic frameworks. Chem Commun 2018;54(77):10812–5.

[131] Ahnfeldt T, Guillou N, Gunzelmann D, Margiolaki I, Loiseau T, et al. [Al4(OH)2(OCH3)4(H2N-bdc)3]·x H2O: a 12-connected porous metal-organic framework with an unprecedented aluminum-containing brick. Angew Chem Int Ed 2009;48(28):5163–6.

[132] Dhakshinamoorthy A, Heidenreich N, Lenzen D, Stock N. Knoevenagel condensation reaction catalysed by Al-MOFs with CAU-1 and CAU-10-type structures. CrystEngComm 2017;19(29):4187–93.

[133] Reinsch H, Feyand M, Ahnfeldt T, Stock N. CAU-3: a new family of porous MOFs with a novel Al-based brick: [Al2(OCH3)4(O2C-X-CO2)] (X = aryl). Dalton Trans 2012;41(14):4164–71.

[134] Heidenreich N, Lieb A, Stock N, Reinsch H. Green synthesis of a new layered aluminium citraconate: crystal structures, intercalation behaviour towards H2O and in situ PXRD studies of its crystallisation. Dalton Trans 2018;47(1):215–23.

[135] Reinsch H, Vos De D, Stock N. Structure and properties of [Al4(OH)8(o-C6H4(CO2)2)2]·H2O, a layered aluminum phthalate. Z Anorg Allg Chem 2013;639 (15):2785–9.

[136] Bon V, Senkovska I, Weiss MS, Kaskel S. Tailoring of network dimensionality and porosity adjustment in Zr- and Hf-based MOFs. CrystEngComm 2013;15(45): 9572–7.

[137] Férey G, Serre C, Mellot-Draznieks C, Millange F, Surblé S, et al. A hhybrid solid with giant pores prepared by a combination of targeted chemistry, simulation, and powder diffraction. Angew Chem Int Ed 2004;43(46):6296–301.

[138] Henninger SK, Jeremias F, Kummer H, Janiak C. MOFs for use in adsorption heat pump processes. Eur J Inorg Chem 2012;2012(16):2625–34.

[139] Wickenheisser M, Jeremias F, Henninger SK, Janiak C. Grafting of hydrophilic ethylene glycols or ethylenediamine on coordinatively unsaturated metal sites in MIL-100(Cr) for improved water adsorption characteristics. Inorg Chim Acta 2013;407:145–52.

[140] Horcajada P, Surblé S, Serre C, Hong DY, Seo YK, et al. Synthesis and catalytic properties of MIL-100(Fe), an iron(iii) carboxylate with large pores. Chem Commun 2007;27:2820–2.

[141] Llewellyn PL, Bourrelly S, Serre C, Vimont A, Daturi M, et al. High uptakes of CO2 and CH4 in mesoporous metal-organic frameworks MIL-100 and MIL-101. Langmuir 2008;24(14):7245–50.

[142] Wang TC, Bury W, Gómez-Gualdrón DA, Vermeulen NA, Mondloch JE, et al. Ultrahigh surface area zirconium MOFs and insights into the applicability of the BET theory. J Am Chem Soc 2015;137(10):3585–91.

[143] Farha OK, Eryazici I, Jeong NC, Hauser BG, Wilmer CE, et al. Metal-organic framework materials with ultrahigh surface areas: is the sky the limit? J Am Chem Soc 2012;134(36):15016–21.

[144] Cmarik GE, Kim M, Cohen SM, Walton KS. Tuning the adsorption properties of UiO-66 via ligand functionalization. Langmuir 2012;28(44):15606–13.

[145] Rode C, Grau K. Moisture buffering and its consequence in whole building hygrothermal modeling. J Build Phys 2008;31(4):333–60.

[146] Rode C, Peuhkuri R, Time B, Svennberg K, Ojanen T. Moisture buffer value of building materials. J ASTM Int (JAI) 2007;4(5):1–12.

[147] Zhang M, Qin M, Rode C, Chen Z. Moisture buffering phenomenon and its impact on building energy consumption. Appl Therm Eng 2017;124:337–45.

[148] Qin M, Belarbi R, Aït-Mokhtar A, Allard F. Simulation of coupled heat and moisture transfer in air-conditioned buildings. Autom ConStruct 2009;18(5): 624–31.

[149] Qin M, Hou P, Wu Z, Wang J. Precise humidity control materials for autonomous regulation of indoor moisture. Build Environ 2020;169:106581.

[150] Daou K, Wang RZ, Xia ZZ. Desiccant cooling air conditioning: a review. Renew Sustain Energy Rev 2006;10(2):55–77.

[151] Shamim JA, Hsu WL, Kitaoka K, Paul S, Daiguji H. Design and performance evaluation of a multilayer fixed-bed binder-free desiccant dehumidifier for hybrid air-conditioning systems: Part I-experimental. Int J Heat Mass Tran 2018;116: 1361–9.

[152] La D, Dai YJ, Li Y, Wang RZ, Ge TS. Technical development of rotary desiccant dehumidification and air conditioning: a review. Renew Sustain Energy Rev 2010; 14(1):130–47.

[153] Kabeel AE. Adsorption-desorption operations of multilayer desiccant packed bed for dehumidification applications. Renew Energy 2009;34(1):255–65.

[154] Hirunlabh J, Charoenwat R, Khedari J, Teekasap S. Feasibility study of desiccant air-conditioning system in Thailand. Build Environ 2007;42(2):572–7.

[155] Zhang LZ, Niu JL. Performance comparisons of desiccant wheels for air dehumidification and enthalpy recovery. Appl Therm Eng 2002;22(12):1347–67.

[156] Yamaguchi S, Saito K. Numerical and experimental performance analysis of rotary desiccant wheels. Int J Heat Mass Tran 2013;60:51–60.

[157] Ge TS, Dai YJ, Wang RZ. Performance study of silica gel coated fin-tube heat exchanger cooling system based on a developed mathematical model. Energy Convers Manag 2011;52(6):2329–38.

[158] Jagirdar M, Lee PS. Mathematical modeling and performance evaluation of a desiccant coated fin-tube heat exchanger. Appl Energy 2018;212:401–15.

[159] Xu F, Bian ZF, Ge TS, Dai YJ, Wang CH, et al. Analysis on solar energy powered cooling system based on desiccant coated heat exchanger using metal-organic framework. Energy 2019;177:211–21.

[160] Cao B, Tu Y, Wang RZ. A moisture-penetrating humidity pump directly powered by one-sun illumination. iScience 2019;15:502–13.

[161] Teo HWB, Chakraborty A, Kitagawa Y, Kayal S. Experimental study of isotherms and kinetics for adsorption of water on aluminium fumarate. Int J Heat Mass Tran 2017;114:621–7.

[162] Feng X, Qin M, Cui S, Rode C. Metal-organic framework MIL-100(Fe) as a novel moisture buffer material for energy-efficient indoor humidity control. Build Environ 2018;145:234–42.

[163] Ge TS, Dai YJ, Wang RZ. Review on solar powered rotary desiccant wheel cooling system. Renew Sustain Energy Rev 2014;39:476–97.

[164] Tu YD, Wang RZ, Ge TS, Zheng X. Comfortable, high-efficiency heat pump with desiccant-coated, water-sorbing heat exchangers. Sci Rep 2017;7:40437.

[165] Tu YD, Wang RZ, Hua LJ, Ge TS. Desiccant-coated water-sorbing heat exchanger: weakly-coupled heat and mass transfer. Int J Heat Mass Tran 2017; 113:22–31.

[166] Hua LJ, Ge TS, Wang RZ. Extremely high efficient heat pump with desiccant coated evaporator and condenser. Energy 2019;170:569–79.

[167] Qin M, Belarbi R, Aït-Mokhtar A, Nilsson LO. Coupled heat and moisture transfer in multi-layer building materials. Construct Build Mater 2009;23(2):967–75.

[168] Abadie MO, Mendonça KC. Moisture performance of building materials: from material characterization to building simulation using the Moisture Buffer Value concept. Build Environ 2009;44(2):388–401.

[169] Woods J, Winkler J, Christensen D. Evaluation of the effective moisture penetration depth model for estimating moisture buffering in buildings. National Renewable Energy Lab. Golden; 2013. U.S.).

[170] Zhang H, Yoshino H, Hasegawa K. Assessing the moisture buffering performance of hygroscopic material by using experimental method. Build Environ 2012;48: 27–34.

[171] Janssen H, Roels S. Qualitative and quantitative assessment of interior moisture buffering by enclosures. Energy Build 2009;41(4):382–94.

[172] Osanyintola OF, Simonson CJ. Moisture buffering capacity of hygroscopic building materials: experimental facilities and energy impact. Energy Build 2006; 38(10):1270–82.

[173] Düren T, Bae YS, Snurr RQ. Using molecular simulation to characterise metal-organic frameworks for adsorption applications. Chem Soc Rev 2009;38(5): 1237–47.

[174] Jhung SH, Lee JH, Yoon JW, Serre C, Férey G, et al. Microwave synthesis of chromium terephthalate MIL-101 and its benzene sorption ability. Adv Mater 2007;19(1):121–4.

[175] Faustini M, Kim J, Jeong GY, Kim JY, Moon HR, et al. Microfluidic approach toward continuous and ultrafast synthesis of metal-organic framework crystals and hetero structures in confined microdroplets. J Am Chem Soc 2013;135(39): 14619–26.
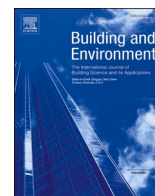
A novel metal-organic frameworks based humidity pump for indoor moisture control

Pumin Hou, Kan Zu, Menghao Qin [*], Shuqing Cui

Department of Civil Engineering, Technical University of Denmark, Lyngby, Denmark

ARTICLE INFO

ABSTRACT

Latent heat load accounts for a significant proportion of energy consumption by air-conditioning, particularly for buildings in humid climates. Traditional vapor-compression refrigeration dehumidification faces problems like refrigerant leakage, overcooling, and complicated mechanical systems. Here, we report a novel humidity pump that uses metal-organic frameworks (MOFs) as desiccant layers to transport moisture from a low-humidity space to a high-humidity one efficiently. The working principle and operation modes of the humidity pump are introduced herein for which the dehumidification performance is investigated at 22.8 °C with 60% RH. The dehumidification rate and moisture removal efficiency of the MIL-100(Fe) based humidity pump reached 26.24 g h^{-1} and 0.87 g Wh^{-1}, respectively, and these are 2.15 and 2.12 times higher than that of the humidity pump with silica gel coating. The maximum dehumidification coefficient of performance (DCOP) of the humidity pump could reach up to ~0.46, higher than the conventional desiccant dehumidification systems. In addition, many factors, such as the cycle time, thermoelectric power, air velocity, etc., which may affect the dynamic characteristics and dehumidification performance, were analyzed. Lastly, the localized humidity management ability of the designed humidity pump using MIL-100(Fe) was validated by a small chamber test. The results indicate that the MOF humidity pump could achieve energy-efficient localized moisture control.

1. Introduction

Energy consumption by buildings has become a worldwide concern. The building sector consumes 40% of the global energy, which is mainly provided by fossil fuels and corresponds to over one-third of carbon dioxide emissions [1,2]. The air conditioning systems account for a significant proportion of the total energy requirement in our living environments. It is worth noting that the latent heat load makes a large proportion of energy for air handling and particularly for buildings in humid climates [3]. Overall, the latent heat load takes up to 20–40% in the air conditioning system [4]. Vapor-compression refrigeration system based on cooling dehumidification is commonly used for indoor temperature and humidity control. During the dehumidification process, the temperature of the air is reduced to the point that is below the dew point in order to condense it. However, this dehumidification method makes the air temperature too low to be directed to the room and needs to be reheated, which causes wastage of energy [5]. By raising the evaporation temperature of 1 °C, the COP of a vapor compression refrigeration system can be increased by about 2.8%, and thus the energy

consumption can be decreased by about 2.5% [6,7]. If the treatment of the latent heat load can be decoupled from the sensible cooling, reducing the temperature of the evaporator to such a low level will not be required. Moreover, it is difficult for vapor compression systems to operate with high performance in small space humidity control applications due to their bulk and complex systems [8]. Therefore, there is a necessity to develop a novel moisture control device for localized humidity management with high efficiency.

To remove the latent heat load separately, many efforts have been dedicated to technologies such as solid dehumidification [9,10], liquid desiccant dehumidification [11,12], membrane dehumidification [13, 14], etc. Combining these dehumidification methods with low-grade energy sources like solar energy and heat pumps can improve dehumidification and energy efficiency [15–17]. However, shortcomings and limitations of these dehumidification methods, such as the problem of re-cooling in rotary solid dehumidification, the growth of bacteria in liquid desiccant dehumidification, have not been solved.

In order to avoid the fresh air dehumidification and to improve air conditioning efficiency, several studies have been done about coating

---

desiccant on the surface of evaporators and condensers [18,19]. Chai et al. combined a desiccant coated heat exchanger (DCHE) with a heat pump for energy saving [20]. Andres et al. investigated the performance of silica gel and sodium acetate composite coated heat exchanger in the summer and winter season [21]. In this case, however, the solid desiccant used is silica gel and its high regeneration temperature reduces the performance of the device significantly. Cui et al. chose porous metal-organic frameworks (MOFs) as advanced sorbents instead of the traditional solid desiccant for which the COP of 7.9 was achieved, demonstrating the superiority of this material [22].

The concept of a humidity pump is inspired by a heat pump. A humidity pump is a device that can transport moisture through the inverse gradient of vapor concentration, i.e., the vapor can be transferred from a relatively low-humidity space to a high-humidity space. For example, in summers, the humidity pump will transfer moisture from cool and less-humid indoor condition to a hot and humid outdoor condition; vice versa, in winters. Li et al. [8] designed a full-solid-state humidity pump based on silica gel, which exhibited good humidity transfer performance without using refrigerant or cooling water. However, the device is limited to the efficiency of mass transfer, and the motor to achieve continuous operation increases the complexity of the device.

Desiccants play an important role in the humidity pump. Traditional desiccants such as silica gel and zeolites possess low adsorption capacity and poor regeneration ability and this limits the development of the adsorption dehumidification system. Though a composite desiccant (silica gel-based, carbon-based, etc.) has been prepared by impregnating hygroscopic salt to enhance the adsorption capacity [23], hygroscopic salts are unstable and deliquesce easily under high humidity. Metal-organic framework (MOF) is a new type of porous crystalline material formed by self-assembly of inorganic metal ions and organic ligands. MOFs possess many good properties like huge internal surface area, large micropore volume, physicochemical and chemical variability as well as low regeneration temperature [24,25]. Although traditional inorganic porous desiccant has been investigated for a humidity pump, the application of MOFs in humidity pump is still worth investigating owing to its high potential in moisture transfer.

In the present study, a humidity pump based on MOFs is fabricated, and its working principle and operation mode are introduced. The performance and impact factors of the device have also been investigated by experiments under different conditions. The localized moisture control ability of the device has been tested experimentally, which provides an important insight to precise moisture control in a confined space.

2. Methodology

2.1. Humidity properties of MIL-100(Fe)

Compared with traditional desiccants, MOFs have greater moisture adsorption capacity and transfer rate due to their huge specific surface area and high porosity. However, the MOFs prepared in early literature had poor water stability, and the pore structure collapsed easily during the process of moisture desorption [26–29]. MOFs prepared by hydrothermal synthesis generally have better water stability. Here, we synthesis MIL-100(Fe) hydrothermally from metal Fe^{3+} ions and trimesic acid. MIL-100(Fe) shows great ability to adsorb moisture from air and can be obtained easily through large-scale synthesis [30–32], making it one of the best choices for humidity pump.

The water adsorption characteristics of MIL-100(Fe) were studied in previous research [21]. Fig. 1 shows the water adsorption isotherms of MIL-100(Fe) at various temperatures. It can be seen that the water adsorption isotherm of MIL-100(Fe) at 20 °C has a stepwise increase between 470 Pa (20% RH) and 1170 Pa (50% RH). This S-shaped isotherm can ensure that the cyclic water uptake is close to the maximum adsorption capacity of dry materials. The maximum difference in moisture content between 20 and 50 °C under 2100 Pa can reach 0.56 kg kg^{-1}, which means the MOF humidity pump possesses the
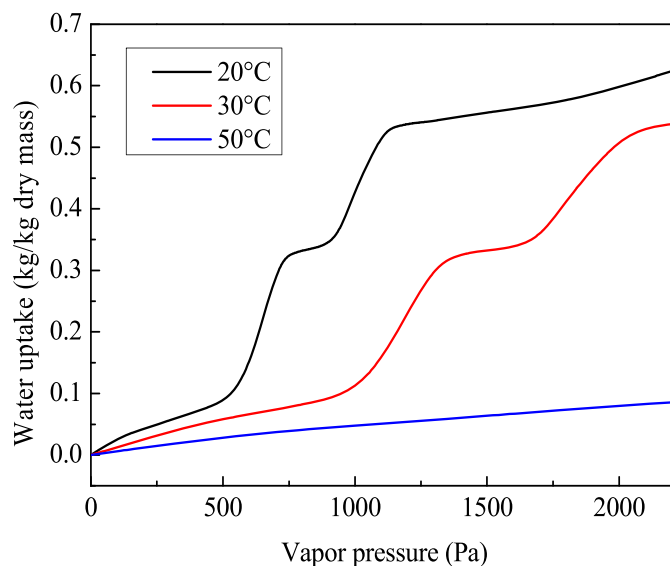
Fig. 1. Water adsorption isotherms of MIL-100(Fe) at different temperatures.

greater potential of adsorption efficiency and has less sensible energy loss by regeneration, as compared to the ones using traditional desiccant such as silica gel.

2.2. Humidity pump based on MIL-100(Fe)

A photograph of MOF based humidity pump is shown in Fig. 2(a). The humidity pump device is fabricated using two MOF coated heat exchangers (MOF-HEx) and two thermoelectric coolers, along with other components. Two aluminum-based plate fins type heat exchangers of the same size (100 mm(L) × 50 mm(W) × 60 mm(H)) are arranged symmetrically as the heat sinks. The plug-in HEx is comprised of 11 fins with a surface area of 0.132 m^2 and 0.5 mm thickness each, while the width of the air channel between each fin is 4 mm. MIL-100(Fe) was coated on the surface of the fins by a water-borne binder of silica sol, which does not affect the water sorption characteristics and capacity. The dry mass of the original heat exchangers and coated MIL-100(Fe) was characterized to be 199.6 g and 45.0 g, respectively. Two thermoelectric coolers (40 mm (L) × 40 mm (W) × 3.8 mm (H)) are stuck in the interlayer between the heat sinks by thermal grease to ensure sufficient contact. The rest of the part of heat sinks not covered by the thermoelectric coolers is blocked by silicon sealant to prevent heat transfer between the hot and cold ends.

Bonded heat sinks and thermoelectric coolers were integrated into an enclosed acrylic box (300 mm(L) × 60 mm(W) × 130 mm(H)) which was divided equally into two volumes by a partition plate. A rectangular cut-out is designed in the middle of the partition plate, corresponding to the size of the surface of the heat sink (100 mm × 50 mm). The periphery of the heat sinks and the partition plate is coated with hot melt adhesive to ensure that it is airtight. Both the upper and lower parts of the acrylic box have two vents of 50 mm diameter connected to the four-way valves and duct fan through the bellows.

A schematic diagram of the MOF based humidity pump is shown in Fig. 2(b). Thermoelectric coolers absorb and release heat at two opposite sides, according to the Peltier effect, when an electrical current passes through it. In this way, the adsorption heat during the dehumidification process is transferred to the other side to improve the temperature of the sink for regeneration. The exchange of dehumidification and regeneration can be achieved by reversal of electrical current and switching four-way valves.
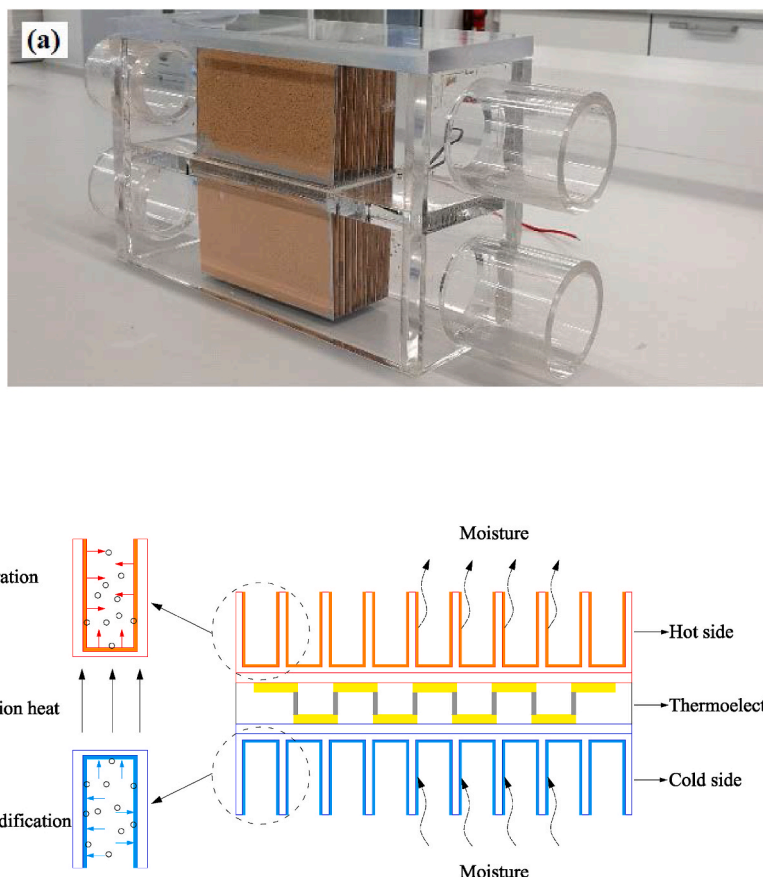
Fig. 2. Photograph and schematic diagram of MOF based humidity pump.

2.3. Working principle

The dehumidification and regeneration processes can be implemented simultaneously when the humidity pump starts running. The detailed working principles can be described in two parts as follows:

Dehumidification: Typically, there are three ways to achieve dehumidification, namely isothermal dehumidification (O→B1), cooling and dehumidification (O→B2), and isenthalpic dehumidification (O→B3). The isothermal methods have been considered as most promising, reported in many refs [8,22], while the other two are, comparatively, not energy-efficient to some extent. In our humidity pump device, moisture can be adsorbed when humid air flows through the surface of MIL-100(Fe) coated fins on the cold side. The dehumidified air can thus be obtained with a subtle temperature rise (O–B shown in Fig. 3). Based on thermodynamic analysis, this can be explained by the total heat transferred on the dehumidification side, which consists of conduction and Joule heat from TEC module, convection heat from inlet air, adsorption heat from the desiccant, and the remaining heat during the switching. Theoretically, by regulating the input power and ventilation quantity, it is feasible to achieve a quick latent load control through a nearly isothermal dehumidification process, the way close to O→B1 (an ideal path).

Regeneration: As for an ideal regeneration condition, desorption of the trapped water vapor in an isothermal regeneration way (O→A1) is preferable. The main reason is that this can lower energy consumption massively. In actual conditions, it is difficult to achieve isothermal regeneration; it is, however, desirable to use fewer energy sources to bring more desorbed water vapor. Considering the interaction between water vapor molecules and desiccant, traditional materials such as zeolite require a high-temperature heat source (>90 °C) to go through the regeneration process (O→A2), while MIL-100(Fe) can be
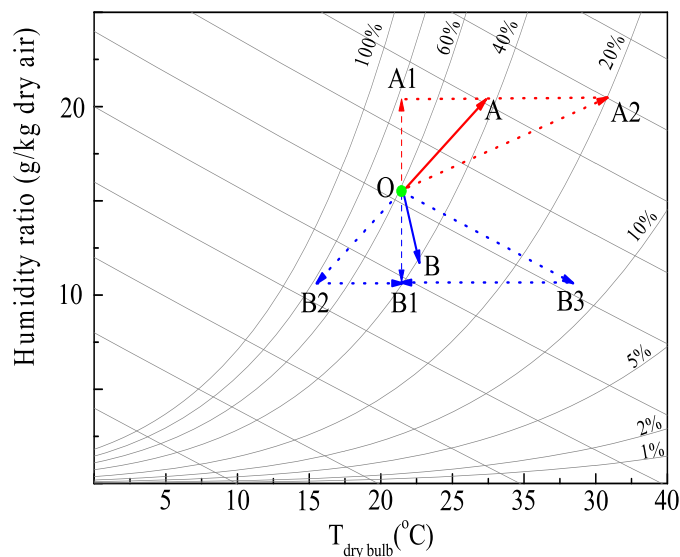

Fig. 3. Working principle: Psychrometric chart of the air treating process in our humidity pump.

regenerated easily with a relatively low-temperature heat source (~50 °C) [22]. In this regard, the heat and mass variation of regeneration air in our device should follow the O→A path, which is specifically between O→A2 and O→A1.

2.4. Operation modes

In this paper, experiments have been carried out in two groups: 1) Mode A- Parameter studies. 2) Mode B- Operation performance of localized humidity control for a small test chamber. The operation parameters including inlet air conditions of dehumidification and regeneration sides are presented in Table 1.

Mode A (Test mode): In this mode, dynamic characteristic and parameter studies have been carried out. The humidity pump device is placed in the test room (like an air cleaner), and the inlet air of both the dehumidification and regeneration sides is the same indoor air. As shown in Fig. 4(a), when the indoor air flows through the dehumidification side, the moisture in the air is adsorbed on the desiccant coated on the fins, leading to a decrease in humidity level. The outlet air from the dehumidification side (dry air) is supplied indoors. Simultaneously, the other batch of indoor air enters the device through the inlet to the regeneration side, flows through the hot side and takes away the moisture released from the desiccant to dry the MOF coatings. The outlet of the regeneration side is exhausted to outdoor. When the desiccant in the dehumidification side saturates, the current flow direction of the thermoelectric cooler is reversed to interchange the roles of dehumidification and regeneration. Meanwhile, only one of the four-way valves (outlet) is rotated by 90° and the state is converted from A1 to A2. Such a reciprocating cycle can realize the continuous operation of the MOF humidity pump.

Mode B (Internal recycle mode): In this intended operation mode for real applications, the inlet air of dehumidification side is always the indoor air, while the inlet air of the regeneration side is always outdoor (ambient) air. The outlet air of the dehumidification side (dry air) is supplied to indoor again. The outlet air of the regeneration side (humid air) is exhausted outdoors. To control the airflow direction, two four-way valves are used as shown in Fig. 4(b), and the airflow passages of the internal recycle channel and external channel are interchanged. The outdoor (ambient) air has no direct heat and mass transfer with the indoor air as these two airflows are completely separated. The outdoor airflow is only used to take away the heat and moisture released by MOF desiccants during the regeneration process. Through a reciprocating cycle, the MOF humidity pump can work continually under internal recycle mode.

2.5. Experimental measurement

Under working mode, the air was supplied to the humidity pump via a duct, and the power of the thermoelectric elements was adjusted and recorded. There were no mechanical operations or moving parts in the whole device. During the dehumidification and regeneration process, temperature and relative humidity of the inlet and outlet air were measured by using digital hygro sensors with accuracy of ±0.2 °C and ±2% RH (SEK-SHTC3-Sensors, Sensirion). The airflow rate was adjusted by variable frequency fan (LH-50P, Jiuyefeng Environmental Technology Co., Ltd.) and recorded by an anemograph (Testo 410-1). The current and voltage of the thermoelectric cooler and the fan under different

Table 1
Operation conditions of different modes.

Operation mode	Parameters	Values
Test mode	Inlet air conditions of De/Re side	22.8 °C, 60%RH
	Cycle time	5min, 10min, 15min
	Thermoelectric power	15 W, 20 W, 25 W
	Air velocity	1.5 m/s, 3.5 m/s, 4.2 m/s
Internal recycle mode	Initial inlet air conditions	23 °C, 81%RH
	Cycle time	10min
	Thermoelectric power	30 W
	Air velocity	2.4 m/s

conditions were recorded for the calculation of power consumed.

2.6. Performance indexes

To evaluate the performance of MOF-based humidity pump as a function of the power input and the temperature and humidity ratio of inlet and outlet air, some parameters herein have been analyzed:

1) Dehumidification rate (E_d): It represents the moisture removal over a period of time, which is computed as follows:

$$E_d = \frac{\int_{t_1}^{t_2} q_a(d_{in} - d_{out})dt}{\Delta t} \tag{1}$$

where E_d (g s^{-1}) is dehumidification rate; q_a (m^3 s^{-1}) is the volume flow. d_{in} and d_{out} (g m^{-3}) are moisture content of inlet and outlet air during dehumidification process, respectively. t_1 and t_2 represent the beginning and end of a dehumidification process when it comes to equilibrium. Δt is the time of one dehumidification process, and can be calculated by $\Delta t = t_2 - t_1$.

2) Moisture removal efficiency (η): It represents the power consumption (P_e) to approach to the dehumidification rate (E_d):

$$\eta = \frac{E_d}{P_e} \tag{2}$$

where η (g Wh^{-1}) indicates the moisture removal efficiency. P_e (kW) is the total power consumption (including thermoelectric coolers and duct fans).

3) Dehumidification coefficient of performance (DCOP) represents the ratio of air enthalpy variation during the dehumidification process to the total power consumption for the regeneration process:

$$DCOP = \frac{q_a(h_{in} - h_{out})}{P_e} \tag{3}$$

where h_{in} and h_{out} are the air enthalpies of inlet and outlet process air.

3. Results and discussion

3.1. Dynamic characteristics

The dynamic characteristics of the device are analyzed in terms of temperature and humidity of inlet and outlet air. In order to compare the cycling performance of dehumidification and regeneration sides, inlet air conditions for these two sides were maintained the same. Thus, the detailed experimental conditions can be shown as follows: the temperature and relative humidity of inlet air are about 22.8 °C and 60%. The velocity of inlet air is 1.5 m/s. The current of the thermoelectric cooler is 2.66 A, its voltage is 11.32 V, and the calculated power is about 30 W.

When it comes to the equilibrium, Fig. 5 shows the variation of temperature and humidity at the inlet and outlet of dehumidification and regeneration sides. The operation consists of dehumidification and regeneration processes, and several cycles are performed until stabilization is reached. The period from 0 to 10 min is the regeneration process corresponding to the regeneration side. It can be seen that the temperature of the outlet air rises sharply at the beginning and then gradually flattens. The moisture content of the outlet air initially increased in line with the temperature, but then decreased gradually. This is because the vapor in MIL-100 (Fe) coatings desorbs as the temperature of the heat exchanger rises sharply. As the desorption proceeds, water vapor content in the desiccant coating decreases gradually, along with the rate of desorption, resulting in a gradual decrease in the moisture content in the outlet air. The dehumidification and regeneration channels are switched over during the period from 10 to 20min. The
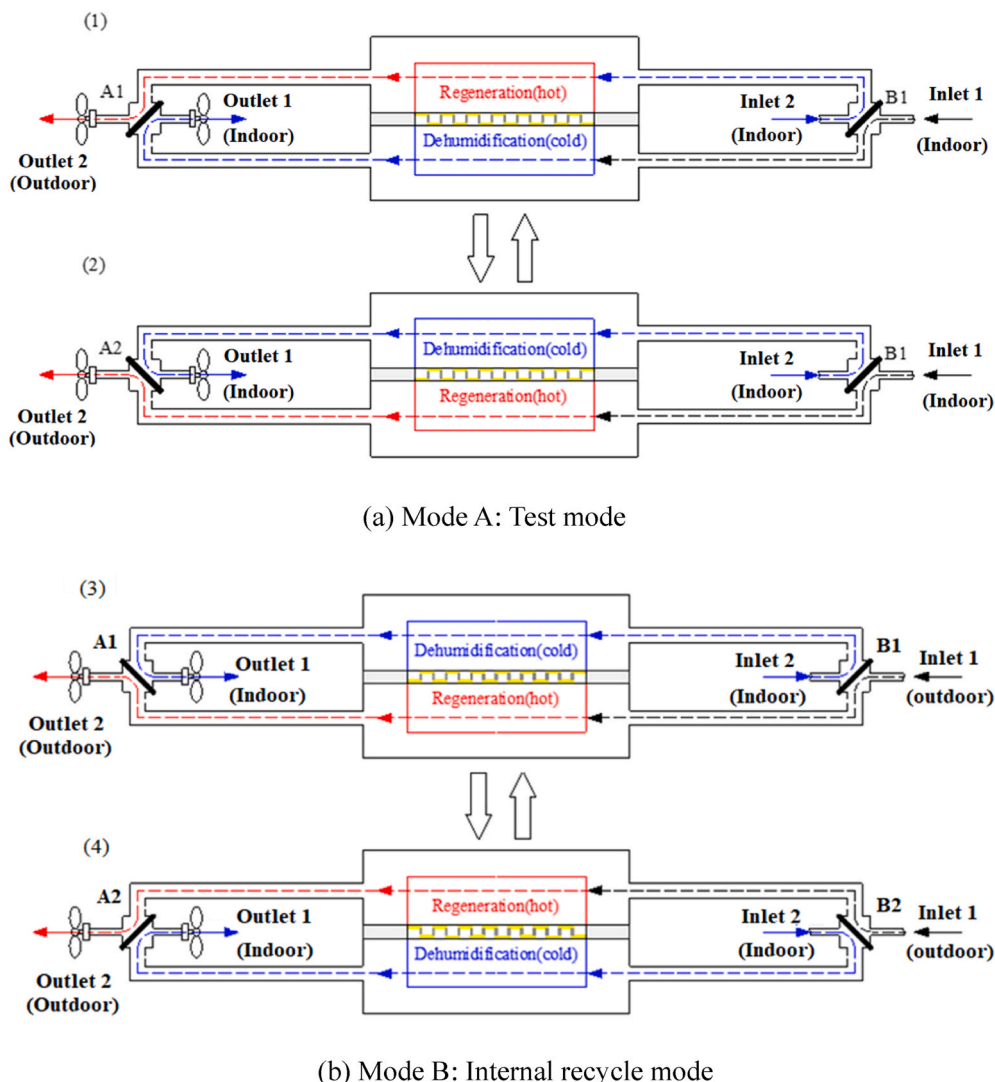
(a) Mode A: Test mode

(b) Mode B: Internal recycle mode

Fig. 4. The operation modes of MOF humidity pump.

outlet air temperature decreases rapidly; but the temperature of the outlet air is, however, still higher than the inlet air. According to the thermodynamic analysis in the previous section, the cooling load of the cold side of TEC cannot remove all the sensible loads to be as cool as the inlet air, but the temperature rise was limited. The average outlet temperature at the dehumidification channel is close to 25.5 °C. Besides, the adsorption heat also increases the temperature of the air. At the same time, when the air flows through the heat exchanger, the water vapor in the air is adsorbed on the MIL-100 (Fe) coating, and the moisture content decreases sharply. As the coating material becomes saturated gradually from the outside to the inside of the layer, the dehumidification rate also decreases gradually.

3.2. Performance of the humidity pump with different desiccants

Based on the same experimental conditions described in Section 3.1, inlet air condition remains at 22.8 °C and 60%RH. Air velocity is set at 1.5 m/s. The power of thermoelectric cooler is around 30 W. From Fig. 6, it shows the difference in moisture content between the inlet and outlet air of the humidity pump with silica gel and MIL-100(Fe) coatings. It can be seen that the humidity pump with MIL-100(Fe) coating shows greater adsorption and desorption rate than that of the silica gel coating while the attenuation rate is slower. This happens because the regeneration temperature of MIL-100 (Fe) is lower, and the moisture storage capacity

is larger than that of silica gel. The operation indices are calculated based on Eqs. (1) and (2). The dehumidification rate and moisture removal efficiency of humidity pump with silica gel coating are 12.23 g h^{-1} and 0.41 g Wh^{-1}, respectively, and for MIL-100(Fe) coating are 26.24 g h^{-1} and 0.87 g Wh^{-1}, respectively. The values of the MOF based humidity pump were 2.15 and 2.12 times greater than that of silica gel.

3.3. Dehumidification performance

3.3.1. Cycle time

According to the previous analysis of dynamic characteristics, it can be observed that as the operating time goes on, the moisture removed by MIL-100(Fe) coating decreases gradually. This indicates that the cycle time has an important effect on the performance of the device. The thermoelectric power is maintained at 30 W while the air speed is 1.5 m/s. A series of experiments with different cycle times were carried out. The moisture content difference between the inlet and outlet air of the humidity pump is shown in Fig. 7. As the cycle time increases from 5 to 10 and 15min, the peak value of moisture content difference decreases from −3.10 to −3.35 and −3.38 g m^{-3} at the dehumidification side, and increases from 2.92 to 3.18 and 3.39 g m^{-3} at the regeneration side, respectively. The absolute values of maximum moisture content difference increase with the increase in cycle time because the regeneration of desiccant becomes sufficient as the cycle time increases. It can also be
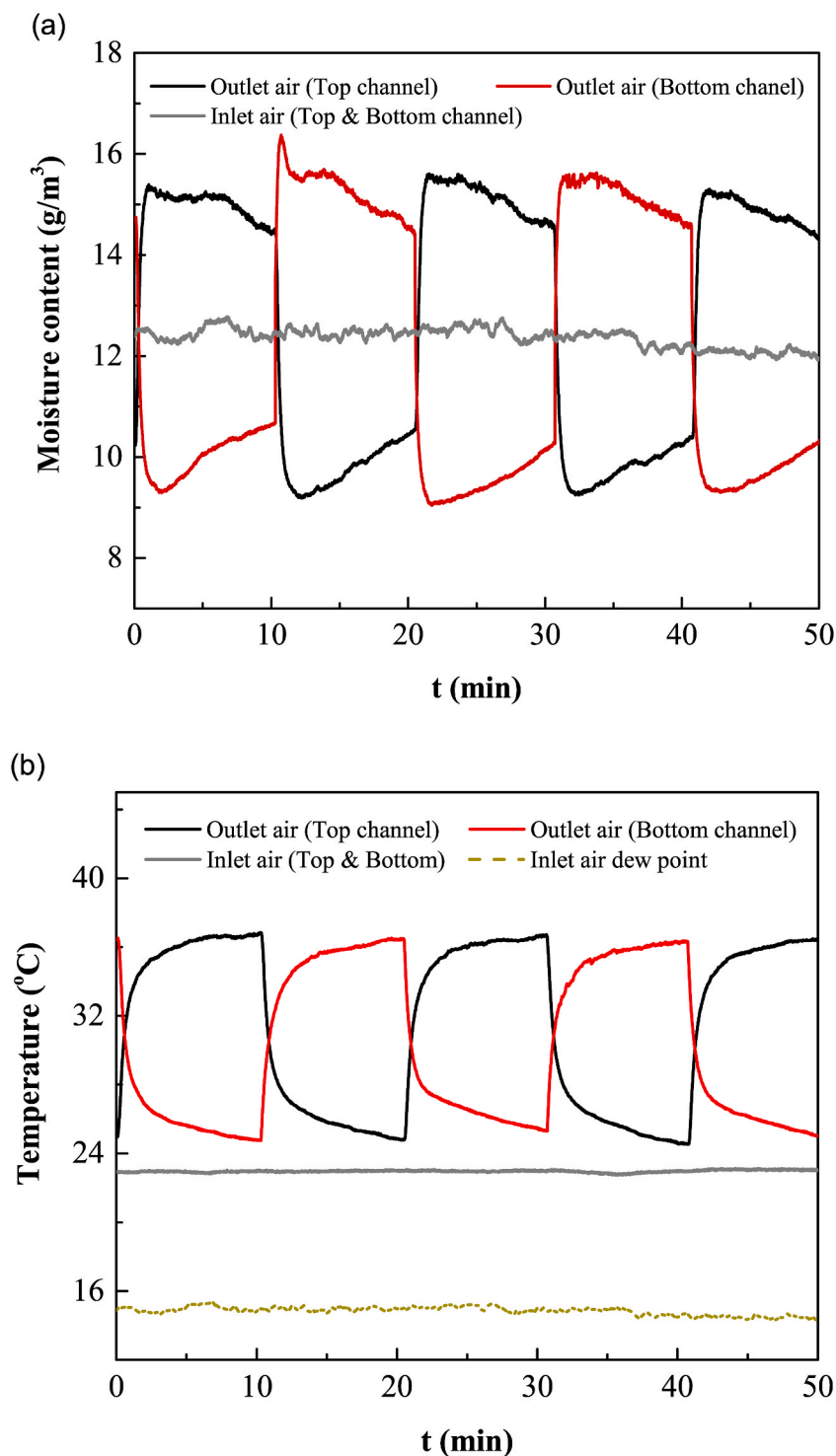
(a)

(b)

Fig. 5. Temperature and moisture content of inlet and outlet air in Mode A.

seen from Fig. 7 that the attenuation of moisture content difference is more serious with the increase in cycle time as the desiccant coating saturates gradually, with the increase of operating cycle time, and the dehumidification capacity decreases.

Fig. 8 shows the effect of cycle time on the performance of the humidity pump. It can be seen that the dehumidification rate and moisture removal efficiency increase at first and then decrease with the increase in cycle time, determined by the peak value of the moisture content difference and the decay degree. This can be attributed to the decay characteristics of the adsorption and regeneration ability of the MIL-100

(Fe) layers at different cycle times. DCOP increases as the cycle time increases, but the rate of the rise is restricted after 10min of cycle time in our case.

3.3.2. Thermoelectric power

Thermoelectric power, which has an important effect on the regeneration of the desiccant layer, determined the temperature difference between the hot and cold sides. The cycle time is set to 10 min and the air speed is 1.5 m/s. Several experiments with different input power of the thermoelectric cooler are carried out and the moisture content

25
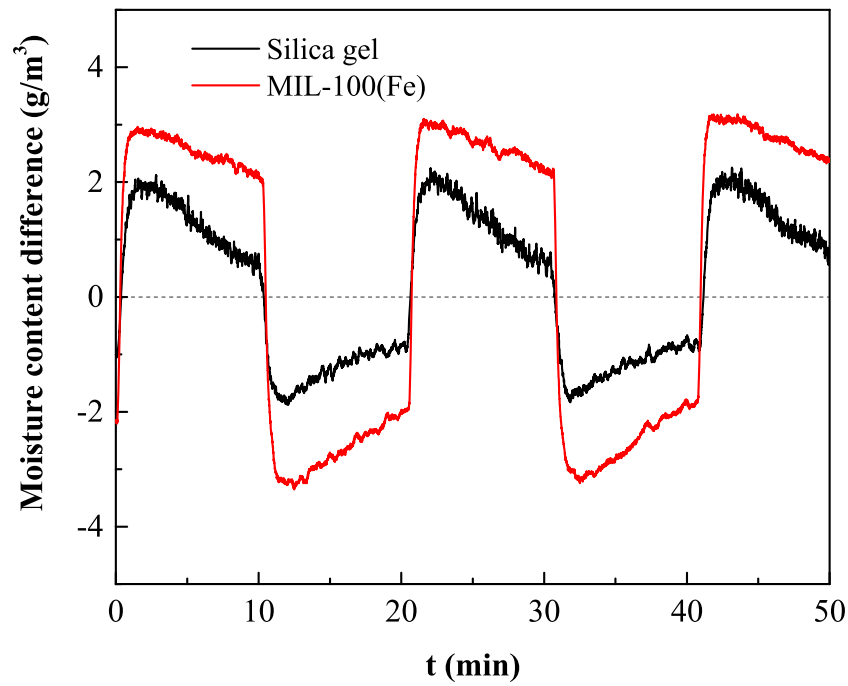
Fig. 6. Moisture content difference of humidity pump using silica gel and MIL-100(Fe).
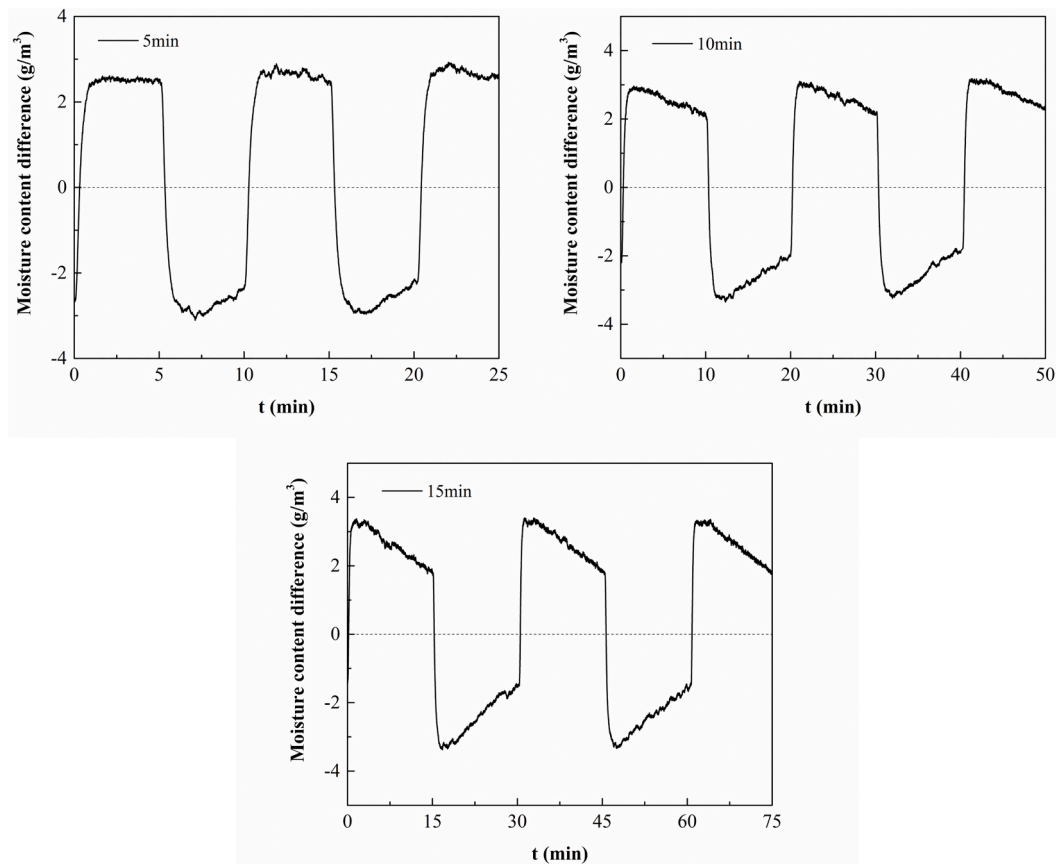

Fig. 7. Moisture content difference of humidity pump with the different cycle times.

differences between the inlet and outlet air of the humidity pump are shown in Fig. 9. Comparing the moisture content difference between the three cases, it can be seen that the lower power, the smaller the moisture content difference between the inlet and outlet air. Particularly

at 15 W, there is almost no dehumidification ability at the end of the cycle time. Further analysis found that as the mode changed from dehumidification to regeneration, the moisture content difference first rises rapidly and then drops sharply, a tip is formed. Thus, the lower the
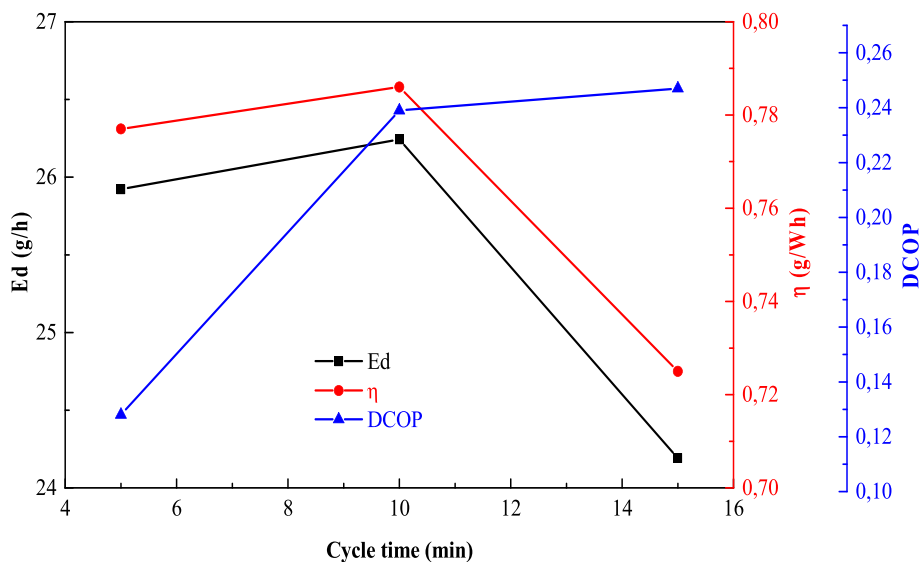
Fig. 8. Effect of cycle time on the performance of humidity pump.
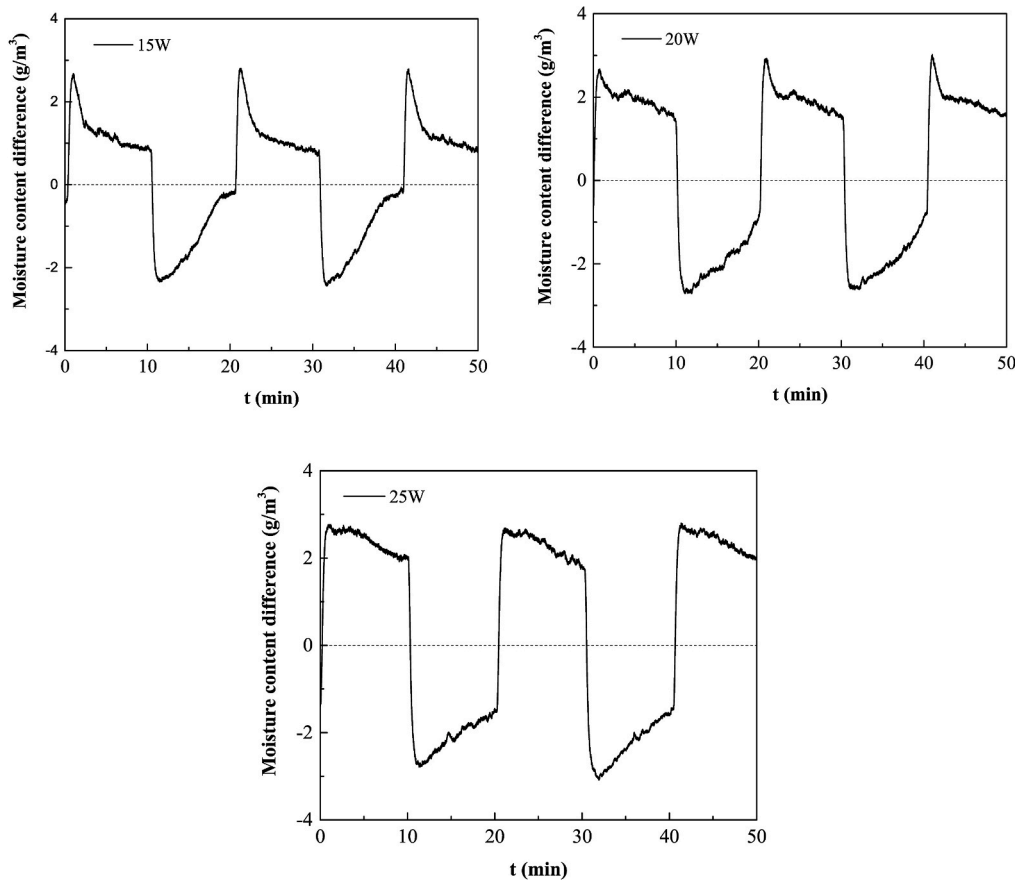
Fig. 9. Moisture content difference of humidity pump with different power.

thermoelectric power, the sharper the tip is. Insufficient power results in lower temperature differences between the hot and cold sides affecting the regeneration of the desiccant layer.

Fig. 10 shows the impact of thermoelectric power on the performance of the humidity pump. With the increase of thermoelectric power from 15 W to 25 W, the dehumidification rate increases from 20.5 to 31.9 g h^{-1}, suggesting that the dehumidification rate increases with the increase of thermoelectric power. The greater the thermoelectric power,

the higher the temperature of the hot side, and the better the regeneration. The moisture removal efficiency increases at first and then decreases with the increase of thermoelectric power showing the same changing trend as DCOP. In this regard, too high thermoelectric power would have a negative impact on moisture removal efficiency and DCOP. As the thermoelectric power increases to a certain degree, the temperature achieved is enough for the regeneration of MIL-100 (Fe). Excessive power will increase the energy consumption and will have no
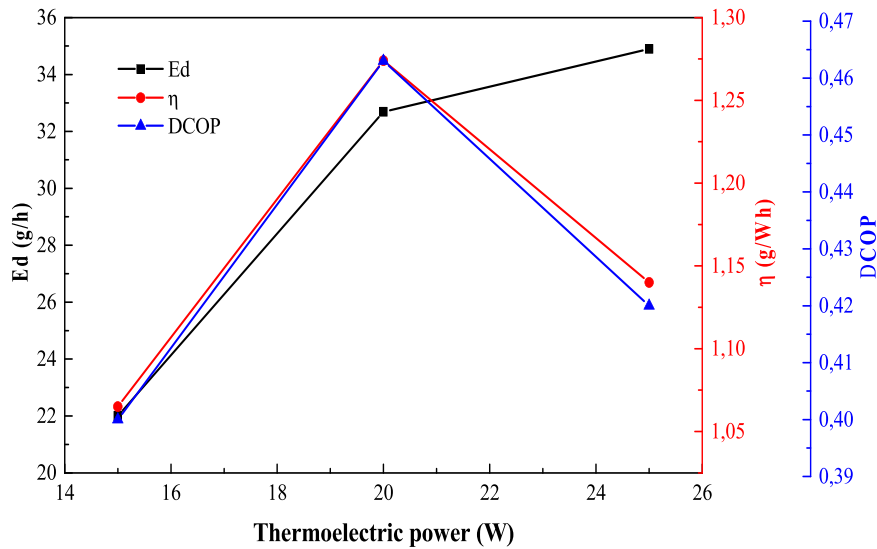
Fig. 10. Effect of thermoelectric power on the performance of humidity pump.

obvious effect on improving regeneration efficiency.

3.3.3. Air velocity

Air velocity is another important factor of the humidity pump. The cycle time is set to 10 min and the thermoelectric power was 30 W. Several experiments with variable air velocity are carried out, and the moisture content difference between inlet and outlet air of the humidity pump is shown in Fig. 11. As the air velocity increases, the peak value of moisture content difference between the inlet and outlet air during dehumidification and regeneration processes decreases. On the one

hand, airflow increases with the increasing air velocity, which would increase the moisture content of the air, while on the other hand, heat transfer of the fins is enhanced by increasing the air velocity. This would reduce the temperature of the heat sink and the regeneration performance.

Fig. 12 shows the effect of air velocity on the performance of the humidity pump. Both the dehumidification rate and moisture removal efficiency increase first and then decrease as the air velocity increases. Also, excessive air velocity has a negative effect on the performance of the humidity pump owing to the reduction in regeneration temperature
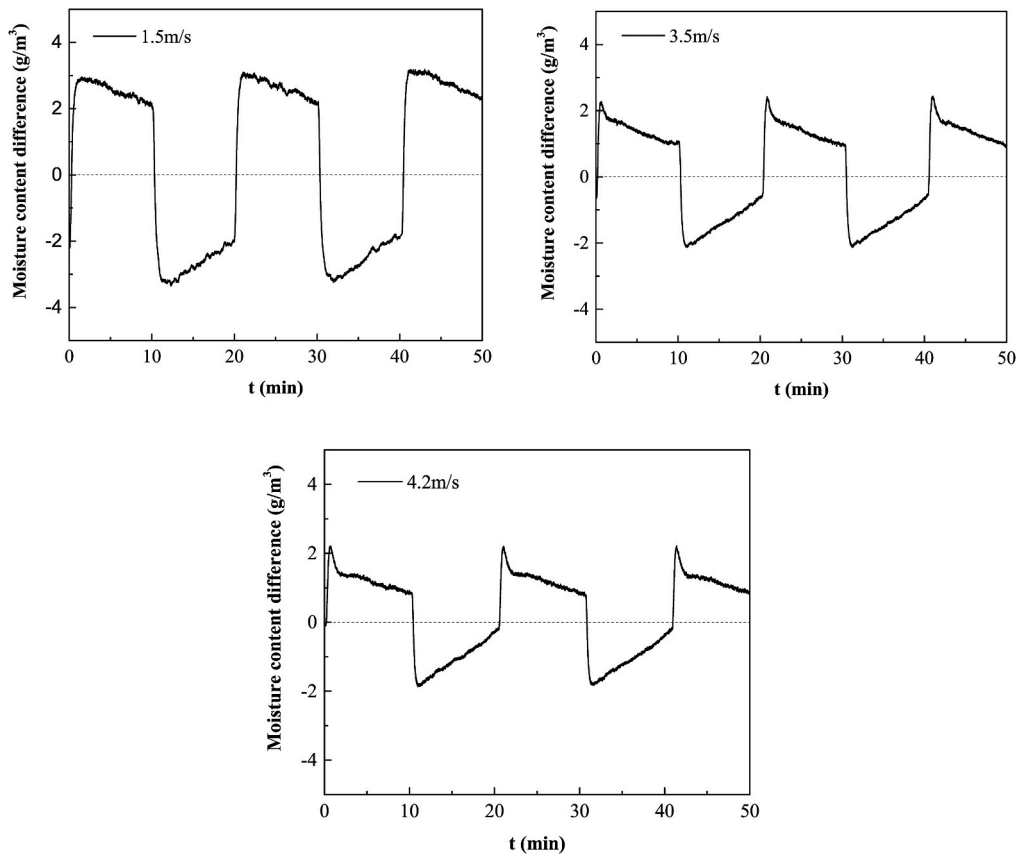

Fig. 11. Moisture content difference of humidity pump with different air velocity.
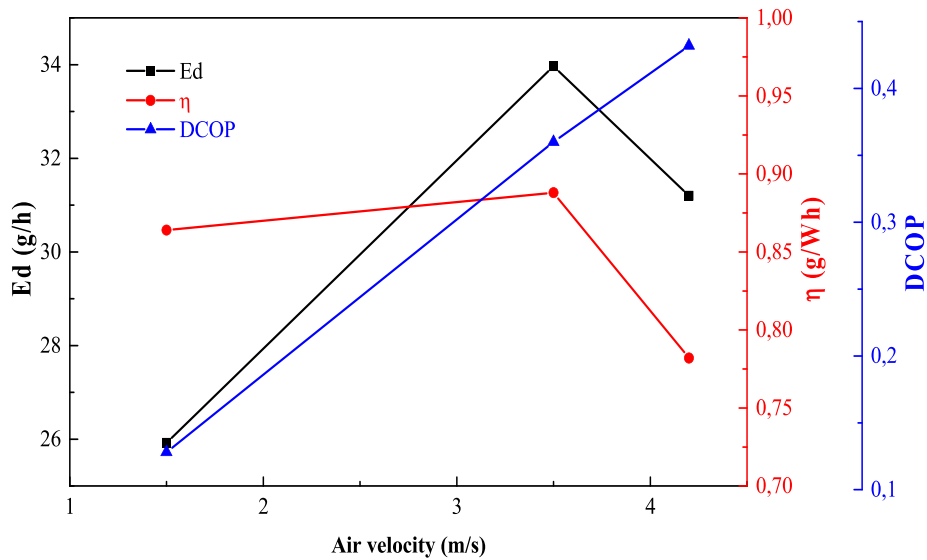
Fig. 12. Effect of air velocity on the performance of the humidity pump.

on the hot sides with the increase in air velocity. Besides, the energy consumption of the pump also increases with increasing air velocity. However, based on our measured results, it can be found that DCOP can be raised linearly with the air velocity. Based on comprehensive consideration (E_d, η and DCOP), there is an equilibrium point for air velocity around 3.5 m/s.

3.4. Humidity control ability

In order to investigate the actual humidity management ability when exposed to a real conditions, a test chamber ($32.5 \times 54 \times 40.3$ cm) made of polystyrene foam (insulation material) is prepared for the humidity pump dehumidification experiment. The initial conditions are maintained at 23 °C and 81% RH (average value), while there are no heat or moisture dissipation sources in the experimental system. The box is connected to the humidity pump by plastic bellows. The schematic diagram of the experimental system is shown in Fig. 13, and the operating conditions are shown as follows: the cycle time is set to 10 min, the thermoelectric power is 30 W, and the air velocity is 2.4 m/s. The digital hygro sensors are installed to record the temperature and humidity variation against time.

Fig. 14 shows the temperature and humidity conditions inside the test chamber during the experiments. Here, the measured results indicate that the temperature in the interior space fluctuates in a zigzag manner. Compared with the environment, the maximum temperature rise in interior space during the experiment is 1.52 °C over 1.3 h, as the
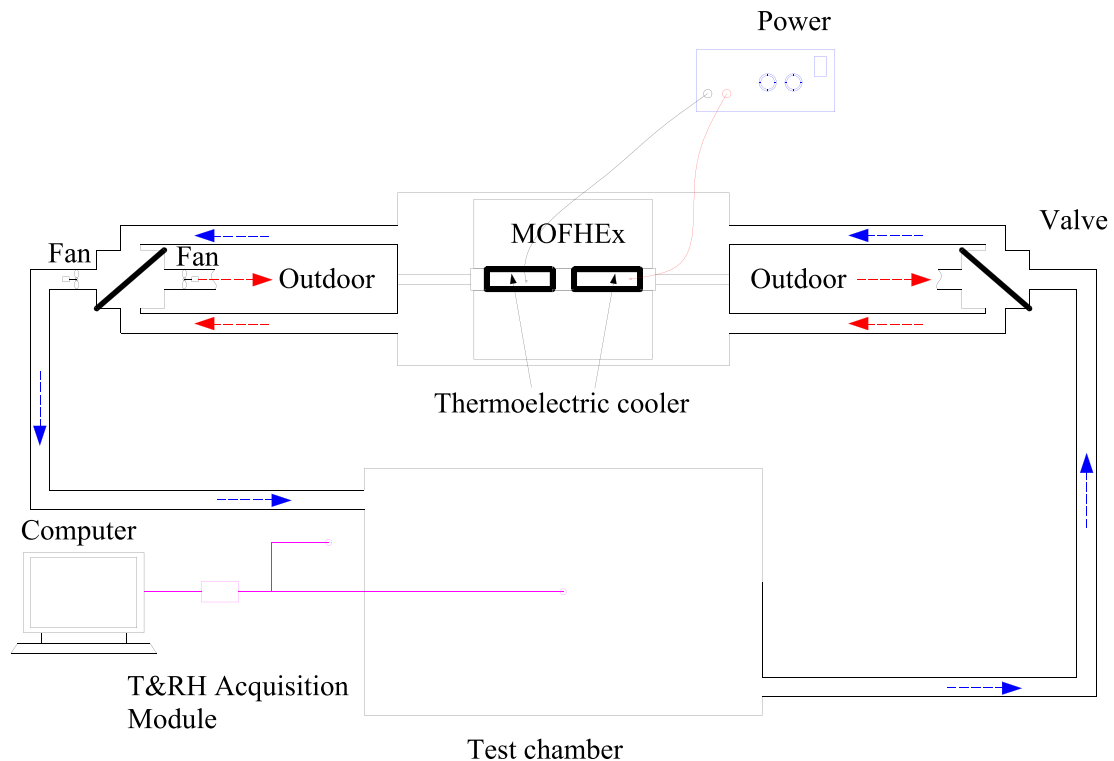

Fig. 13. Schematic diagram of the experimental system.
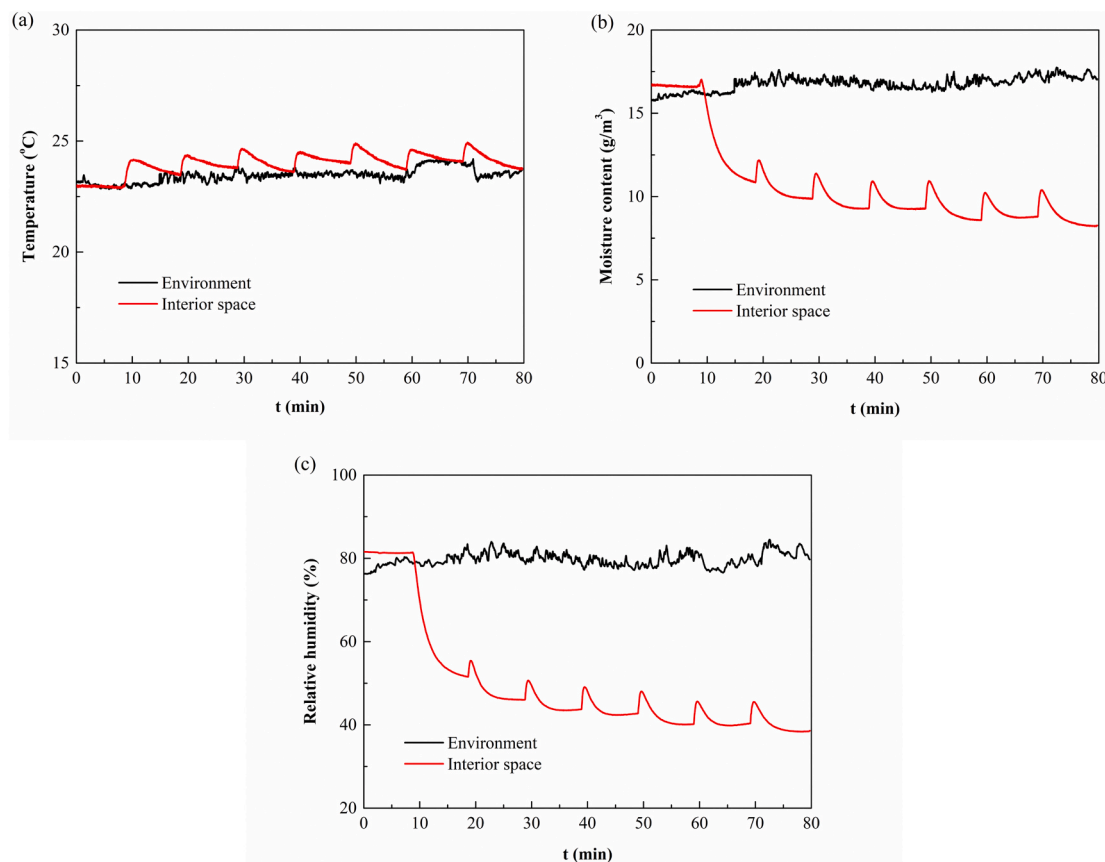
Fig. 14. Temperature and humidity changes inside the test chamber.

fin temperature cannot be reduced immediately when the regeneration process is switched to the dehumidification process. The relative humidity of the interior space is decreased quickly from ~80% to 38%RH, corresponding to the absolute humidity from 16.7 to 8.2 g m^{-3}. There are no heat source and moisture dissipation sources inside the test chamber, as mentioned above. It is important to mention that the interior relative humidity stops decreasing at the trigger point of MOF desiccants, which is around 40% for MIL-100(Fe). It means that MIL-100 (Fe) stops adsorbing a large amount of moisture when the indoor RH is below 40%, and can be seen clearly from the water sorption isotherm of MIL-100(Fe) [33]. It is known that many MOFs have S-shape isotherms and exhibit a steep uptake isotherm at the specific relative humidity depending on the targeted application [34]. For indoor humidity control, the steep uptake should around 40%. This can be noted as one of the main advantages of MOFs over other conventional desiccants. Some MOF materials can control indoor relative humidity autonomously, within the desired comfort range at room temperature [35]. Additionally, different MOFs have different trigger points and can be used for different moisture control applications [34,35]. Based on our measurements, it is seen that MIL-100(Fe) based humidity pump has a satisfactory response to handle the latent load of the test chamber.

4. Conclusion

In this paper, a novel humidity pump that uses MOF as desiccant layers has been demonstrated. A series of experiments were carried out to investigate the dynamic characteristics and factors including cycle time, thermoelectric power, and air velocity. The dehumidification rate, moisture removal efficiency and DCOP were also calculated under different conditions. The conclusions are summarized as follows:

(1) The humidity pump can be used to achieve dehumidification above the dew point temperature, thereby improving the dehumidification efficiency. Latent heat and adsorption heat can be handled by the desiccant layer and thermoelectric cooler, respectively, which can realize the dehumidification and regeneration processes simultaneously. Four-way valves are used to achieve the continuous operation of the humidity pump and the conversion of the operation mode, making the mechanical system simplified.

(2) The dehumidification performance of the humidity pump that uses MIL-100(Fe) as the desiccant layer is superior to that of the humidity pump that uses silica gel. The dehumidification rate, moisture removal efficiency, and DCOP of the MOF based humidity pump are found to be as high as 34.9 g h^{-1}, 1.14 g Wh^{-1}, and 0.46, respectively, which are all around twice higher than that of silica gel coated systems.

(3) The dehumidification rate and moisture removal efficiency increase at first and then decrease with the increase of cycle time and air velocity, while the DCOP increases as the temperature rises. The dehumidification rate also increases with the increase of thermoelectric power. The moisture removal efficiency and DCOP increase first and then decrease with the increase of thermoelectric power. A too high thermoelectric power may have a negative impact on the moisture removal efficiency and DCOP.

(4) The MOF based humidity pump achieves a quick localized humidity control. The internal relative humidity level can thus be maintained at the trigger point of MOF desiccants.

Declaration of competing interest

The authors declare that they have no known competing financial interests or personal relationships that could have appeared to influence

the work reported in this paper.

All authors declare no conflict of interest.

References

[1] IEA, Energy Technology Perspectives, International Energy Agency, 2017, 2017. ISBN978-92-64-27597-3.

[2] Z. Wu, M. Qin, M. Zhang, Phase change humidity control material and its impact on building energy consumption, Energy Build. 174 (2018) 254–261.

[3] M. Qin, J. Yang, Evaluation of different thermal models in EnergyPlus for calculating moisture effects on building energy consumption in different climate conditions, Build. Simulat. 9 (2016) 15–25.

[4] F. Zhang, Y. Yin, X. Zhang, Performance analysis of a novel liquid desiccant evaporative cooling fresh air conditioning system with solution recirculation, Build. Environ. 117 (2017) 218–229.

[5] K. Chua, S. Chou, W. Yang, J. Yan, Achieving better energy-efficient air conditioning–a review of technologies and strategies, Appl. Energy 104 (2013) 87–104.

[6] R. Yumrutaş, M. Kunduz, M. Kanoğlu, Exergy analysis of vapor compression refrigeration systems, Exergy Int. J. 2 (2002) 266–272.

[7] A. Chan, V. Yeung, Implementing building energy codes in Hong Kong: energy savings, environmental impacts and cost, Energy Build. 37 (2005) 631–642.

[8] B. Li, L. Hua, Y. Tu, R. Wang, A full-solid-state humidity pump for localized humidity control, Joule 3 (6) (2019) 1427–1436.

[9] M. Sultan, I. El-Sharkawy, T. Miyazaki, B. Saha, S. Koyama, An overview of solid desiccant dehumidification and air conditioning systems, Renew. Sustain. Energy Rev. 46 (2015) 16–29.

[10] K. Rambhad, P. Walke, D. Tidke, Solid desiccant dehumidification and regeneration methods-A review, Renew. Sustain. Energy Rev. 59 (2016) 73–83.

[11] L. Mei, Y. Dai, A technical review on use of liquid-desiccant dehumidification for air-conditioning application, Renew. Sustain. Energy Rev. 12 (2008) 662–689.

[12] A. Lowenstein, Review of liquid desiccant technology for HVAC applications, HVAC R Res. 14 (2008) 819–839.

[13] C. Isetti, E. Nannei, A. Magrini, On the application of a membrane air—liquid contactor for air dehumidification, Energy Build. 25 (1997) 185–193.

[14] B. Yang, W. Yuan, F. Gao, B. Guo, A review of membrane-based air dehumidification, Indoor Built Environ. 24 (2015) 11–26.

[15] A. Yadav, V. Bajpai, Experimental comparison of various solid desiccants for regeneration by evacuated solar air collector and air dehumidification, Dry. Technol. 30 (2012) 516–525.

[16] K. Gommed, G. Grossman, Experimental investigation of a liquid desiccant system for solar cooling and dehumidification, Sol. Energy 81 (2007) 131–138.

[17] L. Zhang, N. Zhang, A heat pump driven and hollow fiber membrane-based liquid desiccant air dehumidification system: modeling and experimental validation, Energy 65 (2014) 441–451.

[18] T. Ge, Y. Dai, R. Wang, Z. Peng, Experimental comparison and analysis on silica gel and polymer coated fin-tube heat exchangers, Energy 35 (2010) 2893–2900.

[19] X. Sun, Y. Dai, T. Ge, Y. Zhao, R. Wang, Comparison of performance characteristics of desiccant coated air-water heat exchanger with conventional air-water heat exchanger–Experimental and analytical investigation, Energy 137 (2017) 399–411.

[20] S. Chai, X. Sun, Y. Zhao, Y. Dai, Experimental investigation on a fresh air dehumidification system using heat pump with desiccant coated heat exchanger, Energy 171 (2019) 306–314.

[21] S. Andres, X. Sun, T. Ge, Y. Dai, R. Wang, Experimental investigation on performance of a novel composite desiccant coated heat exchanger in summer and winter seasons, Energy 166 (2019) 506–518.

[22] S. Cui, M. Qin, A. Marandi, V. Steggles, S. Wang, et al., Metal-Organic Frameworks as advanced moisture sorbents for energy-efficient high temperature cooling, Sci. Rep. 8 (2018) 15284.

[23] X. Zheng, T. Ge, R. Wang, Recent progress on desiccant materials for solid desiccant cooling systems, Energy 74 (2014) 280–294.

[24] G. Férey, C. Mellot-Draznieks, C. Serre, F. Millange, J. Dutour, et al., A chromium terephthalate-based solid with unusually large pore volumes and surface area, Science 309 (2005) 2040–2042.

[25] O. Yaghi, M. O'Keeffe, N. Ockwig, H. Chae, M. Eddaoudi, et al., Reticular synthesis and the design of new materials, Nature 423 (2003) 705.

[26] A. Cadiau, Y. Belmabkhout, K. Adil, P. Bhatt, R. Pillai, et al., Hydrolytically stable fluorinated metal-organic frameworks for energy-efficient dehydration, Science 356 (2017) 731–735.

[27] D. Alezi, I. Spanopoulos, C. Tsangarakis, A. Shkurenko, K. Adil, et al., Reticular chemistry at its best: directed assembly of hexagonal building units into the awaited metal-organic framework with the intricate polybenzene topology, pbz-MOF [J], J. Am. Chem. Soc. 138 (2016) 12767–12770.

[28] P. Bhatt, Y. Belmabkhout, A. Cadiau, K. Adil, O. Shekhah, et al., A fine-tuned fluorinated MOF addresses the needs for trace CO_2 removal and air capture using physisorption, J. Am. Chem. Soc. 138 (2016) 9301–9307.

[29] J. Low, A. Benin, P. Jakubczak, J. Abrahamian, S. Faheem, et al., Virtual high throughput screening confirmed experimentally: porous coordination polymer hydration, J. Am. Chem. Soc. 131 (2009) 15834–15842.

[30] P. Horcajada, S. Surblé, C. Serre, D. Hong, Y. Seo, et al., Synthesis and catalytic properties of MIL-100 (Fe), an iron (III) carboxylate with large pores, Chem. Commun. (J. Chem. Soc. Sect. D) (2007) 2820–2822.

[31] Y. Seo, J. Yoon, J. Lee, U. Lee, Y. Hwang, et al., Large scale fluorine-free synthesis of hierarchically porous iron (III) trimesate MIL-100 (Fe) with a zeolite MTN topology, Microporous Mesoporous Mater. 157 (2012) 137–145.

[32] P. Hou, M. Qin, S. Cui, K. Zu, Preparation and characterization of metal-organic framework/microencapsulated phase change material composites for indoor hygrothermal control, J. Build. Eng. 31 (2020) 101345.

[33] X. Feng, M. Qin, S. Cui, C. Rode, Metal-organic framework MIL-100(Fe) as a novel moisture buffer material for energy-efficient indoor humidity control, Build. Environ. 145 (2018).

[34] K. Zu, M. Qin, S. Cui, Progress and potential of metal-organic frameworks (MOFs) as novel desiccants for built environment control: a review, Renew. Sustain. Energy Rev. 133 (2020).

[35] M. Qin, P. Hou, Z. Wu, J. Huang, Precise humidity control materials for autonomous regulation of indoor moisture, Build. Environ. 169 (2020).

SCIENTIFIC REP🌣RTS

Metal-Organic Frameworks as advanced moisture sorbents for energy-efficient high temperature cooling

Shuqing Cui [ID]^{1,3}, Menghao Qin^1, Afsaneh Marandi^2, Victoria Steggles^2, Sujing Wang^2, Xiaoxiao Feng^1, Farid Nouar^2 & Christian Serre^2

Latent cooling load accounts for 30% of the total load of air-conditioning, and its proportion is even higher in many tropical and subtropical climates. Traditional vapour-compression air-conditioning (VCAC) has a low coefficient of performance (COP) due to the refrigeration dehumidification process, which often makes necessary a great deal of subsequent re-heating. Technologies using conventional desiccants or sorbents for indoor moisture control are even less competitive than VCAC due to their high regeneration temperature, long cycling time and bulky components. Here, we report a novel high temperature cooling system that uses porous metal-organic frameworks (MOFs) as advanced sorbents for humidity control. We directly coat MOFs on the surface of evaporator and condenser. The system has no additional components compared to a traditional VCAC. The evaporator can simultaneously remove both the sensible and latent loads of the incoming air without reducing the temperature below its dew point. The regeneration of wet MOFs is completely driven by the residual heat from the condenser. The MOF-coated heat exchangers can achieve a cooling power density of 82 W·L^{-1}. We demonstrate that the system has a high COP, up to 7.9, and can save 36.1% of the energy required, compared to the traditional VCAC system with reheating. The amphiphilic MOFs used in the research have high water uptake, are made of low-cost raw materials and have high hydrothermal stability. They thus have the potential for being scaled up for large-scale applications in air conditioning.

Buildings are responsible for 30% of global annual greenhouse gas emissions and consume up to 40% of all energy. Energy demand in the building sector could increase by another 30% in the next forty years if no further actions are taken[1]. Transitions to the 2 °C targets set in the Paris Agreement require the rate of increase to be reduced by 50%. Outpacing other end uses in buildings, the growth in cooling energy demand has multiplied by 2 and 5 times respectively in OECD and non-OECD countries since 1990[1]. There is an urgent need to develop energy-efficient cooling technologies to reduce building energy consumption. Conventional vapour-compression air conditioners normally have a coefficient of performance (COP) around 3 in practice[2]. The low COP is primarily due to the refrigeration dehumidification process. By cooling the air below the dew point, the latent load (humidity load) is removed by condensation. A great deal of subsequent re-heating is required[3] to increase the air temperature to meet the supply-air requirement for indoor thermal comfort[4]. Typically, the latent part accounts for around 30–40% of the working load in air-conditioning, and its proportion is even higher in some hot and humid climates[5]. Considerable efforts have been made to develop alternative air-conditioning technologies[6–8]. High temperature cooling made possible by novel sorbent or desiccant materials is a promising approach[9], where a sorption and heat-driven desorption process handles the removal of moisture. Dealing only with the sensible load, the system can raise the evaporation temperature from a typical 5–7 °C to a higher range (e.g., 15–20 °C[10]) so the COP and energy efficiency of the system can be dramatically improved[11,12].

In principle, sorbent or desiccant materials can be divided into two categories: liquid and solid. Liquid sorbents are mainly based on a solution of hygroscopic salts. Dehumidification by liquid sorbents uses less electrical
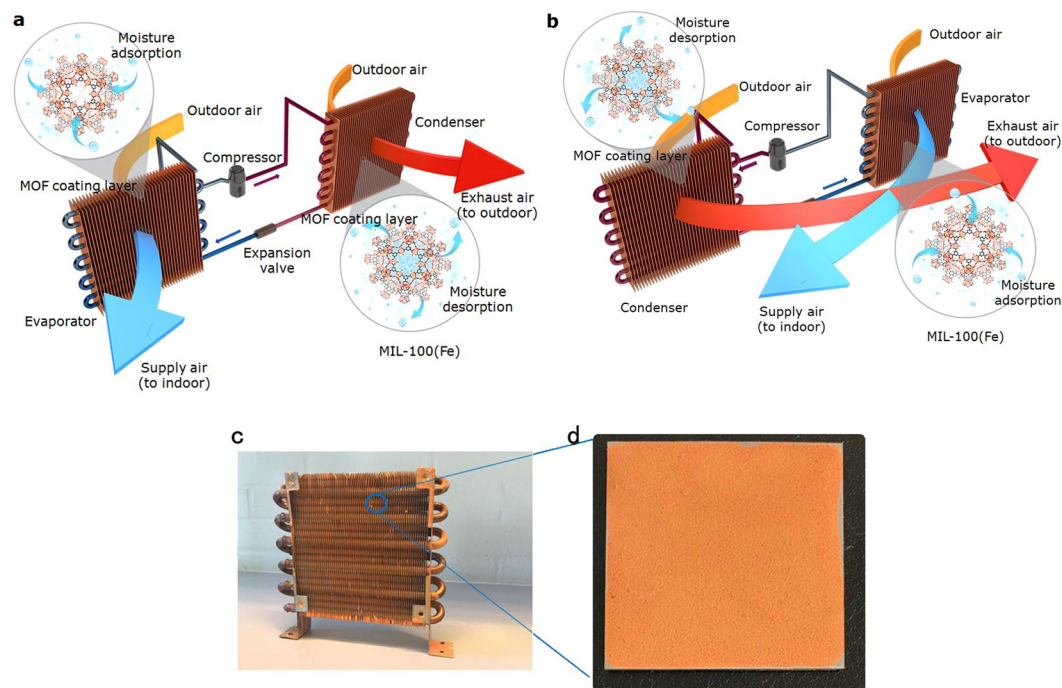
Figure 1. Schematic illustration of the working mechanism of a MOF high temperature cooling system. (**a**) MOFs absorb, store and transfer latent heat loads. The MOF HEx on the left side is in the adsorption mode and works as an evaporator. The MOF HEx on the right side is in the desorption mode and works as a condenser. (**b**) When the MOF coating on the evaporator is saturated, the direction of refrigerant circulation will be reversed, the MOF HEx on the left side becomes a condenser and that on the right side becomes an evaporator. (**c**) Image of a MOF HEx coated with MIL-100(Fe). (**d**) Image of a MOF HEx Element: a single aluminium fin with single-side-coated MIL-100(Fe).

energy than refrigeration, but the relevant technology has distinct drawbacks for commercialization, e.g. it requires a complex system and has corrosion problems[13]. Subject to low water uptake capacity and requiring a high regenerative temperature, conventional solid sorbent systems using silica gel or aluminium-rich zeolites, though less bulky than that of liquid sorbent, are restrained by the availability of heat sources[14]. Some studies have suggested combining liquid and solid sorbents, for example, by encapsulating different salts into a porous matrix[15]. The water uptake capacity of the mixture can be enhanced, but corrosion is still problematic, especially when the composite sorbents are directly applied to a metal surface[16].

Metal-organic frameworks (MOFs) are a class of porous crystalline materials that consist of metal clusters and organic linkers. Due to their high porosity and large specific surface, MOFs can be used for gas storage, purification and catalysis, etc. Recent studies show that MOFs are also promising sorbents for water vapour. The diverse choice of linkers and secondary building blocks (SBU) facilitate the modulation of the hydrophilicity and sorption kinetics[17–22]. Some of us have reported carboxylate-based MOFs showing remarkable uptake for water and requiring lower regeneration temperatures for the desorption compared to conventional sorbents. We found that these MOFs would be excellent sorbents for moisture control in the built environment due to their high hydrothermal stability, non-toxicity and non-corrosion[23].

In this paper, we report a new high temperature cooling system integrated with MOF-coated heat exchangers. The system has no additional components compared to a traditional VCAC (Fig. 1). We directly coated the MOFs on the surface of a metallic heat exchanger (HEx) that works in two modes. In the adsorption mode, the MOF HEx works as an evaporator, maintaininga low temperature that is slightly higher than the dew point of the incoming air. The hot and humid outdoor air passes through the MOF HEx and is dehumidified and cooled to the conditions required for the supply air. In this process, both sensible and latent loadsare removed simultaneously without moisture condensation. In the desorption mode, the MOF HEx acts as a condenser when the sorbent is saturated. The regeneration of the wet MOF coating is completely driven by the heat from condensation of refrigerant. No additional energy is needed. The exhaust air from the condenser is directly discharged to the outdoor environment. Two identical MOF HEx units can ensure the continuous operation of the system by simply reversing the direction of refrigerant and air flow between the two modes.

We selected those amphiphilic MOFs primarily exhibiting a high water-uptake in the pressure range of 25–50% relative humidity (RH). Hydrophilic MOFs often shows the inflection points of water isotherms at a low relative humidity (<25%) and a relatively high sorption enthalpy due to the strong interaction between water molecules and the functional groups/SBUs[24,25]. Overly hydrophobic MOFs, in contrast, are unable to dry the incoming air to the required level of supply air for the building[26,27].

The delicate choices on these MOFs allow the system to maximally exploit the unique S-shape isotherms of the MOFs so that the cyclical water uptake is close to the maximum adsorption of the dry materials. The system
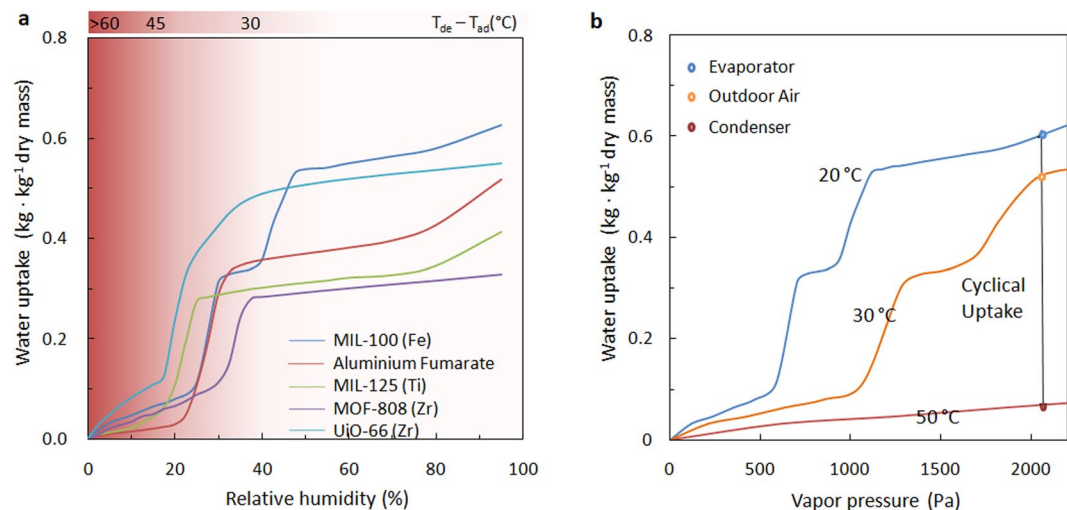
Figure 2. (**a**) Water adsorption isotherms of typical amphiphilic MOFs with simple linkers (MIL-100(Fe), Basolite A520 (Aluminium Fumarate), MIL-125(Ti), UiO-66(Zr), MOF-808(Zr)) at 25 °C, with the steep step located in the narrow range of RH 25–50%. The operation window of a cooling system is illustrated by the difference between the temperatures of the ambient air and the dew point (SI5, $T_{evaporator} > T_{dew\ point}$). The more hydrophilic the materials are, the more significant the temperature lift that can be achieved ($T_{ambient} - T_{evaporator}$), while a higher temperature of desorption is required. (**b**) Temperature swing operation with MIL-100(Fe). Water adsorption isotherms measured at 20 °C, 30 °C and 50 °C show that the cyclical loading difference is 0.56 kg·kg^{-1} dry mass at 2100 Pa vapour pressure (50% RH at 30 °C).

can operate efficiently even though the regeneration is powered by a very low-grade heat source (Fig. 2). With the present concept, the waste heat from the condenser with a temperature lower than 50 °C can be used for moisture desorption. We estimated that the present system can reach a high COP of 7.9 on a typical summer day in an oceanic climate (e.g. Europe) while maintaining high specific cooling power (SCP).

Construction of the MOF Heat Exchanger. In addition to the steep step in the suitable RH range on the isotherms, the sorbent must possess other advantages such as high water-uptake, low-cost, a lack of toxicity and the possibility of scalable production. High-valent metals (III, IV) carboxylates, including hierarchical mesoporous or microporous structures built with the most uncomplicated aromatic rings, e.g., terephthalate/trimesate, and fumarate[28–33], are good candidates to meet all these requirements. The organic linkers without functionalization can be directly purchased on commercial markets, and synthesis can be achieved by robust and straightforward routes.

Many types of MOFs have been synthesized in the past several years[34], but few of them meet the above criteria. We have investigated the performance of a few archetypal amphiphilic MOFs, including MIL-100(Fe), Basolite A520 (Aluminium Fumarate), MIL-125(Ti), UiO-66(Zr), and MOF-808(Zr), etc. With one of the highest water uptake capacity ever reported, MIL-100(Fe) has a better overall performance than any other. We therefore chose MIL-100(Fe) for use in a demonstration of the system concept. The crystalline structure of MIL-100(Fe) has a rigid three-dimensional cubic form, composed of oxo-centred iron(III) octahedral trimers linked to trimesate ligands [Fe$_3$O(H$_2$O)$_2$(OH)(BTC)$_2$], creating two mesoporous cavities of 25 and 29 Å. The heat released from the exothermic adsorption within our operation is very close to the latent heat[23]. The synthesis of MIL-100(Fe) was at the scale of several hundreds of grams in a batch at the laboratory level and can easily be increased to continuous production with high space-time yields[35] (Supplementary Information SI1).

To overcome the inherent problems of weak mechanical strength and low density[36], we shaped the activated MIL-100(Fe) powders into macroscopic layers on a metal surface. The concept of coating also allows the MOFs to rapidly dissipate or absorb heat under isothermal conditions via the evaporator or condenser, which guarantee the desired sorption performance. The coating process used a water-borne binder of silica sol (an aqueous silicic acid solution with water-insoluble silicon dioxide in colloid distribution), enabling the MOF layer to retain its original water sorption features and capacity (besides the "dead volume" on the silicates). The characteristic behaviour of filling the mesopores in two consecutive steps observed in MIL-100(Fe) crystalline material[37] was well conserved. The optimized recipe showed both hydrothermal and mechanical stability after three months of sorption cycle tests without peeling off (SI2).

Water sorption characterization. We investigated the ability of a representative element of the coated MOF HEx to perform the macroscopic ad-/desorption characterization (Fig. 3). Three samples of MIL-100(Fe) were coated on one side of 4 cm × 4 cm × 0.03 cm aluminium plates, obtaining a mass of 0.109 g, 0.203 g, and 0.293 g (90 wt% MOF and 10 wt% binder) and a thickness of 157 ± 37 μm, 313 ± 55 μm, and 463 ± 64 μm. The reverse side of the aluminium plate was attached to a Peltier cooler (TEC) to control the surface temperature, then the MOF Hex Element was placed into a small climate chamber with controlled temperature and RH.
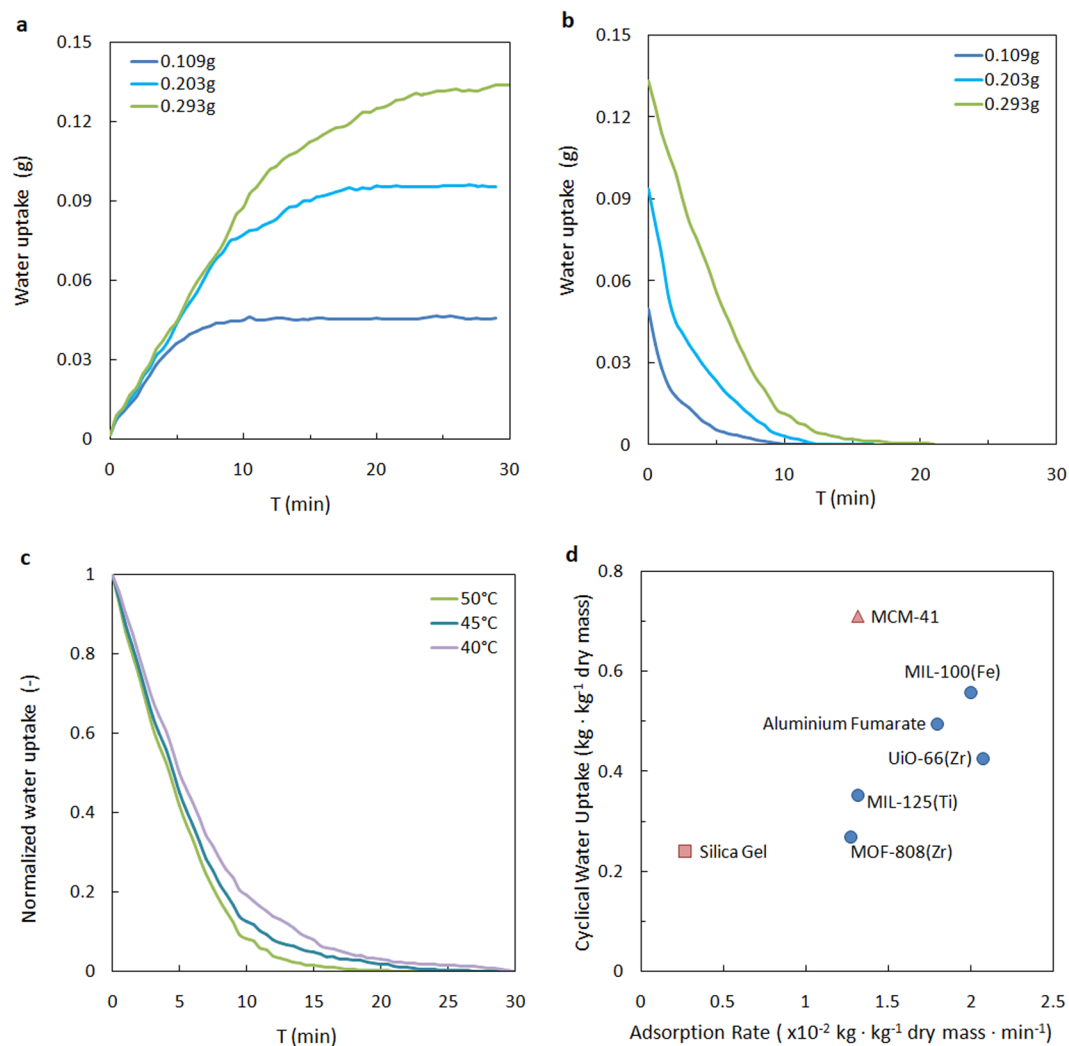
34

Figure 3. Water sorption dynamic achieved by the MOF Hex Element. (**a**) Adsorption curves for three coated MIL-100(Fe) layers of 0.109 g, 0.203 g, and 0.293 g at 20 °C. (**b**) Desorption curves for three coated MIL-100(Fe) layers of 0.109 g, 0.203 g, and 0.293 g at 50 °C. (**c**) Normalized desorption curve for coated MIL-100 layer of 0.293 g at 50, 45 and 40 °C. (**d**) Water cyclical load capacity (20–50 °C) and adsorption rates of common sorbents. In the mass calculation of the MOFs the binder weight was subtracted. The adsorption rates are averaged values for 0–90% water loading with coated layers of 450 μm thick.

The principle of the characterization experiments was the same as under real-life conditions. We provided an isobaric environment with the small climate chamber, with reference to the ambient atmosphere, and represented the evaporator/condenser parts with the TEC (SI3). To represent a typical summer day in Europe, the chamber was set to 30 °C, RH 50%. In the adsorption mode, the surface temperature of the HEx Element was controlled to be 20 °C. The total amount of water that the coated layer could adsorb was 0.45 kg·kg^{-1} dry mass, estimated from the equilibrium states on the isotherms and was measured instantaneously using a gravimetric method. In the desorption mode, the current passing through the TEC was reversed, and the surface temperature of the HEx Element increased to 50 °C. The time-dependent sorption curve validated the tight relation between the layer thickness and the dynamics. The three coating layers reached 90% saturation in 7, 13 and 18 minutes, respectively (Fig. 3a).

We can calculate the energy efficiency of a sorption cycle in which the MOF layer operated as the latent heat storage and transfer media[38]. MIL-100(Fe) has a reversible adsorption/desorption cycle, and the effect of hysteresis within the working range is negligible. The latent load removed is equal to the thermal energy input minus the heat loss, which is mainly due to the parasitic sensible loads during the mode switch between evaporator and condenser. A thinner coating layer implies better heat transfer performance, which is essential to ensure quasi-isothermal sorption of the moisture. However, an augmented metal/sorbent ratio requires a more frequent mode switch, will thus decrease the COP. An optimized thickness of 450 μm was chosen for further demonstration, which allows the MOF to operate with a working cycle of 30 minutes. In this case, the parasitic sensible loads are one order of magnitude smaller than the latent load.
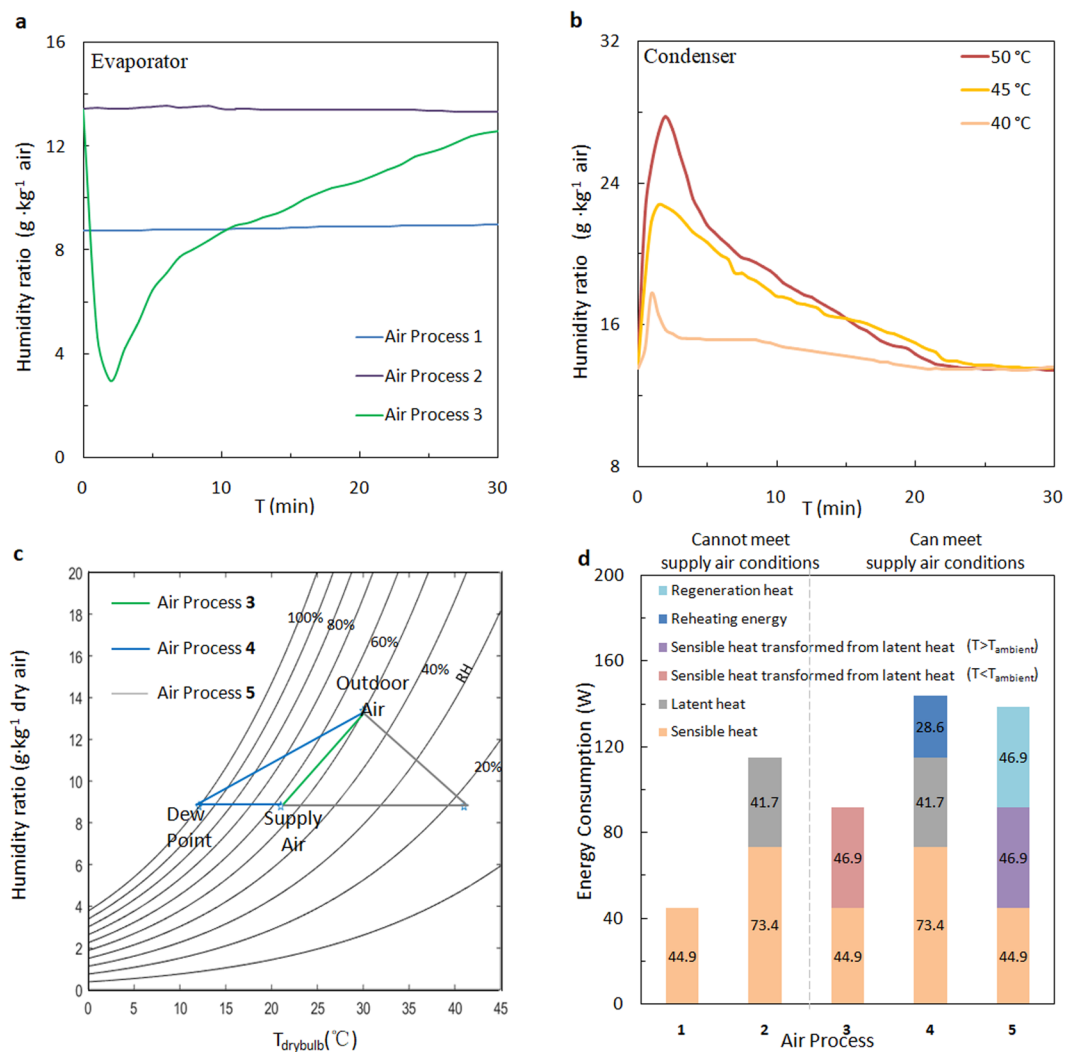
Figure 4. Sorption and energy performance of the proof-of-concept system. (**a**) Supply air humidity ratio from uncoated HEx at evaporation temperature of 19 °C (Air process 1), at 9.5 °C (Air process 2) and MOF HEx at 19 °C (Air process 3). (**b**) Exhaust air humidity ratio from MOF HEx in the desorption mode at 50 °C, 45 °C and 40 °C. (**c**) Psychrometric representation of air process lines for outdoor air of 30 °C, RH 50% and supply air of 21 °C, RH 50%. (**d**) Comparison of energy consumption on sensible and latent heat for the different air processes to reach the same state of supply air.

For comparison, we fabricated other Hex Elements in the same way based on other amphiphilic MOFs and traditional sorbents with an apparent water loading difference within the working range[32,39–44]. Figure 3d shows the thermodynamic and kinetic results of the sorbents. The water sorption cycling speed in MOFs is much more significant than in conventional materials, e.g., the MIL-100(Fe) coating layer adsorbed water 12 times faster than silica gel. The sorption kinetics is important in engineering where the volumetric SCP is a crucial indicator.

MOF HEx dehumidification performance and energy efficiency.

We validated the concept and demonstrated the benefits in operation of high temperature cooling by investigating a fully functional MOF HEx. The full-scale vapour sorption test consisted of a MOF HEx made of 85.6 g MIL-100(Fe) dip-coated[45] on the 0.2 mm-thick aluminium fins and 12 mm-diameter copper tubes. The MOF HEx (20 cm × 5 cm × 15 cm) was placed in a thermally insulated test chamber, through which a hot outdoor airflow was passed (30 °C, RH 50%). Two baselines with uncoated heat exchanger were used in comparison with MOF HEx in Fig. 4a: Air process 1, traditional high temperature cooling without dehumidification; Air process 2, traditional vapour-compression cooling with refrigeration-based dehumidification. The supply air of 1 and 2 was 21 °C, RH 87% and 12 °C, RH 95%, respectively. When the evaporation temperature was set to 19 °C, which is slightly above the dew point, MOF HEx in Air process 3 (the proposed system) reduced the humidity ratio of the airflow from 13.6 g·kg^{-1} to an average of 8.5 g·kg^{-1} within the 90% operation time. It corresponded to the dehumidification performance of an uncoated heat exchanger with an evaporation temperature below 11.7 °C. However, we cannot provide the indoor space directly with supply air from either 1 or 2. The extremely humid air from Air process 1 is outside the occupant comfort zone. A standalone dehumidification step is required in the design of a traditional high temperature

cooling system[4,46]. On the other hand, the over-cooled air from Air process 2 may cause condensation in the indoor environment, which damages building structures and promote microbial growth[47,48]. The process ends up with an additional air mixing or re-heating step, which increase the complexity of the air circulation system and the sensible heat load.

We have evaluated the energy efficiency of the proposed system (Air process 3). Since the latent load is removed by MOF adsorption under quasi-isothermal conditions, the low efficiency in mass and heat transfer related to moisture condensation was eliminated. The total energy input can be roughly estimated as the sum of the adsorption heat of the MOF coating and the sensible load of the outdoor air plus 30% consumption in fans and other losses, as is general industry practice. It is important to note that the desorption of wet MOFs is completely driven by waste heat from the condenser and no extra energy is used. The corresponding COP_{sys} is 6.6 at a condensation temperature of 50 °C. The COP is very sensitive to the temperature differences between the evaporator, the ambient atmosphere, and the condenser. Each 1 °C reduction of the condenser temperature indicates a saving on energy input by 3%[49]. If the condensation temperature dropped to 45 °C, the COP_{sys} would increase to 7.9. On the other hand, reducing the desorption temperature would result in a longer desorption time and would introduce losses of cyclical water uptake. The performance of MIL-100(Fe) was barely affected, whereas the more hydrophilic MOFs would probably be weakened. For instance, the cyclical water uptake of UiO-66(Zr) and MIL-125(Ti) was reduced by 0.2 and 0.13 kg·kg^{-1} dry mass (−45% and −36%), respectively (SI4). Both the thermodynamic and the kinetic properties of the non-trivial sorbents merit individual studies to find the compromise that how they might be better adapted to different climates and engineering demands.

The COP of the proposed system is one of the best values reported for variable space cooling systems. By increasing the evaporation temperature to above the dew point, the high temperature cooling system has a smaller refrigerant pressure difference between the evaporator and the condenser. In other words, the compressor can reject heat more easily and efficiently. Therefore, the COP of high temperature cooling systems is usually higher than vapour-compression air conditioning. However, the supply air from the traditional high temperature cooling system (Air process 1) is very humid, which cannot meet the required conditions for thermal comfort. An additional dehumidification system is needed. To reach the same state of supply air as Air process 3 (i.e. same temperature, RH and flow rate), we added two more scenarios with commercial technology concepts for comparison: Air process 4, vapour-compression air conditioning with reheating; and Air process 5, stand-alone dehumidification by a desiccant wheel combined with a sensible cooling process (Fig. 4c).

Given the same states of outdoor air (30 °C, 50% RH) and supply air (21 °C, 55% RH), Air process 3 demonstrated significant energy savings compared to the other systems. Figure 4d provides detailed information on the breakdown of the energy consumption of the different air processes to reach the same supply air conditions. The MOF HEx in Air process 3 could save 36.1% energy consumption by avoiding over-cooling and reheating compared to 4 while maintaining a high SCP. In Air process 5, the desiccant wheel transforms the latent heat to sensible heat under isenthalpic conditions, which is less efficient than the isothermal adsorption process in Air process 3. Moreover, the same quantity of additional energy input is required to regenerate the desiccant. The total energy consumption of Air process 5 is 33.8% higher than that of Air process 3.

The cooling power of the MOF HEx in our experiment was 91.8 W. Continuous cooling would require two identical MOF HEx units that operated alternately. The MOF HEx can maintain a cooling power density of up to 82 W·L^{-1} including the removal of latent heat by MOF with 274 W·kg^{-1} of MIL-100(Fe). The high cooling power density makes the proposed system very competitive with most commercial cooling systems[50].

Conclusions

We report a new high temperature cooling system that uses amphiphilic MOFs as advanced moisture sorbents with good performance in removing both latent and sensible heat loads simultaneously. The system makes possible an energy-efficient working cycle with a small temperature difference of less than 30 °C between the evaporator and the condenser to exploit the S-shape isotherm of MOFs. The MOF-coated heat exchangers used in the system can remove the cooling load with a power density of 82 W·L^{-1} including latent heat with 274 W·kg^{-1} MIL-100(Fe). In a quasi-isothermal adsorption process, the system eliminates 36.1% of the working load in refrigeration-based dehumidification by a conventional air-conditioner with reheating. The overall COP of the system could be up to 7.9.

We expect that further refinement of the sorbent processing and shaping could optimise the working cycles and enhance the efficiency that can be achieved in different climates. The high COP, high specific power and the minimal modification of existing air conditioning systems that is required makes this new technology suitable for adoption in a broad range of applications and provides a pathway towards highly energy-efficient space cooling.

Methods

Syntheses of MOFs. Large-scale MIL-100(Fe) or $Fe_3O(H_2O)_2OH(BTC)_2$ was prepared as in[29]. The additive free reaction comprising iron nitrate, trimesic acid and water as a sole solvent takes place at low temperature (60 °C) under stirring. The activation conditions consist in washing the solid with water at room temperature. The synthesis procedures of other MOFs can be found in SI1.

Coating on heat exchanger element with MOFs powders. Aluminium sheets (4 cm × 4 cm × 0.03 cm) were cleaned in acetone, and then immersed in 0.3 mol·L^{-1} CH_3COOH and 1 mol·L^{-1} NaOH for 1 min, respectively, before being rinsed with deionized water. A slurry was obtained by dispersing 1.00 g MOF powder in 3.03 g of deionized water with vigorous stirring for 10 min followed by supersonic treatment for 20 min. The binder silicate sol (0.62 mL, 50 wt%) was added to the suspension with continuous stirring. The aluminium sheets were coated manually with the suspension on a single side of the aluminium sheet, using a pipette. The coated sheets were dried at 50 °C for 1 h, and cured at 150 °C for 2 h.

Coating on full-scale heat exchanger with MIL-100 powders.   The MIL-100(Fe) suspension was prepared by using the above procedure (300 g MIL-100(Fe), 600 g deionized water and 102 mL silicate sol). The heat exchanger was dip-coated by immersion in the suspension, dried and cured following the heating procedure described above. Extra slurry on the edges was removed mechanically. The coating was repeated twice to obtain the desired thickness, resulting in 85.6 g of dried coating sorbent.

Water sorption characterization of the MOF HEx Element.   The MOF HEx Element was placed in a small climate chamber (60 cm × 40 cm × 100 cm). A high precision humidity generator (SETARAM Instrumentation, Wetsys) provided the inlet air with controlled temperature and relative humidity. The temperature regulator for the MOF HEx Elements comprised a Peltier cooler (TE Technology, TEC1-12703, 4 cm × 4 cm × 0.4 cm) with two metal heat buffers on each side (Aluminium plates, 4 cm × 4 cm × 3 cm), bonded with thermally resistant grease. A small space (5 mm × 5 mm × 1 mm) was milled out of the aluminium heat buffer at the corner on the MOF HEx side to insert the thermocouple temperature sensors (Omega Type K HFS-4) for the *in-situ* thermal measurement. The TEC was linked to an amplifier (HH-electronic) to guarantee a low power output (the exothermic adsorption power was about 0.1 to 1 W). A small fan (0.2 W) was installed below the heat sink to assist in air mixing. The climate chamber is large enough to be able to maintain an isobaric environment.

The water sorption characterization consisted of two tests: low-temperature adsorption and high-temperature desorption. One temperature-humidity sensor was placed near the HEx Element to measure ambient conditions, and two thermocouples were inserted into the aluminium heat buffers to measure the temperature of the coating layer and heat sink during adsorption. Before the sorption characterization, the MOF HEx Element was dried at 120 °C. After cooled down, the MOF Hex Element was attached to aluminium heat buffer and the TEC. The entire device was sealed and transported to the small climate chamber in an airtight container. The container was removed and the TEC then started to cool the HEx Element. The temperature for cooling was set above the dew point according to the operating intervals in Fig. 2b, i.e., 20 °C. During the desorption test, the current passing through the TEC was reversed, and the coated HEx Element then became the heat sink. The temperature of the HEx Element was raised to 40 °C, 45 °C or 50 °C to represent the condenser. The tests were repeated many times to measure the stabilized cyclical sorption performance.

Air process test for full-scale MOF-coated heat exchanger.   The full-scale coating test was carried out on a water/air finned-tube heat exchanger with aluminium fins 0.2 mm thick pressed onto copper tubes of 7.5 mm diameter. Fin spacing 1.7 mm, fin volume 120 mm × 25 mm × 125 mm = 0.37 L, total dimension 150 mm × 25 mm × 150 mm = 0.56 L, the total mass 225 g. The HEx was placed in a thermally insulated sample box with the same volume, connected to an airflow with controlled humidity and temperature. Temperature and humidity sensors were installed both upstream and downstream of the HEx in the air duct. The water in a thermostatic bath was circulated through the copper tubes to provide accurate temperature control of the HEx. The tests followed the same temperature profiles of the HEx Element sorption characterization. The incoming airflow to the MOF HEx was 200 L·min^{-1}.

Data Availability

The data that support the findings of this study are present in the paper and the Supplementary Information. Additional information is available from the authors upon reasonable request.

References

1. IEA. *Energy Technology Perspectives 2017*, ISBN978-92-64-27597-3 (International Energy Agency, 2017).
2. Shirey, D. B., Henderson, H. I. & Raustad, R. A. *Understanding The Dehumidification Performance Of Air-Conditioning Equipment At Part-Load Conditions* (Florida Solar Energy Center, Cocoa, FL 2006).
3. Chua, K. J., Chou, S. K., Yang, W. M. & Yan, J. Achieving better energy-efficient air conditioning – A review of technologies and strategies. *Appl. Energy* **104**, 87–104 (2013).
4. ASHRAE. *ASHRAE Standard 62.1-2016, Ventilation For Acceptable Indoor Air Quality* (American Society of Heating, Refrigerating, and Air-Conditioning Engineers, Atlanta, GA 2016).
5. Harriman, L. G., Plager, D. & Kosar, D. *ASHRAE J.* November, 37–45 (1997).
6. Papadopoulos, A. M., Oxizidis, S. & Kyriakis, N. Perspectives of solar cooling in view of the developments in the air-conditioning sector. *Renew. Sust. Energ. Rev.* **7**(5), 419–438 (2003).
7. Mazzei, P., Minichiello, F. & Palma, D. HVAC dehumidification systems for thermal comfort: a critical review. *Appl. Therm. Eng.* **25**, 677–707 (2005).
8. La, D., Dai, Y. J., Li, Y., Wang, R. Z. & Ge, T. S. Technical development of rotary desiccant dehumidification and air conditioning: a review. *Renew. Sust. Energ. Rev.* **14**(1), 130–147 (2010).
9. US Department of Energy. Energy Savings Potential and RD&D Opportunities For Non-Vapor-Compression HVAC Technologies, https://doi.org/10.2172/1220817 (2014).
10. Olesen, B. W. *ASHRAE J.* February, 45–52 (2012).
11. Kazanci, O. B., Shukuya, M. & Olesen, B. W. Theoretical analysis of the performance of different cooling strategies with the concept of cool exergy. *Build. Environ.* **100**, 102–113 (2016).
12. Tu, Y. D., Wang, R. Z., Ge, T. S. & Zheng, X. Comfortable, high-efficiency heat pump with desiccant-coated, water-sorbing heat exchangers. *Sci. Rep.* **7**, 40437 (2017).
13. Lowenstein, A. Review of Liquid Desiccant Technology for HVAC Applications. *HVAC&R Res.* **14**, 819–839 (2008).
14. Henning, H. M. Solar assisted air conditioning of buildings-an overview. *Appl. Therm. Eng.* **27**, 1734–1749 (2007).
15. Gordeeva, L. G. & Aristov, Y. I. Composites 'salt inside porous matrix' for adsorption heat transformation: a current state-of-the-art and new trends. *Int. J. Low Carbon Tech.* **7**(4), 288–302 (2012).
16. Rafique, M. M., Gandhidasan, P. & Bahaidarah, H. M. S. Liquid desiccant materials and dehumidifiers - A review. *Renew. Sust. Energ. Rev.* **56**, 179–195 (2016).
17. Zhang, J.-P., Zhu, A.-X., Lin, R.-B., Qi, X.-L. & Chen, X.-M. Pore Surface Tailored SOD-Type Metal-Organic Zeolites. *Adv. Mater.* **23**, 1268–1271 (2011).

18. Canivet, J., Fateev, A., Guo, Y., Coasne, B. & Farrusseng, D. Water adsorption in MOFs: fundamentals and applications. *Chem. Soc. Rev.* **43**, 5594 (2014).
19. Burtch, N. C., Jasuja, H. & Walton, K. S. Water stability and adsorption in metal–organic frameworks. *Chem. Rev.* **114**, 10575 (2014).
20. de Lange, M. F., Verouden, K. J. F. M., Vlugt, T. J. H., Gascon, J. & Kapteijn, F. Adsorption-driven heat pumps: the potential of metal–organic frameworks. *Chem. Rev.* **115**, 12205 (2015).
21. Permyakova, A. *et al.* Synthesis Optimization, Shaping, and Heat Reallocation Evaluation of the Hydrophilic Metal–Organic Framework MIL-160(Al). *Chem Sus Chem* **10**, 1419–1426 (2017).
22. AbdulHalim, R. G. *et al.* A fine-tuned metal−organic framework for autonomous indoor moisture control. *J. Am. Chem. Soc.* **139**, 10715–10722 (2017).
23. Feng, X., Qin, M., Cui, S. & Rode, C. Metal-Organic Framework MIL-100(Fe) as a Novel Moisture Buffer Material for Energy-Efficient Indoor Humidity Control, *Build. Environ.* **145**, 234–243 (2018).
24. Cadiau, A. *et al.* Design of hydrophilic metal organic framework water adsorbents for heat reallocation. *Adv. Mater.* **27**, 4775 (2015).
25. Kim, H. *et al.* Characterization of Adsorption Enthalpy of Novel Water-Stable Zeolites and Metal-Organic Frameworks. *Sci. Rep.* **6**, 19097 (2016).
26. Küsgens, P. *et al.* Characterization of metal-organic frameworks by water adsorption. *Micropor. Mesopor. Mat.* **120**, 325 (2009).
27. Schaate, A. *et al.* Porous interpenetrated zirconium-organic frameworks (PIZOFs): a chemically versatile family of metal-organic frameworks. *Chem. Eur. J.* **17**, 9320–9325 (2011).
28. Cavka, J. H. *et al.* A new zirconium inorganic building brick forming metal organic frameworks with exceptional stability. *J. Am. Chem. Soc.* **130**(42), 13850–13851 (2008).
29. Dan-Hardi, M. *et al.* A new photoactive crystalline highly porous titanium(IV) dicarboxylate. *J. Am. Chem. Soc.* **131**(31), 10857–10859 (2009).
30. Yoon, J. W. *et al.* Controlled reducibility of a metal–organic framework with coordinatively unsaturated sites for preferential gas sorption. *Angew. Chem. Int. Ed.* **49**, 5949 (2010).
31. Furukawa, H. *et al.* Water adsorption in porous metal−organic frameworks and related materials. *J. Am. Chem. Soc.* **136**(11), 4369–4381 (2014).
32. de Lange, M. F. *et al.* Crystals for sustainability – structuring Al-based MOFs for the allocation of heat and cold. *Cryst Eng Comm* **17**, 281–285 (2015).
33. Alvarez, E. *et al.* The structure of the aluminum fumarate metal-organic framework A520. *Angew. Chem. Int. Ed.* **54**, 3664–3668 (2015).
34. Kalmutzki, M. J., Diercks, C. S. & Yaghi, O. M. Metal–Organic Frameworks for Water Harvesting from Air. *Adv. Mater.* 1704304 (2018).
35. Patent pending: European application No. 17305119.4 (2017), International application No. PCT/EP2018/052115 (2018), "Low temperature process for the synthesis of MOF carboxylate nanoparticles".
36. Lenzen, D. *et al.* Scalable green synthesis and full-scale test of the metal-organic framework CAU-10-H for use in adsorption-driven chillers. *Adv. Mater.* 1705869 (2017).
37. Howarth, A. J. *et al.* Chemical, thermal and mechanical stabilities of metal–organic frameworks. *Nature Rev. Mater.* **1**, 15018 (2016).
38. Kolokathis, P. D., Pantatosaki, E. & Papadopoulos, G. K. Atomistic modeling of water thermodynamics and kinetics within MIL-100(Fe). *J. Phys. Chem. C.* **119**, 20074–20084 (2015).
39. Gur, I., Sawyer, K. & Prasher, R. Searching for a better thermal battery. *Science* **335**, 1454–1455 (2012).
40. Jeremias, F., Fröhlich, D., Janiak, C. & Henninger, S. K. Advancement of sorption-based heattrans formation by a metal coating of highly-stable, hydrophilic aluminium fumarate MOF. *RSC Adv.* **4**, 24073 (2014).
41. Kim, S. N., Kim, J., Kim, H. Y., Cho, H. Y. & Ahn, W. S. Adsorption/catalytic properties of MIL-125 and NH$_2$-MIL-125. *Catal. Today* **204**, 85–93 (2013).
42. de Lange, M. F., Verouden, K. J. F. M., Vlugt, T. J. H., Gascon, J. & Kapteijn, F. Adsorption-driven heat pumps: The potential of metal-organic frameworks. *Chem. Rev.* **115**(22), 12205–12250 (2015).
43. Llewellyn, P. L. *et al.* Water sorption on mesoporous alumino silicate MCM-41. *Langmuir* **11**(2), 574–577 (1995).
44. Aristov, Y. I., Tokarev, M. M., Freni, A., Glaznev, I. S. & Restuccia, G. Kinetics of water adsorption on silica Fuji Davison RD. *Micropor. Mesopor. Mat.* **96**(1–3), 65–71 (2006).
45. Freni, A. *et al.* Adsorbent coatings for heat pumping applications: Verification of hydrothermal and mechanical stabilities. *Appl. Therm. Eng.* **50**, 1658–1663 (2013).
46. Sultan, M., El-Sharkawy, I., Miyazaki, T., Saha, B. B. & Koyama, S. An overview of solid desiccant dehumidification and air conditioning systems. *Renew. Sust. Energ. Rev.* **46**, 16–29 (2015).
47. Qin, M., Belarbi, R., Aït-Mokhtar, A. & Nilsson, L. O. Coupled heat and moisture transfer in multi-layer building materials. *Constr. Build. Mater.* **23**, 967–975 (2009).
48. Qin, M. & Belarbi, R. Development of an analytical method for simultaneous heat and moisture transfer in building materials utilizing transfer function method. *J. Mater. Civ. Eng.* **17**, 492–497 (2005).
49. Goldstein, E. A., Raman, A. P. & Fan, S. Sub-ambient non-evaporative fluid cooling with the sky. *Nature Energy* **2**, 17143 (2017).
50. Narayanan, S. *et al.* A thermophysical battery for storage-based climate control. *Appl. Energy* **189**, 31–43 (2017).

Acknowledgements

Author Contributions

S.C. and M.Q. conceived the idea. S.C., M.Q. and C.S. planned the study. S.C. and M.Q. designed the experiment. A.M., V.S. and S.W. contributed to the synthesis of the MOFs. F.N. and C.S. supervised the synthesis and characterization of the MOFs. S.C. and X.F. performed the measurements and analysed the data. S.C. and M.Q. wrote the paper. S.C. and M.Q. contributed equally to this paper. All authors reviewed and commented on the manuscript.

Additional Information

PAPER • OPEN ACCESS

Performance comparison between metal-organic framework (MOFs) and conventional desiccants (silica gel, zeolite) for a novel high temperature cooling system

Performance comparison between metal-organic framework (MOFs) and conventional desiccants (silica gel, zeolite) for a novel high temperature cooling system

Kan Zu[1], Shuqing Cui[1] and Menghao Qin[1,*]

[1] Department of Civil Engineering, Technical University of Denmark, Lyngby, 2800, Denmark
* menqin@byg.dtu.dk

Abstract: The use of desiccant-coated heat exchangers (DCHE) in air conditioning systems possesses great advantages in the independent control of both temperature and humidity, as well as low energy consumption and high coefficient of performance (COP). The paper presents a novel high temperature cooling system that uses metal-organic frameworks (MOFs) as sorbents for humidity control. MOFs are a new class of porous crystalline materials consisted of metal clusters and organic linkers, which have an excellent performance of water sorption due to the large specific surface areas and high porosity. In this research, we directly coat MOFs on the heat exchange surface of evaporator and condenser. The evaporator can simultaneously remove both the sensible and latent loads of the incoming air without reducing the temperature below its dew point. The regeneration of wet MOFs is completely driven by the residual heat from the condenser. We also make comparison between the MOF-coated cooling system and conventional desiccants coated ones (i.e. silica gel, zeolite) by way of tests and calculation. The results indicate that the dehumidification capacity of the MOF-coated heat exchanger outperforms other conventional desiccant coated ones under low regeneration temperature (~50℃). The MOF-coated system has a high COP, up to 7.9, and can save 36.1% of the energy required, compared to the traditional vapour compression system with reheating. The amphiphilic MOFs used in the study have high water uptake and low regeneration temperature, and they thus have the potential for being scaled up for large-scale applications in energy efficient air conditioning systems.

Keywords: Humidity control, MOFs, desiccant-coated heat exchanger, energy efficiency

1. Introduction

Electricity demand for heating, ventilation and air conditioning system (HVAC) has gradually been a significant contributor to building energy consumption in the past decades. This because more buildings are supplied with HVAC system to reach desired indoor thermal comfort [1]. Traditional vapor compression system (VCS) generally operated through refrigeration dehumidification process. By cooling the air below dew point, the humidity load is removed by condensation. Such a large temperature difference generally leads to a low COP and even an additional reheating process, and a lower sensible heat ratio like in some hot and humid climates may further worsen the condition [2-3].

Considerable efforts have been made to develop alternative air-conditioning technologies [4-5]. High temperature cooling made possible by novel sorbent or desiccant materials is a promising approach, where a sorption and heat-driven desorption process handles the removal of moisture. Dealing only with the sensible load, the system can raise the evaporation temperature to a higher range, so the COP and energy efficiency of the system can be dramatically improved [6-7].

In view of this advantages, many configurations of dehumidification units coated with conventional sorbent materials were explored [7-9]. However, the working performance of these systems varies greatly for different sorbent materials. Low water uptake ability and high regeneration temperature are the main limitations for the application of conventional sorbents (e.g. silica gel, zeolite etc.) [10].

1

Metal–organic frameworks (MOFs) are an emerging class of porous materials. Most MOFs can exhibit very high surface areas and large adsorption capacity for gas. Due to their structural and functional tunability, MOFs have become one of the most fascinating classes of materials for both scientists and engineers [11]. Some MOFs with an S-shape isotherm, large water uptake and low regeneration temperature, have been proposed for indoor moisture control [10-12]. With one of the highest water uptake capacity ever reported, MIL-100(Fe) has a better overall performance than other MOFs [10]. We therefore chose MIL-100(Fe) for use in this paper.

In this paper, we first report a new high temperature cooling system integrated with MOF-coated heat exchangers, and secondly, make comparisons between the MOF-coated cooling system and some conventional desiccant-coated systems to investigate their working performance and energy saving potential.

2. Methods

2.1. Adsorption heat exchanger

The main operation component presented here is a fin and tube heat exchanger, in which all the contact surface is coated with MOF including tubes and fins. The MOF-coated heat exchanger can simultaneously process both the sensible and latent load of the incoming air without moisture condensation. There are two working modes as shown in Figure 1(a) and (b). In the adsorption mode, the MOF heat exchanger works as an evaporator, maintaining a low temperature that is slightly higher than the dew point of the incoming air by the cold refrigerant. The hot and humid outdoor air passes through the MOF heat exchanger and is dehumidified and cooled to the conditions required for the supply air by the MOF-coated heat exchanger. This is an isothermal adsorption process. The process continues until the desiccant approaches to its saturation point. In the desorption mode, the MOF heat exchanger acts as a condenser when the sorbent is saturated. The regeneration of the wet MOF coating is completely driven by the heat from condensation of refrigerant. No additional energy is needed. Water vapor previously adsorbed by MOF coating is released and removed by the exhaust air to the outside environment. The MOF coating will be dry and can start a successive dehumidification cycle. Two identical MOF heat exchanger units can ensure the continuous operation of the system by simply reversing the direction of refrigerant and air flow between the two modes.
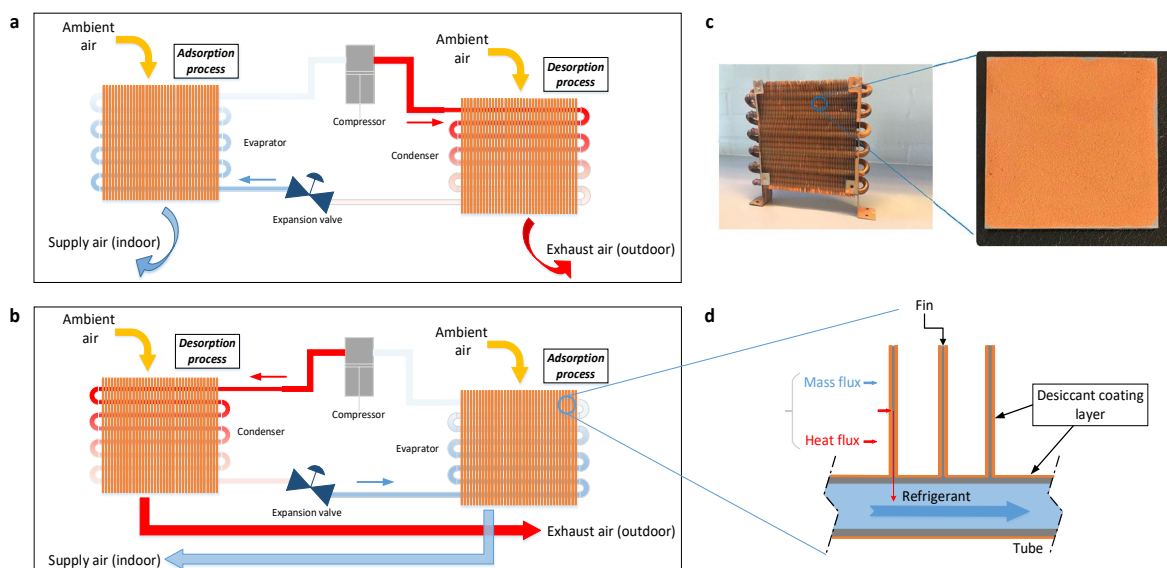

Figure 1. Schematics of heat and mass transfer at desiccant-coated heat exchanger (DCHE).

The MIL-100(Fe) used in this paper was synthesized by the École Normale Supérieure in Paris, France (the main partner of this research). The crystalline structure of MIL-100(Fe) has a rigid three-dimensional cubic form, composed of oxo-centered iron (III) octahedral trimers linked to trimesate

ligands [Fe$_3$O(H$_2$O)$_2$(OH)(BTC)$_2$], creating two mesoporous cavities of 25 and 29Å. The SEM image is shown in Figure 2. The tiny crystal of MIL-100(Fe) is octahedral with the size of 0.5–2 μm. This polymer desiccant, an archetypal amphiphilic MOF, exhibits a distinct water capacity owing to its high porosity, typically showing a sigmoidal curve at middle p/p$_0$. These properties create the condition of using low regeneration temperature (lower than 50℃).
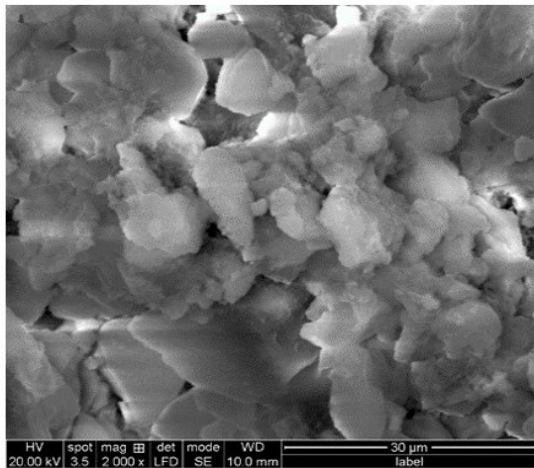

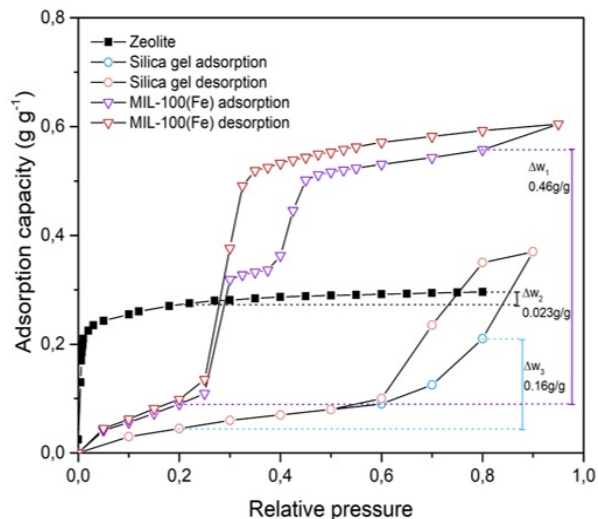**Figure 2.** SEM image of MIL-100(Fe).

Figure 3. Water adsorption isotherms of different desiccant at 298K.

From Figure 3, it can be seen that MIL-100(Fe) has barely ability to adsorb water vapor (below 20%) and its water uptake capacity between a typical relative range (20% for desorption phase and 80%for adsorption phase) is 0.46g/g, which is much higher than other conventional desiccants. In addition, the coating procedures, using a water-borne binder of silica sol, enable MOF layer to retain its water sorption features and capacity. The final configuration of DCHE and schematics of heat and mass transfer are presented in Figure 1(c) and (d), respectively.

2.2. Experimental setup

The experimental setup consists of a traditional vapor compression system with DCHE that can effectively control outlet temperature and humidity, as shown in Fig.1(c). In order to achieve a continuous operation, two of the same DCHEs will take turns as condenser and evaporator. The configuration of heat exchanger (20cm×5cm×15cm) consists of 0.2 mm-thick aluminum fins and 7.5 mm-diameter copper tubes. Fin spacing 1.7 mm, fin volume 120 mm × 25 mm × 125 mm = 0.37 L, total dimension 150 mm × 25 mm × 150 mm = 0.56 L, the total mass 225 g. The coating thickness is less than 1mm with 85.6g MIL-100(Fe) being coated on the surface of fins and tubes.

2.3. Test procedure

The experiments aim to explore the regulation of latent and sensible load during adsorption/ desorption cycle by measuring air and desiccant operational parameters. Temperature and humidity sensors were installed both upstream and downstream of the heat exchanger in the air duct. During adsorption test, the MOF starts in dry condition. The ambient air at a certain temperature and humidity (30℃, 50% RH) passes through the evaporator, and is dehumidified by MOF coating and cooled by the cold refrigerant. In this phase, the adsorption tests can operate at a desired temperature and avoid the influence of adsorption heat. When the water uptake of MOF coating reaches 0.4g/g, the adsorption test finishes. Then the refrigerant (water) flow was switched oppositely from cold flow to hot flow to achieve the regeneration of the saturated MOF. Air humidity ratio and temperature out of evaporator and condenser are continuously measured and logged.

3. Results and discussion

Given the set outdoor air condition, two baselines with uncoated heat exchanger were used in comparison with MOF-coated heat exchanger as shown in Figure 4a: Air process 1, traditional high temperature cooling without dehumidification; Air process 2, traditional vapor compression cooling with refrigeration-based dehumidification (evaporation temperature generally less than 7~9℃). Air process 3, traditional high temperature cooling with MOF-coated heat exchanger. When the evaporation temperature was set to 19℃, slightly above the dew point, the MOF-coated heat exchanger in Air process 3 cut the humidity ratio of air from 13.6g/kg to 8.5g/kg within its operation time. The adsorption operation continues around 10min, with a maximum humidity ratio change value of 10.6g/kg. The regeneration runs at three different regeneration temperature (40℃, 45℃, 50℃). Fig. 4b shows that the maximum exhaust air humidity ratio at 50℃ is twice higher than that of 40℃ of regeneration temperature, which means the system can operate efficiently even though the regeneration is powered by a very low-grade heat source (around 50℃). With the present concept, the waste heat from the condenser with a temperature lower than 50 ℃ can be used for moisture desorption. We estimated that the present system can reach a high COP of 7.9 on a typical summer day in an oceanic climate (e.g. Europe) while maintaining high specific cooling power (SCP).
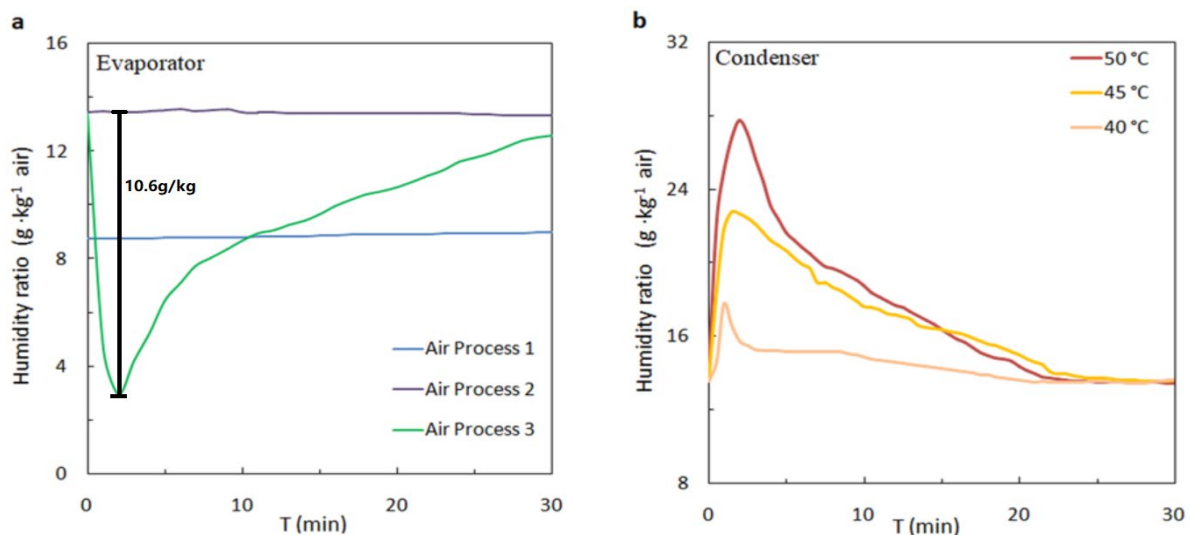

Figure 4. The air humidity change during adsorption and desorption process.

Besides, the test results presented in Figure 5 indicate that the supply air of Air process 1 (21℃, 87%RH) is extremely humid and outside the indoor comfort zone, and supply air of Air process 2 (12℃, 95%RH) may cause vapour condensation in the indoor environment, which promote microbial growth and deteriorate the indoor air quality. To reach the same state of supply air as Air process 3, there should be some extra reheating energy in traditional vapor compression system in Air process 2 (Figure 5). When giving the same test conditions, it can be seen that MOF-coated cooling system can eliminates up to 36.1% of working load in conventional vapor compression system with reheating shown in Figure 6. This means desiccant-coated system can avoid the problems of cooling below dew point.

Theoretically, the integration of desiccant-coated component in traditional cooling system to independently regulate the sensible and latent load gives the possibility to make full use of low-grade energy. The low-temperature heat source for desiccant regeneration (~50℃) is well compatible with the original system. Considering the advantages of desiccant-coated cooling system, some conventional desiccant (i.e. silica gel and zeolite) were also applied and measured in comparison with this MOF-coated cooling system. Thus, we have firstly measured the cyclic water uptake of different desiccant under different temperature pair (evaporation temperature-condensation temperature: 20℃-45℃ and 20℃-50℃). Table 1 shows that the cyclical uptake of MIL-100(Fe) is about 0.56kg/kg dry mass with 30℃, 50% of outdoor air condition, which means it has a low water uptake capacity at a relatively high

temperature and can make the use of low-temperature heat source possible. In addition, it is clear to see that the dehumidification capacity of MIL-100(Fe) is 5 times as that of zeolite below 50°C, so zeolite can barely achieve regeneration under low temperature heat source.
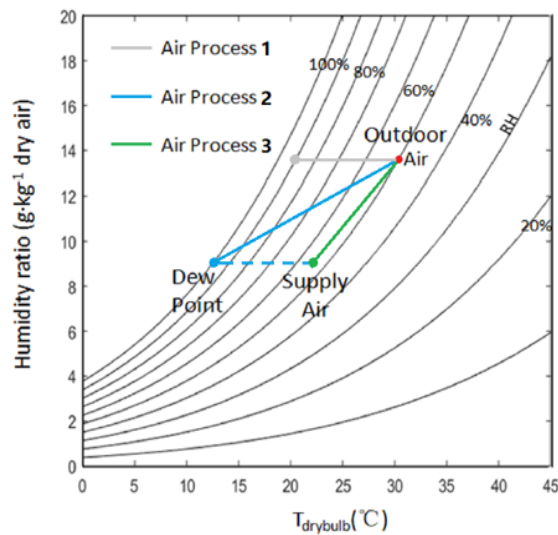

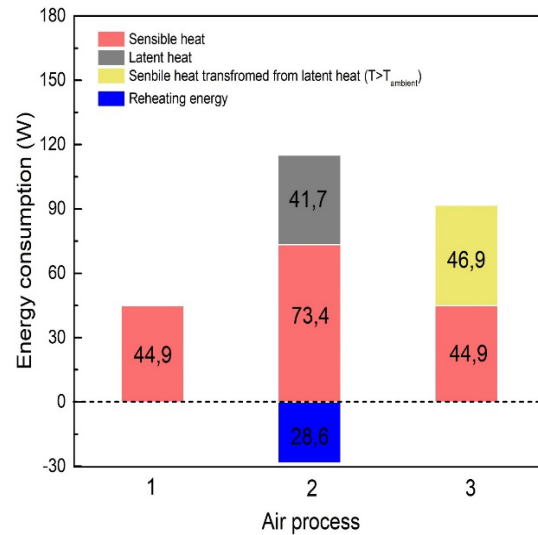**Figure 5.** Psychrometric comparison of different air process.

Figure 6. Comparison of energy consumption for different air processes

Table 1. Cyclical water uptake of different desiccant with 20°C of evaporation temperature.

Regeneration temperature	MIL-100(Fe)	Silica gel	Zeolite
45°C	0.56	0.23	0.09
50°C	0.54	0.24	0.11

Table 2. Outlet air condition under same temperature pair (20°C-50°C).

Average supply air	MIL-100(Fe)	Silica gel	Zeolite
21°C	8.5g/kg (55%)	11.1g/kg (71%)	12.4g/kg (79%)

In view of the adsorption characteristics for these desiccants, there is a comparison presented in Table 2 made to investigate the effect of different desiccant-coated systems with the same sensible load and outdoor air condition (30°C, 50%). It is clear that MOF-coated cooling system can reach the comfort zone, while the silica gel and zeolite cannot achieve it. Compared with Air process 1 above, low temperature can barely help zeolite achieve regeneration. Some recent researches [7, 9] try to use silica gel supported salt desiccant, but the direct contact with metal heat exchange will lead to its corrosion and worsen operation performance. Thus, the proposed system is very competitive with most commercial cooling systems.

4. Conclusions

The MOF coated heat exchanger can achieve a good performance in removing both latent and sensible heat loads simultaneously for a novel high temperature cooling system. The experimental prototype can operate with a cyclical loading difference of 0.56kg/kg dry mass. During a quasi-isothermal adsorption process, the MOF-coated system reduces about 36.1% of the working load in traditional vapor

compression system with reheating. In addition, given the same evaporation and regeneration temperature, the cyclical water uptake of MIL-100(Fe) distinctly outperforms other traditional desiccants (i.e. silica gel, zeolite), which means a strong ability to regulate the humidity load with less operation time and regeneration energy. We also make a comparison among different desiccant coated cooling systems, and the results prove that MIL-100(Fe) is a promising alternatives to conventional desiccants with less regeneration energy source.

Acknowledgement

Reference

[1]   Werner S 2016. European space cooling demands, *Energy* **110** 148-156
[2]   Chua K J, Chou S K, Yang W M and Yan J 2013. Achieving better energy-efficient air conditioning– A review of technologies and strategies, *Appl. Energy* **104** 87-104
[3]   Zouaoui A, Ghedira L Z and Nasrallah S B 2016. Open solid desiccant cooling air systems: a review and comparative study, *Renew. Sust. Energ. Rev.* **54** 889-917
[4]   Papadopoulos A M, Oxizidis S and Kyriakis N 2003. Perspectives of solar cooling in view of the developments in the air-conditioning sector, *Renew. Sust. Energ. Rev.* **7** 419-438
[5]   Mazzei P, Minichiello F and Palma D 2005. HVAC dehumidification systems for thermal comfort: a critical review, *Appl. Therm. Eng.* **25** 677-707
[6]   Kazanci O B, Shukuya M and Olesen B W 2016. Theoretical analysis of the performance of different cooling strategies with the concept of cool exergy, *Build. Environ.* **100** 102-113
[7]   Tu Y D, Wang R Z, Ge T S and Zheng X 2017. Comfortable, high-efficiency heat pump with desiccant-coated, water-sorbing heat exchangers, *Nature Sci. Rep.* **7** 40437
[8]   Narayanan S, Kim H, Umans A, Yang S, Li X S, Schiffres S N, Rao S R, McKay I S, Perez C A R, Hidrovo C H and Wang E N 2017. A thermophysical battery for storage-based climate control, *Appl. Energy* **189** 31-43
[9]   Zheng X, Wang R Z, Ge T S and Hu L M 2015. Performance study of SAPO-34 and FAPO-34 desiccants for desiccant coated heat exchanger systems, *Energy* **93** 88-94
[10] Feng X, Qin M, Cui S, Rode C, Metal-Organic Framework MIL-100(Fe) as a Novel Moisture Buffer Material for Energy-Efficient Indoor Humidity Control, *Build. Environ.* **145** 234-242
[11] Furukawa H, Cordova K, O'Keeffe M, Yaghi O 2013. The Chemistry and Applications of Metal-Organic Frameworks, *Science* **341** 1230444.
[12] Cui S, Qin M, Marandi A, Steggles V, Wang S J, Feng X, Nouar F and Serre C 2018. Metal-Organic Frameworks as advanced moisture sorbents for energy-efficient high temperature cooling, *Nature Sci. Rep.* **8** 15284
[13] Jeremias F, Khutia A, Henninger S K and Janiak C 2012. MIL-100(Al, Fe) as water adsorbents for heat transformation purposes—a promising application, *J. Mater. Chem.* **22** 10148-51

Precise humidity control materials for autonomous regulation of indoor moisture

Menghao Qin [a,*], Pumin Hou [a], Zhimin Wu [b], Juntao Wang [c]

[a] Department of Civil Engineering, Technical University of Denmark, Lyngby, Denmark
[b] School of Architecture and Urban Planning, Nanjing University, Nanjing, China
[c] Department of Chemistry, Technical University of Denmark, Lyngby, Denmark

ABSTRACT

Indoor relative humidity is an important parameter to determine indoor air quality, occupants' thermal comfort and building energy consumption. As recommended by ASHRAE, the appropriate indoor relative humidity range for a healthy and comfortable indoor environment is between 40% and 65% RH. In order to meet the requirements, the most commonly used method is mechanical dehumidification/humidification system by using electricity. However, this approach is energy consuming. In this paper, a novel precise humidity control material (PHCM) based on Metal-Organic Frameworks (MOFs) is synthesized and its application in built environment is investigated. This material has an S-shape isotherm, high porosity and very high water vapor uptake of 1.62 g/g at 80% RH. It can rapidly adsorb moisture as the indoor relative humidity exceeds 60%, and release moisture as relative humidity drops below 45%. Unlike the conventional desiccants, e.g. zeolites, silica gel etc., MOF-PHCM can autonomously control indoor relative humidity within the desired comfort range at room temperature. Hygrothermal properties of the new material are measured. Numerical simulations have been carried out to study the effect of MOF-PHCM on indoor hygrothermal conditions and building energy consumption in five different climates worldwide (i.e. hot desert, semi-arid, Mediterranean, temperate, and humid subtropical). The results show that MOF-PHCM can effectively control indoor relative humidity fluctuations and reduce building energy consumption in most climates without any additional energy input. MOF-PHCM can be easily regenerated by either night ventilation (e.g. in hot desert, semi-arid, Mediterranean climates) or heating system powered by low-grade energy (e.g. in humid climates).

1. Introduction

Latent cooling load accounts for around one third of the total load of air-conditioning, and its proportion is even higher in some subtropical and tropical areas [1]. In order to maintain indoor comfort and to prevent microorganism growth, the American Society of Heating, Refrigerating, and Air-Conditioning Engineers (ASHRAE) recommends that indoor relative humidity should be maintained between 40% and 65%, which is the desired comfort relative humidity range for human being. In the conventional air-conditioning system, air is cooled and dehumidified simultaneously. The latent cooling load is removed by the refrigeration dehumidification process. Air is cooled to the dew point first, and then re-heated to the set-point for indoor environment, which results in wasting a lot of energy [2]. Desiccants help the system to independently control both temperature and humidity and thus contribute to the

reduction of the energy used [3,4]. Silica gels and zeolites are the most commonly used solid desiccants, but they are not very efficient for dehumidification owing to their high regeneration temperature, long cycling time and the fact that a larger part of their water vapor sorption occurs outside the desired comfort relative humidity range or the operating vapor pressure windows (i.e. between 40% and 65% RH) [5]. Dehumidification by liquid sorbents uses less electrical energy than refrigeration, but the relevant technology has distinct drawbacks for commercialization, e.g. the system is complex and bulky, and has corrosion problems [6,7].

The ideal materials for autonomous regulation of indoor relative humidity should meet the following criteria:

(1) The material should have an IUPAC-type V [8] S-shape isotherm and exhibit a steep uptake isotherm at a specific relative humidity

---

depending on the targeted application. For indoor humidity control for thermal comfort, the adsorption isotherm must have a steep rise around 65% RH, and the desorption isotherm must have a steep decrease around 40% RH (see Fig. 1);

(2) High water vapor uptake within the operating vapor pressure window;

(3) Low regeneration temperature and high reproducible cycling performance;

(4) High hygrothermal stability, non-toxicity and non-corrosion.

Solid porous material that meets all above four criteria is named as Precise Humidity Control Material (**PHCM**).

Many studies have been carried out to investigate existing solid desiccants that exhibit a water vapor sorption isotherm with a sigmoidal or S-shape [9,10]. However, studies show that almost no traditional or conventional porous sorbent can meet all of the four above criteria. Most conventional porous materials have a limited water vapor uptake ability at room conditions, and are not able to autonomously control the indoor humidity level within a small range precisely. Therefore, developing novel desiccants with large water vapor uptake and precise humidity control ability is needed.

Metal-organic frameworks (MOFs) are an emerging class of porous materials [11]. Most MOFs can exhibit very high surface areas and large adsorption capacity for gas [12]. Due to their structural and functional tunability, MOFs have become one of the most fascinating classes of materials for both scientists and engineers [12–14]. MOFs can be used for gas storage, purification, catalysis, sensor and drug delivery, etc. [12]. Recent studies show that MOFs are also promising sorbents for water vapor [6,13,14]. The diverse choice of linkers and secondary building blocks (SBU) facilitate the modulation of the hydrophilicity and sorption kinetics [15–18]. The carboxylate-based MOFs show remarkable uptake for water vapor and require lower regeneration temperatures for the desorption compared to conventional sorbents [6,14]. Some MOFs, such as Al-fumarate [19] and CAU-10-H [20], PIZOF-2 [21], 33R [22], Cr-MIL-101 [23], Cr-MIL-101-NH$_2$ [23,24], Cr-MIL-101-NO$_2$ [25], Y-shp-MOF5 [26], MIL-100(Fe) [27] and Al-MIL-53-OH [28] show good water vapor adsorption properties for

humidity control, and have different operating pressure windows in a general range of 20%–80% relative humidity. However, to the best of our knowledge, only very few of MOF materials can meet the all criteria for PHCM. In addition, most previous studies about MOFs are from chemistry discipline, and mainly focus on the synthesis and characterization of new materials. Detailed investigations of the effect of MOFs on indoor hygrothermal conditions and building energy performance have not been reported.

This paper aims to synthesis a MOF-based precise humidity control material (PHCM) that can realize the autonomous regulation of indoor relative humidity, and study the performance of the new MOF-PHCM for the indoor humidity control in different climates. First, the synthesis procedure and hygrothermal characterizations of the new MOF-PHCM will be reported, and the moisture buffer value (MBV) of the material will also be measured. Secondly, the energy saving potential by using MOF-PHCM in different climates will be discussed.

2. Synthesis and characterization

2.1. Synthesis of MOF based PHCM

Typically, MOFs are constructed from linking metal centers or clusters with organic linkers via relatively strong coordination bonds. The detailed processes of the MOF-PHCM are presented as follows. 0.3 ml 0.1 M FeCl$_3$·6H$_2$O in Dimethylformamide (DMF) (0.03 mmol) was added to a 23 ml glass scintillation vial containing 3,3″,5,5″-tetrakis (4-carboxyphenyl)-p-terphenyl (H$_4$TCPT) (H$_4$Ll) (The numbers 3,3″ and 5,5″ refer to the positions on the terphenyl ring where the tetrakis (4-carboxyphenyl) is attached [29].) (0.01 mmol), 1 ml DMF, 1 ml CH$_3$CN, and 1.5 ml nitric acid (3.5 M in DMF). The vial was sealed and placed into a preheated oven at 115 °C for 3 days. Pure orange cube-shaped crystals were obtained and washed with CH$_3$CN and air-dried [29]. The molecular formula of the orange crystals is [Fe$_3$(μ$_3$-O)(H$_2$O)(O$_2$C$^-$)$_6$]. Since the orange crystals are not very water stable, the following steps were carried out to replace Fe^{3+} with other more water stable ions, for example, zirconium [21], aluminum [29] and chromium [23,24] etc. The DVS tests show that Cr-MOF has the largest water vapor uptake
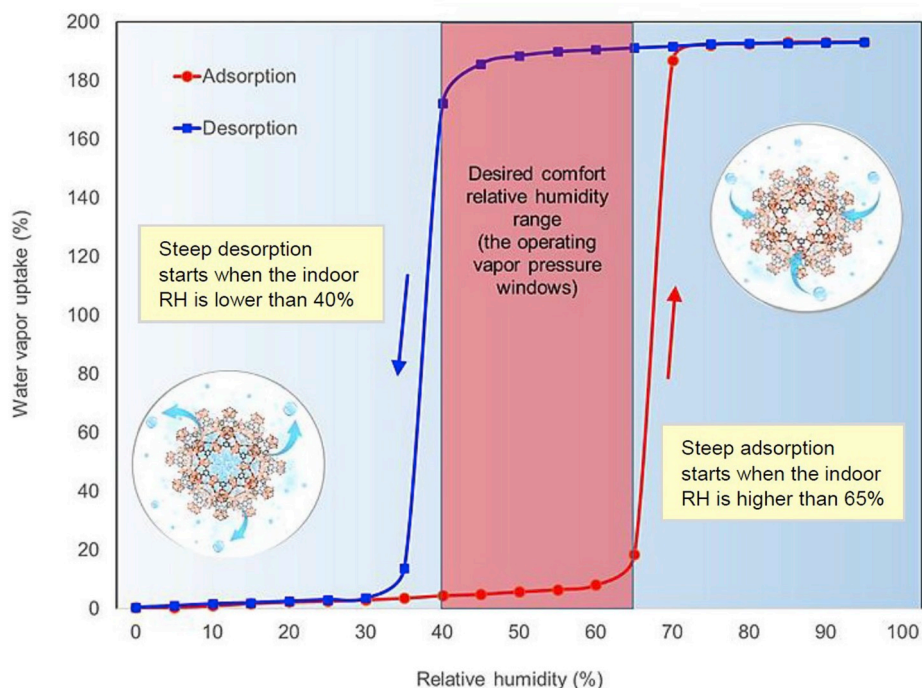

Fig. 1. Working principle of the ideal PHCM for autonomous indoor humidity control.

among other MOFs. Therefore, chromium is selected to replace Fe^{3+} for the second step of the synthesis. 25 mg of orange crystals was added in a 20 ml scintillation vial. In another vial, 150 ml of $CrCl_2$ was dissolved in 3 ml of DMF. The solution was then added to the first vial [24]. The vial was capped and incubated at 115 °C for 36 h, and then was cool to room temperature. Pure green crystals were obtained and washed with DMF several times (see Fig. 2). The molecular formula of the green crystals is $[Cr_3(\mu_3\text{-}O)(H_2O)(O_2C^-)_6]$.

Finally, the green crystals were coated into macroscopic layers on a metal surface. The concept of coating allows the MOFs to rapidly dissipate or absorb heat under isothermal conditions via a heat exchanger, which guarantee the desired sorption performance. The coating process used a water-borne binder of silica sol [6] (an aqueous silicic acid solution with water-insoluble silicon dioxide in colloid distribution), enabling the MOF layer to retain its original water vapor sorption features and capacity.

2.2. Characterization

2.2.1. Morphology

Scanning electronic microscope (SEM) has been used to analyze the geometry of the new crystal. The images were taken by an FEI Quanta 200 ESEM FEG microscope equipped with an energy-dispersive X-ray (EDS) spectrometer. The SEM image is shown in Fig. 3. The size of single cubic crystal is around 25 μm. The average pore size is around 2 nm.

2.2.2. Water vapor sorption experiments

The water vapor sorption isotherm is one of the most important hygric properties of a porous material. The water vapor isotherms of the MOF-PHCM were measured by a DVS (Dynamic vapor sorption) instrument (Surface Measurement Systems DVS Adventure). The sample was first dried in DVS by the airflow with the temperature of 23 °C and RH of 0% until weight did not change. Then the RH of the airflow increases from 0% to 100%. DVS will automatically record the weight of the sample when the weight of the sample retains constant at each RH step. The test results are shown in Fig. 4. The temperature during the measurements remains at 23 °C. The mass of sample used for the DVS test is around 30 mg.

The steep adsorption occurs at 60% RH and steep desorption occurs around 45% RH, respectively. Saturation approaches when the relative humidity reaches 80%. The water vapor uptake of MOF-PHCM at 80% RH is 1.62 g/g, which is much higher than most conventional sorbents and many MOFs [21]. Adsorption occurs in the inter-particulate voids. For the desorption curve, a visible hysteresis occurs. The water vapor isotherms show that the new MOF-PHCM meets the first and second criteria of the ideal PHCM for autonomous indoor humidity control. Fig. 4 also shows the water vapor isotherms of the material after 100 cycles. We can see there are only very minor changes to the isotherms, which means the adsorption and desorption of MOF-PHCM always take place in that specific way.
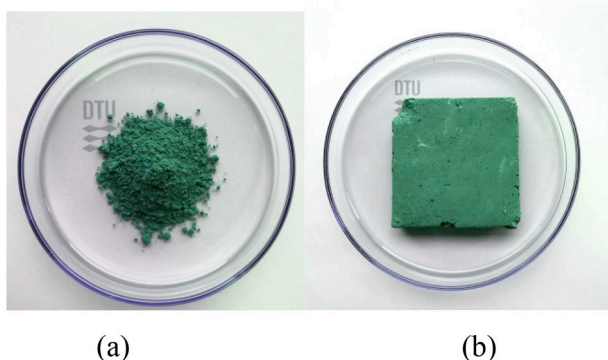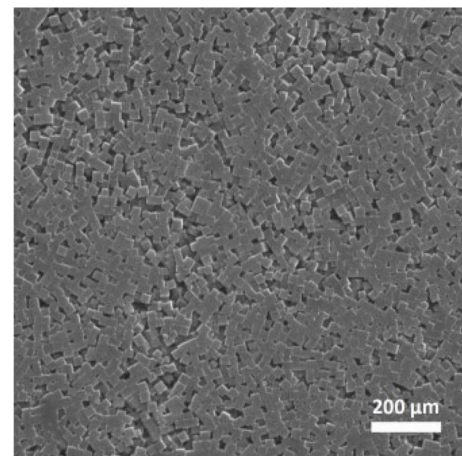

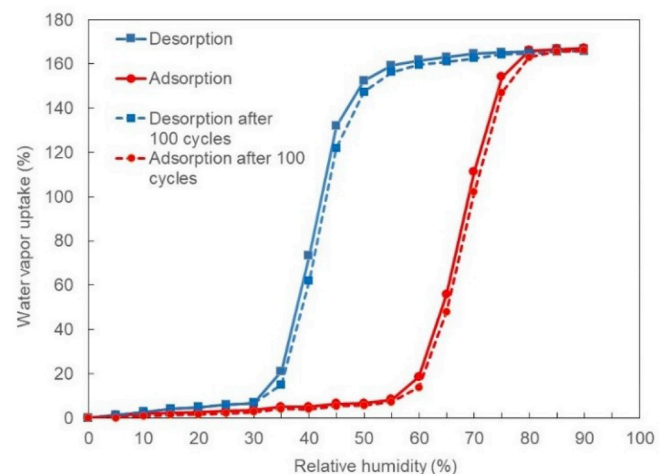
Fig. 3. SEM image of MOF-PHCM crystals.

Fig. 4. Water vapor sorption isotherms of MOF-PHCM.

2.2.3. Moisture buffer value (MBV)

The moisture buffering through adsorption and desorption of the hygroscopic surface materials of building envelopes and furnishing (e.g. wood furniture, curtains, carpet, textiles etc.) has an important effect on indoor hygrothermal conditions and energy performance of buildings [14,30–32]. Hygroscopic surface materials can uptake moisture from the air when its relative humidity increases and release moisture to the air when its relative humidity falls.

In order to evaluate the moisture buffer capacity of different hygroscopic materials, Rode et al. [33] proposed the concept of moisture buffer value (MBV), which indicates the amount of moisture uptake/release by a material when it is exposed to diurnal relative humidity variations between two given values. According to the test protocol proposed in NORDTEST [33], the MBV is a direct measurement of the amount of water vapor absorbed or desorbed by a hygroscopic material when it is exposed to a square wave in daily cycles (for example, 8 h of high relative humidity at 75% followed by 16 h of low relative humidity at 33%). Recently, Qin et al. [30] have improved the MBV theory and test methods.

The moisture buffer value (MBV) of the MOF-PHCM was measured according to the classic MBV test method proposed by NORDTEST. First, the sample (27 mm × 27 mm × 20 mm) was dried in an oven for 10 h at 60 °C. The thickness of the sample is larger than the penetration depth of the material, which is about 1.5 cm for MOF-PHCM in this research. Then the sample was sealed in a glass container in the climate chamber

Fig. 2. (a) MOF-PHCM powder, (b) MOF-PHCM in the form of a brick.

until the temperature of the samples dropped to the chamber temperature, which was 23 °C. The measurement was conducted in a climate chamber. The temperature inside the chamber is 23 °C. The external ambient temperature is between 20 and 25 °C. The temperature and humidity sensors measure the temporal temperature and relative humidity, and the signal is sent back to a PID regulator and computer. Saturated air and dry air can be mixed in different proportion controlled by the PID regulator to maintain a stable humidity in the chamber. The temperature and humidity inside the climate chamber are uniform as a small axial fan is installed to make the inside air well mixed. The relative humidity inside the chamber was set as 75% for 8 h and 33% for 16 h in one period of time. The air humidity was switched swiftly.

The MOF sample was placed inside the climate chamber, and only the upper surface of the sample was exposed to the air in the chamber. The rest five surfaces were sealed to avoid moisture transport. The weight of MOF sample was measured and logged automatically by the balance every minute. The measurement was performed in several cycles to get a relatively constant MBV of the material.

The mass variation during the MBV test is presented in Fig. 5. The test results show that the MBV of MOF-PHCM is 20.50 g m^{-2}·RH^{-1} at 8 h in the experimental conditions, which is almost 45 times higher than that of laminated wood and 36 times higher than gypsum [33]. The MBV test results indicate that the new MOF-PHCM has an exceptional performance of moisture buffering capacity within the hygroscopic range. Its MBV value is one magnitude higher than that of traditional/conventional building materials, and also much higher than other MOF desiccants, for example, MOF-100(Fe) [14] (see Table 1). MOF-PHCM has a great potential to be an ideal moisture sorbent for indoor humidity control. The MBVs of some traditional building materials and conventional materials are listed in the same table for comparison.

In addition, the vapor transfer coefficient of the new material was measured by the traditional cup method (see Appendix A for more details). It is 1.26×10^{-7} kg m^{-1} s^{-1}.

3. Indoor hygrothermal simulation

Both the moisture sorption isotherms and the MBV test show that the MOF based PHCM has an extraordinary moisture buffering capacity, which makes it very promising for indoor passive moisture control. Numerical simulations will be carried out to study the effect of MOF-PHCM on indoor humidity condition and building energy consumptions. The energy saving potential of applying MOF-PHCM in built environment in different climates will be investigated in this section.
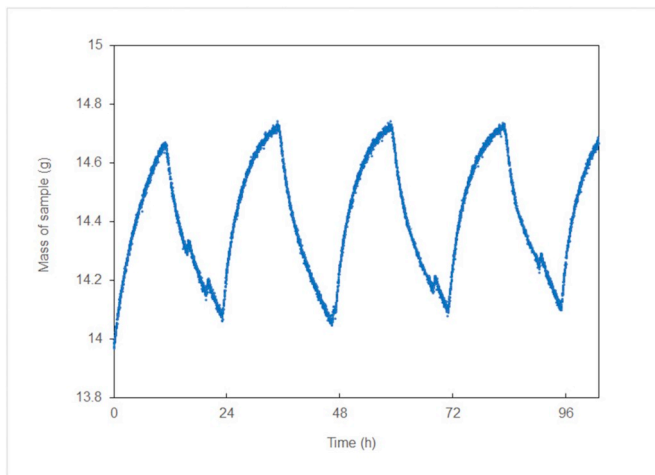

Fig. 5. Mass variation during the MBV test.

Table 1
MBVs of some porous materials [30–35] (23 °C, 33%/75%).

Material	MBV (g·m^{-2}·RH^{-1})
MOF-PHCM	20.50
MOF-100(Fe)	7.40
Spruce boards	1.22
Cellular concrete	1.05
Brich panels	0.91
Vesuvianite	0.79
Gypsum	0.57
Sepiolite	0.54
Laminated Wood	0.46
Concrete	0.42
Brick	0.39

3.1. Indoor latent load model

In order to investigate the buffering effect of MOF-PHCM on indoor environment, a simplified latent load model was developed. The model mainly focuses on the moisture balance/transfer in buildings because hygroscopic materials only affect the indoor moisture variation and their effect on indoor temperature can be neglected [36–38]. Generally, the indoor moisture conditions are mainly affected by the following factors: internal sources/sinks, moisture adsorption/desorption of internal hygroscopic materials, mechanical ventilation and infiltration, moisture diffusion through building envelopes, and heating and cooling systems. Vapor diffusion through building walls are not take into account in the current model since well-insulated modern buildings are normally equipped with vapor barrier, and are almost water impenetrable. There is no heating and cooling systems in the model. The indoor air is assumed to be well mixed, so the humidity at the ventilation exhaust is the same as the indoor humidity. The humidity of outside air varies with time depending on the outdoor weather condition. The variation rate of the indoor humidity ratio can be expressed as:

$$m_{in}\frac{dc_{in}}{dt} = m_{ven}(c_{out}(t) - c_{in}) + M_{PHCM}V_r + M_g V_r \qquad (1)$$

Where, m_{in} is the mass of indoor air, kg; m_{ven} is mass of ventilation air, kg·s^{-1}; c_{out} is the humidity ratio of outdoor air, kg·kg$_{air}^{-1}$; c_{in} is the humidity ratio of indoor air, kg·kg$_{air}^{-1}$; V_r is the room volume, m^3; t is the time, s; M_g is the vapor generation rate, kg·m^{-3}·s^{-1}; M_{PHCM} is the absorption/desorption rate by MOF-PHCM multiplies the surface area of material and divides by the room volume, kg·m^{-3}·s^{-1}, which can be calculated from the MBV theory [33].

By solving the differential equation (1), the indoor humidity ratio can be expressed as follows:

$$c_{in} = e^{-\frac{m_{ven}}{m_{in}}t}\left(\frac{m_{ven}}{m_{in}}\int c_{out}(t)e^{\frac{m_{ven}}{m_{in}}t}dt + c_{in}(0) - \frac{(M_g + M_{MOF})V_r}{m_{ven}}\right)$$
$$+ \frac{(M_g + M_{MOF})V_r}{m_{ven}} \qquad (2)$$

Where, $c_{in}(0)$ is the initial humidity ratio of indoor air.

The time-dependent indoor air humidity can be calculated by Eq. (2), and the influence with and without the moisture buffering of MOF-PHCM can be evaluated. Then the latent load removed by MOF-PHCM can be derived by comparing the moisture fluctuation with and without MOF-PHCM.

$$Q_l = r_0 m_r \int_{t_1}^{t_2}(c_{rno} - c_{rPHCM})dt \qquad (3)$$

Where, Q_l is the latent load removed by MOF-PHCM, kW; r_0 is the latent heat of vaporization, kJ·kg^{-1}; t_1 and t_2 are the start and end time of occupied period, s; c_{rno} is the indoor air humidity ratio without MOF-PHCM, kg·kg$_{air}^{-1}$; c_{rPHCM} is the indoor air humidity ratio with MOF-

PHCM, kg·kg$_{air}^{-1}$. If the indoor air humidity level with MOF-PHCM drops below the lower limit of the comfort zone (i.e. 40% RH in this research), c_{rPHCM} equals to the humidity ratio corresponding to the set-point condition.

3.2. Model validation

The International Energy Agency (IEA) Annex 41 project [39] has published a series of experimental tests for the validation of moisture buffer models. The experimental tests were carried out in Frauhofer Institut Fur Bauphysik, Germany. The volume of the test room is approx. 50 m^3, and the total surface of the room is approx. 67 m^2. All walls and ceiling surfaces of the test room were initially covered with aluminum foil to prevent the moisture sorption. A PVC covering was installed in order to avoid moisture flow to or from the ground. During the test, 50 m^2 of uncoated gypsum boards were attached on top of the walls with aluminum foil inside. The moisture buffering effect of the gypsum boards were measured.

The rooms were equipped with calibrated heating, ventilation and moisture production systems. The indoor air temperature of the test room was held at 20 °C. The tests were performed with a constant air change rate (ACH) of 0.66 h^{-1}. The solar radiation through the windows were ignored. The moisture production in the test room corresponds to a normal four-person household. The total moisture production is 2.4 kg d^{-1}. A basic moisture production rate of 0.025 kg h^{-1} was assumed with peaks in the morning and in the evening (0.4 kg h^{-1} from 6:00 to 8:00 a. m. and 0.2 kg h^{-1} from 16:00 to 22:00 p.m. every day). More detailed information of the experiments can be found in the report [39].

Fig. 6 shows the comparison between experiment and simulations. The simulation results from WUFI is also added. The indoor temperature was treated as a constant (20 °C) in the simulations. The calculated indoor relative humidity from the current model is slightly higher than the measured data. The mean relative error (MRE) is 2.7%. Nevertheless, a considerably good agreement is found between the predicted results and the measures values. Therefore, it shows that the model is capable of simulating the indoor moisture buffering.

3.3. Climate cases

Outdoor climatic conditions have a significant effect on the indoor humidity variations and the performance of porous humidity control materials. The humidity level of the outdoor air directly affect the regeneration efficiency of humidity control materials. In order to research the performance of the new MOF-PHCM on indoor humidity control and its energy saving potential in different climates, five typical climates/cities worldwide are selected. They are: Phoenix (hot desert climate), Salt Lake City (semi-arid climate), Madrid (moderate Mediterranean climate), Paris (temperate climate) and Shanghai (humid subtropical climate). These five climates cover the most populous areas in the world.

3.4. Test building

The BESTEST base case building from the IEA ECBCS Annex 21 [40] and Annex 41 [41] is selected as the test building. It is an 8 m × 6 m × 2.7 m single zone room (see Fig. 7). The current study only uses the characteristics of the BESTEST case in terms of volume and surface area to calculate the moisture buffering effect of interior porous materials on the indoor humidity variation and the latent heat load. There are no windows on the wall. The building is assumed to be a normal office room, which is only occupied from 9:00 am to 5:00 pm. The internal moisture gain during the occupied period is 5 g m^{-3}h^{-1}. There is no internal moisture gain during the unoccupied period. The building has a ventilation rate of 0.5 ACH throughout the day (for the cases with night ventilation, the ventilation rate during the unoccupied period is 1 ACH). The sensible load and latent load are handled independently. The indoor temperature is maintained at 25 °C by a high temperature cooling (HTC) system [6,42] during the occupied period. The HTC system uses higher temperature chilled water (e.g., 15–20 °C) compared to the conventional system (typical 5–7 °C). The HTC system only handles the sensible load, and the latent load will be handled by independent dehumidification system. Since the HTC system can largely raise the evaporation temperature, the corresponding COP is also much higher than conventional AC systems [6,42]. There is no temperature control during the unoccupied period. The permissible max indoor relative humidity is 65%. If the indoor RH is higher than 65%, the latent load should be removed by an independent dehumidification system. All external surfaces are assumed to be covered with aluminum foil where no vapor diffusion/transfer are possible.

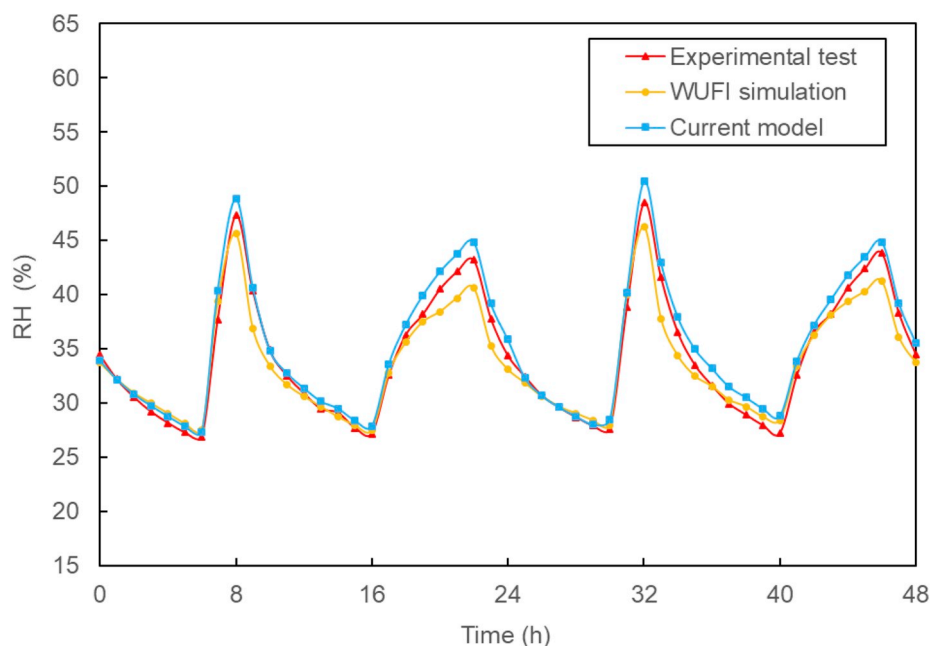For the cases without humidity control materials, all internal

Fig. 6. The comparison of simulated results from the current model and WUFI with the measured data (17–19 Feb. 2005).
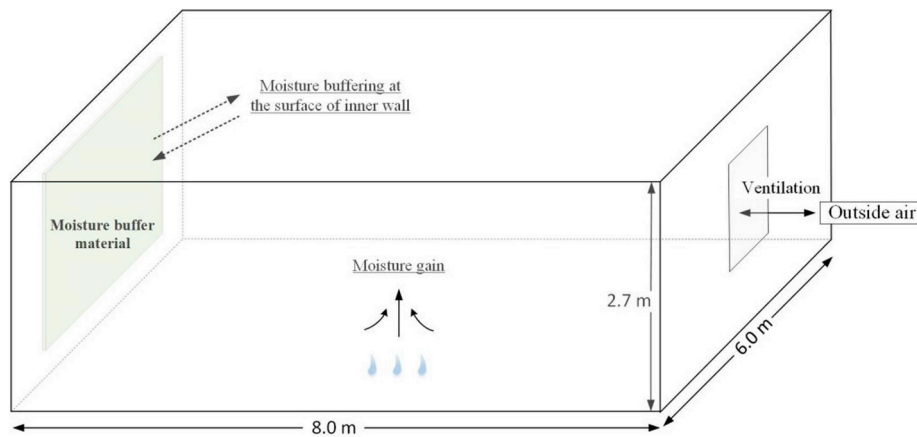
Fig. 7. A single office room model.

surfaces are supposed to be water-tight, and no moisture adsorption and desorption at the internal surface. For the cases with humidity control materials, an 8 m² wall panel made by MOF-PHCM is installed on the west internal wall, which is the only moisture buffer material indoors. All other internal wall surfaces are also supposed to be water-tight. The numerical simulation aims to evaluate the performance of the MOF-PHCM panel on passive regulation of the internal humidity condition.

The program used for the simulation was written in MATLAB based on the model presented in the paper. The time-step is 1 h. The calculations were run for as many years as it was necessary to achieve quasi-steady conditions. The results were reported for the last year of calculation.

3.5. Results and discussion

The simulation results of indoor humidity variations with and without MOF-PHCM materials in different climates are presented in this section. The corresponding energy saving potentials for latent load in different cases have also been calculated and discussed.

3.5.1. Phoenix (hot desert climate)

Hot desert climates are typically found under the subtropical ridge in the lower middle latitudes, often between 20° and 33° north and south latitude. Phoenix in the USA is one of the largest cities in this climate zone. Phoenix has hot and dry summers and mild winters. The average

annual percentage of humidity is 36.0%. On average, June and July are the driest months. Fig. 8 shows the indoor humidity ratio profiles for two weeks in July with and without MOF-PHCM in the Phoenix climate. The results indicate that in the case without moisture buffering materials, the indoor humidity ratio during the occupied period of the day exceeds 0.013 kg kg⁻¹ (65% RH at 25 °C) twice a week; while in the case with MOF-PHCM, the indoor humidity ratio is all below 0.012 kg kg⁻¹ (60% RH at 25 °C). No additional dehumidification is needed when MOF-PHCM is installed in the room. During the unoccupied period (the evening), the indoor humidity ratio in the case with MOF-PHCM is higher than that of the case without moisture buffer materials. The night ventilation of outside dry air (1 ACH) can regenerate the wet MOF-PHCM. MOF-PHCM will release moisture that was adsorbed during the occupied period, and the dry MOF-PHCM will be ready for the next cycle. The simulation of the whole summer shows the indoor relative humidity of the case with MOF-PHCM varies between 60% and 35%, which is perfect for indoor comfort and health. No additional humidity adjustment is needed in the case with MOF-PHCM in the hot desert climate.

3.5.2. Salt Lake City (hot semi-arid climate)

Hot semi-arid climates are most commonly found around the fringes of subtropical deserts. This climate tends to have hot summers and warm to cool winters, with some to minimal precipitation. Salt Lake City in the USA has a typical semi-arid climate. The average relative humidity in
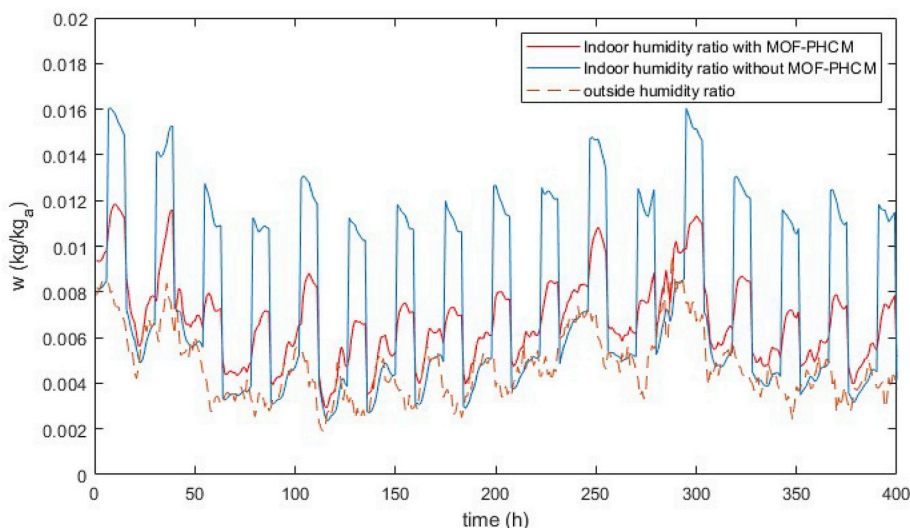

Fig. 8. Simulated indoor humidity ratio (July) with and without MOF-PHCM in Phoenix.

summer (June, July and August) is 33.2%. The simulated indoor humidity ratio for two weeks in July with and without MOF-PHCM in Salt Lake City are presented in Fig. 9. The results indicate that in the case without moisture buffering materials, the indoor humidity ratio during the occupied period exceeds 0.013 kg kg^{-1} (65% RH at 25 °C) almost every day. Additional dehumidification is needed for this case. However, in the case with MOF-PHCM, the indoor humidity ratio reaches 0.013 kg kg^{-1} only one day per week. The indoor relative humidity variation with MOF-PHCM during the occupied period is between 65% and 42%, which very close to the ASHRAE comfort zone. In the unoccupied period (night), the outdoor air with low RH could be used to dry the MOF-PHCM. The moisture released by MOF-PHCM will also be removed by night ventilation. Therefore, there is no need for extra humidity control for this case, which means MOF-PHCM could autonomously control the indoor humidity within the conform zone in semi-arid climates.

3.5.3. Madrid (moderate mediterranean climate)

Mediterranean climate zones are typically located along the western sides of continents, between roughly 30° and 45° north and south of the equator. A Mediterranean climate is characterized by dry summers and mild, wet winters. Madrid in Spain has a very typical Mediterranean climate. The average outdoor relative humidity in summer is 38.2%. The simulation results (see Fig. 10) show that the indoor humidity ratio without moisture buffer materials exceeds 0.017 kg kg^{-1} (85% RH at 25 °C) most time of the occupied period. The maximum indoor RH reaches 100% in several days. The high indoor humidity level will lead to mold formation, material deterioration and bad indoor comfort. Dehumidification is needed for the case without moisture buffering. In the case with MOF-PHCM, the indoor humidity ratio reaches 0.013 kg kg^{-1} two days per week. The indoor relative humidity with MOF-PHCM varies between 70% and 50% in the most time of the occupied period. Although it is slightly higher than the thermal comfort zone, it is still within the up limit of acceptable indoor humidity level. Very few days of high humidity will not cause mold and health problems. Therefore, there is no need for dehumidification in most days in the summer of Madrid climate with MOF-PHCM. Since the average outdoor humidity in the evening is quite low (below 40% RH), MOF-PHCM could be regenerated by night ventilation of outdoor dry air. When most MOF-PHCM has been regenerated, the night ventilation should be stop to avoid the dry materials to start adsorb moisture in the evening. With proper control ventilation strategies, MOF-PHCM could also be used to automatous regulation of indoor air during the occupied period in the Mediterranean climates.

3.5.4. Paris (temperate climate)

Paris has a temperate maritime climate, which features mild summers and mild winters, with a relatively narrow annual temperature range and few extremes of temperature. The precipitation is evenly dispersed throughout the year. It is the predominant climate type across much of Western Europe including the United Kingdom, the Pacific Northwest region of the United States and Canada etc. As to outdoor relative humidity, January is the most humid, and May is the least humid month. The average percentage of humidity in summer is around 65%. The simulated indoor humidity ratio for two weeks in July in Paris is presented in Fig. 11. For the case without moisture buffering, indoor humidity during the occupied period is higher than 0.016 kg kg^{-1} (80% RH at 25 °C) in 78% of the time. For the case with MOF-PHCM, the indoor humidity ratio reaches 0.015 kg kg^{-1} (75% RH at 25 °C) three to four days per week. There is a need for dehumidification for both cases. Since the outdoor air in the evening in Paris is more humid than that of the three previously discussed climates, MOF-PHCM could not be completely regenerated by night ventilation. The statistics result shows that in around half of the summer days, the outdoor humidity level in the evening meets the requirement for MOF regeneration. It means that MOF-PHCM cannot be completely regenerated in the rest half of the summer days. If the MOF-PHCM cannot be regenerated in the evening (the unoccupied period), its moisture buffer capacity will be significantly affected on the next day (the occupied period). Day 5 and 6 in Fig. 11 is an example. In these cases, additional regenerate method (e.g. heating etc.) may be needed. The detailed regeneration methods of MOF-PHCM will be discussed in the next section.

The calculation also indicates that the indoor latent load is 11.8 W m^{-2} in Paris climate. A stand-alone MOF-PHCM wall panel regenerated by night ventilation can remove 51.5% (6.08 W m^{-2}) of the total latent load in the temperate Paris climate without any additional energy input. The night ventilation rate is 1 ACH. If the material is completely dried by a proper regeneration system (e.g. heating system powered by low-grade energy), MOF-PHCM can handle all indoor latent load.

3.5.5. Shanghai (humid subtropical climate)

A humid subtropical climate is a zone of climate characterized by hot and humid summers, and cool to mild winters. Although many subtropical climates tend to be located at or near coastal locations, in some cases they extend inland, most notably in China and the United States. Shanghai has a typical humid subtropical climate. The average annual relative humidity is 80.3% and average monthly relative humidity
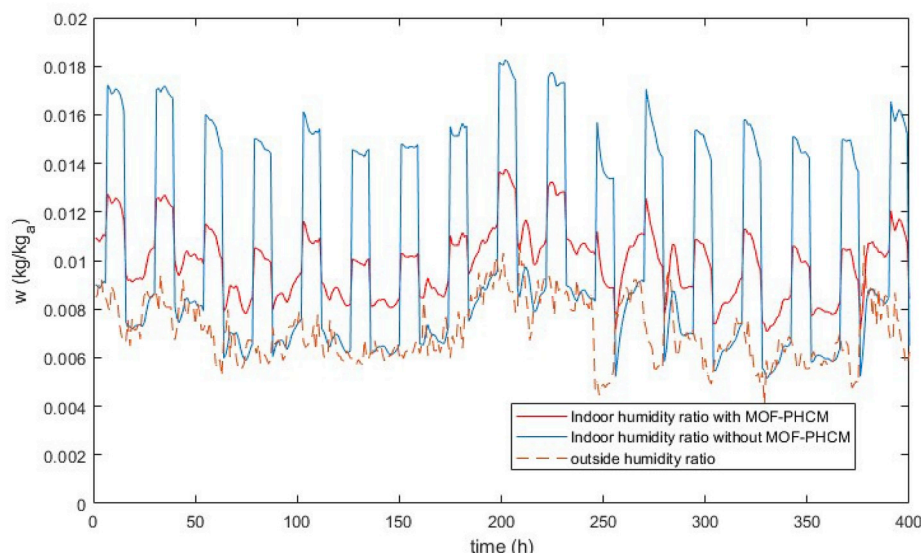

Fig. 9. Simulated indoor humidity ratio (July) with and without MOF-PHCM in Salt Lake City.
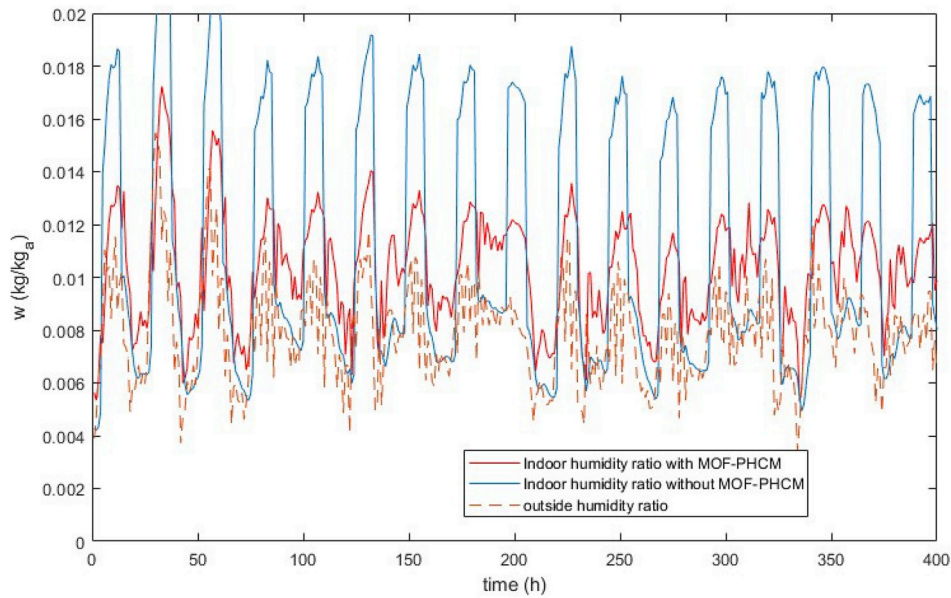
Fig. 10. Simulated indoor humidity ratio (July) with and without MOF-PHCM in Madrid.
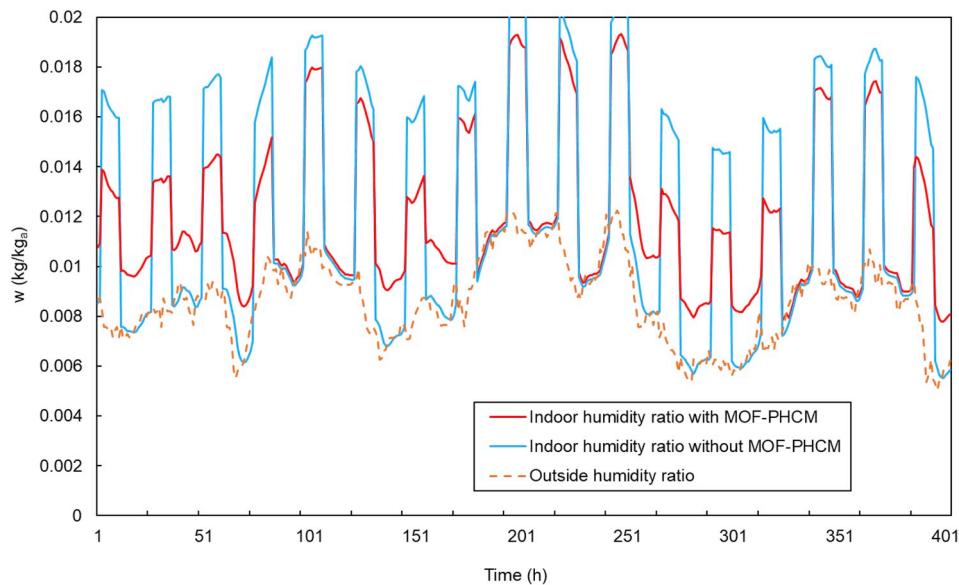

Fig. 11. Simulated indoor humidity ratio (July) with and without MOF-PHCM in Paris.

ranges from 77% in December to 84% in June. The simulation shows that MOF-PHCM cannot work properly in this climate since the outside RH in the unoccupied period is much higher than the desorption RH of MOF-PHCM. Once the MOF-PHCM gets saturated, it is impossible to dry the wet MOF-PHCM purely by passive approach (e.g. night ventilation etc.)

In order to make MOF-PHCM work in the Shanghai climate, two modifications have been proposed: (1) double the amount of MOF-PHCM, i.e. add one more MOF wall panel on the east wall; (2) regenerate the wet MOF-PHCM by a heating system powered by low-grade energy. The heat source for the heater could be solar energy or waste heat from thermal power plants etc. Fig. 12 shows the simulated indoor humidity profiles with and without MOF-PHCM for two weeks in July in Shanghai after the improvements. The results indicate that MOF-PHCM could adsorb most moisture load in the occupied period as long as it can be completely regenerated in the following unoccupied period. In the case with MOF-PHCM, the humidity ratio is below 0.014 kg kg^{-1} (70%

RH at 25 °C) most time of the week. No additional dehumidification other than MOF-PHCM is needed. If the heat for the regeneration of the material is from renewable energy or waste heat, the whole system is still very much energy efficient compared to the traditional refrigeration dehumidification. The study confirms that MOF-PHCM with a proper regeneration system can be used for passive control of the indoor humidity condition in very humid climates.

In summary, MOF-PHCM could be used for indoor moisture control in all climates. In hot desert climate, semi-arid climate and Mediterranean climate, MOF-PHCM could autonomously regulate indoor relative humidity within the comfort zone without any additional energy input. In temperate maritime climate, a stand-alone MOF-PHCM wall panel could remove 51.5% of the total indoor latent load without additional energy input. If the material is regenerated by a proper regeneration system, for example, heating systems powered by renewable energy, enough MOF-PHCM could also realize the autonomous control of indoor relative humidity in temperate climate. In humid subtropical climates,
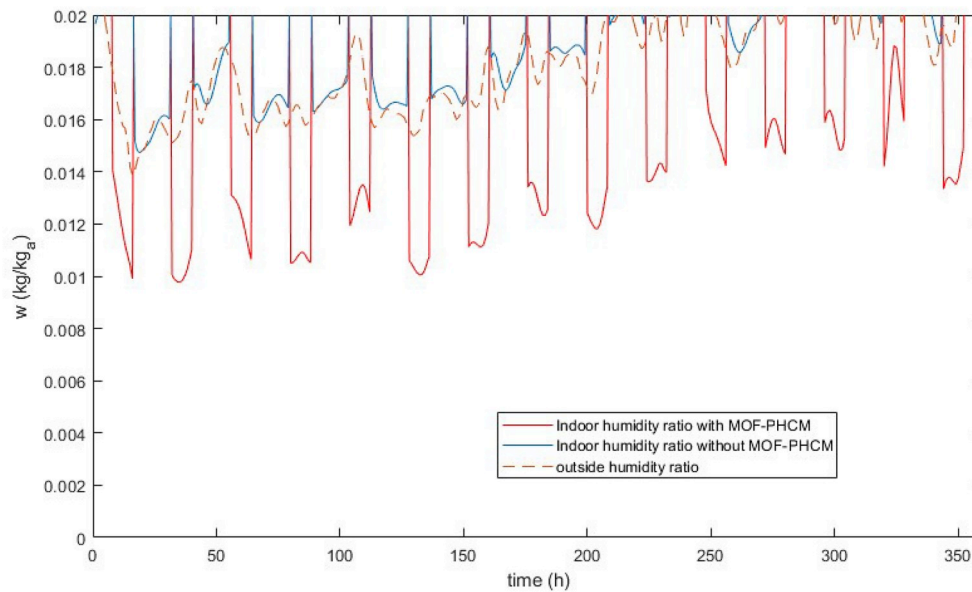
Fig. 12. Simulated indoor humidity ratio (July) with and without MOF-PHCM in Shanghai.

MOF-PHCM must be integrated with a proper regeneration system to realize the indoor humidity control. It is important to note that the amount of MOF-PHCM for moisture control in different climates should be calculated according to the indoor moisture load and outdoor weather condition.

Finally, it is necessary to mention again that the current research mainly focuses on the moisture buffer effect on the latent load of a building. We assume that the sensible load is the same for both cases with and without moisture buffer materials [36–38]. All energy-saving potentials presented in the paper refer to the latent load saving rate, and the values are evaluated based on the numerical simulation. There might be some extra energy consumption due to the night ventilation at 1 ACH in some cases. However, take the BESTEST room as an example, the night ventilation rate at 1 ACH is 130 m³ h⁻¹. The power consumption of a fan for this ventilation rate is normally around 20 W, which is negligible compared to the energy consumption of the air-conditioning system. In addition, the current research mainly focuses on the preparation, characterization and potential application of the new material. More detailed investigation of its integration into a specific AC system in a real building will be carried out next step. We will report the details in future papers.

3.6. Regeneration of MOF-PHCM

Metal-organic frameworks (MOFs) can be regenerated either by dry air or by heating. In general, the regeneration temperature of MOFs is much lower than that of conventional sorbents or desiccants [6,12,13], which makes it possible to use some low-grade energy (e.g. solar energy, waste heat from thermal power plants etc.) to regenerate it. There are many ways to regenerate the MOF-PHCM materials. The simplest way is to expose the wet MOF-PHCM to the sun, and regenerate it by using low-grade heat from natural sunlight [13]. In order to maintain a continuous operation, two MOF-PHCM panels are needed. One is in use and the other one is under regeneration by natural sunlight, and switch them every day at the beginning of the occupied period. The other simple way is to integrate the MOF-PHCM wall panel with a heater (e.g. coat the MOFs on the surface of a panel heater), and then maintain the surface temperature around 60 °C for 20–30 min [6]. The MOF-PHCM coating will be regenerated. The heat and moisture released to the indoor space could be removed by forced ventilation, and will not significantly affect the indoor temperature. The heat source for the

heater could be solar energy or waste heat from other process. Of course, this process is better completed when the room is unoccupied.

Since the energy used for regeneration is renewable, the energy efficiency of the whole MOF dehumidification system is still much higher than other normal dehumidification technologies (e.g. refrigeration, conventional solid desiccants and liquid desiccant etc.) However, due to the limitation of the paper length, a detailed description of the mechanical regeneration system for MOF-PHCM is not within the scope of this paper. We will report the system in the future studies.

4. Conclusion

The paper first proposes the concept of the ideal precise humidity control material (PHCM) for autonomous regulation of indoor relative humidity, and the selection criteria of PHCM. A new PHCM based on metal-organic frameworks (MOFs) has been prepared. Hygrothermal properties of the new material have been measured. This material has an S-shape isotherm, high porosity and very high water vapor uptake of 1.62 g/g at 80% relative humidity. It can rapidly adsorb moisture as the indoor relative humidity level exceeds 60%, and release moisture when the indoor relative humidity drops below 45%. Compared with conventional dissidents, e.g. zeolites and silica gel etc., MOF-PHCM has high water vapor uptake capacity, lower regeneration temperature, and more importantly, MOF-PHCM can autonomously control the indoor relative humidity within the desired comfort range at room temperature.

Numerical simulations have been carried out to study the effect of MOF-PHCM on indoor hygrothermal conditions and building energy consumption in five different climates (i.e. hot desert, semi-arid, Mediterranean, temperate, and humid subtropical climates). The results show that MOF-PHCM can effectively moderate the indoor moisture fluctuation, and maintain the indoor relative humidity within the desired range in most climates as long as it can be properly regenerated. In hot desert climate, semi-arid climate and Mediterranean climate, MOF-PHCM can be regenerated by night ventilation without any additional energy input. MOF-PHCM can remove all indoor latent load passively. In temperate maritime climate, MOF-PHCM could remove up to 51.5% of the total indoor latent load by using night ventilation as the only regeneration method. Additional regeneration by heating could be used to completely dry MOF-PHCM. In humid subtropical climate, MOF-PHCM should be integrated with a proper regeneration system to realize the indoor humidity control. Since the regeneration temperature of MOF-PHCM is

around 60–70 °C, it is easy to reach that temperature by using low-grade energy (e.g. solar energy, waste heat from thermal power plants etc.) The whole MOF dehumidification system is zero-energy consumption as the heat for regeneration is from renewable sources.

To sum up, MOF-PHCM is a promising material for automatous regulation of indoor moisture in different climates. The MOF-PHCM synthesized in the paper focuses on the operating range of 40–65% RH, which is mainly for the human comfort. No refrigeration dehumidification is needed when using enough MOF-PHCM indoors. The MOF-PHCM can be easily regenerated by either night ventilation or heating system powered by renewable energy. Further studies will focus on the development of new MOF-PHCMs with different operating RH ranges for different applications and processes in industry, for example, 10–30% RH range for the microelectronics industry, and 20–30% RH for the storage of artworks in the museums etc.

Declaration of competing interest

Acknowledgements

Appendix A

The isothermal cup method was used to measure the vapor transfer coefficient of the material. The saturated salt solution (NaCl, sodium chloride) provides a constant relative humidity (75.3 ± 0.12% at 25 °C) inside the cup. The cup was placed in a climate chamber with a constant temperature and relative humidity (33 ± 0.5% %, 25 ± 0.2 °C). Then a vapor pressure gradient appears across the test sample. The cup test was conducted under the conditions of a constant temperature and a given RH difference.
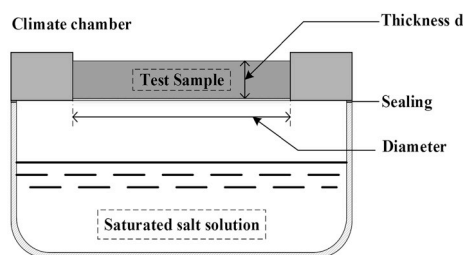

Fig. A1. Schematic of cup method.

Fig. A1 shows the schematic of the cup method test. The weight change of the cup with time was measured regularly until the mass loss reaches a steady state. The vapor transfer coefficient can be expressed as:

$$\delta = \frac{g_v \cdot d}{\Delta RH} \tag{A.1}$$

Where, g_v is the moisture flow (kg s^{-1}), d is the thickness of the sample (m), and ΔRH is the difference of relative humidity on both sides of the sample. In this case, the thickness is 1.5 cm; the diameter of the test sample is 2.5 cm. The vapor transfer coefficient of MIL-100(Fe) can thus be calculated, and it is 1.26×10^{-7} kg m^{-1} s^{-1}.

References

[1] P. Mazzei, F. Minichiello, D. Palma, HVAC dehumidification systems for thermal comfort: a critical review, Appl. Therm. Eng. 25 (2005) 677–707.
[2] K. Chua, S. Chou, W. Yang, J. Yan, Achieving better energy-efficient air conditioning – a review of technologies and strategies, Appl. Energy 104 (2013) 87–104.
[3] P. Mazzei, F. Minichiello, D. Palma, HVAC dehumidification systems for thermal comfort: a critical review, Appl. Therm. Eng. 25 (2005) 677–707.
[4] X. Liu, Y. Jiang, Temperature and Humidity Independent Control (THIC) of Air-Conditioning System, Springer, 2013.
[5] P.K. Tsobnang, E. Hastürk, D. Fröhlich, et al., Water vapor single-gas selectivity via flexibility of three potential materials for autonomous indoor humidity control, Cryst. Growth Des. 19 (5) (2019) 2869–2880.
[6] S. Cui, M. Qin, et al., Metal-Organic Frameworks as advanced moisture sorbents for energy-efficient high temperature cooling, Sci. Rep. 8 (2018).
[7] A. Lowenstein, Review of liquid desiccant technology for HVAC applications, HVAC R Res. 14 (2008) 819–839.
[8] M. Thommes, K. Kaneko, A.V. Neimark, et al., Physisorption of gases, with special reference to the evaluation of surface area and pore size distribution (IUPAC Technical Report), Pure Appl. Chem. 87 (2015) 1051–1069.
[9] J. Dieckmann, Air-to-air energy recovery heat exchangers, ASHRAE J. 45 (2003) 15–16.
[10] W. Wang, L. Wu, Z. Li, Y. Fang, et al., An Overview of adsorbents in the rotary desiccant dehumidifier for air dehumidification, Dry. Technol. 31 (2013) 1334–1345.
[11] G. Férey, Hybrid porous solids: past, present, future, Chem. Soc. Rev. 37 (2008) 191–214.
[12] H. Furukawa, K. Cordova, M. O'Keeffe, O. Yaghi, The Chemistry and Applications of Metal-Organic Frameworks, Science, Aug, 2013.
[13] H. Kim, S. Yang, S. Rao, S. Narayanan, A. Umans, O. Yaghi, E. Wang, et al., Water harvesting from air with metal-organic frameworks powered by natural sunlight, Science 356 (6336) (2017) 430–434. Apr.
[14] X. Feng, M. Qin, S. Cui, C. Rode, Metal-Organic Framework MIL-100(Fe) as a Novel Moisture Buffer Material for Energy-Efficient Indoor Humidity Control, vol. 145, Building and Environment, 2018.
[15] E. Ng, S. Mintova, Nanoporous materials with enhanced hydrophilicity and high water sorption capacity, Microporous Mesoporous Mater. 114 (2008) 1–26.
[16] J. Bauer, R. Herrmann, W. Mittelbach, W. Schwieger, Zeolite/aluminum composite adsorbents for application in adsorption refrigeration, Int. J. Energy Res. 33 (2009) 1233–1249.
[17] D. Wragg, R. Johnsen, P. Norby, H. Fjellvåg, The adsorption of methanol and water on SAPO-34: in situ and ex-situ X-ray diffraction studies, Microporous Mesoporous Mater. 134 (2010) 210–215.
[18] A. Dhakshinamoorthy, M. Alvaro, H. Garcia, Commercial metal–organic frameworks as heterogeneous catalysts, Chem. Commun. 48 (2012) 11275.

[19] F. Jeremias, D. Frolich, C. Janiak, S.K. Henninger, Advancement of sorption-based heat transformation by a metal coating of highly-stable, hydrophilic aluminum fumarate MOF, RSC Adv. 4 (2014) 24073–24082.

[20] D. Frohlich, E. Pantatosaki, P.D. Kolokathis, et al., Water adsorption behavior of CAU-10-H: a thorough investigation of its structure property relationships, J. Mater. Chem. 4 (2016) 11859–11869.

[21] H. Furukawa, F. Gndara, T. Zhang, et al., Water adsorption in porous metal organic frameworks and related materials, J. Am. Chem. Soc. 136 (2014) 4369–4381.

[22] S.Y. Zhang, S. Jensen, K. Tan, et al., Modulation of water vapor sorption by a 4th generation metal-organic material with a rigid framework and self-switching pores, J. Am. Chem. Soc. 140 (2018) 12545–12552.

[23] J. Ehrenmann, S. Henninger, C. Janiak, et al., Water adsorption characteristics of MIL-101 for heat transformation applications of MOFs, Eur. J. Inorg. Chem. (2011) 471–474, 2011.

[24] T. Abtab, D. Alezi, P. Bahtt, et al., Reticular Chemistry in Action: A Hydrolytically Stable MOF Capturing Twice Its Weight in Adsorbed Water, Chem 4 (1) (2018) 94–105.

[25] J. Canivet, J. Bonnefoy, C. Daniel, A. Legrand, et al., Structure property relationships of water adsorption in metal organic frameworks, New J. Chem. 38 (2014) 3102–3111.

[26] R.G. AbdulHalim, P.M. Bhatt, Y. Belmabkhout, A. Shkurenko, et al., A fine-tuned metal organic framework for autonomous indoor moisture control, J. Am. Chem. Soc. 139 (2017) 10715–10722.

[27] P. Horcajada, S. Surble, C. Serre, D. Hong, et al., Synthesis and catalytic properties of MIL-100(Fe), an iron(III) carboxylate with large pores, Chem. Commun. 27 (2007).

[28] S.K. Ghosh, J.P. Zhang, S. Kitagawa, Reversible topochemical transformation of a soft crystal of a coordination polymer, Angew. Chem. Int. Ed. 46 (2007) 7965–7968.

[29] D.A. Alezi, Reticular Chemistry and Metal-Organic Frameworks: Design and Synthesis of Functional Materials for Clean Energy Applications, PhD thesis, King Abdullah University of Science and Technology, 2017.

[30] M. Zhang, M. Qin, C. Rode, Z. Chen, Moisture buffering phenomenon and its impact on building energy consumption, Appl. Therm. Eng. 124 (2017) 337–345.

[31] Z. Wu, M. Qin, M. Zhang, Phase change humidity control material and its impact on building energy consumption, Energy Build. 174 (2018) 254–261.

[32] Z. Chen, D. Su, M. Qin, G. Fang, Preparation and characteristics of composite phase change material (CPCM) with SiO2 and diatomite as endothermal-hydroscopic material, Energy Build. 86 (2015) 1–6.

[33] C. Rode, R. Peuhkuri, B. Time, K. Svennberg, T. Ojanen, et al., Moisture buffer value of building materials, J. ASTM Int. (JAI) 4 (2007) 1–12.

[34] M. Rahim, O. Douzane, A. Tran Le, G. Promis, et al., Characterization and comparison of hygric properties of rape straw concrete and hemp concrete, Constr. Build. Mater. 102 (2016) 679–687.

[35] Z. Chen, M. Qin, Preparation and hygrothermal properties of composite phase change humidity control materials, Appl. Therm. Eng. 98 (2016) 1150–1157.

[36] M. Qin, R. Belarbi, F. Allard, Simulation of Whole Building Coupled Hygrothermal-Airflow Transfer in Different Climates, Energy Conversion and Management, 2011, p. 52.

[37] H. Künzel, A. Holm, D. Zirkelbach, A. Karagiozis, Simulation of indoor temperature and humidity conditions including hygrothermal interactions with the building envelope, Sol. Energy 78 (2005) 554–561.

[38] M. Qin, R. Belarbi, Development of an analytical method for simultaneous heat and moisture transfer in building materials utilizing transfer function method, J. Mater. Civ. Eng. 17 (2005) 492–497.

[39] C. Rode, M. Woloszyn, IEA Annex 41, MOIST-ENG Subtask 1 – Modelling Principles and Common Exercises, Final report, 2007.

[40] R. Judkoff, J. Neymark, International Energy Agency Building Energy Simulation Test (BESTEST) and Diagnostic Method, NREL, National Renewable Energy Laboratory, Golden, 1995.

[41] C. Rode, M. Woloszyn, Common exercises in whole building HAM modelling, in: C. Rode, H. Hens, H. Janssen (Eds.), Proceedings of the IEA ECBCS Annex 41 Closing Seminar, 2008. Copenhagen, Denmark.

[42] E. Saberab, K. Thama, H. Leibundgutc, A review of high temperature cooling systems in tropical buildings, Build. Environ. 96 (2016) 237–249.

58

Metal-organic framework MIL-100(Fe) as a novel moisture buffer material for energy-efficient indoor humidity control

Xiaoxiao Feng, Menghao Qin*, Shuqing Cui, Carsten Rode

Department of Civil Engineering, Technical University of Denmark, Lyngby, 2800, Denmark

ARTICLE INFO

ABSTRACT

Metal-organic frameworks (MOFs) are a new class of porous materials composed of a three-dimensional network of metal ions held in place by multidentate organic molecules. MIL-100(Fe) (molecular formula: $Fe_3O(H_2O)_2OH$ $(BTC)_2$), as one kind of MOFs, has an excellent performance of water sorption due to the large specific surface areas and high porosity. The paper proposes an innovative application of MIL-100(Fe) as a new kind of moisture buffer material to control the indoor humidity passively. MOFs can moderate indoor moisture fluctuation, which will greatly reduce the energy consumption of HVAC systems and improve the building energy efficiency. In the paper, microstructure and moisture characterizations of MIL-100(Fe) have been carried out. The moisture buffer value (MBV) of MIL-100(Fe) has been measured and compared to the typical building materials. The results show that MIL-100(Fe) can absorb up to $15 \, g \, m^{-2} \cdot RH^{-1}$ at 8 h, which is 33 times higher than the laminated wood. A novel lumped model for building latent load simulation has been developed. The energy saving potential by using MOFs in a typical office in different climates was calculated. The results show that a $5 \, m^2$ MOF wall panel can remove most of the latent load in dry and moderate climates without any energy input; MOFs can be regenerated by night ventilation. In the hot and humid climate, the MOF materials can remove 73.4% of the latent load, and can be easily regenerated by using low-grade energy.

1. Introduction

Buildings account for about 40% of the world's total energy consumption [1,2], and more than 50% of the primary energy consumed in buildings is for the heating and air-conditioning system [3]. To ensure adequate supplies of energy and to curtail the growth of CO_2 emissions, it is essential to improve the building energy efficiency and reduce the energy consumption of HVAC systems. One way to achieve this goal is through the introduction of innovative passive building materials that can regulate the indoor humidity, and maintain the indoor environment at a stable and comfortable level.

The loads of HVAC systems consist of sensible load and latent load. In some hot and humid climates, the latent load takes a significant proportion of the total cooling load [4], leading to considerable energy consumption in air dehumidification [5]. Hygroscopic materials and components in buildings, such as porous building materials and furniture, can adsorb/release moisture from/to the indoor air, and have a positive effect on moderating the indoor relative humidity (RH) fluctuations. Since the moisture buffer phenomenon occurs without energy use, the moisture buffer materials can reduce the energy use for humidification or dehumidification in buildings [6].

Previous studies on the moisture buffer materials for indoor humidity control mainly focus on the traditional and conventional building materials, such as concrete, drywall, brick, plywood, gypsum and combination of them [7,8]. In 2005, Rode et al. proposed the concept of the moisture buffer value (MBV) to evaluate the moisture buffer performance of different materials [7]. The MBVs of many traditional and conventional building materials have been measured according to the NORDTEST method [6,7]. The test results show that the MBV of most traditional and conventional building materials is relatively low and imply a limited ability to moderate the indoor moisture variation [9–16]. The MBVs of some traditional building materials and conventional materials are listed in Table 1. The test temperature is 23 °C and RH is 33%/75%. As a result, the energy saving potential by using the traditional or conventional hygroscopic building materials for moisture buffering is limited. Further studies on new materials are needed.

Conventional desiccants, such as silicates, aluminophosphates, zeolites and activated charcoal, have high hydrophilicity, and show large water sorption capacity, and are widely used in many industrial and civil applications [17–20]. However, the regeneration temperature of most traditional desiccants is very high (normally higher than

* Corresponding author.
  E-mail address: menqin@byg.dtu.dk (M. Qin).

Table 1
MBV of some traditional/conventional materials [7,10,14–16] (23 °C, 33%/75%).

Material	MBV (g·m^{-2}·RH^{-1})
Gypsum	0.26
Diatomite	0.33
Concrete	0.38
Brick	0.4
Laminated Wood	0.45
Sepiolite	0.54
Vesuvianite	0.79
Spruce boards	1.15

100 °C), which means these desiccants cannot release moisture in indoor conditions. Thus, these desiccants are not suitable for passive moisture regulation in buildings.

The ideal moisture buffer materials should have both high water uptake capacity and low regeneration temperature (i.e. the material could release moisture in room temperature when the indoor humidity is low.). Metal–organic frameworks (MOFs), a novel class of porous crystalline materials, have drawn large attention recently. Some MOFs possess the largest surface area, pore volume and lowest framework density among the existing porous solids and have high water uptake capacity [21–23]. Compared to some microporous materials, such as the desiccants mentioned above, the structure of MOFs has the potential for more flexible rational design [24], and the pore size of MOFs is tunable, leading to some unusual patterns of water sorption isotherm [21,25]. Some MOFs can be regenerated under room temperature and humidity owing to their unique water sorption isotherms. However, in previous studies, applications on MOFs mainly focus on catalysis, gas sorption and storage, adsorption heat pump, sensor, and drug delivery [23,26]. The application of MOFs in buildings as a moisture buffer material for energy-saving has not been reported yet.

In addition to the large adsorption ability, the MOFs for built environment application must possess other advantages such as water stable, a lack of toxicity, low regeneration temperature, low-cost and the possibility of scalable production. Many types of MOFs have been synthesized in the past several years, but few of them meet the above criteria [27–29]. We have investigated the performance of a few archetypal amphiphilic MOFs, including MIL-100(Fe), Basolite A520 (Aluminium Fumarate), MIL-125(Ti), UiO-66(Zr), and MOF-808(Zr) etc [30–33]. With one of the highest water uptake capacity ever reported, MIL-100(Fe) has a better overall performance than any other. We therefore chose MIL-100(Fe) for use in this paper.

This paper aims to apply MIL-100(Fe) as a novel moisture buffer material for the passive control of indoor humidity in different climates. First, the microstructure and moisture characterizations of MOF MIL-100(Fe) will be studied, and the moisture buffer value of the material in various conditions will also be measured. Secondly, a mathematical model will be set up to study the energy performance of MOF MIL-100(Fe) in a typical office room. Finally, the energy saving potential by using MOF materials in different climates will be discussed.

2. Characterization

The sample of MIL-100(Fe) analyzed in this paper is synthesized by the École Normale Supérieure in Paris, France (the main partner of this research). The microstructure and moisture characterizations of MIL-100(Fe) have been measured and discussed in this section.

2.1. Morphology

Scanning electronic microscope (SEM) has been used to analyze the geometry of MIL-100(Fe) crystal. The sample of MIL-100(Fe) is not purified further after acquiring from the French partner. The images
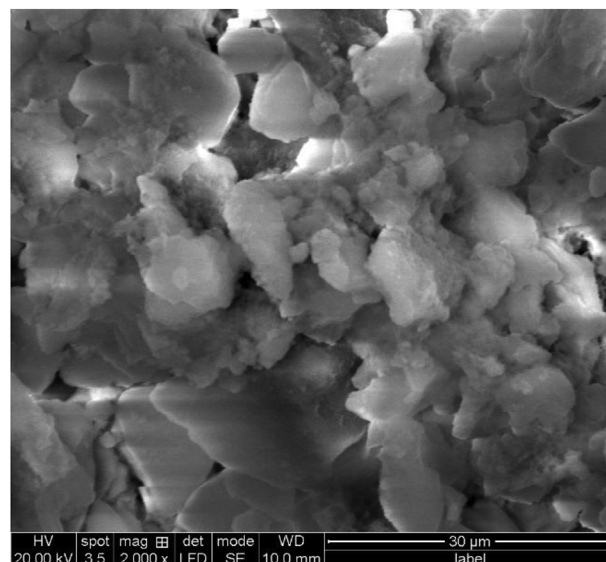

Fig. 1. SEM images of MIL-100(Fe).

were taken by an FEI Quanta 200 ESEM FEG microscope equipped with an energy-dispersive X-ray (EDS) spectrometer. The SEM image is shown in Fig. 1. The tiny crystal of MIL-100(Fe) is octahedral with the size of 0.5–2 μm.

2.2. Water sorption isotherms

Water sorption isotherms illustrate a clear image of water sorption performance under different relative humidity. The isotherms were measured by a DVS (Dynamic vapor sorption) instrument (Surface Measurement Systems DVS Adventure). The sample of MIL-100(Fe) was first dried in DVS by the airflow with the temperature of 23 °C and RH of 0% until weight did not change. Then the RH of the airflow could be set, such as 0%, 10%, 20%, etc. DVS will automatically record the weight of the sample when the weight of the sample retains constant at each RH point. The test result is shown in Fig. 2. The temperature during the measurements remains at 23 °C. The steep adsorption occurs at RH = 25% and RH = 40%, respectively. This is mainly because that MIL-100(Fe) has a polymodal pore size distribution, from both 25 Å and 29 Å mesopores. Saturation approaches when the relative humidity reaches 50%. When the relative humidity is higher than 50%, the mass
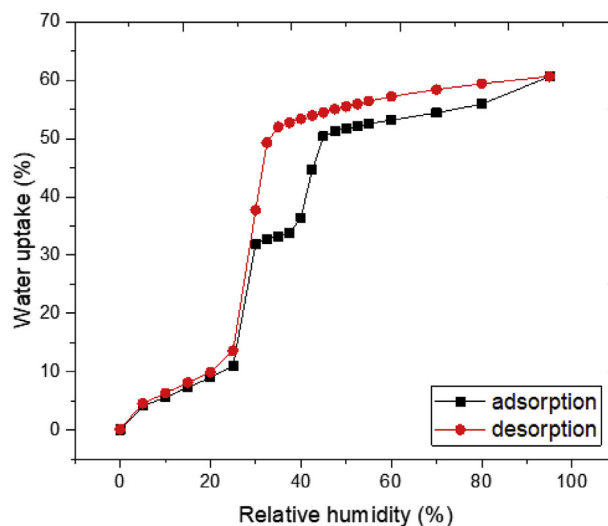

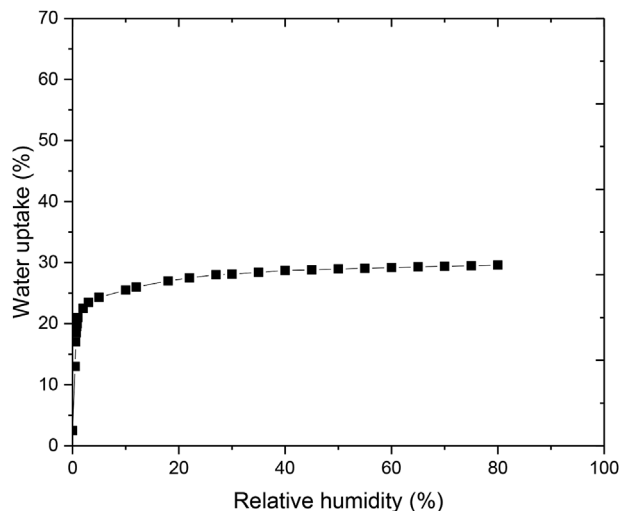**Fig. 2.** Water sorption isotherm of MIL-100(Fe) at 23 °C.

Fig. 3. Water vapor adsorption isotherm of zeolite 13X (Sigma-Aldrich) at 25 °C [34].

increase is slight. Adsorption occurs in the inter-particulate voids. For the desorption curve, a visible hysteresis occurs, especially for the 29 Å meso-pores. The test result has a good agreement with the previous studies [23,25].

Figs. 3 and 4 show that the water sorption of typical zeolite and silica gel [34,36]. The steep uptake of zeolite occurs when relative humidity is low (RH = 5%), which means zeolite will not release moisture in room humidity. In addition, the regeneration temperature of zeolite is quite high (more than 95 °C) [35]. Moreover, the water uptake capability is lower than MOF MIL-100(Fe). Water uptake is defined as the mass of the moisture adsorbed by sorbents.

On the contrary, the adsorption of some types of silica gel occurs slowly in room humidity (40% < RH < 60%) and accelerates when relative humidity is high (RH = 80%). Water sorption isotherms of the conventional desiccants also demonstrate a low adsorption capability and limited moisture buffer performance.

However, the water sorption isotherms of MIL-100(Fe) shows a promising result for the passive indoor moisture control. Since the steep adsorption begins at RH = 25% and ends at RH = 50% at 23 °C, MIL-100(Fe) can adsorb the moisture when the indoor relative humidity is higher than 50%, and release the moisture when the relative humidity is lower than 25%. Therefore, MIL-100(Fe) is suitable to be used to keep the interior hygrothermal condition in the thermal comfort [37] zone
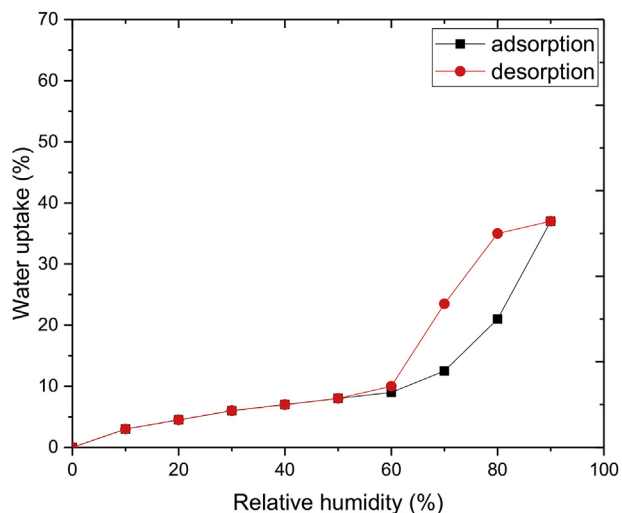

Fig. 4. Isotherms of silica gel at 25 °C [36].

passively.

3. Moisture buffer value

3.1. Definition of moisture buffer value (MBV)

The moisture buffer performance of a room is the ability of the materials within the room to moderate variations in the relative humidity. These variations can be seasonal or diurnal.

Most attention is paid to the moisture buffering of diurnal variations. The moisture buffer performance depends on the moisture buffer capacities of each material combination and furniture in the room together with the moisture production and air change rate and ratio between the material surface area and the air volume.

To evaluate the moisture buffer effect of materials, moisture buffer value (MBV) has been proposed [6,7]. MBV is defined as a characteristic of material, equals to the moisture uptake per relative humidity change during one cycle of moisture adsorption or release. An ideal MBV can be derived by assuming that the material is isotropic and semi-infinite, the boundary conditions are the alternating high and low relative humidity of the surface, neglecting the surface moisture convection.

The expression of ideal MBV is as follows.

$$MBV = \frac{G(t)}{\Delta RH} = 0.00568 b_m p_s \sqrt{t_p} \tag{1}$$

where, b_m is the moisture effusivity, $kg \cdot m^{-2} \cdot Pa^{-1} \cdot s^{-1/2}$; p_s is the saturated vapor pressure, Pa; t_p is the time period, s.

The b_m can be expressed as follows.

$$b_m = \sqrt{\frac{\delta_p \cdot \rho_0 \cdot \frac{\partial u}{\partial \varphi}}{p_s}} \tag{2}$$

where δ_p is the water vapor permeability, $kg \cdot m^{-1} \cdot s^{-1} \cdot Pa^{-1}$; ρ_0 is the dry density of the material, $kg \cdot m^{-3}$; u is the moisture content, $kg \cdot kg^{-1}$; φ is the relative humidity, %.

Meanwhile, MBV can be measured directly by experiment without acquiring the thermal properties of the material. The MBV tested by experiments named practical MBV. In a certain period of time, the ambient humidity alternates between high level and low level. The moisture transports into or out of the material during the period of time is reported per open surface area and per % RH variation, and it is the definition of practical MBV, with a unit of $g \cdot m^{-2} \cdot RH^{-1}$. Therefore, the definition of practical MBV is the principle of MBV measurement.

3.2. MBV measurement

3.2.1. Method

Based on the definition of the practical MBV, the MBV of MIL-100(Fe) has been measured. First, the sample of MIL-100(Fe) (L × W × H = 2.8 × 2.5 × 3 cm) was dried in an oven for 10 h at 60 °C. Then the sample was sealed in a glass container in the climate chamber until the temperature of the samples dropped to the chamber temperature, which was 23 °C.

The measurement was conducted in a climate chamber (Fig. 5). The temperature inside the chamber is 23 °C. The external ambient temperature is between 20 and 25 °C. The temperature and humidity sensors measure the temporal temperature and relative humidity, and the signal is sent back to a PID regulator and computer. Saturated air and dry air can be mixed in different proportion controlled by the PID regulator to maintain a stable humidity in the chamber. A heater is placed in the chamber and also controlled by the regulator to keep a stable temperature. An axial fan disturbs the air in the chamber to approach a uniform hydrothermal condition in the chamber. Fig. 5 shows the schematic diagram of the climate chamber.

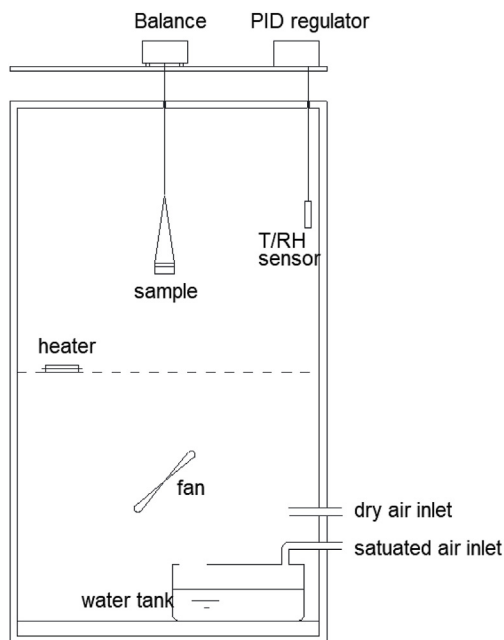The MIL-100(Fe) sample was placed in a small box and was

Fig. 5. Schematic diagram of the climate chamber.

Fig. 6. Photo of the climate chamber.

suspended in the climate chamber connected with a balance above the chamber (Fig. 5). Only the upper surface of the sample (7 cm²) was exposed to the air inside the climatic chamber. The rest five surfaces were sealed to avoid moisture transport. The test conditions in the climate chamber were set according to the NORDTEST method [7]. The temperature and humidity inside the climate chamber are uniform as a small axial fan is installed to make the inside air well mixed. The temperature inside the chamber was maintained at 23 °C, and the relative humidity was set as 75% for 8 h and 20% for 16 h in one period of time. The air humidity was switched swiftly. The weight of MIL-100(Fe) sample was weighed and logged automatically with the balance every minute. The measurement was performed in several cycles to get a relatively constant MBV of the material. Fig. 6 is the photo of the
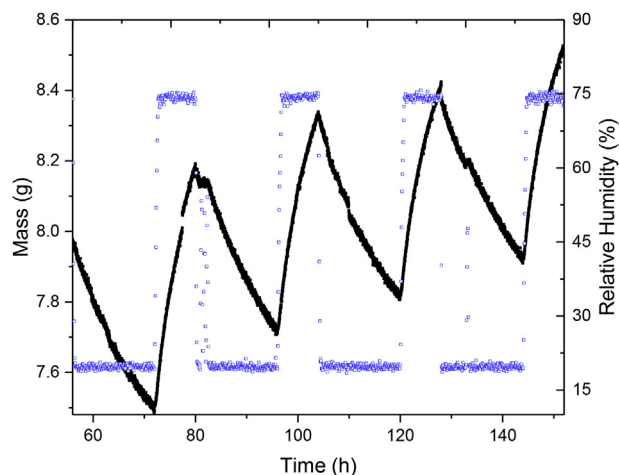

Fig. 7. MBV test at 23 °C (RH = 20%/75%).

climate chamber when the measurement is performing.

3.2.2. Results

The measurement results are shown in Fig. 7. The mass change of the sample corresponds rapidly with the surrounding humidity change. The sharp peak of the curve shows that the sample is far from saturation when the humidity begins to fall. The MBV of the MIL-100(Fe) is $15 \pm 0.2 \, g \, m^{-2} \cdot RH^{-1}$ at 8 h in the experimental conditions. Fig. 8 shows the MBV test results with a different low humidity level 33%. Other conditions maintain the same. The MBV of MIL-100(Fe) is $7.4 \pm 0.2 \, g \, m^{-2} \cdot RH^{-1}$ at 8 h, which is lower than the result in the 75%/20% condition.

3.2.3. Discussion

According to the expression of the moisture effusivity b_m (Eq. (2)), b_m has a significant relation to the sorption isotherm. The term $\frac{\partial u}{\partial \varphi}$ represents the moisture capacity, i.e. the ratio of the moisture added to a material to the resulting humidity change. It is not a constant and varies according to the water sorption isotherm. Therefore, the MBV value (shown in Eq. (1)) is also not a constant, and will change according to different upper and lower boundary of RH. In the case of MIL-100(Fe), If the low-level relative humidity is above the first steep adsorption point (RH = 25%), which is also the end of desorption, the moisture buffer performance of the material will be hindered. Therefore, the MBV in an alternative 75%/33% condition is lower than that of 75%/20%.
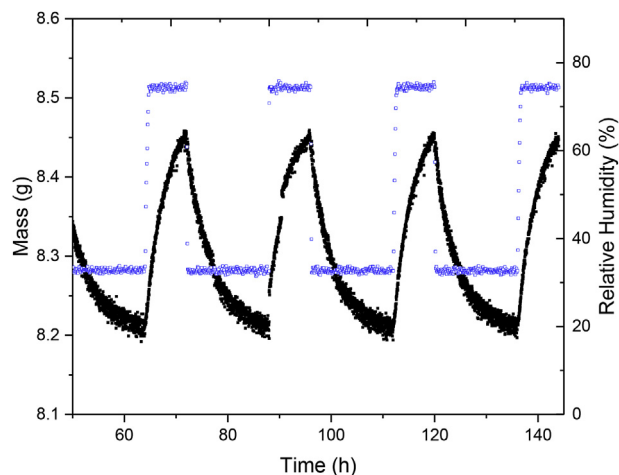

Fig. 8. MBV test at 23 °C (RH = 33%/75%).

Table 2
Classification of MBV.

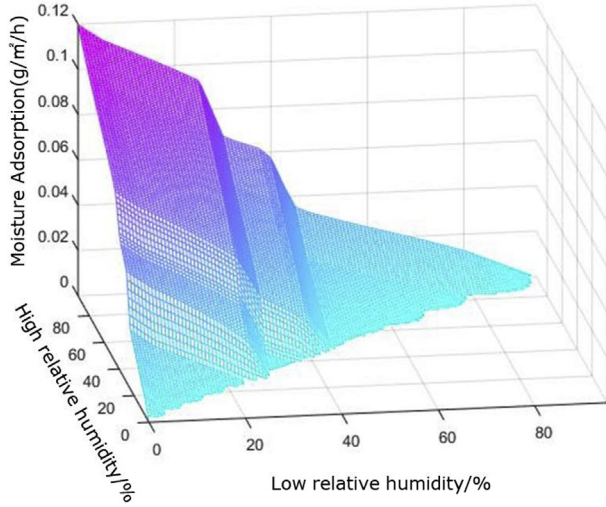| MBV	negligible	limited	moderate	good	excellent	exceptional
Lower limit	0	0.25	0.50	1.00	2.00	5.00
Upper limit	0.25	0.50	1.00	2.00	5.00	> 5.00

Fig. 9. Moisture adsorption with the different high and low relative humidity.

The MBVs of some typical building materials are listed in Table 1. In line with different levels of MBV, Materials can be classified into six categories, shown in Table 2. Therefore, MBV of the MIL-100(Fe) is one order of magnitude larger than the traditional hygroscopic building materials, and the moisture buffering ability of MIL-100(Fe) is in the exceptional group.

Furthermore, the moisture adsorption in different conditions can be calculated based on the water sorption isotherm and MBV formula. Fig. 9 shows the water vapor uptake of MIL-100(Fe) per hour and square meter varies with the different high and low RH levels. The variation of the moisture adsorption in different conditions can be further implemented in the simulation of energy saving potential in buildings.

4. Energy saving potential

The MBV measurement shows MIL-100(Fe) has an excellent performance of moisture buffering, which makes it very promising for indoor passive moisture control. The energy saving potential of applying MIL-100(Fe) in buildings will be discussed in this section.

Since only the hydro environment is considered, humidity ratio has been used instead of relative humidity in this section. The relation between humidity ratio and relative humidity is as follows.

$$\omega = 0.622 \frac{\varphi p_s}{p_{at} - \varphi p_s} \tag{3}$$

where ω is the humidity ratio, kg/kg$_{air}$; p_{at} is the atmospheric pressure, Pa.

4.1. Lumped energy model

Since the moisture buffer materials only affect the indoor humidity variation, the model in this paper mainly focuses on the moisture transfer in buildings. The indoor humidity conditions are mainly affected by (1) internal sources and sinks, (2) moisture diffusion through building envelopes, (3) infiltration, (4) mechanical ventilation, and (5) air conditioning. In the lumped model, the internal sources and sinks

are considered (e.g. human activities, moisture adsorption or desorption of moisture buffer materials). Infiltration and mechanical ventilation are expressed together as ventilation rate. Moisture diffusion through building envelopes are neglected in this case since well-insulated modern buildings are normally equipped with vapor barrier, and are almost impenetrable in terms of moisture. There is no air conditioning in the model. The indoor air is assumed to be well mixed, so the humidity at the ventilation exit is the same as the indoor humidity. The humidity of fresh air varies with time. The variation rate of the indoor humidity ratio should follow the equation below:

$$m_r \frac{d\omega_r}{dt} = m_a(\omega_{fr}(t) - \omega_r) + M_g V_r + M_{MOF} V_r \tag{4}$$

where, m_r is the mass of indoor air, kg; m_a is mass of ventilation air, kg; V_r is the room volume, m³; t is the time, s; M_g is the vapor generation rate, kg·m⁻³·h⁻¹; M_{MOF} is the absorption or desorption rate by moisture buffer material multiplies the surface area of material and divides by the room volume, kg·m⁻³·h⁻¹; ω_{fr} is the humidity of fresh air, kg·kg$_{air}$⁻¹; ω_r is the humidity of indoor air, kg·kg$_{air}$⁻¹;

Therefore, in the simplified case, the indoor humidity ratio can be expressed in equation (8). $\omega_r(0)$ is the initial humidity indoor.

$$\omega_r = e^{-\frac{m_a}{m_r}t}\left(\frac{m_a}{m_r} \int \omega_{fr}(t) e^{\frac{m_a}{m_r}t} dt + \omega_r(0) - \frac{(M_g + M_{MOF})V_r}{m_a} \right)$$
$$+ \frac{(M_g + M_{MOF})V_r}{m_a} \tag{5}$$

The time-dependent indoor air humidity can be calculated with the equation above. The influence with and without the moisture buffer phenomenon of MIL-100(Fe) will be both reckoned. Then the latent load removed by MIL-100(Fe) can be derived by comparing the moisture fluctuation with and without MIL-100(Fe).

$$Q_l = r_0 m_r \int_{t_1}^{t_2} (\omega_{rno} - \omega_{rMOF}) dt \tag{6}$$

where, Q_l is the latent load removed by MIL-100(Fe), kW; r_0 is the latent heat of vaporization, kJ·kg⁻¹; t_1 and t_2 are the time when human activities began and end, respectively, s; ω_{rno} is the air humidity ratio without MIL-100(Fe), kg·kg$_{air}$⁻¹; ω_{rMOF} is the air humidity with MIL-100(Fe), kg·kg$_{air}$⁻¹.

4.2. Building model

The BESTEST base case building (shown in Fig. 10) from the IEA ECBCS Annex 21 [38] was selected as the test building in this study, where it serves as a typical office room. The room is occupied during the daytime from 9:00 a.m. to 17:00 p.m. and unoccupied the rest of the day. The dimension of the building is 8 m × 6 m × 2.7m. Internal moisture source, sink, and ventilation cause the indoor humidity variation. The ventilation rate of the room is 0.5 ACH for 24 h. The internal moisture gain during the occupied period is assumed as 5 g m⁻³ h⁻¹, which is mainly from the human activities. There is no internal moisture gain during the unoccupied period.

In the case with moisture buffer materials, a 5 m² wall panel with the thickness of 1.5 cm made by 7.5 kg MIL-100(Fe) was installed on the internal surface. The MOF material will absorb and release moisture when there is humidity difference between the day and night. The moisture buffering effect is given by Fig. 9. In the case without moisture buffer materials, it is assumed that there is no moisture adsorption and desorption phenomenon at the internal wall surface.

4.3. Climate

The geographical locations (weather) of the building have a significant effect on indoor moisture fluctuations and moisture buffer phenomenon. To investigate the effect of MOF on indoor hygrothermal
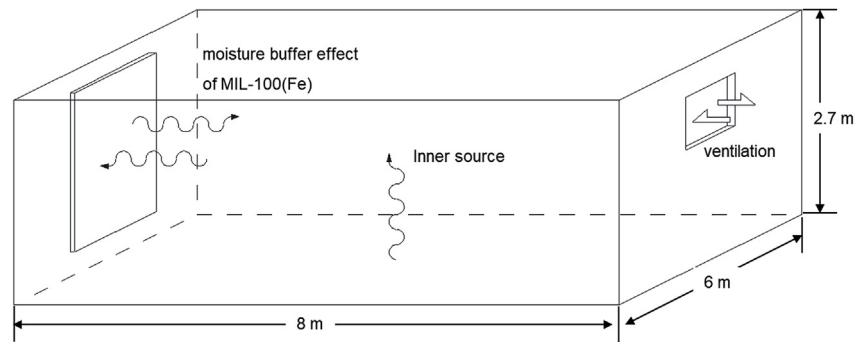
Fig. 10. A single office room model.

environment and building energy consumption under different climates, four cities in the United States are selected. They are San Francisco (moderate Mediterranean climate), Phoenix (hot desert climate), Salt Lake City (semi-arid climate) and Norfolk (humid subtropical).

The temporal climatic data is derived from the Typical Meteorological Year version 3 data sets [39]. For each city, the dry bulb temperature and relative humidity in one typical summer month have been used to calculate the humidity of fresh air in ventilation.

4.4. Results and discussion

The indoor moisture variations with and without the MOF materials for different locations have been calculated and presented in this section. Since the outside relative humidity plays an important role of the regeneration of MOFs, the following discussion will be divided into two parts according to the climatic conditions.

4.4.1. Dry and moderate climates

The monthly average outdoor air humidity ratio is $6\,g\,kg^{-1}$ in Phoenix, $7\,g\,kg^{-1}$ in Salt Lake City, and $8\,g\cdot kg^{-1}$ in San Francisco. The outdoor air with low humidity during the night of these locations could be directly used to regenerate the MOF materials that have adsorbed water vapor during the daytime. The simulated results of the indoor humidity variations with and without moisture buffer materials (MIL-100(Fe)) for dry and moderate climates are shown in Figs. 11–13 and Table 3.

Fig. 11 shows the variation of indoor humidity in a typical summer month in Phoenix. In the case without MOF materials, the indoor humidity often exceeds the upper limit of the thermal comfort zone (i.e. RH 60%). The indoor air should be dehumidified by air conditioning, which causes extra energy use. However, in the case with MOF materials, the indoor hygrothermal environment is well within the comfort zone during most time of the occupied period. The moisture buffer

material successfully moderates the fluctuation of indoor humidity.

The daily and monthly indoor moisture fluctuations in Salt Lake City and San Francisco are shown in Figs. 12 and 13. The humidity of the fresh air determines the low level of indoor humidity, and the moisture buffer capacity will be hindered when the low level of indoor humidity is higher than the start of steep adsorption of the water sorption isotherm of MIL-100(Fe). Therefore, building located in Phoenix has the most prominent moisture buffer phenomenon because of the dry climate. The moisture buffer phenomenon is weaker in San Francisco due to its higher outdoor humidity.

Table 3 shows the amount of the latent heat removed by MOF in different conditions. In the daytime when the building is occupied, the moisture buffer material MIL-100(Fe) functions as a desiccant and removes a large portion of the latent load without extra energy use. The amount of adsorbed moisture can be calculated since the moisture variations with and without moisture buffer material have been shown in simulation results, then the removed latent load can be further calculated. The results are presented in Table 3. The calculated indoor latent loads are $6.5\,W\,m^{-2}$, $8.6\,W\,m^{-2}$, $12.1\,W\,m^{-2}$ in Phoenix, Salt Lake City, and San Francisco respectively. The latent loads removed by MIL-100(Fe) are $5.0\,W\,m^{-2}$, $4.1\,W\,m^{-2}$, $2.4\,W\,m^{-2}$ in the three cities. Therefore, the latent load saving rates are 76.9%, 47.7% and 19.8% for hot dry climate (Phoenix), semi-arid climate (Salt Lake City), and moderate Mediterranean climate (San Francisco) respectively. The air change rate of night ventilation in the above simulation is 0.5 ACH.

In order to remove more latent load, the night ventilation should be enhanced. The higher night ventilation rate will remove more indoor moisture released by MIL-100(Fe), and contributes to the lower indoor humidity ratio and higher regeneration rate of MIL-100(Fe). The MBV will increase, and more latent load will be removed by the dryer MIL-100(Fe) during the daytime. According to the simulation results, when the night ventilation rate is raised to 2 ACH from 6 p.m. to 8 a.m., (the ventilation rate during the day remains as 0.5 ACH), the latent loads will be totally removed by MIL-100(Fe) in Phoenix and Salt Lake City

Table 3
Latent load removed by MIL-100(Fe) in different cases.

| Climate (City)	Load and efficiency	Ventilation rate is 0.5 ACH for 24 h	MOF regenerated by enhanced night ventilation (2 ACH)	MOF regenerated by low-grade energy
Hot dry (Phoenix)	Latent load removed by MOF $(W\cdot m^{-2})$	5.0	6.5	–
	Energy saving (latent load) (%)	76.9	100	–
Semi-arid (Salt Lake City)	Latent load removed by MOF $(W\cdot m^{-2})$	4.1	8.6	–
	Energy saving (latent load) (%)	47.7	100	–
Moderate (San Francisco)	Latent load removed by MOF $(W\cdot m^{-2})$	2.4	8.0	–
	Energy saving (latent load) (%)	19.8	66.1	–
Humid (Norfolk)	Latent load removed by MOF $(W\cdot m^{-2})$	0.5	–	16.3
	Energy saving (latent load) (%)	2.3%	–	73.4

64
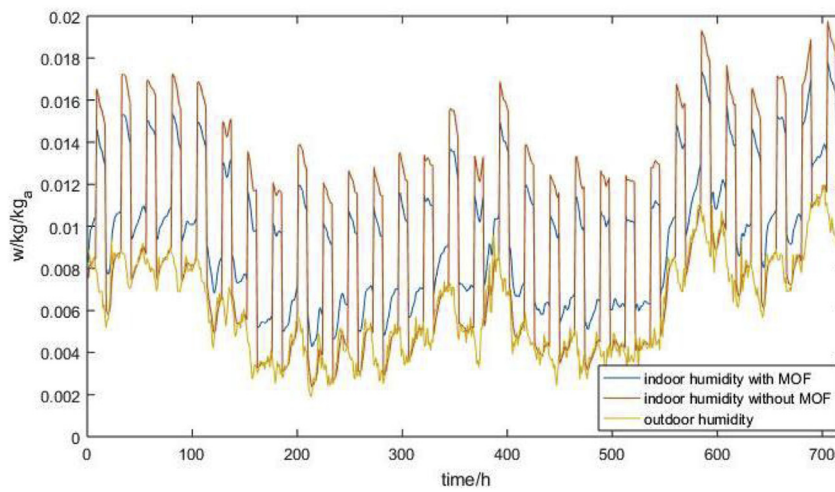
Fig. 11. Indoor humidity variation with and without MIL-100(Fe) in Phoenix.
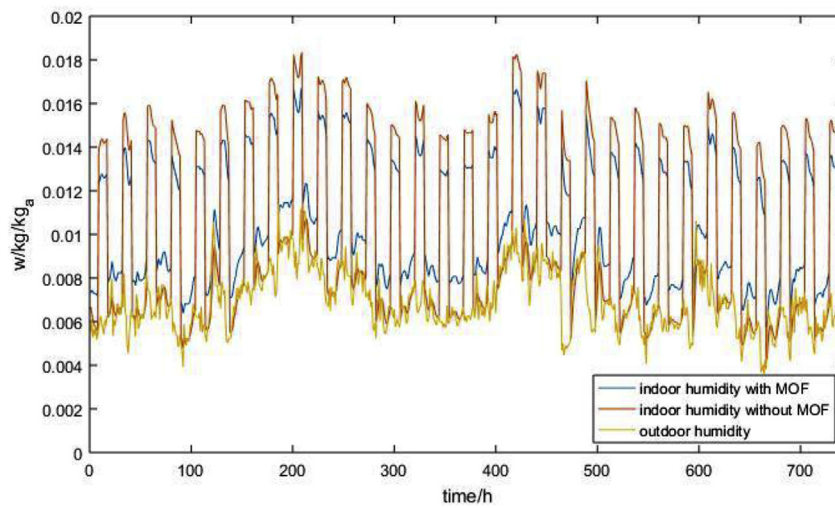

Fig. 12. Indoor humidity variation with and without MIL-100(Fe) in Salt Lake City.
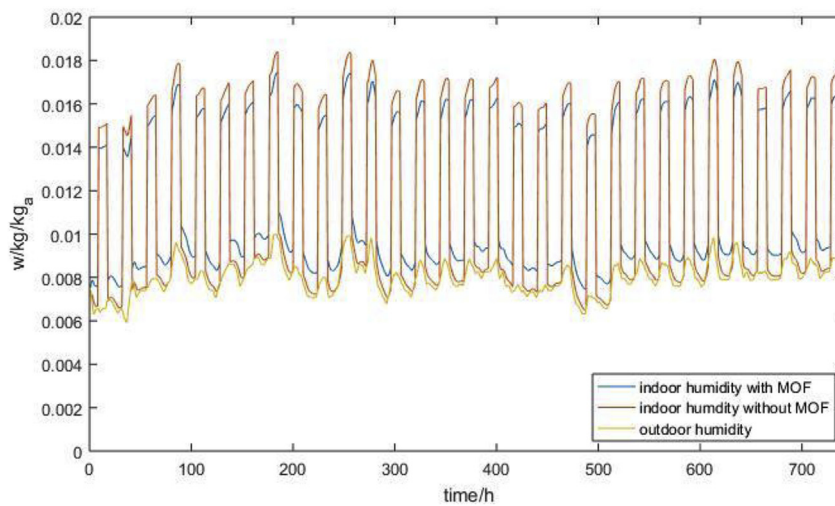

Fig. 13. Indoor humidity variation with and without MIL-100(Fe) in San Francisco.

without extra energy use. The percentage of latent load removed by MIL-100(Fe) is 66.1% in San Francisco. Night ventilation is a very effective way to regenerate the MOF materials in dry and moderate climates.

4.4.2. Humid climates

In Norfolk, the monthly average outdoor air humidity ratio is 15 g kg^{-1}. Fig. 14 shows the indoor moisture variations with and without the MOF in Norfolk. In Table 3, the simulation results show
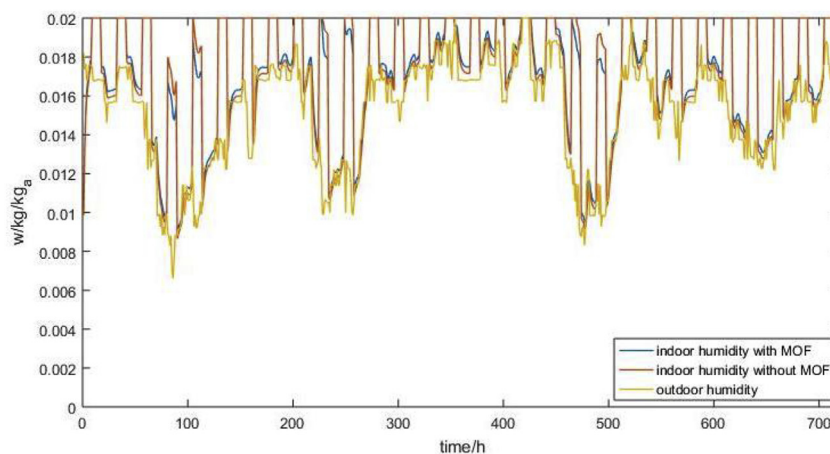
65

Fig. 14. Indoor humidity variation with and without MIL-100(Fe) in Norfolk.

that the indoor latent load is $22.2\,W\,m^{-2}$ in Norfolk. The latent load removed by MIL-100(Fe) is $0.5\,W\,m^{-2}$, which is only 2.3% of the total latent load. Therefore, the energy saving potential is limited, due to the high outdoor humidity throughout the day. Night ventilation cannot effectively reduce the indoor humidity and regenerate the MIL-100(Fe) since the outdoor humidity is still quite high in the evening.

In order to use MIL-100(Fe) for continuous passive control of indoor moisture in the humid climate, it needs to be regenerated with some low-grade energy, such as solar energy or waste heat from thermal power plants etc. Since the regeneration temperature of MIL-100(Fe) is quite low (around 50 °C), it is not difficult to find such a heat source. The simulation results show that $16.3\,W\,m^{-2}$ can be removed by the regenerated dry MIL-100(Fe), which is 73.4% of the latent load. The efficiency of the whole system is still very high as there is no need for refrigeration dehumidification. Therefore, MIL-100(Fe) is also applicable for the passive control of indoor moisture in humid climates with proper regeneration strategies. Due to the limitation of the paper length, a detailed description of the regeneration system for MIL-100(Fe) is not within the scope of this paper. We will report the system in the future studies.

Overall, in dry and moderate climates, most of the indoor latent loads can be removed by MIL-100(Fe) with a night ventilation at 2 ACH, which will significantly save the energy for dehumidification of the air-conditioning system. In the cases without the MOF buffer material, all latent loads have to be removed by the air conditioning system via refrigeration dehumidification, which causes a lot of energy use. In the humid climate, the MIL-100(Fe) could remove 73.4% of the total latent load with the help of a proper regeneration system powered by low-grade energy. Since the regeneration temperature of MIL-100(Fe) is around 50 °C, it is easy to regenerate it by solar energy or other waste heat from different processes. Therefore, MOF buffer materials have a large energy saving potential in buildings under different climate conditions.

5. Conclusion

MOF is a new class of crystalline materials with porous structures. Due to its high surface area, porosity, pore volume and low framework density, MOFs have a high capability to adsorb water vapor. MIL-100(Fe) is one type of metal-organic frameworks with large water vapor uptake capacity. Besides the high moisture sorption ability, MIL-100(Fe) is nontoxic, water-stable, and can be produced on a large scale.

The paper proposed an innovated application of metal-organic framework MIL-100(Fe) as a passive moisture buffer material in buildings. The MIL-100(Fe) has a strong ability to adsorb or release water vapor, and thus can moderate the daily indoor humidity fluctuation. The water sorption isotherms of MIL-100(Fe) have been measured. The steep

adsorption occurs between RH = 25% and 50%, which is inside of indoor thermal comfort zone. The practical MBV of MOF MIL-100(Fe) has been measured and proved to be one order of magnitude larger than typical building materials, leading to an exceptional moisture buffer ability.

The energy saving potential of applying MIL-100(Fe) to control the indoor humidity has been calculated. In the study, a $5\,m^2$ wall plate filled with MIL-100(Fe) was used to control the latent load of an office room with a size of $48\,m^2$. The simulation results show that most of the latent loads can be removed by MIL-100(Fe) with a night ventilation at 2 ACH in dry and moderate climates. In the humid climate, the MIL-100(Fe) could remove 73.4% of the total latent load with the help of a proper regeneration system powered by low-grade energy.

In summary, MIL-100(Fe) is a very promising moisture buffer material for the passive control of indoor humidity in different climates. The MOF buffer materials could be easily integrated with mechanical cooling systems to realize the temperature and humidity independent control. Since the MOF materials could handle most of the indoor latent load passively, the refrigeration dehumidification process can be avoided. Dealing only with the sensible load, the evaporation temperature of the cooling system can be raised to above the dew point so the coefficient of performance (COP) and energy efficiency of the system can be dramatically improved. Furthermore, new MOFs with higher water uptake capacity and low regeneration temperature will be the focus of future studies.

Acknowledgements

References

[1] P. Huovila, Buildings and Climate Change, United Nations Environment Programme, Sustainable Consumption and Production Branch, Paris, France, 2009.
[2] L. Pérez-Lombard, J. Ortiz, C. Pout, A review on buildings energy consumption information, Energy Build. 40 (2008) 394–398.
[3] M. Karimpour, M. Belusko, K. Xing, F. Bruno, Minimising the life cycle energy of buildings: review and analysis, Build. Environ. 73 (2014) 106–114.
[4] P. Mazzei, F. Minichiello, D. Palma, HVAC dehumidification systems for thermal comfort: a critical review, Appl. Therm. Eng. 25 (2005) 677–707.
[5] K. Chua, S. Chou, W. Yang, J. Yan, Achieving better energy-efficient air conditioning – a review of technologies and strategies, Appl. Energy 104 (2013) 87–104.
[6] M. Zhang, M. Qin, C. Rode, Z. Chen, Moisture buffering phenomenon and its impact on building energy consumption, Appl. Therm. Eng. 124 (2017) 337–345.
[7] C. Rode, R. Peuhkuri, B. Time, K. Svennberg, T. Ojanen, P. Mukhopadhyaya, et al.,

Moisture buffer value of building materials, J. ASTM Int. 4 (2007) 1–12.

[8] M. Rahim, O. Douzane, A. Tran Le, G. Promis, B. Laidoudi, A. Crigny, et al., Characterization of flax lime and hemp lime concretes: hygric properties and moisture buffer capacity, Energy Build. 88 (2015) 91–99.

[9] E. Latif, M. Lawrence, A. Shea, P. Walker, Moisture buffer potential of experimental wall assemblies incorporating formulated hemp-lime, Build. Environ. 93 (2015) 199–209.

[10] M. Rahim, O. Douzane, A. Tran Le, G. Promis, T. Langlet, Characterization and comparison of hygric properties of rape straw concrete and hemp concrete, Construct. Build. Mater. 102 (2016) 679–687.

[11] M. Abadie, K. Mendonça, Moisture performance of building materials: from material characterization to building simulation using the Moisture Buffer Value concept, Build. Environ. 44 (2009) 388–401.

[12] S. Hameury, Moisture buffering capacity of heavy timber structures directly exposed to an indoor climate: a numerical study, Build. Environ. 40 (2005) 1400–1412.

[13] M. Qin, R. Belarbi, Development of an analytical method for simultaneous heat and moisture transfer in building materials utilizing transfer function method, J. Mater. Civ. Eng. 17 (2005) 492–497.

[14] Z. Chen, D. Su, M. Qin, G. Fang, Preparation and characteristics of composite phase change material (CPCM) with SiO2 and diatomite as endothermal-hydroscopic material, Energy Build. 86 (2015) 1–6.

[15] Z. Wu, M. Qin, M. Zhang, Phase change humidity control material and its impact on building energy consumption, Energy Build. 174 (2018) 254–261.

[16] Z. Chen, M. Qin, J. Yang, Synthesis and characteristics of hygroscopic phase change material: composite microencapsulated phase change material (MPCM) and diatomite, Energy Build. 106 (2015) 175–182.

[17] E. Ng, S. Mintova, Nanoporous materials with enhanced hydrophilicity and high water sorption capacity, Microporous Mesoporous Mater. 114 (2008) 1–26.

[18] J. Bauer, R. Herrmann, W. Mittelbach, W. Schwieger, Zeolite/aluminum composite adsorbents for application in adsorption refrigeration, Int. J. Energy Res. 33 (2009) 1233–1249.

[19] D. Wragg, R. Johnsen, P. Norby, H. Fjellvåg, The adsorption of methanol and water on SAPO-34: in situ and ex situ X-ray diffraction studies, Microporous Mesoporous Mater. 134 (2010) 210–215.

[20] R. AbdulHalim, P. Bhatt, Y. Belmabkhout, A. Shkurenko, K. Adil, L. Barbour, et al., A fine-tuned metal–organic framework for autonomous indoor moisture control, J. Am. Chem. Soc. 139 (2017) 10715–10722.

[21] A. Dhakshinamoorthy, M. Alvaro, H. Garcia, Commercial metal–organic frameworks as heterogeneous catalysts, Chem. Commun. 48 (2012) 11275.

[22] D. Peralta, G. Chaplais, A. Simon-Masseron, K. Barthelet, G. Pirngruber, Synthesis and adsorption properties of ZIF-76 isomorphs, Microporous Mesoporous Mater. 153 (2012) 1–7.

[23] M. Bahri, F. Haghighat, H. Kazemian, S. Rohani, A comparative study on metal organic frameworks for indoor environment application: adsorption evaluation, Chem. Eng. J. 313 (2017) 711–723.

[24] H. Li, M. Eddaoudi, M. Keeffe, O. Yaghi, Design and synthesis of an exceptionally stable and highly porous metal-organic framework, Lett. Nat. 402 (1999) 276–279.

[25] S. James, Metal-organic frameworks, ChemInform 34 (2003).

[26] P. Horcajada, S. Surblé, C. Serre, D. Hong, Y. Seo, J. Chang, et al., Synthesis and catalytic properties of MIL-100(Fe), an iron(iii) carboxylate with large pores, Chem. Commun. (2007) 2820–2822.

[27] G. Férey, Hybrid porous solids: past, present, future, Chem. Soc. Rev. 37 (2008) 191–214.

[28] F. Jeremias, A. Khutia, S. Henninger, C. Janiak, MIL-100(Al, Fe) as water adsorbents for heat transformation purposes—a promising application, J. Mater. Chem. 22 (2012) 10148–10151.

[29] C. Volkringer, D. Popov, T. Loiseau, G. Férey, M. Burghammer, C. Riekel, et al., Synthesis, single-crystal X-ray microdiffraction, and NMR characterizations of the giant pore metal-organic framework aluminum trimesate MIL-100, Chem. Mater. 21 (2009) 5695–5697.

[30] J. Canivet, A. Fateeva, Y. Guo, B. Coasne, D. Farrusseng, Water adsorption in MOFs: fundamentals and applications, Chem. Soc. Rev. 43 (2014) 5594–5617.

[31] N. Burtch, H. Jasuja, K. Walton, Water stability and adsorption in metal–organic frameworks, Chem. Rev. 114 (2014) 10575–10612.

[32] Y. Seo, J. Yoon, J. Lee, Y. Hwang, C. Jun, J. Chang, et al., Energy-Efficient dehumidification over hierachically porous metal-organic frameworks as advanced water adsorbents, Adv. Mater. 24 (2011) 806–810.

[33] P. Küsgens, M. Rose, I. Senkovska, H. Fröde, A. Henschel, S. Siegle, et al., Characterization of metal-organic frameworks by water adsorption, Microporous Mesoporous Mater. 120 (2009) 325–330.

[34] S. Narayanan, X. Li, S. Yang, I. McKay, H. Kim, E. Wang, Design and Optimization of High Performance Adsorption-based Thermal Battery, (2018).

[35] K. Ng, H. Chua, C. Chung, C. Loke, T. Kashiwagi, A. Akisawa, et al., Experimental investigation of the silica gel–water adsorption isotherm characteristics, Appl. Therm. Eng. 21 (2001) 1631–1642.

[36] J. White, Computational Fluid Dynamics Modelling and Experimental Study on a Single Silica Gel Type B, Modelling and Simulation in Engineering vol 2012, (2012), pp. 1–9.

[37] ANSI/ASHRAE Standard 55-2013, ASHRAE, Atlanta, 2013.

[38] R. Judkoff, J. Neymark, International Energy Agency Building Energy Simulation Test (BESTEST) and Diagnostic Method, NREL, National Renewable Energy Laboratory, Golden, Colo, 1995.

[39] Users Manual for TMY3 Data Sets (Revised), United States, Dept. of Energy, Washington, D.C, 2008.

Nomenclature

Latin letters

b_m: moisture effusivity kg·m^{-2}·Pa^{-1} s$^{-1/2}$
G: moisture transfer in a cycle period g·m^{-2}
m_a: mass of ventilation air kg
m_r: mass of indoor air kg
MBV: moisture buffer value g·m^{-2}·RH^{-1}
M_g: vapor generation rate kg·m^{-3}·h^{-1}
M_{MOF}: absorption rate kg·m^{-3}·h^{-1}
p_a: atmospheric pressure Pa
p_s: saturated vapor pressure P$_a$
Q_l: latent load kW
r_0: latent heat of vaporization kJ·kg^{-1}
t: time s
t_1: the time when human activities began s
t_2: the time when human activities end s
t_p: time period s
u: moisture content kg·kg^{-1}
V_r: room volume m^3

Greek letters

δ_p: water vapor permeability kg·m^{-1}·s^{-1} Pa^{-1}
ρ_0: dry density of the material kg·m^{-3}
φ: relative humidity %
ω: humidity ratio kg/kg$_{air}$
ω_{fr}: humidity of fresh air kg·kg$_{air}$$^{-1}$
ω_r: humidity of indoor air kg·kg$_{air}$$^{-1}$
ω_{rno}: air humidity ratio without MIL-100(Fe) kg·kg$_{air}$$^{-1}$
ω_{rMOF}: air humidity with MIL-100(Fe) kg·kg$_{air}$$^{-1}$

67

Preparation and characterization of metal-organic framework /microencapsulated phase change material composites for indoor hygrothermal control

Pumin Hou, Menghao Qin [*], Shuqing Cui, Kan Zu

Department of Civil Engineering, Technical University of Denmark, Lyngby, 2800, Denmark

ARTICLE INFO

ABSTRACT

Building materials with high thermal and hygric inertia can moderate the fluctuation of indoor temperature and relative humidity, and thus can improve the indoor thermal comfort and reduce the building energy consumption passively. In this study, a novel hygrothermal control material was prepared based on Metal-Organic Frameworks (MOFs) and microencapsulated phase change material (MicroPCM). The new MOF/MicroPCM composite has a dual functionality of adsorption and desorption of both heat and moisture, can offer an accurate passive control of the indoor hygrothermal environment. N-octadecane was encapsulated by polymethylmetracrylate (PMMA) as MicroPCM for the thermal buffering. MIL-100(Fe) was prepared by the hydrothermal reaction method as the humidity buffering material. A series of hygrothermal control composite materials were obtained by grinding MicroPCM and MIL-100(Fe). Physicochemical properties of the synthesized materials were characterized by SEM, TEM, XRD, FTIR, N_2 physisorption, Water vapor sorption isotherm, DSC and TGA techniques. Hygrothermal properties of the composites were analyzed in comparison to pure MicroPCM and MIL-100(Fe). The thermal and humidity buffering behavior of the composites containing 50% MicroPCM was analyzed by numerical simulations. The results show that the composites possess an excellent thermal and humidity buffer capacity, which can be used for building energy-saving and improving thermal comfort.

1. Introduction

The building sector accounts for 40% of global energy which is mainly provided by fossil fuel and corresponding to over one-third of carbon dioxide emissions [1,2]. Reducing building energy consumption plays an active part in mitigating global problems such as energy fuel depletion, environmental pollution, and global warming. Passive design method is an effective method to reduce building energy consumption and improve indoor thermal comfort [3,4].

Among various passive design methods, the integration of phase change material with the building envelope has been widely studied to improve the thermal inertia and reduce temperature fluctuation [5–7]. However, this solution has little effect on the regulation of relative humidity, which also has a significant impact on building energy consumption and occupants' comfort [8,9]. Hygroscopic porous materials can automatically adjust the relative humidity of the indoor environment rely solely on their own moisture absorption and desorption properties [10].

Normally it is difficult to regulate both temperature and humidity at the same time by a single PCM or porous material. Recently, some researches have combined microencapsulated PCMs with conventional porous materials (e.g., diatomite, vesuvianite, sepiolite, and zeolite, etc.) to simultaneously regulate temperature and humidity in the building [11–13]. These hygrothermal materials show a promising energy saving potential and the maximal energy-saving rate could be up to 19.57% [14]. However, the conventional hygroscopic materials are suffering from low moisture absorption capacity and high requirements for desorption (e.g. high regeneration temperature, etc.) [15]. In order to make the hygrothermal material have a certain moisture absorption capacity by simple physical mixing as mentioned in previous research, the porous material has to occupy a considerable proportion, which will make the enthalpy of the composite materials greatly reduced. Another disadvantage is that the pore size distribution of the conventional porous materials is irregular and the corresponding water adsorption isotherms do not satisfy the V-type adsorption curve, which is considered to be the most beneficial for thermal comfort in buildings [16].
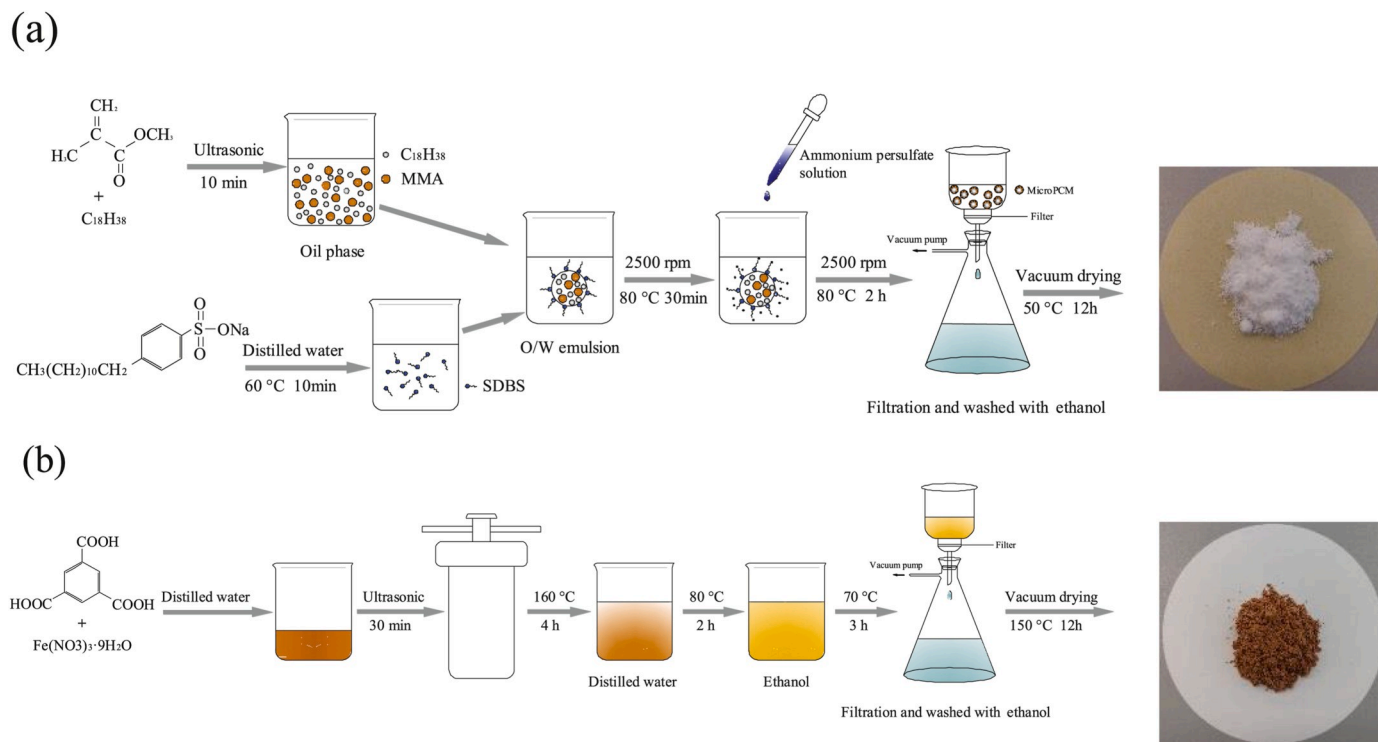

(a)

(b)

Fig. 1. Schematic representation of the fabrication procedure of (a) MicroPCM and (b) MIL-100(Fe).

Metal-organic framework (MOF) is a new kind of porous crystalline material with a periodic network structure formed by self-assembly of inorganic metal nodes and organic linkers [17,18]. MOF is becoming a promising alternative for moisture adsorption due to its high specific surface area, permanent porosity, tunable crystalline structure, and organic functionality [19–22]. MIL-100(Fe) as one of the major crucial MOF that possesses high water uptake capacity, hydrothermal and cycle stability [23]. In addition, the main constituent element iron atom is non-toxic, widely sourced, inexpensive, and environmentally friendly [24], making MIL-100(Fe) a priority for this work.

In this paper, a series of MIL-100(Fe)/MicroPCM composites were prepared and studied for temperature and humidity control. Firstly, the MicroPCM and MIL-100(Fe) were prepared by interfacial polymerization [25] and hydrothermal reaction method [24] respectively. Then two ingredients mixed sufficiently by gridding. The homogeneous composites were characterized by SEM, TEM, N_2 adsorption, XRD, FTIR, Water Isotherm, DSC and TGA techniques. Finally, the thermal and humidity buffering behavior of the composites is evaluated by numerical simulations.

2. Materials preparation

2.1. Raw materials

Methyl methacrylate (MMA), n-octadecane, Sodium dodecyl benzene sulfonate (SDBS) and ammonium persulfate were offered by Sinopharm chemical. Ferric sulfate nonahydrate ($Fe(NO_3)_3 \cdot 9H_2O$) and Benzene-1,3,5-tricarboxylic acid (H_3BTC) were purchased from Sigma-Aldrich. All chemicals used in the experiment are analytical reagents without further purification.

2.2. Synthesis of MicroPCM

MicroPCMs were prepared by encapsulating the core material n-octadecane with PMMA using interfacial polymerization. The schematic production process is illustrated in Fig. 1(a). 21 g n-octadecane and 9 g

MMA were mixed by ultrasonic for preparing the oil phase. 3% SDBS was added into 30 g distilled water and agitated with 2500 rpm in a flask at 60 °C for preparing the water phase. Then the oil phase was added to the water phase and improved the temperature to 80 °C and stirred for 30 min to prepare the O/W emulsion. Finally, 1% ammonium persulfate solution (0.13 g/ml) of MMA quality was dropwise added into the above emulsion as initiator and maintained the temperature and stirring rate until the end of the polymerization after 2 h. The products were covered by filtration and washed with distilled water 3 times. The white powders were obtained by vacuum drying at 50 °C for 12 h.

2.3. Synthesis of MIL-100(Fe)

MIL-100(Fe) was prepared by the hydrothermal reaction method. The schematic production process is illustrated in Fig. 1(b). 5 g Fe$(NO_3)_3 \cdot 9H_2O$ and 1.73 g H_3BTC (molar ratio 1.5:1) were dissolved in 1 g distilled water by sonication for 10 min. Then the solution was transferred to a 100 ml Teflon-lined autoclave and heated in an oven at 160 °C for 4 h. The obtained reaction product purified using 100 ml distilled water at 80 °C for 2 h and 100 ml ethanol at 70 °C for 3 h. The products were covered by filtration at each purification step and washed with ethanol 3 times. Finally, claybank solid was obtained by vacuum drying at 150 °C for 12 h.

2.4. Synthesis of MIL-100(Fe)/MicroPCM composites

MIL-100(Fe)/MicroPCM composites were obtained by hand gridding. Firstly, the MicroPCM and MIL-100(Fe) were dried in a vacuum oven at 50 and 70 °C for 24 h, respectively. Then different ratios of MIL-100 (Fe) and MicroPCM were mixed and ground in ambient atmosphere at least 5 min until homogeneous. Finally, a series of composites containing different proportions of MIL-100(Fe) and MicroPCM were obtained.
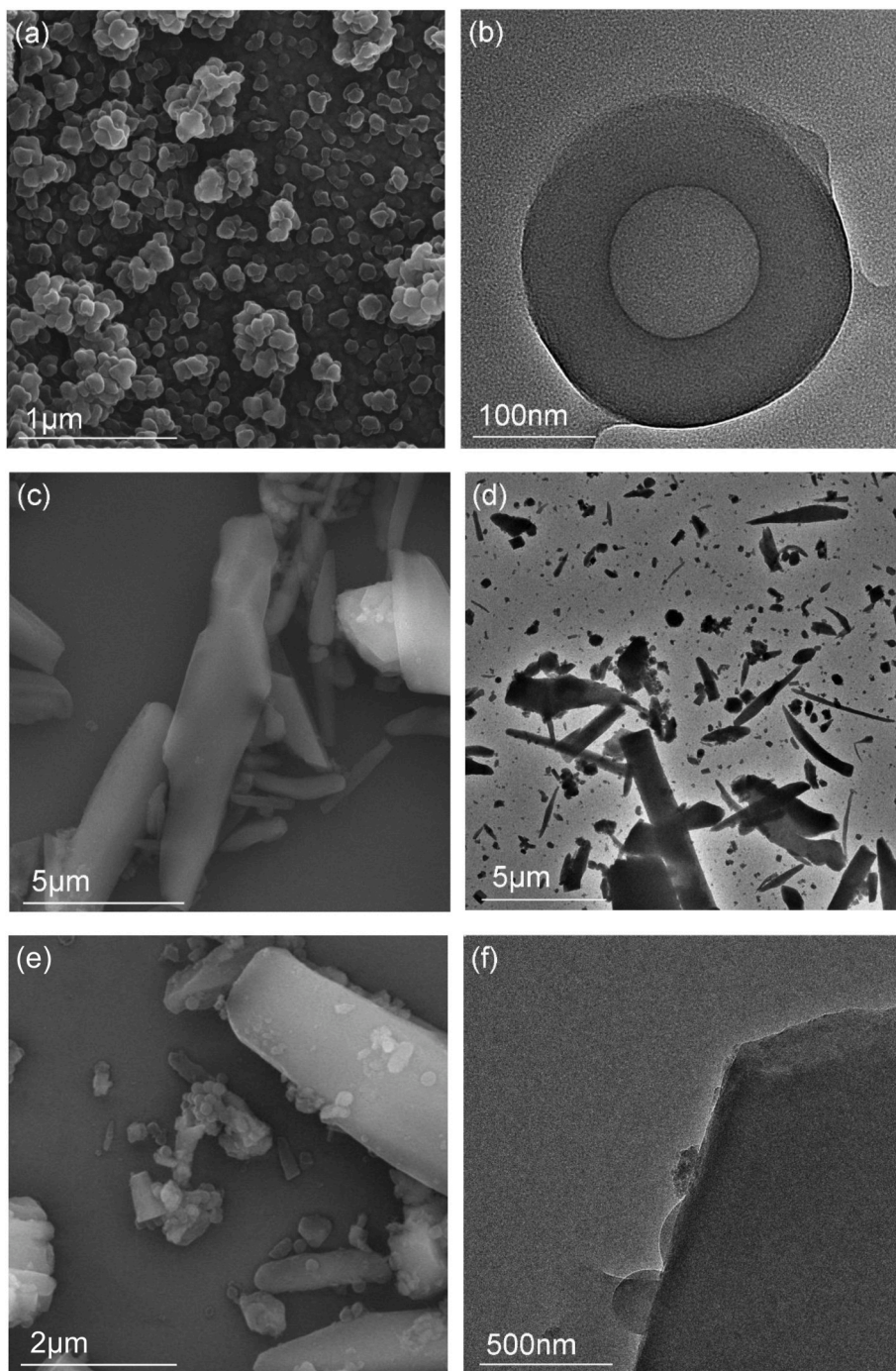
Fig. 2. SEM and TEM image of MicroPCM (a and b), MIL-100(Fe) (c and d) and MIL-100(Fe)/MicroPCM (e and f).
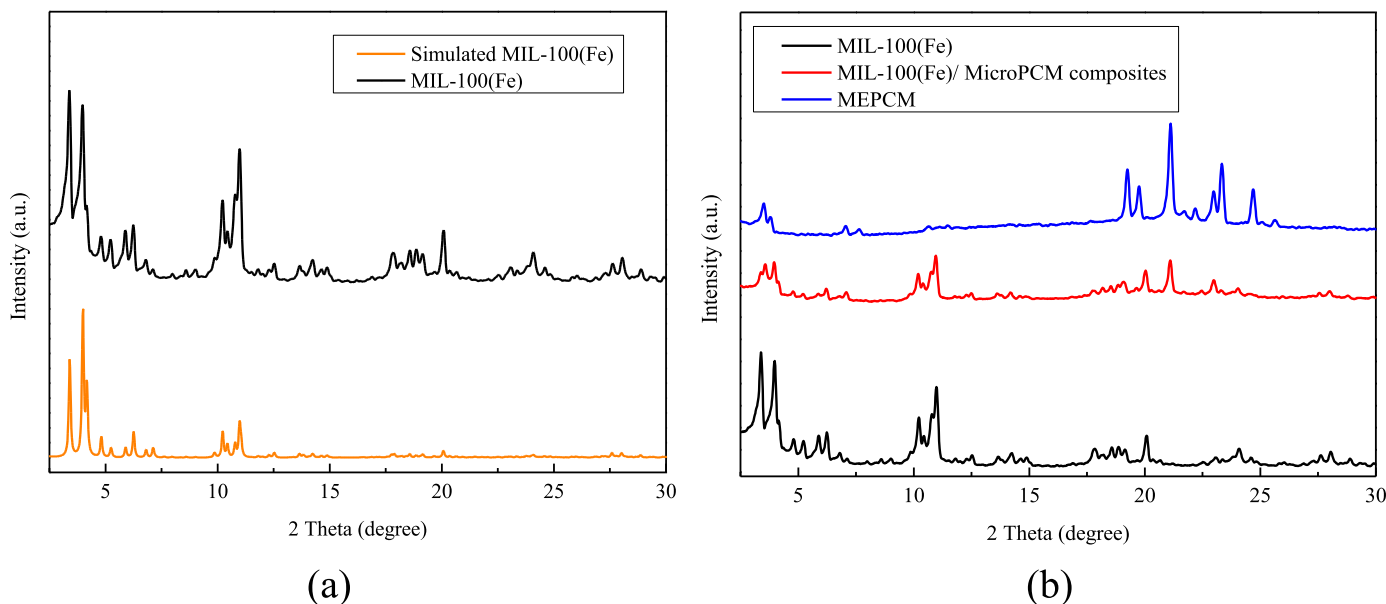
Fig. 3. XRD Patterns of simulated and as-synthesized MIL-100(Fe), MicroPCM and MIL-100(Fe)/MicroPCM composites.
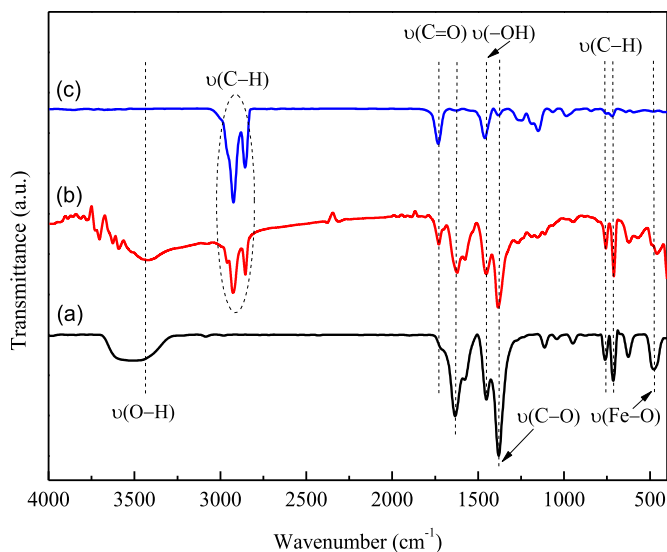

Fig. 4. FTIR spectra of as synthesized (a)MIL-100(Fe), (b)MicroPCM and (c) MIL-100(Fe)/MicroPCM composites.

3. Characterization

Morphologies of the materials were investigated by scanning electron microscope (SEM; FEI Nova Nano SEM 450) at an accelerating voltage of 15 kV. Detail structures of the microcapsules were researched on a transmission electron microscopy (TEM; FEI Tecnai F30) at 200 kV. N_2 sorption isotherms were obtained on an ASAP 2020 micromeritics at $-196\,°C$. Water sorption isotherms were measured by a dynamic vapor sorption (DVS intrinsic; SMS) instrument. Powder X-ray diffraction (XRD) patterns were recorded on a diffractometer (Rigaku Smartlab9) from 2 to 90°. Fourier transform infrared (FTIR) spectra were measured on a spectrometer (Bruker Verte-80). Differential scanning calorimeter (DSC) curves were obtained by TA Q200 from $-10\,°C$ to $50\,°C$ with the heating rate of $10\,°C/min$ under N_2 atmosphere. The thermal stability was tested by thermal gravimetric analyzer (TGA; TA Q50) from ambient temperature to $600\,°C$ with the heating rate $20\,°C/min$ under N_2 atmosphere.

3.1. Microscopic morphology and chemical characterization

SEM image of the MicroPCM is shown in Fig. 2(a). It can be observed that the synthesized microcapsules have relatively uniform sizes in hundreds of nanometers. As illustrated in the TEM image (Fig. 2 (b)) of MicroPCM, the microsphere is composed of n-octadecane core and PMMA shell, clearly exhibiting a core-shell structure. Fig. 2(c) and (d) present the SEM and TEM pictures of MIL-100(Fe), it is obvious that the MIL-100(Fe) is mainly composed of stick-like crystals. As shown in Fig. 2 (e) and (f), MicroPCM and MIL-100(Fe) were mixed, and some of the MicroPCM is adsorbed on the surface of the MIL-100(Fe).

XRD patterns of as-synthesized MIL-100(Fe) are presented in Fig. 3 (a). In order to facilitate comparison, the XRD patterns of the simulated data is also shown in Fig. 3(a). Diffraction peaks of MIL-100(Fe) synthesized in this work at 2θ values of 3.4, 4.0, 5.2, 11.0, 14.2, 18.2, 27.6° are consistent with the simulated one from crystal structure data [26]. The XRD patterns of MIL-100(Fe), MicroPCM and MIL-100 (Fe)/MicroPCM composite mixtures were collected and presented in Fig. 3 (b). Though the intensities of the diffraction peaks of composite mixtures attenuated a lot, all peaks in the composite mixtures curve corresponding to the peaks in MIL-100(Fe) and MicroPCM, indicating that two substances still retain good crystallinity after grinding mixing.

In order to get the chemical structures and compositions of the materials, the MIL-100(Fe), MicroPCM and MIL-100(Fe)/MicroPCM composites were studied by FTIR spectra and the results are shown in Fig. 4. FTIR spectra of as-synthesized MIL-100(Fe) shown in Fig. 4 is similar to the previous research [27,28], which further confirmed that the MIL-100(Fe) was synthesized successfully. It can be observed that the MIL-100(Fe) has a higher purity due to the disappearance of the C=O stretching vibration around $1714\,cm^{-1}$, which usually belongs to the residual H_3BTC over from reaction. Compared three spectra curves, the peak at $3400\,cm^{-1}$ due to O–H corresponding water can only be found in MIL-100(Fe) and composites, which means that the MicroPCM is extremely hydrophobic. FTIR spectra reveal additional bands in the MIL-100(Fe)/MicroPCM composites corresponding to n-octadecane at 2924 and $2856\,cm^{-1}$ attributed to the alkyl C–H stretching vibration of $-CH_2$ and-CH_3. Besides, the peak at$1732\,cm^{-1}$ denote C=O stretching vibrations of the ester group, which acted as a packaging material for capsuling phase change materials. The peak at $1622\,cm^{-1}$ is attributed to the carboxylate groups, which provides interaction between COOH and Fe ion [29]. While the bands at $1452\,cm^{-1}$ and $1381\,cm^{-1}$ are
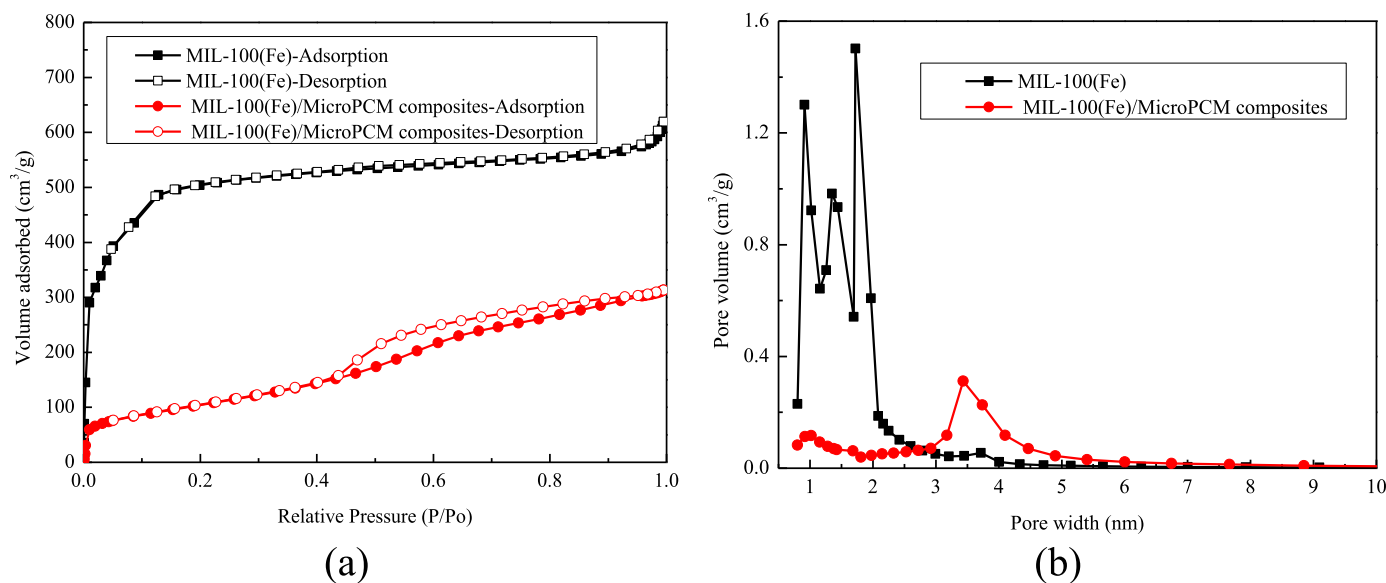
Fig. 5. (a) N_2 adsorption-desorption isotherms and (b) pore size distributions of MIL-100(Fe) and composites containing 50% MicroPCM.

mainly due to the symmetric –COOH group. Another two peaks at 760 and 714 cm^{-1} mainly due to C–H bending vibrations of benzene. The peak at 476 cm^{-1} stretching vibrations is caused by Fe–O. By comparing three FTIR spectra curves in Fig. 4, it can be seen that the curve (b) contained all vibration peaks occurred in the curve (a) and (c), which confirms that no chemical reaction occurred during the mixing process of MIL-100(Fe) and MicroPCM.

3.2. Sorption isotherms

Fig. 5(a) presents the N_2 adsorption-desorption isotherms of MIL-100 (Fe), MicroPCM and composites containing 50% MicroPCM. The Brunauer-Emmett-Teller (BET) specific surface area and total pore volume of MIL-100(Fe) and composites containing 50% MIL-100(Fe) is 1672 and 377 m^2/g, 0.93 and 0.49 cm^3/g, respectively. Both the two values of the composites are less than pure MIL-100(Fe), which is primarily due to the addition of nonporous MicroPCM. Fig. 5(b) shows the pore size distributions of MIL-100(Fe) and composites containing 50% MicroPCM. It was revealed that the pore size distribution of MIL-100(Fe) changed a lot after being ground with MicroPCM. The pore size of MIL-100(Fe) dominates at 0.9, 1.4 and 1.7 nm, while the pore size of composites containing 50% MIL-100(Fe) is mainly concentrated around 3.4 nm.

Water adsorption isotherms of MIL-100(Fe), MicroPCM and composites with varying content of MicroPCM were achieved by changing the relative humidity from 0 to 95% at 25 °C, the results were shown in Fig. 6. The relative humidity gradient during the test was 10% while the last step was 5%. When the mass change of the sample in each stage was less than 0.001%·min^{-1}, it was considered that the adsorption reached equilibrium at this stage and automatically entered the next stage. As presented in Fig. 6(a), the water adsorption isotherm of MIL-100(Fe) rises significantly from 20% to 50%, then increases slowly over the relative humidity, has the characteristic of "S" type. While the MicroPCM shows linear shape. The water uptake of MIL-100(Fe) at RH = 95% is 57.75%, which indicates that MIL-100 (Fe) as a moisture buffer material shows great potential in building energy-saving applications over traditional materials. The water uptake of MicroPCM is 0.85%, which again confirms its hydrophobicity. According to Fig. 6(b)–(d), the water uptake of composites was decreased with increasing the MicroPCM proportion. And the composites containing 30%, 50% and 70% MicroPCM reduced to 30.27%, 24.16% and 15.76%, respectively. Besides, the adsorption curve changed dramatically by adding

MicroPCM. The trigger point of steep adsorption of MIL-100(Fe) moved from 20% RH to 70% RH. This is caused by the pore size change of MIL-100 (Fe). Besides, the trigger point of steep desorption moved from 40% to 70%, which means the composites are easier to desorb than the pure MIL-100(Fe). Compared the difference of water adsorption isotherm between pure MIL-100(Fe) and MIL-100(Fe)/MicroPCM composites, it can be found that the step (between 30% and 40% RH) caused by polymodal pore size distribution is disappeared as the percentage of MicroPCM increased to 50%. This can be confirmed from the pore size distribution of the composites above.

As shown in Fig. 6(b)–(d), the hysteresis loop between the sorption and desorption curves of composites is wider than pure MIL-100(Fe). Fig. 7 shows detail hysteresis data of MIL-100(Fe), MicroPCM and the composites at different relative humidity. It can be observed that the maximum hysteresis of pure MIL-100(Fe) and composites occurred at 40% and 70%, respectively. And the maximum value shows different degrees of reduction as the proportion of MicroPCM increased. This may be caused by two reasons. On the one hand, the addition of nonporous MicroPCM leads to the reduction of the water uptake. On the other hand, the PMMA-encapsulated MicroPCM increased the hydrophobicity of the composites.

3.3. Thermal properties

DSC curves of MIL-100(Fe), MicroPCM and MIL-100(Fe)/MicroPCM composites are presented in Fig. 8 and corresponding detailed thermal properties are listed in Table 1. As shown in Fig. 8 that all samples showed a single endothermic peak except for pure MIL-100(Fe), indicating that MIL-100 (Fe) has no phase transition during the test temperature range and the addition of MIL-100(Fe) does not change the crystallization form of MicroPCM. As shown in Table 1, both of the melting temperature (onset temperature) and peak temperature of MIL-100(Fe)/MicroPCM composites were reduced in various degrees compared with pure MicroPCM, which may be caused by the surface tension, capillary action and intermolecular force between the nanoparticles. The enthalpy value reduced rapidly as the proportion of MIL-100(Fe) increased. This is because both MicroPCM and MIL-100(Fe) were dried sufficiently before grinding. The MIL-100(Fe)/MicroPCM composites would adsorb moisture during grinding and the period before the DSC testing, which directly increased the weight of MIL-100 (Fe) and decreased the relative proportion of MicroPCM.

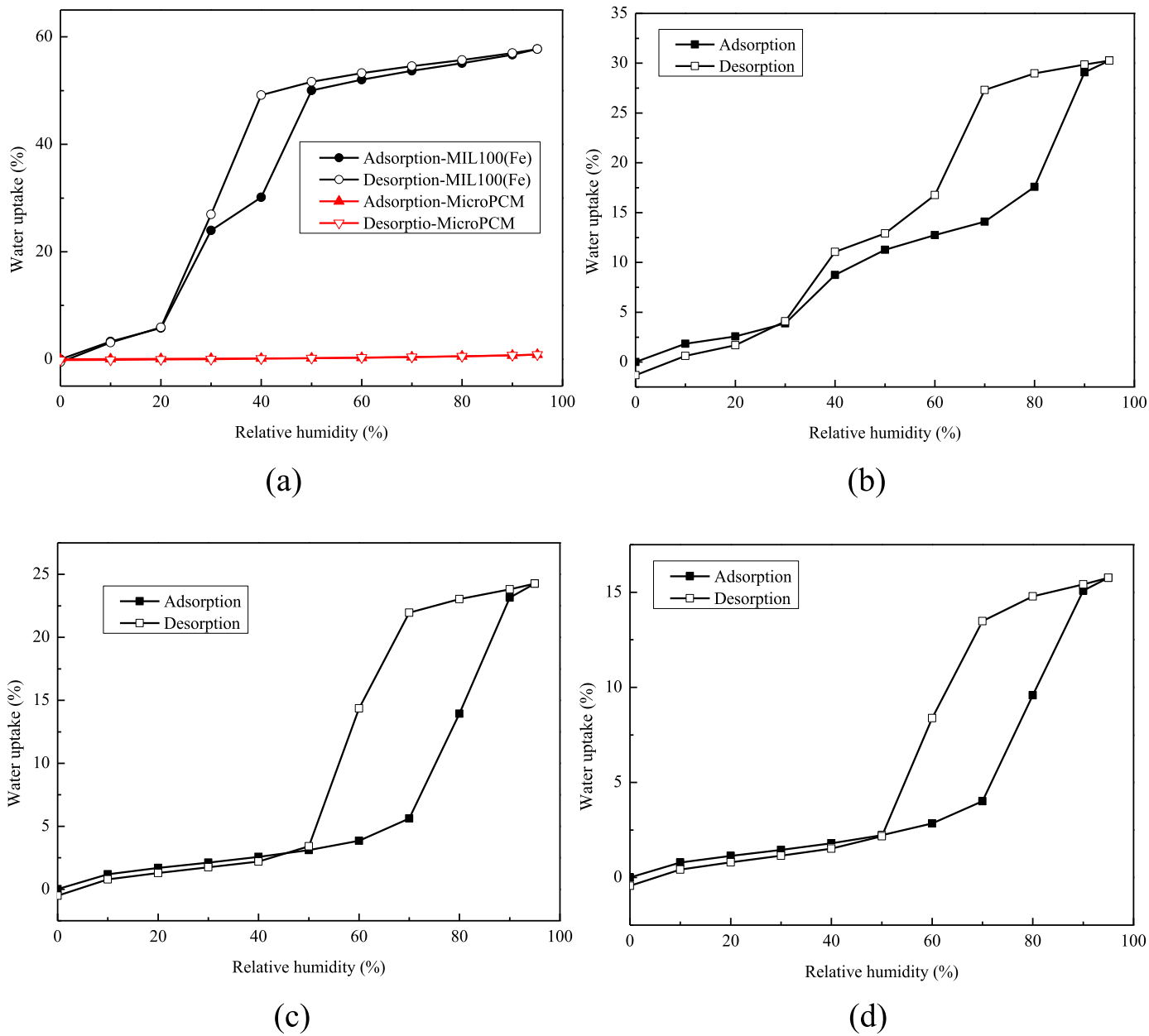The thermal stability of the composites with varying content of MIL-

Fig. 6. Water adsorption isotherms of (a) MIL-100(Fe) and MicroPCM and (b)–(d) MIL-100(Fe)/MicroPCM composites containing 30%, 50% and 70% MicroPCM.
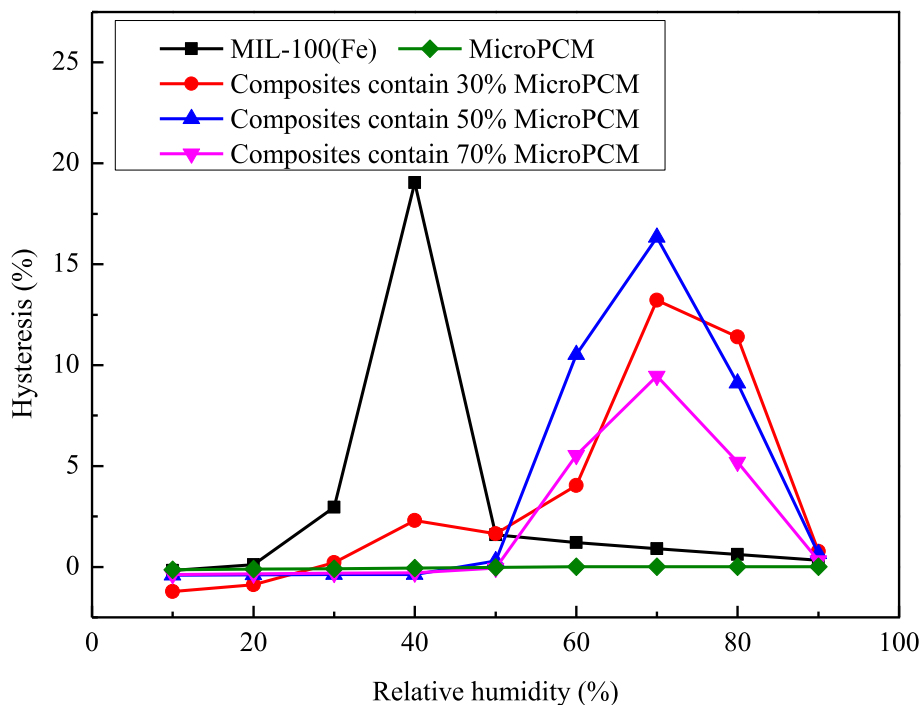
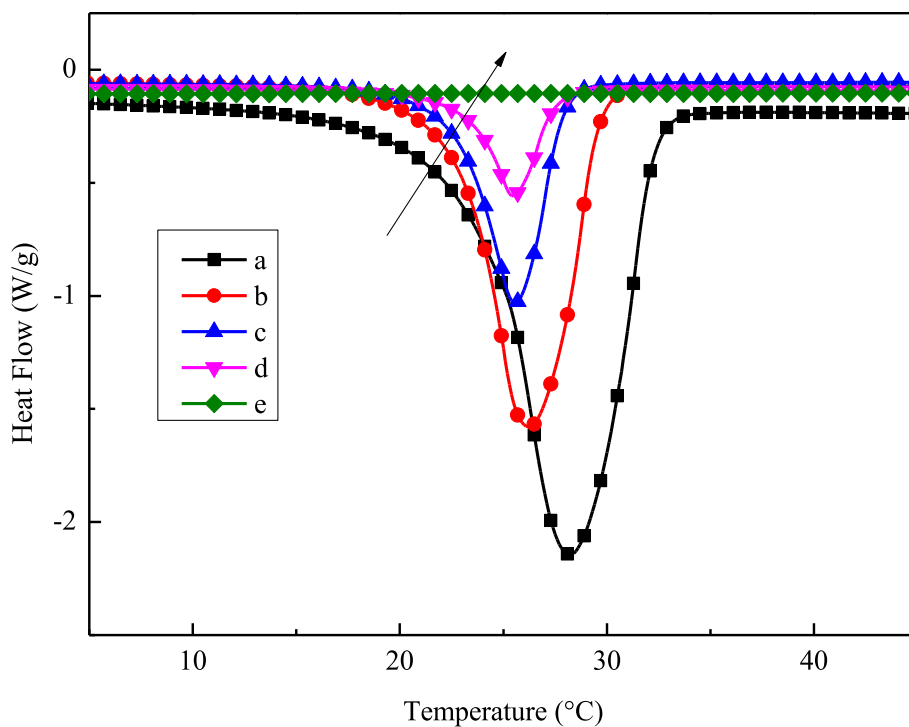**Fig. 7.** Hysteresis of MIL-100(Fe), MicroPCM and the composites.

Fig. 8. DSC curves of MIL-100(Fe)/MicroPCM composites (a)–(e): containing 100%, 70%, 50%, 30%, 0% MicroPCM.

100(Fe) and MicroPCM was measured by a TG analyzer. Fig. 9 demonstrates the TG results of the composites and Table 2 shows the degradation data including initial decomposition temperature and residual mass. The weight loss process of MIL-100(Fe) is roughly divided into three stages [30]. The initial weight loss (about 14 wt%) bellow 100 °C due to the desorption of free water. The second step (about 13 wt%) from 100 to 300 °C is ascribed to the loss of bonded water. The last step (about 31 wt%) occurred at the temperature between 300 and 520 °C is

caused by the decomposition of trimesic acid. The degradation of MicroPCM has three steps and the initial decomposition temperature starts at roughly 192 °C and completely loses its weight at around 465 °C. At the first step, the mass drop sharply between 105 and 237 °C due to the evaporation of octadecane, which is comprised of linear alkane with low thermal decomposition temperature [31]. The second and third step was ascribed to the monomer evolution and the random bond scission of the PMMA shell, respectively [32]. The weight loss rate of the

Table 1
Thermal properties of composites with varying content of MIL-100(Fe) and MicroPCM.

Sample	MicroPCM contents (%)	Melting temperature (°C)	Peak temperature	Enthalpy (J/g)
a	100	24.05	28.16	144.20
b	70	22.90	26.27	90.76
c	50	22.67	25.66	44.78
d	30	23.27	25.43	18.45
e	0	–	–	0

composites is improved with the increase of the content of MIL-100(Fe) at the beginning. Along with the rise of temperature, the curves show a reverse trend. This is because that the weight loss at lower temperatures is mainly caused by evaporation of water, while the composite with higher MIL-100(Fe) can adsorb more water vapor. Once the temperature rises to the thermal decomposition point of octadecane, the weight loss rate of composites with lower MIL-100(Fe) content will quickly exceed others. Finally, the composites with lower MIL-100(Fe) have less residual mass at 600 °C.

4. Hygrothermal buffering behavior of MIL-100(Fe)/MicroPCM composites

In order to evaluate the effect of MIL-100(Fe)/MicroPCM composites on the indoor climate of building. Hygrothermal buffering behavior of the composites containing 50% MicroPCM was analyzed by numerical simulation [33] using software WUFI Plus. A single-room model was built based on the case 600 from the International Energy Agency (IEA) ECBCS Annex 21 [34]. Detail dimensions of the building are shown in Fig. 10. The selected building faces south with a floor area of 48 m^2 and volume of 129.6 m^3. Two south-facing double-glazed windows with dimensions of 2 m × 3 m. The properties of the materials used in different layers are shown in Table 3. It should be noted that the underfloor insulation assumed with the minimum density and specific heat. The light weight building was assumed in Rome with a typical Mediterranean climate. The mechanical ventilation rate is 0.5 ACH for the whole day. The case 600 model with hygrothermal buffering

material installed 2 cm thickness composites containing 50% MicroPCM on the internal wall. For comparison, the reference room added 2 cm thickness plasterboard.

Figs. 11–13 show the fluctuation in indoor temperature and humidity for a typical summer week in July. Compared with the reference room, the room with MIL-100(Fe)/MicroPCM composites has a significant reduction of periodic fluctuations in temperature. This is mainly due to the thermal storage of phase change material. It can be seen from Figs. 12 and 13, both of the relative and absolute humidity have smaller amplitudes for room with MIL-100(Fe)/MicroPCM composites. This is because that the composites show good buffering capacity that can absorb and release moisture.

Further analysis found that the greater the temperature and relative humidity difference between day and night, the great the advantages of MIL-100(Fe)/MicroPCM composites for indoor hygrothermal control. For example, the temperature difference between day and night on July 1 was 9 °C and the relative humidity difference was 39% RH. For the room with MIL-100(Fe)/MicroPCM composites as enclosure, the temperature and moisture content at 2:00 p.m. were 30.5 °C and 16.38 g/kg, respectively. While for the reference room with plaster, the temperature and moisture content were 33.6 °C and 18.0 g/kg, respectively. Conclusions can be drawn that the MIL-100(Fe)/MicroPCM composites can make full use of the temperature and humidity gradient between day and night and significantly reduce the daytime peak temperature and moisture content.

Table 2
TG data of composites with varying content of MIL-100(Fe) and MicroPCM.

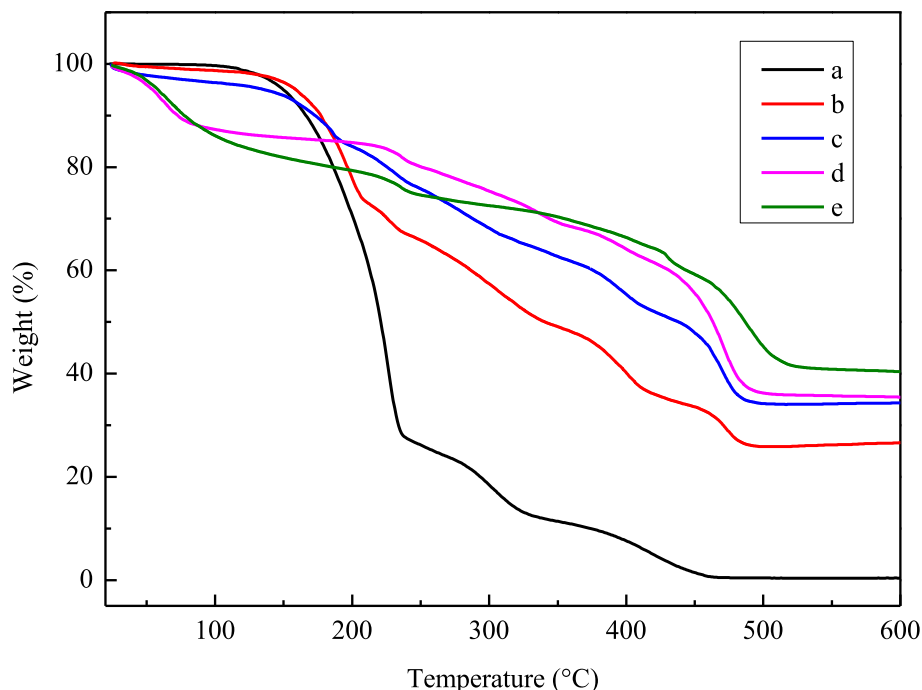| Sample	MicroPCM contents (%)	Initial decomposition temperature (°C)	Residual mass at 600 °C (%)
a	100	192.2	0
b	70	168.9	26.7
c	50	168.4	34.2
d	30	49.9	35.3
e	0	49.0	40.5

Fig. 9. TG curves of MIL-100(Fe)/MicroPCM composites (a)–(e): containing 100%, 70%, 50%, 30%, 0% MicroPCM.
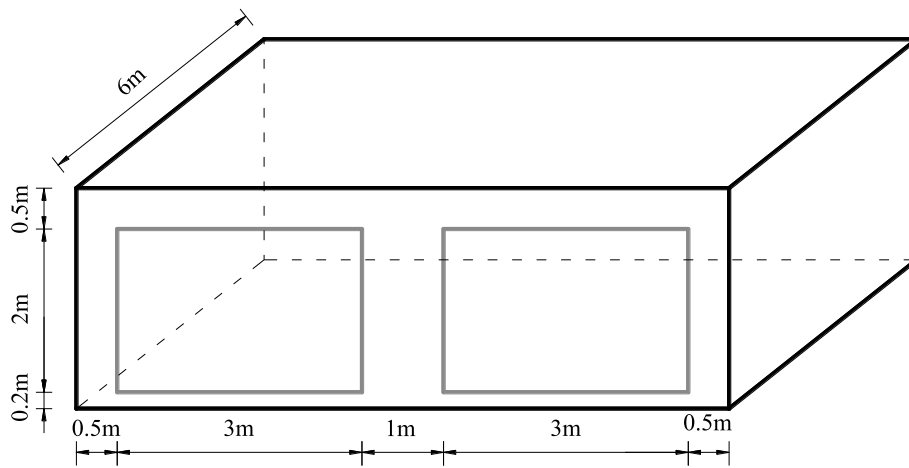
Fig. 10. The BESTEST lightweight case building.

Table 3
Properties of the envelop materials.

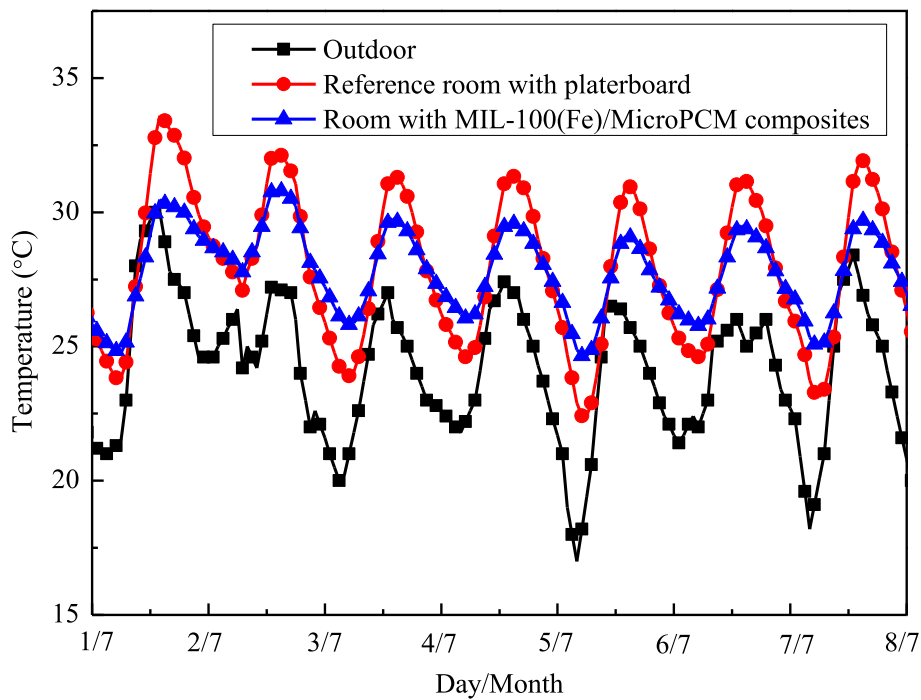| Construction	Material	Thickness (m)	Dry density (kg/m³)	Porosity (m³/m³)	Specific heat capacity (J/kg·K)	Thermal conductivity (W/m·K)	U (W/ m²·K)	Vapor diffusion resistance (−)
Wall (outside to inside)	Ext surf coef						29.3	
	Wood siding	0.009	530	0.666	900	0.14	15.556	53.1
	Fibreglass quilt	0.066	12	0.99	840	0.04	0.606	1.3
	Plasterboard	0.012	950	0.61	840	0.16	13.333	9
	Int Surf Coef						8.29	
Floor (outside to inside)	Insulation	1.003	1	0.01	1	0.04	0.04	500
	Timber flooring	0.025	650	0.47	1200	0.14	5.6	200
	Int Surf Coef						8.29	
Roof (outside to inside)	Ext surf coef						29.3	
	Roofdeck	0.019	530	0.1	900	0.14	7.368	13
	Fiberglass quilt	0.1118	12	0.99	840	0.04	0.358	1.3
	Plasterboard	0.01	950	0.61	840	0.16	16	9
	Int Surf Coef						8.29	
Window	Double glazing unit	–	2500	–	750	1.06	3	–

Fig. 11. Outdoor and simulated indoor temperature of reference room and room with MIL-100(Fe)/MicroPCM composites.
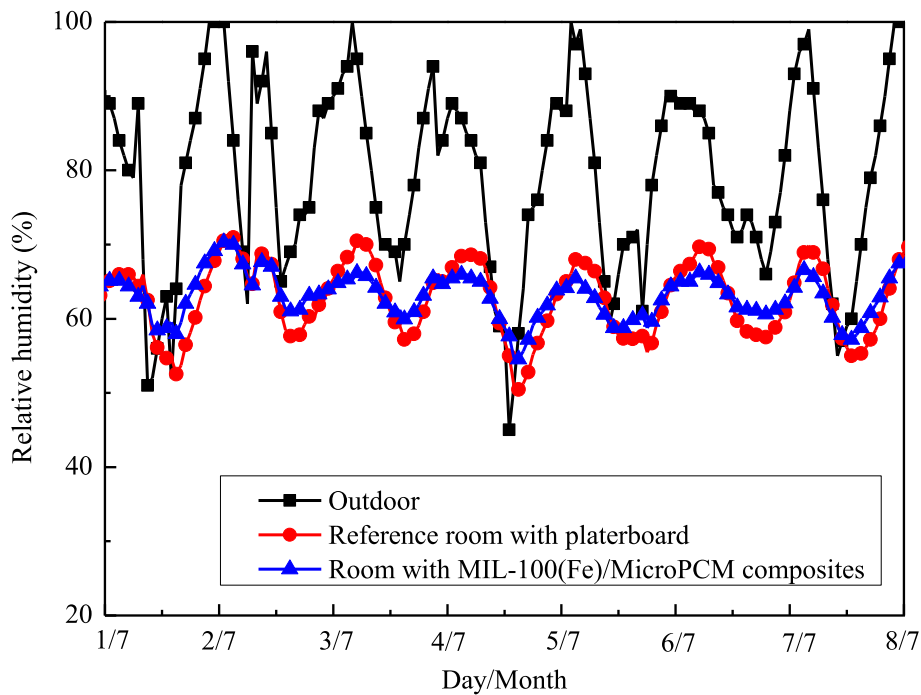
Fig. 12. Outdoor and simulated indoor relative humidity of reference room and room with MIL-100(Fe)/MicroPCM composites.
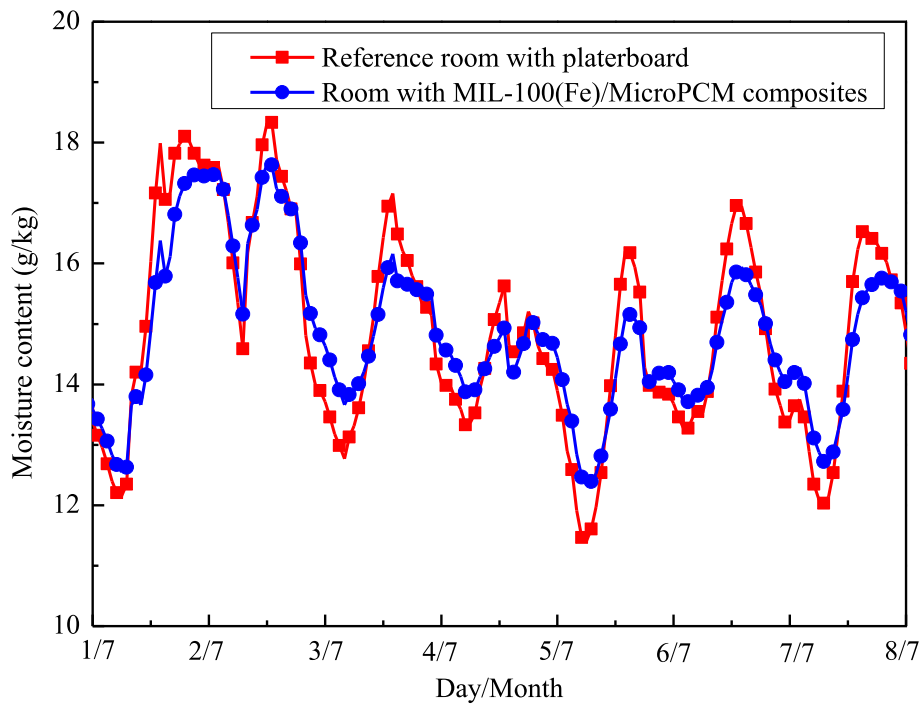

Fig. 13. Absolute humidity of reference room and room with MIL-100(Fe)/MicroPCM composites.

5. Conclusion

In this study, MicroPCM synthesized as thermal buffering material and MIL-(100) synthesized as humidity buffering material. A series of composites containing different proportions of MicroPCM and MIL-(100) were obtained by gridding two ingredients. The hygrothermal properties of the composites were characterized by experimental measurements. Hygrothermal buffering behavior of the composites containing 50% MicroPCM in a lightweight building was obtained by the simulation method. The results show as follows.

(1) When the content of MicroPCM in the composites is more than 50%, the trigger point of steep adsorption and desorption of MIL-100(Fe)/MicroPCM moved from 20% to 40% RH to 70% and 70% RH, respectively. That means composites are easier to be regenerated than pure MIL-100 (Fe), which will increase its application in passive buildings.

(2) There is no chemical reaction between the MicroPCM and MIL-100(Fe) by simple grinding. The addition of MIL-100(Fe) doesn't change the crystallization form of MicroPCM. The enthalpy decreased with the increase of MIL-100(Fe) in the composites. The temperature and humidity control ability of composites has a trade-off relationship.

(3) Numerical results show that the composites show excellent thermal and moisture buffering behavior. Compared with the same thickness of the plasterboard, the composites can significantly reduce the temperature and humidity fluctuations. Thus the comfort of the room with MicroPCM/MIL-100 (Fe) composites is improved.

Declaration of competing interest

The authors declare that they have no known competing financial interests or personal relationships that could have appeared to influence the work reported in this paper.

CRediT authorship contribution statement

Pumin Hou: Writing - original draft, Investigation. **Menghao Qin:** Conceptualization, Supervision. **Shuqing Cui:** Methodology. **Kan Zu:** Data curation.

Acknowledgements

References

[1] A. Waqas, Z. Ud Din, Phase change material (PCM) storage for free cooling of buildings-A review, Renew. Sustain. Energy Rev. 18 (2013) 607–625.

[2] British Petroleum (B.P), Statistical Review of World Energy, 2010.

[3] E. Maleviti, W. Wehrmeyer, Y. Mulugetta, An empirical assessment to express the variability of buildings' energy consumption, Int. J. Energy Optim. Eng. 2 (3) (2013) 55–67.

[4] R. Yao, V. Costanzo, X. Li, et al., The effect of passive measures on thermal comfort and energy conservation. A case study of the hot summer and cold winter climate in the Yangtze River region, J. Build Eng. 15 (2018) 298–310.

[5] H. Akeiber, P. Nejat, M.Z.A. Majid, et al., A review on phase change material (PCM) for sustainable passive cooling in building envelopes, Renew. Sustain. Energy Rev. 60 (2016) 1470–1497.

[6] M. Song, F. Niu, N. Mao, et al., Review on building energy performance improvement using phase change materials[J], Energy Build. 158 (2018) 776–793.

[7] F. Kuznik, D. David, K. Johannes, et al., A review on phase change materials integrated in building walls[J], Renew. Sustain. Energy Rev. 15 (1) (2011) 379–391.

[8] M. Zhang, M. Qin, C. Rode, et al., Moisture buffering phenomenon and its impact on building energy consumption, Appl. Therm. Eng. 124 (2017) 337–345.

[9] A. Trabelsi, R. Belarbi, K. Abahri, M. Qin, Assessment of temperature gradient effects on moisture transfer through thermogradient coefficient, Build. Simulat. 5 (2) (2012) 107–115.

[10] R. El Diasty, P. Fazio, I. Budaiwi, Modelling of indoor air humidity: the dynamic behaviour within an enclosure, Energy Build. 19 (1) (1992) 61–73.

[11] Z. Chen, M. Qin, J. Yang, Synthesis and characteristics of hygroscopic phase change material: composite microencapsulated phase change material (MPCM) and diatomite, Energy Build. 106 (2015) 175–182.

[12] Z. Chen, M. Qin, Preparation and hygrothermal properties of composite phase change humidity control materials, Appl. Therm. Eng. 98 (2016) 1150–1157.

[13] Z. Chen, D. Su, M. Qin, et al., Preparation and characteristics of composite phase change material (CPCM) with SiO2 and diatomite as endothermal-hydroscopic material, Energy Build. 86 (2015) 1–6.

[14] Z. Wu, M. Qin, M. Zhang, Phase change humidity control material and its impact on building energy consumption, Energy Build. 174 (2018) 254–261.

[15] X. Feng, M. Qin, S. Cui, et al., Metal-organic framework MIL-100 (Fe) as a novel moisture buffer material for energy-efficient indoor humidity control, Build. Environ. 145 (2018) 234–242.

[16] X. Zheng, T.S. Ge, R.Z. Wang, Recent progress on desiccant materials for solid desiccant cooling systems, Energy 74 (2014) 280–294.

[17] G. Férey, C. Mellot-Draznieks, C. Serre, et al., A chromium terephthalate-based solid with unusually large pore volumes and surface area, Science 309 (5743) (2005) 2040–2042.

[18] O.M. Yaghi, M. O'Keeffe, N.W. Ockwig, et al., Reticular synthesis and the design of new materials, Nature 423 (6941) (2003) 705.

[19] O.M. Yaghi, M. O'keeffe, N.W. Ockwig, et al., Reticular synthesis and the design of new materials, Nature 423 (6941) (2003) 705.

[20] G. Férey, Hybrid porous solids: past, present, future, Chem. Soc. Rev. 37 (1) (2008) 191–214.

[21] S.M. Cohen, Modifying MOFs: new chemistry, new materials, Chem. Sci. 1 (1) (2010) 32–36.

[22] H. Furukawa, F. Gándara, Y.B. Zhang, et al., Water adsorption in porous metal–organic frameworks and related materials, J. Am. Chem. Soc. 136 (11) (2014) 4369–4381.

[23] P. Horcajada, S. Surblé, C. Serre, et al., Synthesis and catalytic properties of MIL-100 (Fe), an iron (III) carboxylate with large pores, Chem. Commun. (27) (2007) 2820–2822.

[24] Y.K. Seo, J.W. Yoon, J.S. Lee, et al., Large scale fluorine-free synthesis of hierarchically porous iron (III) trimesate MIL-100 (Fe) with a zeolite MTN topology, Microporous Mesoporous Mater. 157 (2012) 137–145.

[25] J. Shi, X. Wu, X. Fu, et al., Synthesis and thermal properties of a novel nanoencapsulated phase change material with PMMA and SiO2 as hybrid shell materials, Thermochim. Acta 617 (2015) 90–94.

[26] R. Canioni, C. Roch-Marchal, F. Sécheresse, et al., Stable polyoxometalate insertion within the mesoporous metal organic framework MIL-100 (Fe), J. Mater. Chem. 21 (4) (2011) 1226–1233.

[27] L. Han, H. Qi, D. Zhang, et al., A facile and green synthesis of MIL-100 (Fe) with high-yield and its catalytic performance, New J. Chem. 41 (22) (2017) 13504–13509.

[28] S.E. Moradi, S. Dadfarnia, A.M. Haji Shabani, et al., Removal of Congo red from aqueous solution by its sorption onto the metal organic framework MIL-100 (Fe): equilibrium, kinetic and thermodynamic studies, Desalination Water Treat. 56 (3) (2015) 709–721.

[29] J.W. Yoon, Y.K. Seo, Y.K. Hwang, et al., Controlled reducibility of a metal–organic framework with coordinatively unsaturated sites for preferential gas sorption, Angew. Chem. Int. Ed. 49 (34) (2010) 5949–5952.

[30] S. Huang, K.L. Yang, X.F. Liu, et al., MIL-100 (Fe)-catalyzed efficient conversion of hexoses to lactic acid, RSC Adv. 7 (10) (2017) 5621–5627.

[31] C. Alkan, A. Sarı, A. Karaipekli, Preparation, thermal properties and thermal reliability of microencapsulated n-eicosane as novel phase change material for thermal energy storage, Energy Convers. Manag. 52 (1) (2011) 687–692.

[32] A. Sarı, C. Alkan, A. Karaipekli, Preparation, characterization and thermal properties of PMMA/n-heptadecane microcapsules as novel solid–liquid microPCM for thermal energy storage, Appl. Energy 87 (5) (2010) 1529–1534.

[33] M. Qin, J. Yang, Evaluation of different thermal models in EnergyPlus for calculating moisture effects on building energy consumption in different climate conditions, Build. Simulat. 9 (2016) 15–25.

[34] R. Judkoff, J. Neymark, International Energy Agency Building Energy Simulation Test (BESTEST) and Diagnostic Method, National Renewable Energy Lab., 1995.

Development of a moisture buffer value model (MBM) for indoor moisture prediction

Kan Zu[a], Menghao Qin[a,*], Carsten Rode[a], Michele Libralato[b]

[a] Department of Civil Engineering, Technical University of Denmark, Lyngby, Denmark
[b] Polytechnic Department of Engineering and Architecture, University of Udine, Udine, Italy

HIGHLIGHTS

- Moisture buffer values (MBVs) under different boundary conditions are proposed.
- Time-average MBV is introduced to calculate the indoor moisture conditions.
- A new moisture buffer value model (MBM) is developed for building simulation.
- The MBM model can provide a fast and accurate indoor moisture prediction.

ARTICLE INFO

ABSTRACT

Hygroscopic materials could be used to passively regulate indoor moisture fluctuations, and thus reduce building energy consumption. It is essential to accurately calculate the moisture buffering effect in building energy simulations. However, in many building simulation tools, moisture buffering has been neglected. In those building tools that include moisture model, moisture buffering either has been estimated by very simple approximations or has been calculated by complex coupled heat-air-moisture transfer models that require orders of magnitude more computing time than simple energy prediction. Here, we have developed a new moisture prediction model with fast solution time and reasonable accuracy based on the moisture buffer value (MBV) theory. The MBV was originally designed to evaluate the moisture buffering capacity of building materials. Little research has been carried out to directly use MBV for building energy simulations. This paper first investigates MBVs under different boundary conditions. Secondly, a time-average MBV has been proposed, and its parameters can be obtained from the practical MBV test. Finally, comparison tests between the new moisture buffer value model (MBM) and other moisture prediction models have been carried out. The results indicate that the MBM can provide a fast and reasonably accurate prediction for indoor moisture variation.

1. Introduction

In the process of achieving the desirable thermal comfort, more and more buildings are supplied with heating, ventilation and air-conditioning systems (HVAC) to reach the demand, while its usage is responsible for more than 50% of primary energy used within building blocks [1]. This continuous growth of building energy consumption has drawn people's attention on the energy-efficient control of hygrothermal conditions, and it is noted that latent cooling load accounts for around 40% of the total load of air-conditioning, and its proportion is even higher in many tropical and subtropical climates [2]. As the building codes have become much stricter, the improvement of insulation technology have contributed to the decrease of sensible load

(refers to the temperature changes), but latent load (refers to the humidity changes) remains unchanged. This urges the improvement of indoor humidity regulations. It is known that a wet environment may cause fungus growth and hence people are susceptible to respiratory diseases and allergies, while dry environment leads to skin allergy and eye irritation etc. [3]. Furthermore, moisture accumulation within the material of a building envelop can lead to degradation of organic materials, metal corrosion and structure deterioration [4,5]. The most commonly used dehumidification method is vapor-compression air-conditioning powered by electricity. This system is energy consuming and has a low coefficient of performance (COP) due to the refrigeration-dehumidification process, which often makes necessary a great deal of subsequent re-heating [6]. Some research have indicated that one

Nomenclature

a	Air exchange rate (h^{-1})	T	Periodic time (s)
A	Contact surface area (m^2)	v	Air velocity ($m\ s^{-1}$)
c	Vapor concentration ($kg\ m^{-3}$)	V	Indoor volume (m^3)
$\bar{c}$	Equilibrium vapor concentration ($kg\ m^{-3}$)	x	Spatial coordination (m)
c_0	Constant component of the indoor vapor concentration ($kg\ m^{-3}$)		

Greek letters

c_{air}	Vapor concentration of indoor air ($kg\ m^{-3}$)
c_{sat}	Saturated vapor concentration ($kg\ m^{-3}$)
D	Moisture diffusivity ($m^2\ s^{-1}$)
G	Moisture gain ($kg\ s^{-1}$)
G_w	The accumulated moisture mass ($kg\ s^{-2}$)
MBV	Moisture buffer value ($g\ m^{-2}\%RH^{-1}$)
N	Ratio factor (m^{-1})
P_{sat}	Saturated vapor pressure (Pa)
t	Time (s)

ρ	Density of hygroscopic material ($kg\ m^{-3}$)
μ	A dimensionless function related to the time ratio
ξ	Moisture capacity ($kg\ kg^{-1}$)
φ	Relative humidity (%)
δ	Vapor transfer coefficient ($kg\ m^{-1}\ s^{-1}$)
δ_{total}	Lumped total vapor transfer coefficient ($kg\ m^{-1}\ s^{-1}$)
$\varnothing_v$	Moisture flux ($kg\ m^{-2}\ s^{-1}$)
ω	Harmonic phase (s^{-1})
γ	Time ratio ($h\ h^{-1}$)

promising approach to control indoor moisture fluctuations within a desirable range is to use hygroscopic materials to benefit the moisture buffering (i.e. adsorption and desorption) at indoor surfaces [7–9].

Indoor humidity conditions have a significant effect on building energy consumption (e.g. latent load), thermal comfort of residents and indoor air quality [8]. The relative humidity (RH) in a building is mainly affected by the following factors: internal moisture sources or sinks, ventilation and infiltration, air-conditioning equipment, and moisture buffering (adsorption and desorption) of indoor hygroscopic materials. Many energy consumption models have ignored the last term, which may lead to overestimation of peak latent loads [10,11]. Moisture buffer capacity of building materials has been defined to disclose the phenomenon that hygroscopic materials can adsorb moisture from the ambient air when the indoor relative humidity rises, and release moisture to the ambient air when the indoor relative humidity drops [7,10,12]. It is a promising passive method to achieve moisture control or regulation without adding energy costs.

Over the past decades, many researchers have investigated the moisture-buffering phenomenon from the aspects of theory, experiment and simulation [4,13–16]. Time [17] proposed the method to characterize the moisture buffer effect of hygroscopic materials. Then Padfield [18] has investigated the effect of different adsorbent building materials on indoor moisture variation in detail. Simonson et al. [19] have experimentally and numerically proved that the hygroscopic wood-based materials can reduce the peak of indoor humidity and improve the perceived air quality. In 2005, Rode et al. [14] have introduced the concept of Moisture Buffer Value (MBV) in NORDTEST project, which represents the weight change of test samples when subjected to cyclic relative humidity variations under the set temperature. The test protocol proposed by NORDTEST defines the cyclic RH step-change between 75% of high humidity level for 8 h and 33% of low humidity level for 16 h. The amount of moisture exchanged during the adsorption or desorption period per exposed surface area and per % RH variation gives the practical MBV in $kg\ m^{-2}(\%RH)^{-1}$. Table 1 presents the different MBV test protocols [14,20,21].

The MBV theory was originally developed to evaluate the moisture buffering capacity of different building materials. Although the definition and test method of MBV is clear and easy to understand and conduct, its application in building simulation is very limited. Little research has been carried out to directly use MBV for building energy simulations. There are two main obstacles: (1) the NORDTEST assumes that the indoor moisture variation is a square-wave function that is very rare in real built environment; (2) the ideal MBV formula has ignored the surface resistance between the material and indoor air, while the measured MBV has taken into account the influence of moisture resistance at the material surface.

Regarding the indoor moisture prediction, some numerical models, such as the effective capacitance (EC) model [22,23], the effective moisture penetration depth (EMPD) model [22,24,25] and the coupled heat, air and moisture transfer (HAMT) model [22,23,26] have been developed and interagted into building energy simulation tools (e.g. EnergyPlus, WUFI Plus, TRANSYS etc.). The EC model uses a moisture capacitance multiplier to estimate the moisture buffering effect, which is an improvement over neglecting the moisture buffering of the materials entirely. However, it does not appropriately model the physical process of moisture adsorption and desorption at the material surface, and the multiplier is empirical and difficult to predict for different materials. The effective moisture penetration depth (EMPD) [8,10] model is based on the assumption that the moisture transfer takes place between the zone air and a thin fictitious layer of uniform moisture content of thickness d_{EMPD}. There are two formulations of the EMPD model. The one-layer EMPD model only has a thin surface layer to account for short-term transients, and may cause errors in energy simulations [27]. The two-layer EMPD model has introduced a deep layer for long-term moisture events, but the model is isothermal and the thickness of deep layer is empirical [22]. Abadie et al. [25] have developed an EMPD based lumped model for building simulation. The parameters in the model can be determined from the MBV test concept. Many researchers have developed finite-difference models (i.e. the HAMT models) to predict the moisture transport in hygroscopic materials. The HAMT model is more physically realistic than the EC and EMPD models, but it requires much more computation time (10^2-10^4 longer than the EC model [22]). In addition, the HAMT model requires many material properties and parameters (e.g. permeability, porosity and sorption isotherm etc.) that are normally difficult to obtain. There is a need to develop new moisture models with fast solution time and reasonable accuracy. Since the moisture buffer value indicates the quantity of water vapor absorbed or released by hygroscopic materials when a periodic variation of RH imposed at its surface directly, it is possible to evaluate and predict the indoor moisture variations by directly using the MBV theory and test method.

The purpose of this paper is to develop a new moisture prediction model based on the theory of moisture buffer value (MBV). The paper first investigates the MBV under different boundary conditions. A ratio

Table 1
Different test protocols of Moisture buffer.

	Time intervals (h)	RH range (%)
NORDTEST [14]	8/16	33–75
DIS 24353 [20]	12/12	33–53; 53–75; 75–93
JIS A 1470-1 [21]	24/24	33–53; 53–75; 75–93

factor has been introduced by mathematic deduction to convert MBVs from square wave to harmonic wave. Secondly, a time-average MBV has been proposed, and a lumped vapor transfer coefficient containing the surface resistance will be introduced, which can be obtained from the normal MBV measurements. Finally, comparison tests between the new moisture buffer value model (MBM) and other moisture prediction models (e.g. EC, EMPD and HAMT models) have been carried out.

2. Theory deduction

Indoor humidity load generally exhibits a cyclic variation in a day. Such variation, taking place at the surface of hygroscopic materials, leads to moisture adsorption or desorption between indoor air and the materials. For homogenous porous materials, it is possible to obtain analytical solutions for moisture transfer under cyclic boundary conditions. One-dimensional governing equation of moisture transfer in porous materials can be expressed as below [12]:

$$\frac{\partial c}{\partial t} = D\frac{\partial^2 c}{\partial x^2} = \frac{\delta}{\rho\xi}\frac{\partial^2 c}{\partial x^2} \tag{1}$$

where c is vapor concentration [kg m^{-3}]; ρ and ξ are density [kg m^{-3}] and moisture capability of materials [kg kg^{-1}], respectively; D is moisture diffusivity [m^2 s^{-1}]; δ is vapor transfer coefficient [kg m^{-1}s^{-1}]. Derived from the analogy of heat transfer, Eq. (2) correlates moisture flux $\varnothing_v$ [kg m^{-2} s^{-1}] with vapor concentration variation.

$$\varnothing_v = -\frac{\delta}{c_{sat}}\frac{\partial c}{\partial x} = -\delta\frac{\partial \varphi}{\partial x} \tag{2}$$

The corresponding initial and boundary condition can be described as:

$$\begin{cases} t = 0, c(x) = \bar{C} \text{ (Initial condition)}; \\ x = 0, \frac{\partial c}{\partial x} = N(c_{air} - c) \text{ (Boundary condition)}; \end{cases}$$

where N is ratio factor ($N = \frac{P_{sat}}{R \cdot \delta}$) [m^{-1}]; R is the surface resistance [Pa m^2 s kg^{-1}]; c_{air} is the vapor concentration for indoor air [kg m^{-3}]; $\bar{C}$ is the initial vapor concentration [kg m^{-3}]. The boundary condition here indicates the balance of moisture gradients at the interface between the air and material.

In the present analysis, the temperature is set as a constant, which eliminates the thermal effect on hygroscopic materials, and therefore makes it reasonable to assume that moisture properties of the materials are constant. The vapor transfer coefficient (δ) is measured by the cup method (see appendix A).

2.1. The ideal MBV

The ideal MBV represents the weight change of hygroscopic materials when subjected to cyclic relative humidity variations. Within a periodic time T, the surface condition of materials with time is a γT hours of high humidity (c_{high}) followed by (1-γ)T hours of low humidity (c_{low}). The boundary conditions can be expressed as:

$$c_0 = \begin{cases} c_{high}, 0 < t < \gamma T \\ c_{low}, \gamma T < t < T \end{cases} \tag{3}$$

By using Fourier transform that can convert the square wave function of Eq. (3) into the sum of simple waves mathematically represented by sines and cosines, the indoor vapor concentration variation can be rewritten as [12]:

$$c_0(t) = C + \sum_{n=1}^{\infty}(A_n\cos\frac{n\pi t}{T} + B_n\sin\frac{n\pi t}{T}) \tag{4}$$

where

$$A_n = \frac{1}{T}\int_{-T}^{T} c_0(t)\cdot\cos\frac{n\pi t}{T}dt = \frac{c_{high} - c_{low}}{n\pi}(\sin\gamma n\pi - \sin(1 - \gamma)n\pi)$$

$$B_n = \frac{1}{T}\int_{-T}^{T} c_0(t)\cdot\sin\frac{n\pi t}{T}dt$$
$$= \frac{c_{high} - c_{low}}{n\pi}(1 + \cos n\pi - \cos\gamma n\pi - \cos(1 - \gamma)n\pi)$$

$$C = \frac{A_0}{2} = \gamma c_{high} + (1 - \gamma)c_{low}$$

From the Eq. (4), it can be found that the variable items against time include sine and cosine function. However, C is a fixed value determined by the value of high humidity, low humidity and the time period ratio of high humidity. It has no influence on the moisture flux against time [12,25]. Therefore, it's neglected in the following discussion. Based on those harmonic function items ($\sum_{n=1}^{\infty}(A_n\cos\frac{n\pi t}{T} + B_n\sin\frac{n\pi t}{T})$), the moisture flux over the surface of materials can be presented from Eqs. (1)–(3) as:

$$\varnothing_0(t)$$
$$= \sum_{n=1}^{\infty}\left(\frac{A_n}{c_{sat}}\sqrt{\frac{n\pi}{T}\cdot\delta\cdot\rho\xi}\cos\left(\frac{n\pi t}{T} + \frac{\pi}{4}\right) + \frac{B_n}{c_{sat}}\sqrt{\frac{n\pi}{T}\cdot\delta\cdot\rho\xi}\sin\left(\frac{n\pi t}{T} + \frac{\pi}{4}\right)\right) \tag{5}$$

The accumulated moisture uptake/release G_w can be evaluated and simplified as [14]:

$$G_w = \int_0^{\gamma T}\varnothing_0(t)dt = 1.27(\gamma(1 - \gamma))^{0.535}\frac{c_{high} - c_{low}}{c_{sat}}\sqrt{\delta T\rho\xi} \tag{6}$$

All hygroscopic materials will reach to an equilibrium state after several cycles, which means the amount of moisture uptake equals to that of moisture release. During the time interval with high humidity, air moisture is transferred towards the materials. Thus, by using Eqs. (4)–(6), the ideal moisture buffer value under a square-wave moisture variation can be can be defined as:

$$MBV_{Ideal} = \frac{G_w}{\Delta RH} = 1.27(\gamma(1 - \gamma))^{0.535}\frac{\sqrt{\delta T\rho\xi}}{100} \tag{7}$$

2.2. MBV under a harmonic wave of indoor humidity

When considering a real living space, the indoor moisture variation will more likely change in a fluctuant wave but not a square wave mentioned above. It is hard to maintain a constant high/low humidity level without the assistance of mechanical systems in built environment, thus it is improper to use the ideal MBV (obtained under square wave) to directly evaluate the cyclic moisture uptake in real conditions [25,28]. Mathematical deductions can pave the way for the transformation of MBVs under different climates. The conversion from the square-wave to the harmonic-wave humidity change is presented in this section. Similar to the square-wave moisture variation, the assumed indoor vapor concentration variation in the real condition can be expressed as:

$$c_0 = \begin{cases} \bar{c} + (c_{high} - \bar{c})\sin\frac{\pi}{\gamma T}t, 0 < t < \gamma T \\ \bar{c} + (\bar{c} - c_{low})\sin\frac{\pi}{(1 - \gamma)T}t, \gamma T < t < T \end{cases} \tag{8}$$

where $\bar{c}$ is the equilibrium vapor concentration of material [kg m^{-3}].

Under a certain condition (23 °C, γ = 0.5), Eq. (3) and Eq. (8) can be described as in Fig. 1, which has clearly shown how indoor vapor concentration varies within a periodic time T (24 h).

According to its harmonic change during the cycle, the moisture flux of sorption process can be written as [12]:

$$\varnothing_{0\_ad}(t) = \frac{c_{high} - \bar{c}}{c_{sat}}\sqrt{\frac{\pi}{\gamma T}\cdot\delta\rho\xi}\sin\left(\frac{\pi}{\gamma T}t + \frac{\pi}{4}\right) \tag{9}$$

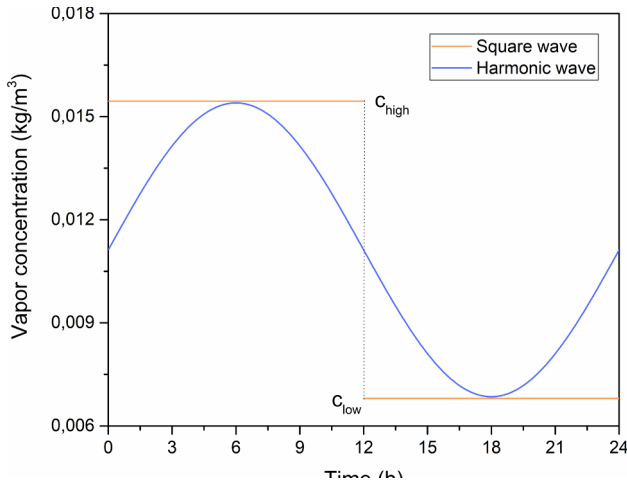Then the accumulated moisture mass (G_{w_ad}) can be integrated by Eq. (9) from 0 to γT.

3

Fig. 1. Square-wave and harmonic-wave vapor concentration variation (33–75% RH).

$$G_{w\_ad} = 2\frac{c_{high} - \bar{c}}{c_{sat}}\sqrt{\frac{\gamma T}{\pi} \cdot \delta\rho\xi} \tag{10}$$

The desorption process is similar to the adsorption process, the integrated equation can be written as:

$$G_{w\_de} = 2\frac{\bar{c} - c_{low}}{c_{sat}}\sqrt{\frac{(1-\gamma)T}{\pi} \cdot \delta\rho\xi} \tag{11}$$

When it comes to an equilibrium state, the moisture uptake is equal to the moisture release, so the only unknown parameter $\bar{c}$ can therefore be evaluated by Eq. (12).

$$\bar{c} = \frac{c_{high}\sqrt{\gamma} + c_{low}\sqrt{1-\gamma}}{\sqrt{\gamma} + \sqrt{1-\gamma}} \tag{12}$$

Plugging the Eq. (12) into Eq. (10), the accumulated moisture mass can be written as:

$$G_w = 2\frac{c_{high} - c_{low}}{c_{sat}}\frac{\sqrt{\gamma(1-\gamma)}}{\sqrt{\gamma} + \sqrt{1-\gamma}}\sqrt{\frac{\delta\rho\xi T}{\pi}} \tag{13}$$

Compared with Eq. (7), $MBV_{Harmonic}$ can be expressed as:

$$MBV_{Harmonic} = \frac{G_w}{\Delta RH} = 0.888\frac{(\gamma(1-\gamma))^{-0.035}}{\sqrt{\gamma} + \sqrt{1-\gamma}}MBV_{Ideal} = \mu(\gamma)MBV_{Ideal} \tag{14}$$

where the time interval γ is the only independent variable to the ratio factor μ. In addition, Eq. (14) indicates that for a complete cycle, the moisture uptake (or release) under the harmonic wave is different from that the under square wave due to the ratio factor $\mu(\gamma)$, which is always less than 1.

In Fig. 2, the ratio factor μ characterizes the accumulated mass change under different boundary conditions. The vapor transfer coefficient is given as $1.0 \times 10^{-8}\,\mathrm{kg\,m^{-1}\,s^{-1}}$, and the density and moisture capacity keeps constant as $800\,\mathrm{kg\,m^{-3}}$ and $0.1\,\mathrm{kg\,kg^{-1}}$, respectively. When time interval γ approaches to 0.5, the accumulated mass reaches the maximum, but the ratio factor μ decreases to the minimum.

2.3. Time-average MBV

As a material property, the ideal MBV represents the total amount of water vapor exchanged during the adsorption or desorption period. It is not suitable for building energy simulation, which is normally based on the hourly data. Therefore, a time-average MBV has been proposed. First, the cycle has been divided into several time intervals $\triangle t$, then considering the MBVs under different boundary conditions that have been presented in previous section, the expression of time-average MBV

at time t_1 can be defined by:

$$MBV_i = \frac{\int_{t_1}^{t_1+\Delta t} \varnothing_0(t)dt}{\Delta t * \Delta RH} \tag{15}$$

For square wave:

$$
\begin{aligned}
MBV_i &= \sum_{n=1}^{\infty} \left[\frac{A_n}{c_{high} - c_{low}}\sqrt{\frac{n\pi}{T} \cdot \delta \cdot \rho\xi}\cos(\frac{n\pi t}{T} + \frac{\pi}{4}) + \frac{B_n}{c_{high} - c_{low}}\sqrt{\frac{n\pi}{T} \cdot \delta \cdot \rho\xi} \right. \\
&\quad \left. \sin(\frac{n\pi t}{T} + \frac{\pi}{4}) \right]
\end{aligned}
\tag{16}$$

For harmonic wave:

$$MBV_i = \frac{c_{high} - \bar{c}}{c_{high} - c_{low}}\sqrt{\frac{\pi}{\gamma T} \cdot \delta\rho\xi}\sin(\frac{\pi}{\gamma T}t + \frac{\pi}{4}) \tag{17}$$

It can be found that the time-average MBV is related to the average moisture flux over one time step. Within one time step, the value can be approximated with a constant. In the real condition, the time-average MBV can be obtained from the MBV test, so the moisture flux at any time interval can be calculated by Eq. (17). Note that $\triangle$RH is a constant equal to the maximum RH difference in a day. In building simulation, the RH difference can be estimated when considering the air exchange and indoor moisture gain.

2.4. Surface resistance

In the building physics literatures it is usually assumed that the surface resistance to transfer of moisture in vapor form is nearly zero or insignificant, and some researchers [14,29] indicate that the intrinsic moisture transfer resistance is larger than the surface resistance. However, Roels et al. demonstrated that it is unreasonable to ignore the influence of external resistance over the materials in the real building simulation [10]. It is important to note that the ideal MBV is characterized at the *Material level* [14,25] by using standard material properties (e.g. moisture effusivity, vapor transfer coefficient etc.) obtained under stationary conditions. The practical MBV is characterized at the *System level* [14,25] that represents the material-environment combination, which is a function of the moisture effusivity, the air RH variation period and the air-film resistance [14]. This may be the main reason that discrepancy exists between the ideal MBVs and practical ones.

Here, in order to include the system-level surface resistance in the ideal MBV formulas, a lumped total vapor transfer coefficient (δ_{total}) has been introduced. This lumped value combines the surface moisture
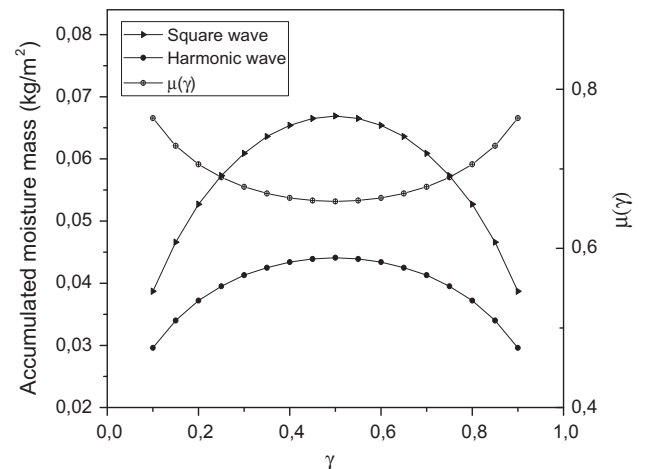

Fig. 2. The correlation of accumulated moisture mass under different boundary conditions.

transfer and the vapor diffusion across the material and thin air layers to be a lumped coefficient, in which all factors related to the vapor transfer is considered. This lumped total vapor transfer coefficient can be easily obtained from the MBV test by data fitting. The procedure will be described in the following experiment section. In this paper, the lumped total vapor transfer coefficient (δ_{total}) will be used to replace the vapor diffusion coefficient (δ) in the above MBV deductions. Then the new MBVs together with indoor moisture gain and ventilation will be used to calculate the indoor moisture variation.

3. Experimental method

The MBV test has been carried out to measure the time-average MBV and other parameters required in the moisture flux calculations. The amount of moisture uptake/release with time under both the square wave and harmonic wave conditions have been recorded with the nearly same airflow condition in the following simulation. The material used in the tests are MIL-100(Fe), which is a kind of Metal-Organic Frameworks (MOFs). MOFs are a new class of porous crystalline materials that consist of metal clusters and organic linkers. Owing to their high porosity and large specific surface, MOFs are promising sorbents for water vapor. As shown in Fig. 3, the sorption isotherms indicate that MIL-100 (Fe) has a high moisture adsorption capacity due to the polymodal pore size distribution [30,31]. Meanwhile, recent research [31] shows the MBV of MIL-100(Fe) with 0.92 cm^3 g^{-1} of pore volume and over 1600 m$^2 \cdot$g^{-1} of surface area could be up to 15 g·m^{-2}·RH^{-1} at 8 h, which is 33 times higher than the laminated wood. Here, all measurements last until the system reaches an equilibrium.

3.1. MBV test

The climate chamber can provide a constant temperature at 23 °C as shown in Fig. 4. The test sample (diameter: 26 mm; thickness: 20 mm) was prepared with all sides sealed except one exposed to the air inside the climate chamber. Before test, the sample was dehydrated at 50 °C in an oven, and then put in the climate chamber cooling down to the set temperature. The mix of dry air and saturated air in proportion regulates the RH of the climate chamber, and the heater controls the chamber temperature. The temperature and humidity were measured by sensors and regulated by PID regulator. A fan stirred the chamber air to keep the climate chamber in an even hygrothermal condition.

During the MBV test, the sample was hung on the supporter connected to the balance. For the square wave measurement, the test condition refers to the NORDTEST protocol test (0.1 m/s of airflow condition over the material surface). The test cycle consists of 12 h of high RH (75%) and 12 h of low RH (33%) [14]. As for the harmonic wave measurement, the RH changes from 33% to 75% within a day (here γ equals 0.5). Then the mass change of the test sample was recorded every minute in terms of moisture uptake or release, and automatically plotted by the connected computer. The tests were conducted in several cycles until the mass change was below 5% for the last three days.

3.2. Results and discussion

Fig. 5(a) shows that a sharp change appears when vapor concentration switches from high level to low level and vice versa. However, under a harmonic vapor concentration variation in Fig. 5(b), it presents a more continuous change, which is much closer to the real condition. The moisture flux change with different boundary conditions show a different evolution. Based on the mathematic deduction described in the Section 2, the calculated moisture flux over time matches well with the measured results, thus it is reasonable to calculate the lumped total vapor transfer coefficient (δ_{total}) by fitting the curve of the MBV tests. In Table 2, it can be seen that MBV using lumped total vapor

transfer coefficient (δ_{total}) is much closer to the measured MBV. The remaining gap may be the error during the experiments. Therefore, the method of fitting curve is capable of providing a reasonable value to the following simulation. In the MBV tests, the lumped total vapor transfer coefficients under different boundary conditions (i.e. square wave and harmonic wave) are very much alike. So in this paper, the value of lumped total vapor transfer coefficient (δ_{total}) is set an average (1.6 × 10^{-7} kg m^{-1}s^{-1}), and it considers all transfer resistances to be a symbolically lumped parameter for simulation (detailed calculation steps are presented in the Section 4), which is a more reliable value.

4. Indoor moisture simulation

In the following part, the numerical prediction of the indoor relative humidity variation will use the MBM model (i.e. the harmonic MBV model) followed by the corresponding results and analysis. The lumped total vapor transfer coefficient (δ_{total}) obtained from the MBV tests will be applied to the proposed MBM model for indoor moisture simulation. The procedures are the following:

- Measurements of the moisture uptake or release between the test samples and its surrounding air when the samples are subjected to square-wave moisture variation and harmonic moisture variation of the surrounding air, respectively.
- Curve fitting evaluation of the experimental data to obtain the lumped total vapor transfer coefficients that include the surface resistance. These parameters (δ_{total}) could be estimated by taking the Eqs. (5) and (9) as the fitting functions, respectively. Software, such as Matlab, Origin, etc., can be used to create user-defined functions employing Eqs. (5) and (9) to calculate the parameters.
- Determination of the expression of time-average MBV (Eq. (15)) and calculation of the ideal MBV in Eqs. (7) and (14) by using the lumped total vapor transfer coefficients.
- The integration of the expression of time-average MBV, and calculation of the indoor vapor balance equation.

The present case measured the mass variation of test sample subjected to square-wave and harmonic-wave vapor concentration variation, respectively. A 24-h periodic relative humidity varies from 33% RH to 75%RH under a constant temperature (23 °C) at which the saturated vapor concentration is 20.5 g m^{-3}. The sample's properties mainly include material density (790 kg m^{-3}), moisture capacity (0.45 g g^{-1}). The corresponding experiments set γ equal to 0.5 under different boundary conditions.

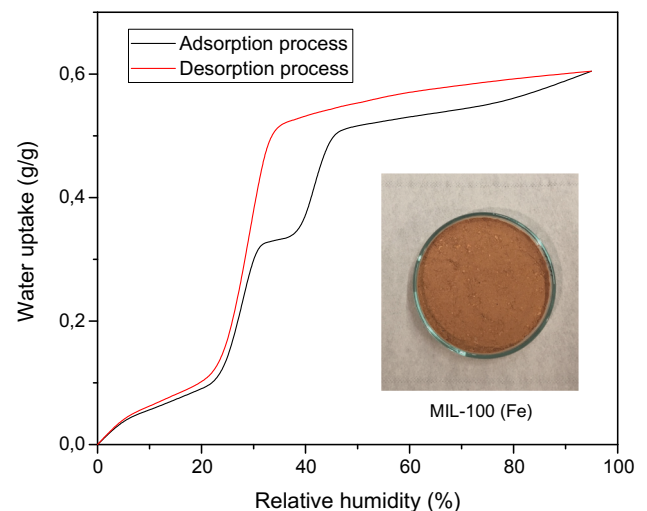In view of the correlation between the water uptake/release of
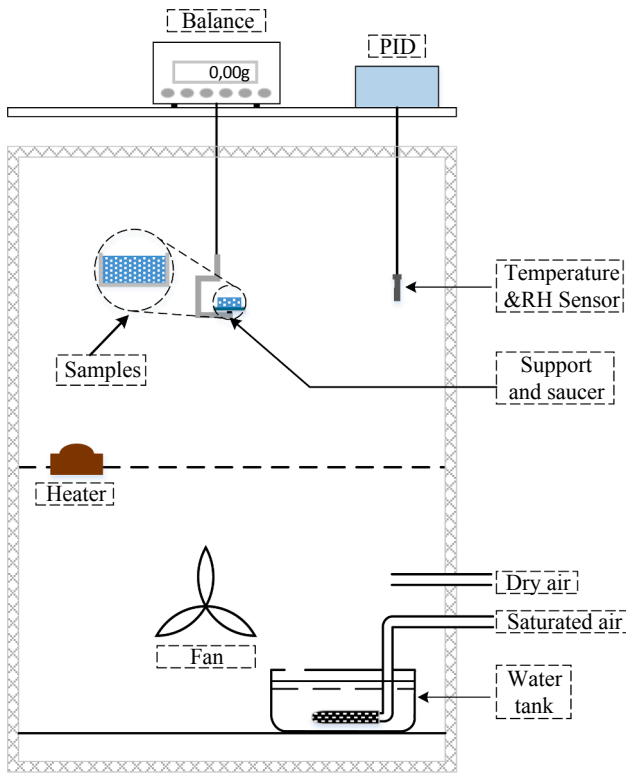
Fig. 3. Sorption isotherms of MIL-100 (Fe).

Fig. 4. Schematic view of experiment system.

hygroscopic materials and the moisture buffer capability, MBV affects the indoor moisture balance. The theory deduction indicates that the ideal MBV characterizes the material property without considering the surface resistance and environmental impact, while the time-average MBV represents the feedback to the indoor moisture variation against time through the lumped total vapor transfer coefficient (δ_{total}). The moisture buffer phenomenon at the room level is related to exposure areas of the surface materials, moisture load, ventilation rate and indoor climate etc. The following simulation takes the BESTEST benchmark building geometry as a reference shown in Fig. 6 [32].

The indoor vapor balance equation can be expressed as:

Table 2
The measured parameters under different boundary conditions.

	Square wave	Harmonic wave
Lumped total vapor transfer coefficient (MBV test) ($\times 10^{-7}$ kg m^{-1}s^{-1})	1.52	1.69
Measured MBV (g m^{-2} RH%$^{-1}$)	11.9	8.3
Calculated MBV using δ_{total} (g m^{-2}RH%$^{-1}$)	13.1	9.1
Ideal MBV (g m^{-2}RH%$^{-1}$)	20.8	13.7

$$V\frac{dc_i}{dt} = a(c_0 - c_i)V + G + A \cdot MBV_i \cdot \Delta RH \tag{18}$$

where a is air exchange rate [h^{-1}]; G is moisture gain [kg h^{-1}]; A is the surface area of the moisture buffer material [m^2]; V is indoor volume [m^3].

The room size is 8 m × 6 m × 2.7 m, and the wall thickness is 20 cm. A wall panel made of MOF-100(Fe) is installed on the west wall to act as the moisture buffer material (see Fig. 6), and the surface area of the wall panel is 12 m^2 with a 15 mm of thickness. The total vapor transfer coefficient is 1.6×10^{-7} kg m^{-1}s^{-1}, a more accurate value obtained from the experimental measurements. All external surfaces of this room are assumed impermeable and waterproof, which means there is no moisture transfer across the building envelopes. The indoor moisture variation is mainly affected by the moisture adsorption or desorption of the wall panel made of moisture buffer materials. The initial indoor air concentration is set 6.15 g m^{-3}, and the outside air concentration varies as a 24 h harmonic function starting from 6.15 g m^{-3} with an a (=0.5) ACH of air exchange rate. Additionally, moisture perturbations occurred between 9:00 am and 5:00 pm with a 0.5 kg h^{-1} of moisture gain. The calculation of indoor vapor balance is conducted by using Eq. (18) with an explicit discrete scheme. The moisture flux over the surface of materials is calculated by: (1) the finite volume method (with a 0.01 m of spatial step and a 1/60 h of time step); (2) the EMPD model and (3) the MBM model (under harmonic vapor concentration variation).

Fig. 7 shows the indoor moisture variation when a periodic moisture gain occurs. Since the HAMT model has been widely validated against both experimental tests and analytical solutions [22,23,26,33], we assumed that the results from HAMT is *correct*. The MBM model appears to be the most accurate. We quantify this accuracy by calculating the percent difference between the indoor humidity predicted by the HAMT
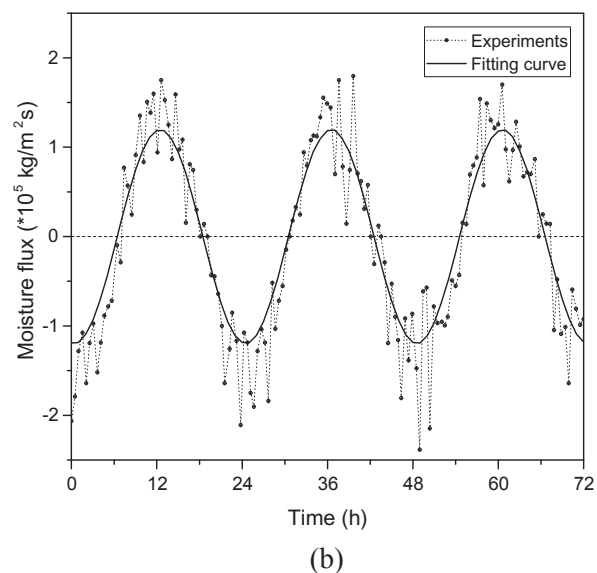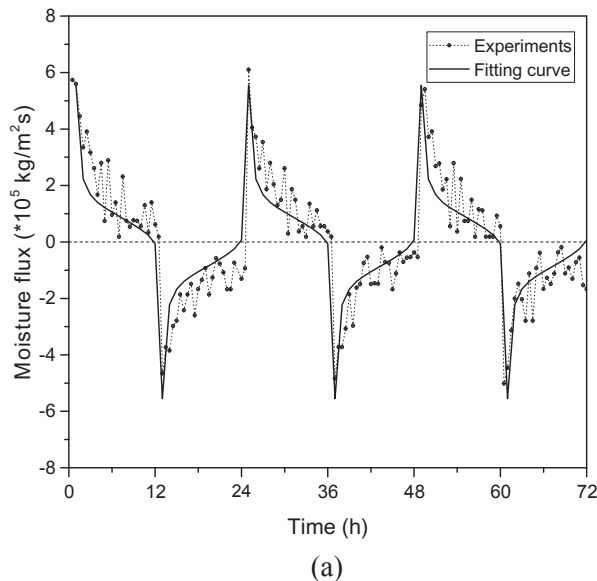

Fig. 5. Measured average moisture flux under a 24-h vapor concentration variation (RH = [33%, 75%]). a) Square wave; b) Harmonic wave.
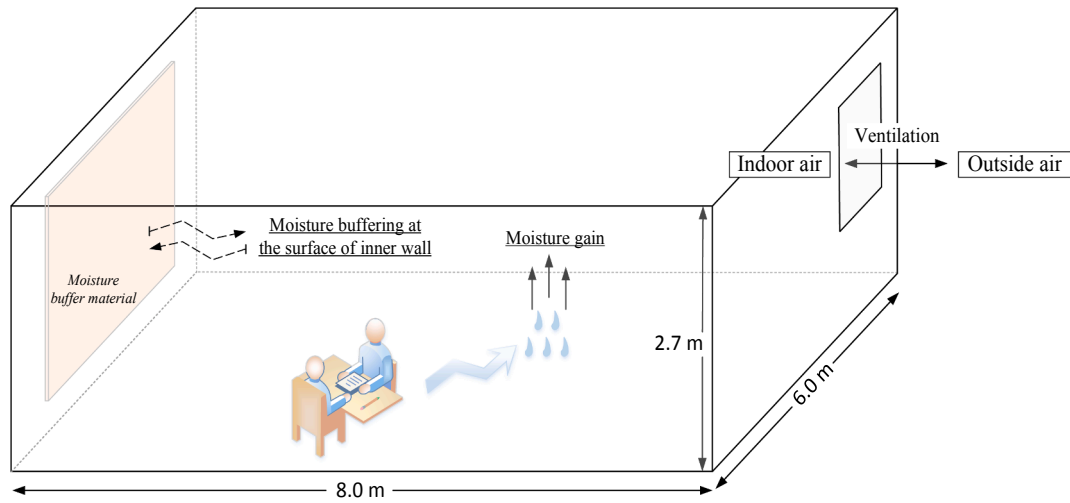
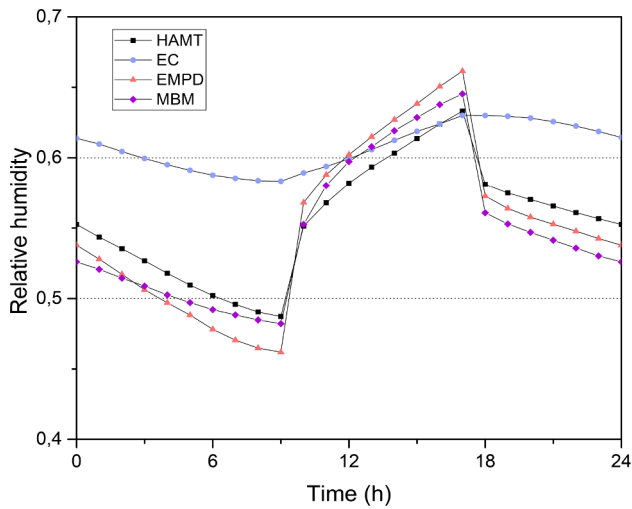**Fig. 6.** Schematic of BESTEST benchmark building.

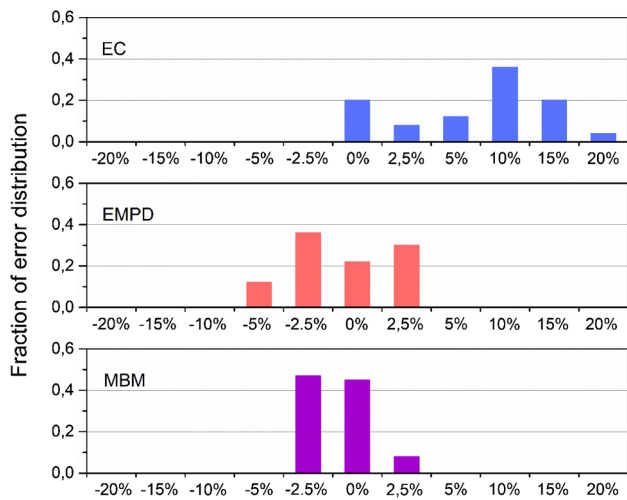**Fig. 7.** Indoor moisture variation prediction.

Fig. 8. Histogram of errors for EC, EMPD and MBM models. Error is calculated as deviation from HAMT model.

model and that predicted by the other models at each time step. The errors are presented in Fig. 8, where the bins are centered at the label on the x-axis.

Fig. 8 shows that the MBM model matches the HAMT model within ± 2.5% at all time steps and is within ± 1% for more than 45% of the simulation. One possible reason to the small differences (or errors) between the MBM model and the HAMT model might be that the current MBM model is isothermal and the HAMT is non-isothermal. The minor temperature change due to the adsorption heat may affect the value of relative humidity, and the error from the experimental setup may bring the uncertainty (i.e. the response of humidity sensor) to the moisture variation prediction as well. Nevertheless, compared with the results from other models, the MBM model is outperforming the EC and EMPD model [22] in the prediction of indoor humidity variation. Since the EC model simplifies moisture buffer effect into a single moisture capacitance multiplier, the result from the EC model is far from that of the HAMT model with errors up to 20%. The EMPD model is also less accurate than the MBM model as it matches the HAMT within ± 1% for only 20% of the simulation.

As to the computing time of the MBM model, it is close to that of the EC model, which is 2–4 orders of magnitude faster than the HAMT model [22]. In summary, the MBM model can provide a fast and reasonable prediction for indoor moisture variation.

5. Conclusion

Moisture buffering of indoor hygroscopic materials has a significant effect on indoor moisture condition and building energy consumption. This paper has developed a new moisture prediction model – the MBM model, which is based on the theory of the moisture buffer value (MBV). Since the MBV from NORDTEST was originally designed to classify the moisture buffering capacity of different building materials, some improvements of the MBV theory have been proposed to make the MBV suitable for building simulation. First, the theoretical MBV under a harmonic-wave indoor moisture variation has been proposed, which is more practical than the original MBV obtained under the square-wave test for calculating indoor moisture condition in the near real condition. Although the ambient RH in a building room may not vary exactly like a harmonic wave, it is not deviating too much from a harmonic condition, and the conversion of MBVs under different climate can be achieved in a mathematical deduction [28]. Meanwhile, the surface resistance between the material and indoor air has also been taken into account. Secondly, the time-average MBV has been developed and integrated into the vapor balance along with the transformation to a harmonic-wave variation. From this perspective, the time-average MBV can directly correspond to the hourly moisture uptake or release of materials when indoor RH increases or decreases.

In order to get the required parameters for the MBM model, the

MBV tests under both the square-wave and harmonic-wave moisture variation have been carried out. Curve fitting evaluation of the experimental data can provide the fitting parameters for the calculation of indoor humidity conditions. Finally, comparison tests between the new moisture buffer value model (MBM) and other moisture prediction models (e.g. EC, EMPD and HAMT models) have been carried out. The results indicate that the MBM model can provide a fast and reasonable prediction for indoor moisture variation.

Although the current MBM model is isothermal, and the temperature effect on MBVs has not been considered, the proposed model does work well to predict the indoor moisture variation. Further research will be carried out to investigate the temperature effect (e.g. adsorption/desorption heat) on the MBV and indoor hygrothermal conditions.

CRediT authorship contribution statement

Kan Zu: Data curation, Writing - original draft. **Menghao Qin:** Conceptualization, Methodology, Supervision. **Carsten Rode:** Supervision. **Michele Libralato:** Writing- review & editing.

Declaration of Competing Interest

The authors declare that they have no known competing financial interests or personal relationships that could have appeared to influence the work reported in this paper.

Appendix A

The isothermal cup method was used to measure the vapor transfer coefficient of the material. The saturated salt solution (NaCl, sodium chloride) provides a constant relative humidity (75.3 ± 0.12% at 25 °C) inside the cup. The cup was placed in a climate chamber with a constant temperature and relative humidity (33%, 23 °C). Then a vapor pressure gradient appears across the test sample. The cup test was conducted under the conditions of a constant temperature and a given RH difference.

Fig. A1 shows the schematic of the cup method test. The weight change of the cup with time was measured regularly until the mass loss reaches a steady state. The vapor transfer coefficient can be expressed as:

$$\delta = \frac{g_v \bullet d}{\Delta RH} \tag{A.1}$$

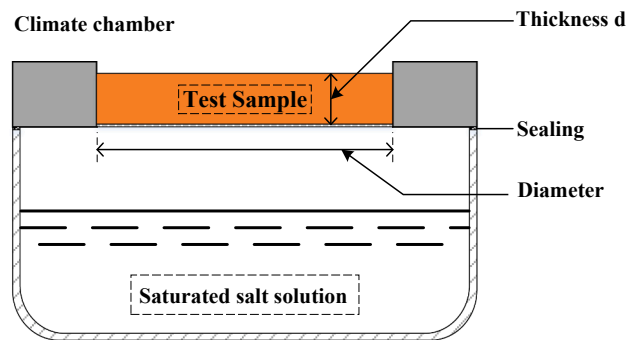**Fig. A1.** Schematic of cup method.

where g_v is the moisture flow (kg s^{-1}), d is the thickness of the sample (m), and ΔRH is the difference of relative humidity on both sides of the sample. In this case, the thickness is 1.5 cm; the diameter of the test sample is 2.5 cm. The vapor transfer coefficient of MIL-100(Fe) can thus be calculated, and it is 2.82×10^{-7} kg m^{-1} s^{-1}.

It is important to note that the vapor transfer coefficient from the cup method is a material level property under stationary conditions, which is normally different from the lumped total vapor transfer coefficient of the system level obtained from the MBV test [14].

References

[1] L.Z. Zhang, F. Xiao, Simultaneous heat and moisture transfer through a composite supported liquid membrane, Int. J. Heat Mass Tran. 51 (2008) 2179–2189.

[2] M. Qin, P. Hou, Z. Wu, J. Wang, Precise humidity control materials for autonomous regulation of indoor moisture, Build. Environ. 169 (2020).

[3] A.C. Lowen, S. Mubareka, J. Steel, P. Palese, Influenza virus transmission is dependent on relative humidity and temperature, PLOS Pathog. 3 (2007) 151.

[4] O.F. Osanyintola, C.J. Simonson, Moisture buffering capacity of hygroscopic building materials: Experimental facilities and energy impact, Energy Build. 38 (2006) 1270–1282.

[5] M. Sultan, I. El-Sharkawy, T. Miyazaki, B.B. Saha, S. Koyama, An overview of solid desiccant dehumidification and air conditioning systems, Renew. Sust. Energ. Rev. 46 (2015) 16–29.

[6] S. Cui, M. Qin, et al., Metal-Organic Frameworks as advanced moisture sorbents for energy-efficient high temperature cooling, Sci. Rep. 8 (2018).

[7] H. Zhang, H. Yoshino, K. Hasegawa, Assessing the moisture buffering performance of hygroscopic material by using experimental method, Build. Environ. 48 (2012) 27–34.

[8] J.W. Meissner, N. Mendes, K.C. Mendonca, L.M. Moura, A full-scale experimental set-up for evaluating the moisture buffer effects of porous material, Int. Commun. Heat Mass. 37 (2010) 1197–1202.

[9] Z. Wu, M. Qin, M. Zhang, Phase change humidity control material and its impact on building energy consumption, Energy Build. 174 (2018) 254–261.

[10] S. Roels, H. Janssen, Is the moisture buffer value a reliable material property to characterize the hygric buffering capacities of building materials? Working paper A41-T2-B-05-7 for IEA Annex 41 Project, Whole Building Heat, Air and Moisture Response, Trondheim, Norway, 2005.

[11] M. Qin, R. Belarbi, F. Allard, Simulation of whole building coupled hygrothermal-

airflow transfer in different climates, Energy Convers. Manage. 52 (2011).

[12] M. Zhang, M. Qin, C. Rode, Z. Chen, Moisture buffering phenomenon and its impact on building energy consumption, Appl. Therm. Eng. 124 (2017) 337–345.

[13] S. Hameury, Moisture buffering capacity of heavy timber structures directly exposed to an indoor climate: a numerical study, Build. Environ. 40 (2005) 1400–1412.

[14] C. Rode, Moisture Buffering of Building Materials, Department of Civil Engineering, Technical University of Denmark, 2005.

[15] A. Trabelsi, R. Belarbi, K. Abahri, M. Qin, Assessment of temperature gradient effects on moisture transfer through thermogradient coefficient, Build. Simul. 5 (2) (2012) 107–115.

[16] M. Qin, R. Belarbi, Development of an analytical method for simultaneous heat and moisture transfer in building materials utilizing transfer function method, J. Mater. Civ. Eng. 17 (2005) 492–497.

[17] B. Time, Hygroscopic Moisture Transport in Wood, Ph.D. Thesis Norwegian University of Science and Technology, Trondheim, Norway, 1998.

[18] T. Padfield, The role of absorbent building materials in moderating changes of relative humidity, Ph.D. Thesis The Technical University of Denmark, Copenhagen, Denmark, 1998.

[19] C.J. Simonson, M. Salonvaara, The effect of structures on indoor humidity – possibility to improve comfort and perceived air quality, Indoor Air 12 (2002) 243–251.

[20] International Organization for Standardization (ISO), Hygrothermal Performance of Building Materials and Products Determination of Moisture Adsorption Desorption Properties in Response to Humidity Variation, ISO 24353, 2008.

[21] Japanese Standards Association (JSA), Test Method of Adsorption/Desorption Efficiency for Building Materials to Regulate an Indoor Humidity - Part 1: Response Method of Humidity, JIS A 1470-1, 2002.

[22] J. Woods, J. Winkler, D. Christensen, Evaluation of the Effective Moisture Penetration Depth Model for Estimating Moisture Buffering in Buildings, National Renewable Energy Laboratory, The U.S. Department of Energy, USA, 2013.

[23] M. Qin, J. Yang, Evaluation of different thermal models in EnergyPlus for calculating moisture effects on building energy consumption in different climate conditions, Build. Simul. 9 (2016) 15–25.

[24] M.J. Cunningham, Effective penetration depth and effective resistance in moisture transfer, Build. Environ. 27 (1992) 379–386.

[25] M.O. Abadie, K.C. Mendonça, Moisture performance of building materials: from material characterization to building simulation using the Moisture Buffer Value concept, Build. Environ. 44 (2009) 388–401.

[26] H. Kunzel, Simultaneous heat and moisture transport in building components, Ph.D. Thesis Fraunhofer Institute of Building Physics, Suttgart, German, 1995.

[27] A. Karagiozis, L. Gu, The EMPD model, IEA/ECBCS Annex 41 Meeting, Glasgow, Scotland, (2004).

[28] V. Cascione, D. Maskell, A. Shea, P. Walker, A review of moisture buffering capacity: From laboratory testing tofull-scale measurement, Constr. Build. Mater. 200 (2019) 333–343.

[29] C. Rode, K. Peuhkuri, K. Hansen, B. Time, J. Svennberg, T. Arfvidsson, T. Ojanen, NORDTEST Project on moisture buffer value of materials, AIVC Conference 'Energy performance regulation', Brussels, Belgium September 21–23, 2005.

[30] J. Canivet, A. Fateeva, Y. Guo, B. Coasne, D. Farrusseng, Water adsorption in MOFs: fundamentals and applications, Chem. Soc. Rev. 43 (2014) 5594–5617.

[31] X. Feng, M. Qin, S. Cui, C. Rode, Metal-organic framework MIL-100(Fe) as a novel moisture buffer material for energy-efficient indoor humidity control, Build. Environ. 145 (2018) 234–242.

[32] R. Judkoff, J. Neymark, International Energy Agency Building Energy Simulation Test (BESTEST) and Diagnostic Method, National Renewable Energy Laboratory, USA, 1995.

[33] M. Qin, R. Belarbi, A. Ait-Mokhtar, F. Allard, Simulation of coupled heat and moisture transfer in air-conditioned buildings, Automat. Constr. 18 (2009) 624–631.